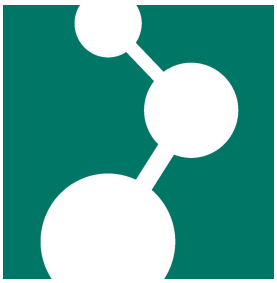

Complex Colloids by the Emulsion Solvent Evaporation Process

Dissertation
zur Erlangung des Grades
„Doktor der Naturwissenschaften“
im Promotionsfach Chemie

am Fachbereich Chemie, Pharmazie und Geowissenschaften
der Johannes Gutenberg-Universität Mainz

Roland Hinrich Staff

geboren in Hildesheim

Mainz, 2013

Die vorliegende Arbeit wurde am Max-Planck-Institut für Polymerforschung in Mainz unter der Betreuung von [redacted] von April 2011 bis November 2013 angefertigt. Ich versichere, die vorliegende Arbeit selbstständig angefertigt zu haben. Alle verwendeten Hilfsmittel und Quellen habe ich eindeutig als solche kenntlich gemacht.

Dekan: [redacted]

1. Berichterstatterin: [redacted]

2. Berichterstatter: [redacted]

Tag der mündlichen Prüfung: 31.01.2014

Für [redacted]

Table of Contents

1. Motivation

> "Complexity is the prodigy of the world.
> Simplicity is the sensation of the universe.
> Behind complexity, there is always simplicity to be revealed.
> Inside simplicity, there is always complexity to be discovered." [1]

This quote by Gang Yu beautifully describes the relation of complexity and simplicity – they are the two sides of the same coin. Highly complex systems can be broken down into smaller pieces that are more simple to handle and to understand. At the same time, complex systems are diverse in terms of the quantity and the diversity of their subunits and of their interactions with each other.

Thus, it is the task of a scientist to "reveal simplicity behind complexity" and to "discover complexity inside simplicity". It is also the duty of a scientist to find new solutions to existing problems, and indeed these two tasks go hand in hand as one entails the other. The problems to solve can often be highly complex, as the world itself is complex. Furthermore, the world becomes more and more complex since its subunits such as people and their interactions, the available materials and technology as well as the laws and regulations governing them increase and advance.

Today, many complex problems such as health, nutrition, communication, and diminishing resources are calling for complex solutions. One possible solution is to invent new technologies and to adapt old technologies to new needs. By this, physical objects such as food, clothes, housing and other materials can be generated that even have better properties than the ones in use nowadays. In addition, the production can be done more efficiently and consume less resources. Humanity has been inventing new technologies and new materials for millennia with great success, albeit having needed more and more resources in the process. Therefore, the focus should be on producing complex materials in a way that they can still fulfill their function but only with a fraction of the material needed before.

One way of fabricating complex materials with a significantly lower amount of material than before is to divide the material's abilities into functional and stabilizing parts. The former provide the functionality of the material while the latter act as stabilizer. Furthermore, the functional parts can be distributed heterogeneously along the material, allowing for a more efficient use of the functional parts.

A highly useful class of functional materials are polymers – indeed, today we live in the Polymer Age, following the Stone Age, the Bronze Age and the Iron Age.[2,3] In contrast to stone, bronze and iron, the mechanical properties of polymers can be varied over a wide range. Furthermore, they can carry diverse functional groups which can fulfill a function on the molecular level. In addition, polymers can have different architectures such as being star-shaped or being linear.[4,5] Among linear polymers, the functionality can be located homogeneously along the polymer chain, at the beginning and/or at the end of the polymer chain, or heterogeneously along the polymer chain as it is the case for block copolymers. In block copolymers, there is also a built-in heterogeneity since the two blocks in a diblock copolymer can phase separate and hence form a heterogeneous system.[6,7]

Having functional groups that can be distributed homogeneously or heterogeneously, the polymer needs to be formulated into a usable system for the problem at hand. As water is the common solvent in many technical and biological systems, the use of colloids seems obvious: Colloids can be dispersed in water, there are numerous ways to produce them, and they are already abundantly used both as a starting material for further modification or as the final product. In addition, one colloid can consist not only of one, but of several different materials,[8] which again could phase separate to form a heterogeneous structure. Thus, functionality in addition to potentially two different levels of morphology control can be achieved in colloids prepared from a preformed polymer. One level of morphology control is a property of the polymer and the other is a property of the colloid. Furthermore, colloids can be extremely small, which allows to use only minute amounts of material, thus preserving valuable resources. To form the colloids, a method to formulate the preformed polymer into a colloid is needed. The methods of choice is the process of solvent evaporation from emulsion droplets (SEED), as it allows to produce colloids and to control their morphology.

Thus, it is the objective of this thesis to prepare complex polymeric colloids by the SEED process. By complex, it is understood that they should have some addressable functionality and that the colloids have not a homogeneous but a heterogeneous structure. In this context, "simplicity behind complexity" shall be revealed by using new approaches, methods, and materials. Additionally, "complexity inside simplicity" will be discovered as new approaches, methods, and materials create new, unforeseen obstacles.

The SEED process is used throughout this thesis – however, its mechanism has not been completely understood yet. Therefore, it was investigated in detail, especially concerning the question whether coalescence of droplets occurs in the process or not. For this, different techniques were applied. Some of them were employed for the first time in regard to coalescence. Furthermore, the SEED process was used to prepare polymeric Janus particles that were functionalized with clickable alkyne groups on one face and azide groups on the other face. By choosing different synthetic routes for the polymers used in the process, the density of the functional groups could be varied. Another, even more complex type of matter

are stimulus-responsive materials. Such materials are highly interesting because they can first encapsulate and then release other substances[9] such as self-healing materials,[10–13] or drugs.[14–17] In this thesis, stimulus-responsive capsules were prepared by the SEED process. The stimulus-responsiveness was programmed into the polymer by having stimulus-responsive side groups. Complex morphologies could be generated, as not homopolymers but block copolymers were used. These morphologies formed a direct structure-function relationship which could be efficiently used to trigger a release from the nanocapsules. In addition, not only block copolymers responsive to one stimulus but also to two different stimuli could be employed to form capsules that showed release upon application of one or both stimuli, thus broadening the range of possible stimuli and enlarging the scope of their applications.

This thesis is structured into different chapters, whose function and content will be shortly summarized here. The first chapter consists of the present general motivation for the entire thesis. In Chapter 2, the basic foundations of colloidal materials such as particles and capsules are laid out. The SEED process used to generate the particles and capsules is introduced in detail. Furthermore, the possible morphologies of colloids that contain more than one material are depicted. In Chapter 3, the different characterization methods mainly used in this thesis are described from a theoretical point of view. Both the general set-up as well as the physical processes used are emphasized with regard to their application in this thesis. The actual results obtained in the course of this thesis are presented, discussed and critically examined in Chapter 4. The chapter is divided into different sections which correspond to the topics described in the last paragraph. In these sections, a short introduction and motivation to the different topics is given after an abstract. In the following, the results are discussed, conclusions are drawn and an outlook is given. The experimental details can be found in Chapter 5.

2. Theoretical Background

In this chapter, the basic theoretical foundations of colloidal systems, of the preparation of nanoparticles and nanocapsules by the solvent evaporation process from emulsion droplets and of the morphology of nanoparticles, especially Janus particles are laid out.

2.1. Colloidal Systems

Colloidal system are everywhere, although they are often not noticed as such. For example, milk, fog, and many paints are colloidal systems. In general, these are heterogeneous systems consisting of one material which is dispersed in another material. The dispersed and the continuous phase are often differentiated from each other.[18] There are different names for colloidal systems depending on the physical state of both phases, which are shown in Tab. 2.1. The size of the colloids dispersed in the continuous phase varies between several micrometers down to a few nanometers. However, once the dispersed phase is smaller than a few nanometers it is called a true solution. In contrast to colloidal systems, a true solution is homogeneous. Many colloids have sizes of 380 nm to 780 nm, e.g. the size of colloids is similar to the wavelength of visible light. Therefore, they scatter light which leads to an apparent turbidity of the system, as for example in milk.

Tab. 2.1.: Different colloidal systems and their respective composition.

Type	Continuous Phase	Dispersed Phase	Example
Mixture	solid	solid	polymer blend
Gel	solid	liquid	gelatin
Solid Foam	solid	gaseous	styrofoam™
Dispersion	liquid	solid	paints
Emulsion	liquid	liquid	milk
Foam	liquid	gaseous	soap foam
Solid Aerosol	gaseous	solid	clouds
Liquid Aerosol	gaseous	liquid	fog

2.1.1. Emulsions and their Stability

A heterogeneous mixture of droplets of one liquid dispersed in another liquid is called an emulsion. A prerequisite for an emulsion is the immiscibility of the two liquids. There are three subgroups of emulsions: Macro-, micro-, and miniemulsions.[19,20] Their differences originate from the size of the dispersed droplets, their thermodynamic stability, and the method of their preparation. However, in almost all cases a surfactant is employed to stabilize the droplets sufficiently and over longer periods of time. Also, quite often the droplet formation is not spontaneous, i.e. energy has to be put into the system in order to generate the droplets. The energy input can consist of simple stirring, ultrasonication or flow systems, among others. Another differentiating factor of emulsions is the polarity of the dispersed phase. Direct emulsions consist of an non-polar phase that is dispersed in a polar phase, while inverse emulsions consist of a polar phase dispersed in a non-polar phase. Especially the direct emulsions have found many applications and technical uses, as the most common solvent water is usually the polar phase.[21]

Macroemulsions are prepared by fast stirring and by adding relatively high amounts of surfactant.[19] As the system is stirred, droplets are formed which are kinetically stabilized by the surfactant. However, they are not stable thermodynamically, therefore phase separation occurs with time. The size of the dispersed droplets can be varied and ranges from about 10 µm to 0.1 µm, often having a broad size distribution.

In contrast to macroemulsions, microemulsions contain very high amounts of surfactant, often between 50 % and 200 % relative to the total weight of the dispersed phase.[19] The surfactant concentration is far above the critical micelle concentration. Additionally, a co-surfactant is most often added as well. The co-surfactant does not form micelles by itself, but it adds to the lowering of the surface tension between the continuous and the dispersed phase. In contrast to macroemulsions, microemulsions are thermodynamically stable. The size of the dispersed droplets varies between 5 nm and 100 nm.

Another type of emulsions are miniemulsions. Here, the concentration of the surfactant is very low, usually between 0.1 % and 20 % relative to the dispersed phase.[22–24] Thus, the surfactant does not cover the entire surface area of the stabilized droplet. Furthermore, the size of the droplets is very small, usually between 30 nm and 500 nm. To obtain droplets of these sizes, very strong shear forces are employed to break up larger droplets. Such shear forces can be obtained by ultrasonication, for example.

The stability of miniemulsions is determined by two different and competing processes: coalescence and Ostwald ripening (see Fig. 2.1).[23,25] The process of collision and subsequent merging of two or more droplets is named coalescence.[23,25] The probability of coalescence of three or more droplets at the same time is highly unlikely but the collision of a droplet that

already has undergone coalescence with another droplet is possible. In order for coalescence to occur, the droplets have to collide first, e.g. they have to move. The movement is usually a consequence of stirring or of the ever-present Brownian motion of the droplets. Coalescence can be suppressed by adding a suitable surfactant to stabilize the droplets. The surfactant shields the droplet either electrostatically or sterically from each other. Other possibilities to suppress coalescence are to increase the viscosity of the continuous phase, thereby decreasing the motion of the droplets,[26] or the presence of dissolved polymers[27] which add additional stabilizing forces to the dispersion.

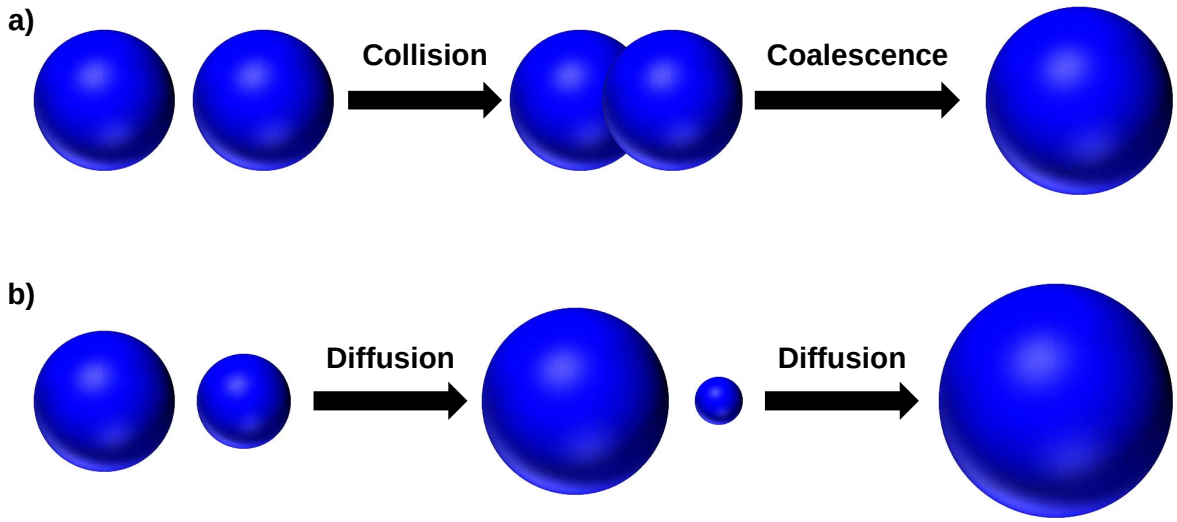

Fig. 2.1.: Both coalescence (a) and Ostwald ripening (b) lead to larger droplets while the total number of droplets is diminished.

The surfactants hindering the collision and subsequent merging of the droplets can be of ionic or non-ionic nature, which results in different mechanisms of droplet stabilization. Whereas ionic surfactants stabilize the droplets by electrostatic repulsion, non-ionic surfactants function by purely steric hindrance (see Fig. 2.2).[25] The type of surfactant also plays a role in determining the droplets diameter. Quite often, ionic surfactants lead to smaller droplets than non-ionic surfactants. Usually, the amount of surfactant is also of very high importance for the size of the droplets in any case. The more surfactant is used, the more surface can be stabilized, hence the droplets become smaller.[28]

Another process of droplet destabilization in emulsions is Ostwald ripening.[23,29] Ostwald ripening describes the growth of larger droplets, which are fed by smaller droplets. The process is not only found in emulsions, but also applies to crystals and other systems. It is based on the high Laplace pressure of small droplets, which allows material to diffuse out to larger droplets with a lower Laplace pressure.[23] The Laplace pressure $p_{Laplace}$ can be calculated by the ratio of the surface tension γ_{ij} between continuous and dispersed phase

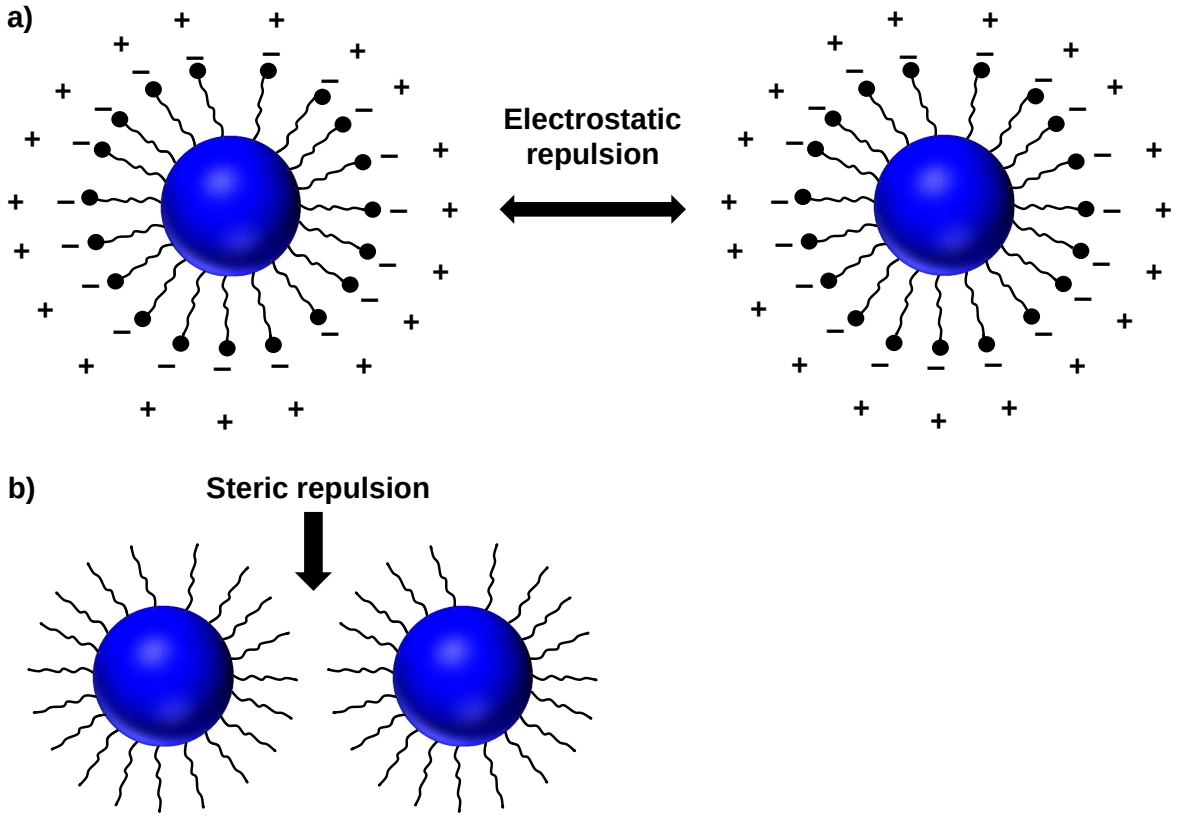

Fig. 2.2.: Electrostatic stabilization of droplets by ionic surfactants (a) and steric stabilization by non-ionic surfactants (b).

and the hydrodynamic diameter D of the droplet according to

$$p_{Laplace} = \frac{4\gamma_{ij}}{D} \qquad \text{Eq. 2.1}$$

To suppress Ostwald ripening, the Laplace pressure needs to be counterbalanced. For this, the osmotic pressure $\Pi_{osmotic}$ of the droplets can be increased by adding a suitable agent that is insoluble in the continuous phase (see Fig. 2.3). The thus generated osmotic pressure can be calculated by

$$\Pi_{osmotic} = \frac{R_{gas} T c}{M} \qquad \text{Eq. 2.2}$$

where R_{gas} represents the universal gas constant, T the temperature, c the concentration of the added agent and M its the molecular weight. Usually hexadecane (HD) or other high alkanes are used in direct miniemulsions whereas salts are used in inverse miniemulsions.

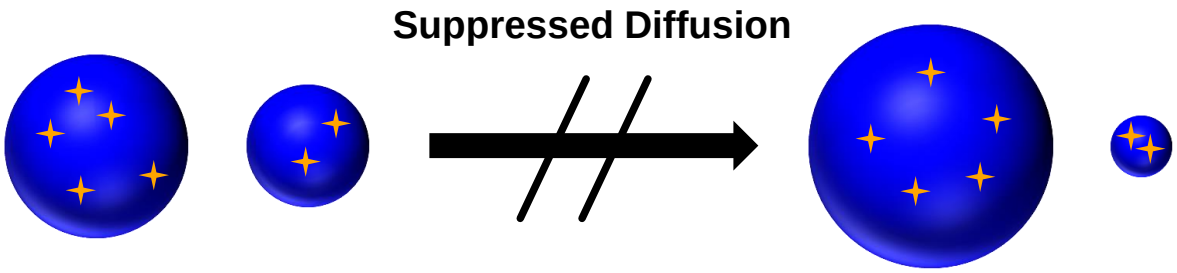

Fig. 2.3.: By adding an osmotic agent, Ostwald ripening can be suppressed.

2.1.2. Preparation of Nanoparticles

As mentioned in Section 2.1.1, emulsions can be used to generate nano-scaled droplets. From these droplets, dispersions of solid nanoparticles can be generated. Primary and secondary dispersions can be distinguished, which are generated by different means.

2.1.2.1. Primary Dispersions

Primary dispersions are generated by polymerization reactions in or on the emulsion droplets, e.g. a monomer is reacting with other monomers to form a polymer which precipitates out to form solid particles in dispersion.[30] A possibility to generate polymer nanoparticle dispersions is the direct miniemulsion process,[24] shown in Fig. 2.4. In this process, the organic monomer phase is first stirred in water containing a suitable surfactant and then ultrasonicated to form nano-sized droplets. Afterwards, the temperature is increased to start the polymerization of the monomer by using an initiator. In an ideal miniemulsion process, one particle corresponds to one droplet, i.e. one droplet is one nano-reactor.[31] The preparation of nanocapsules by the miniemulsion process is also possible.[32] For preparation of capsules, a hydrophobic oil such as HD has to be added in significant amounts. Since the growing polymer chain is insoluble in the oil, phase separation occurs and hence a core-shell structure is formed. The processes occurring and the underlying physical parameters are discussed in Section 2.3. Another reaction type to produce nanoparticles or nanocapsules is the condensation of alkoxy silanes such as tetraethoxysilane (TEOS) to silica in miniemulsion droplets.[10] Here, TEOS is emulsified in water and condenses on the interface of the droplets to the surrounding aqueous environment.

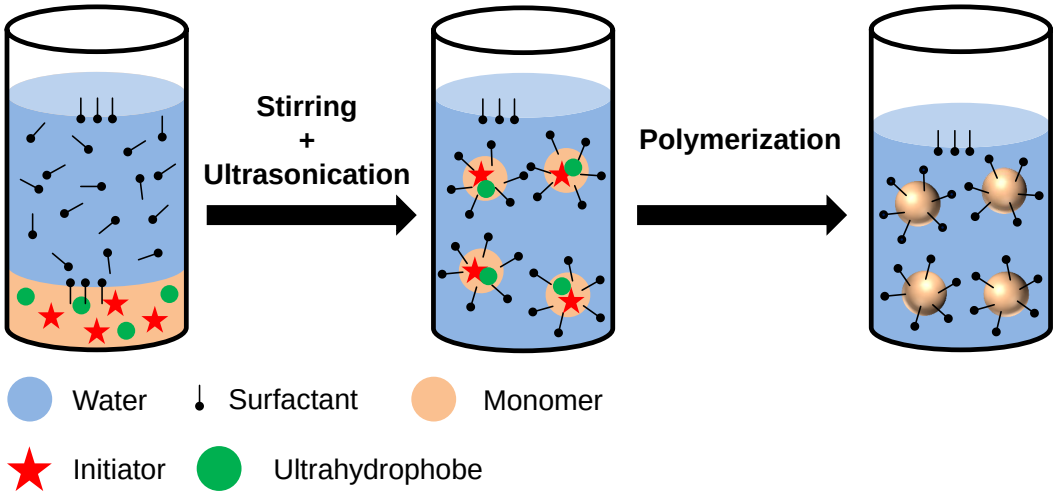

Fig. 2.4.: Polymer nanoparticles can be prepared by polymerizing a hydrophobic monomer by the direct miniemulsion process.

2.1.2.2. Secondary Dispersions[1]

Although primary dispersions are very useful, they have their limitations: Imagine that you have synthesized a highly functional and advanced polymer. You want to formulize it as nanoparticles or nanocapsules dispersed in an organic or in an aqueous medium. Unfortunately, your synthesis does not allow the use of emulsion,[33,34] miniemulsion,[24,35] or microemulsion polymerization[36,37] because of demanding reaction conditions. Or let us imagine that you can perform the aforementioned polymerization in dispersed media but you cannot get rid of some residual monomer and/or initiator/catalyst without destabilizing the nanoparticles. What are the possibilities to prepare polymer nanoparticles directly from your polymer?

A way to solve these problems is to separate the polymerization from the emulsification. Firstly, the polymer can be synthesized and purified. Secondly, the polymer is formulated into a colloidal form. Here, three techniques have emerged:

1. The Ouzo-Effect[38,39] is based on the spontaneous emulsification of a solution of a strongly hydrophobic oil or polymer in a water-miscible solvent. Once the hydrophobic solution is in contact with water, the water can diffuse into the droplets, which causes supersaturation of the oil or polymer. As a result, an emulsion or dispersion of finely dispersed droplets or particles is obtained.
2. The nanoprecipitation-technique[40] is based on the precipitation of a polymer from a polymer solvent which comes into contact with a non-solvent for the polymer. The polymer solvent and the non-solvent are chosen to be miscible, hence the polymer precipitates out and a dispersion of polymer nanoparticles is obtained.

[1]Parts of the subsequent sections have been published in the the paper "Recent Advances in the Emulsion Solvent Evaporation Technique for the Preparation of Nanoparticles and Nanocapsules" by Roland H. Staff, Katharina Landfester and Daniel Crespy, published in 2013 in *Adv. Polym. Sci.*, DOI: 10.1007/12_2013_233.[8] It is reprinted here with kind permission of Springer Science+Business Media.

3. In the solvent evaporation process from emulsion droplets, the polymer is dissolved in a good solvent, mixed with water and the solvent is subsequently evaporated, leaving a dispersion of nanoparticles. In the following section, this process, its mechanism and applications are laid out.

2.2. The Emulsion Solvent Evaporation Process from Miniemulsion Droplets

Burton and O'Farrell invented the SEED process, also called emulsion solvent evaporation process preparing a variety of elastomers and resin latexes.[41] In this process, a pre-synthesized polymer or a mixture of different polymers and possibly an hydrophobic oil are dissolved in a suitable solvent and mixed with another immiscible liquid containing a surfactant (see Fig. 2.5). After the formation of droplets by ultrasonication or other high energy means, the solvent can be evaporated by heating the emulsion or applying a low vacuum.[42] If a hydrophobic oil is added, capsules can be obtained (see Section 2.3) Two years after the invention of the SEED process, Vanderhoff, El-Aasser, and Ugelstad proposed detailed preparation procedures for a large variety of polymers in their patent application.[43] Thereafter, the process was mainly adopted in pharmaceutical science to encapsulate drugs in biodegradable polymers,[44,45] especially in micron- and nano-sized capsules as well as in particles.[46]

2.2.1. Mechanism of the Emulsion Solvent Evaporation Process

Surprisingly, little has been known for many years about the mechanisms governing the SEED process. The main physical processes underlying the method are quite simple: a polymer is dissolved in a good solvent, which is then emulsified in an aqueous medium containing a surfactant. The slow evaporation of the polymer solvent leads to nucleation of the polymer on the water-solvent interface.[47] The mechanism for the removal of the solvent is based on its, albeit low, solubility in the continuous phase, therefore both the temperature and the nature of the solvent play an important role in the rate of evaporation. The completion of the evaporation can be monitored by gas chromatography (GC)[48] or nuclear magnetic resonance spectroscopy (NMR)[49] and is usually realized in a few hours.[50] After the evaporation of the solvent, the dispersions can be dialyzed to remove unwanted or low-molecular weight polymer and/or can be freeze-dried to obtain the polymer back from the dispersion.

The evaporation plays an important role on the hardening kinetics of the particles provided that the continuous phase is saturated with the solvent mainly present in the dispersed phase

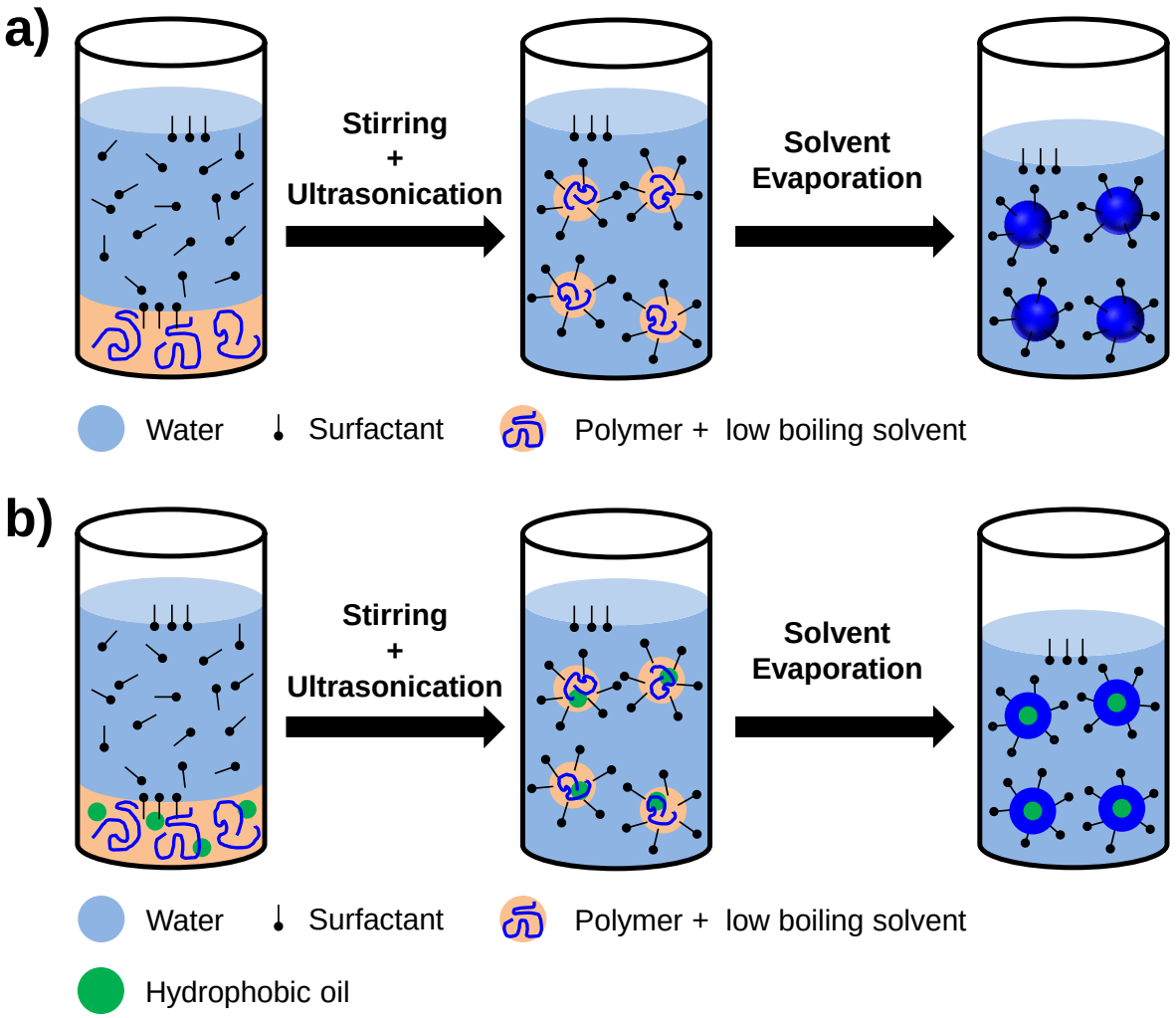

Fig. 2.5.: In the SEED process, the polymer solvent is evaporated from droplets containing the pre-synthesized polymer. Thus, nanoparticles (a) or nanocapsules (b) can be formed. For the preparation of the latter, a hydrophobic oil such as HD needs to be added to the dispersed phase. Here, the case of a direct emulsion is depicted, i.e. the continuous phase consists of an aqueous solution.

and that the diffusion rate of the solvent of the dispersed phase to the continuous phase is fast compared to the solvent evaporation kinetics. In an experimental study performed with dichloromethane, ethyl acetate, and acetonitrile as solvents, Wang and Schwendeman demonstrated that the rate limiting step for mass transport of solvent is depending on the solvent's properties.[48] Dichloromethane at room temperature was found to be liquid-side transport limited whereas ethyl acetate and acetonitrile were gas-side transport limited. As expected, the evaporation rate was largely affected by the diameter of the impeller, its rotational speed, and the temperature. The hardening profile of the particles could be determined and predicted without needing to measure the concentration of polymer in the solvent in time, but by measuring the concentration of the solvent and by knowing the permeability coefficient of the solvent at the liquid/air interface.[48]

One of the most critical property of nanoparticles is their size, hence their control is of utmost importance. As the particles are formed from droplets, their sizes are largely depending on the size of the droplets. In the case of miniemulsions, the size of the droplets is controlled by the concentration of surfactant.[51] Other parameters such as the nature of the solvent[52] or the stirring rate or ultrasonication time[53] also influence the particle size and their size distribution. Longer and/or stronger emulsification usually leads to lower and more narrowly distributed particle sizes to a certain extent.[53] However, it is difficult to ascribe an observed effect upon changing one parameter to this sole parameter, because most of the parameters are not independent.

Furthermore, physical processes responsible for the destabilization of emulsions such as Ostwald ripening and coalescence are of crucial importance for the determination of the final particle size and size distribution. It is known that the addition of a small amount of a chemical that is preferentially soluble in the dispersed phase can hinder Ostwald ripening (also see Section 2.1.1).[54]

In the SEED process, usually no additional osmotic pressure agent is added as the polymer itself can act as an osmotic pressure agent because it is insoluble in the continuous phase. However, the concentration of polymer must be above a threshold value to effectively hinder Ostwald ripening.[55] Loxley and Vincent supposed that the relatively broad size distribution of the obtained particles is caused by coalescence.[56] The size of emulsion droplets and the obtained nanoparticles was measured by dynamic light scattering (DLS).[50] Based on these measurements, it was concluded that coalescence plays an important role in the particle formation under certain conditions. However, if coalescence is indeed the cause for the broad size distribution obtained will be discussed in depth in Section 4.1.

2.2.2. Selected Applications

Although most reports deal with the preparation of microparticles, nano-sized particles and capsules are also accessible. To this aim, most often ultrasonication is employed to form very small droplets,[47] from which the solvent is evaporated. Usually, the continuous phase is an aqueous solution. Inverse systems, in which water is the solvent, have been reported[57,58] as well as non-aqueous emulsions[59] such as dimethyl formamide (DMF) in paraffin,[60] dichloromethane in fluorinated solvent for microparticles,[61] and formic acid in paraffin for nanocapsules.[62] Nowadays, the SEED process is widely used to generate both micro- and nano-sized particles and capsules from a wide variety of different polymers, including, but not limited to, semiconducting,[63] biodegradable,[64–66] or naturally occurring polymers such as cellulose derivatives.[67] Such materials are also used to encapsulate other materials such as magnetic nanoparticles,[68,69] biomaterials,[70] perfluorocarbons as contrast agents for ultrasonic imaging,[71,72] dyes for up-conversion,[73] or self-healing agents.[74,75] It was shown that nanocapsules with a hydrophobic liquid core could successfully be fabricated with polymers having completely different thermal and mechanical properties such as poly(L-lactic acid) (PLLA), poly(methyl methacrylate) (PMMA), poly(2,6-dimethyl-1,4-phenylene oxide) (PPO), poly(vinylformal) (PVF), poly(vinylcinnamate) (PVCi), and poly(vinylacetate) (PVAc).[74] The use of different polymer mixtures or architectures such as polymer blends,[63,76–78,78–80] statistical copolymers,[75] and block copolymers is also possible.[51,81–84] Especially, the latter polymer architecture is interesting for introducing an additional spatial segregation in nanoparticles to yield new multicompartment structures, such as nanocapsules or polymer particles with two or more phases, that are discussed in more detail in Section 2.3.

The main advantages of the SEED process are its versatility with respect to the polymer that can be used, the simplicity and speed of the method, and the fact that the produced polymer dispersions do not contain any non-reacted monomers or residual initiator when the pre-synthesized polymer is purified before as opposed to heterophase polymerizations. The drawbacks lie in the usually broad size distribution (20 % to 50 %) of the produced particles and capsules, the usually low solid content of the dispersions, and the presence of residual surfactants. However, the last two issues can be overcome by concentrating the dispersions in vacuo[43] and by dialysis,[85] respectively. Recently, both issues were solved simultaneously by employing a copolymer with masked amphiphilic and pH-responsive properties.[86] Indeed, the masked groups yielded ionic groups for electrostatic repulsion of the colloids upon reaction with water during the emulsification. The produced carboxylic acid groups were in a sufficient amount not only to allow a reversible aggregation/redispersion upon changes, but also to create the emulsions without additional surfactant. The solid content was increased by successive cycle aggregation/redispersion in a lower amount of water to concentrate the dispersion of nanocapsules.

Among different possible morphologies (also see Section 2.3), capsules, i.e. core-shell particles with a liquid core, are often targeted morphologies for the protection and encapsulation of substances. When nanocapsules are produced by the SEED process, the liquid core material is usually non-functional. However, functional non-solvents were also used, for example in the form of self-healing agents[73,74] or of a pH-responsive non-solvent.[87] The encapsulation of Grubbs catalysts and of monomers for a self-healing reaction based on ring opening metathesis polymerization by the SEED method was found to be advantageous over other methods such as the use of silica nanocapsules or direct encapsulation by miniemulsion polymerization. While silica nanocapsules with hydrophobic liquid core are porous and therefore cannot be used as fillers in a hydrophobic matrix,[10] it was not possible to encapsulate Grubbs catalysts in nanocapsules fabricated by free-radical polymerization in miniemulsion polymerization.[12] For the pH-responsive core, tertiary amines with long alkyl chains were embedded as liquid core in nanocapsules and could be released to the continuous phase after protonation of the amine.[87] The diffusion of the core out of the nanocapsules allowed for an unprecedented chemical transformation of the liquid core from hydrophobic to aqueous.

2.2.3. Solvent Evaporation from Unconventional Emulsions

Whereas the preparation of particles and capsules with solvent evaporation from non-polar droplets is largely reported, their preparation from polar droplets is still unusual.[57–62] The challenge is to find a suitable polar solvent with a low boiling point that can solubilize both the polymer and the substance to be encapsulated. In such cases, water as dispersed phase is not always suitable and has been replaced in non-aqueous emulsions by other polar solvents[59] to allow reactions sensitive to water such as anionic polymerization[88] or reactions requiring high temperature and the absence or removal of water.[89] Polar solvents such as DMF, formic acid, formamide, or dimethyl sulfoxide (DMSO) can be used but are difficult to remove because of their high boiling points. Recently, hexafluoroisopropanol (HFIP) was proposed as a suitable candidate to prepare polymer nanoparticles via the SEED method. It also has the property to be a good solvent for metallo-pharmaceuticals that need to be embedded in a carrier material to be delivered in the body.[90] A ruthenium nitrosyl complex designed for phototherapy that is polar but not soluble in water could be successfully encapsulated in polymer nanoparticles after the evaporation of HFIP from HFIP in alkane miniemulsions.[73] Various polymer matrices such as gelatin, PLLA, poly(ethylene terephtalate) (PET), and PVF could be used for the physical entrapment of the metal complex. The colloidal stability of the particles was improved by matching the density of the continuous phase to the density of HFIP, and hence *cis*-decalin was found to be more suitable to obtain stable dispersions than cyclohexane, HD, and isooctane. The nanoparticles could be redispersed in aqueous solutions after removal of the alkane and the release of nitric oxide upon irradiation of the aqueous dispersion with a low intensity UV-light could be demonstrated.

In addition, the SEED process can also be used for non-polymeric materials[91,92] such as inorganic nanocrystals of $BaCrO_4$ and others dispersed in an organic solvent. Upon emulsification and evaporation of the organic phase, spherical aggregates of the nanocrystals are formed. Also, this method has also recently been exploited to prepare manganese ferrite/graphene oxide nanocomposites[93] and siRNA-loaded magnetic metal nanoparticles.[94]

2.3. Morphologies of Nanoparticles

> "It is the pervading law of all things organic and inorganic,
> Of all things physical and metaphysical,
> Of all things human and all things super-human,
> Of all true manifestations of the head,
> Of the heart, of the soul,
> That the life is recognizable in its expression,
> That form ever follows function. This is the law." [95]

"Form follows function" - this highly important principle from design and architecture can also be applied to systems on the nano-scale. A system can be rationally designed for the function it should have - be it to study anisotropic materials or to release a material from a nanocapsule upon a certain stimulus. However, the important parameters governing the system's form have to be known in order to design it. Therefore, this section will deal with the morphology of nanoparticles, both in general and in view of thermodynamic and kinetic aspects.

2.3.1. Simple Morphologies and their Origin

The general theory describing the thermodynamically stable morphologies obtained when three immiscible liquids are mixed with two of them present in a dispersed phase was formulated by Torza and Mason,[96] using the spreading coefficient s_i that depends on the interfacial tensions of the oil and water phases. The morphology of a system consisting of two different, non-miscible oils (1 and 3) dispersed in an aqueous phase (2) can be calculated by

$$s_i = \gamma_{jk} - (\gamma_{ij} + \gamma_{ik}) \qquad \text{Eq. 2.3}$$

In this equation, γ represents the interfacial tension between the components i, j and k, while s_i represents the spreading coefficient of the component i. Therefore, the spreading coefficient can be calculated after determining the different surface tensions. The morphologies (see Fig. 2.6 for details) can then be deduced from their values according to the different possible cases:

I. Oil 3 is significantly more hydrophilic than oil 1 ($\gamma_{12} > \gamma_{23}$) and the surface tension between the oils is low ($\gamma_{31} < \gamma_{12} + \gamma_{23}$). It follows that $s_1 < 0$, $s_2 < 0$ and $s_3 > 0$, which results in a core-shell morphology.

II. Oil 3 is about as hydrophilic as oil 1 ($\gamma_{12} \approx \gamma_{23}$) and the surface tension between the oils is low ($\gamma_{31} < \gamma_{12} + \gamma_{23}$). It follows that $s_1 < 0$, $s_2 < 0$ and $s_3 < 0$, which results in a partial engulfing of oil 1.

III. Oil 3 is about as hydrophilic as oil 1 ($\gamma_{12} \approx \gamma_{23}$) and the surface tension between the oils is high ($\gamma_{31} > \gamma_{12} + \gamma_{23}$) It follows that $s_1 < 0$, $s_2 > 0$ and $s_3 < 0$, which results in separate droplets.

The theoretical values of s_i can be employed to predict the morphologies of emulsion droplets or particles consisting of two immiscible materials. Depending on the sign of the spreading coefficients, one of the substances can be completely engulfed in another material (see Fig. 2.6).

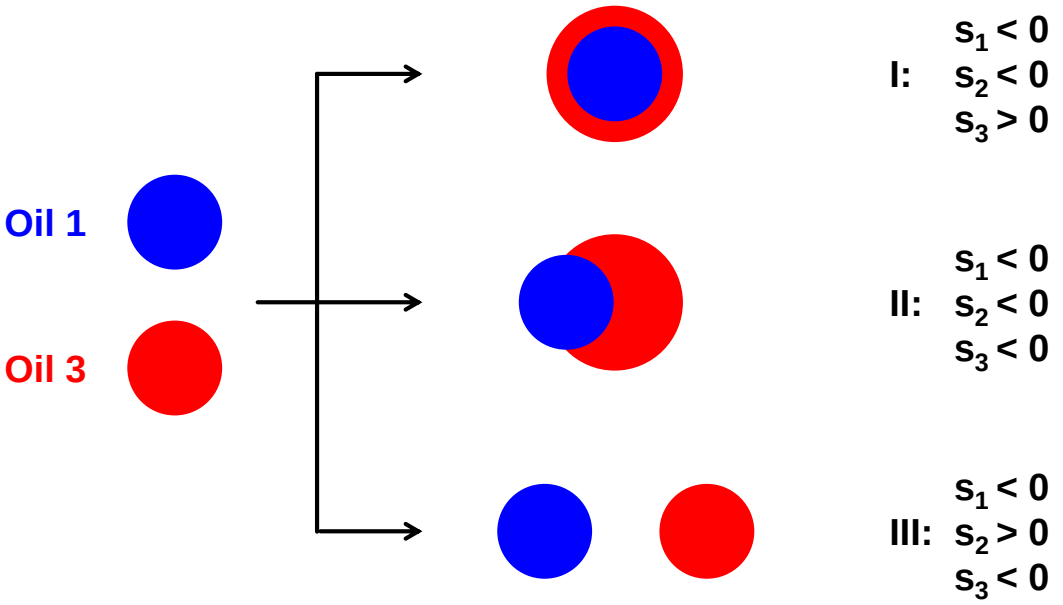

Fig. 2.6.: The spreading coefficients determine the final particle morphology: In I, oil 1 is completely engulfed in oil 3, in II the engulfment is only partial and in III there is no engulfment.[97]

2.3.1.1. Thermodynamic Aspects

The method from Section 2.3.1 can also be applied to systems in which the materials are not liquid oils but solid polymers.[97] Thermodynamically, the final morphology will be the one with the lowest free Gibbs enthalpy G, which can be calculated by

$$G = \sum_{i,j}^{n} \gamma_{ij} A_{ij} \qquad \text{Eq. 2.4}$$

Here, γ_{ij} represents the surface tension of the phases i and j, while A_{ij} represents the area of the interface. Therefore, the surface tensions between the different phases are of utmost importance for the final morphology. The surface tensions are in turn determined by the nature of the polymers used and the amount of surfactant in the system. In addition, the amounts of the polymers also have an impact on the final, thermodynamically stable morphology because the interfacial area is also important.

2.3.1.2. Kinetic Aspects

However, what happens if G cannot be minimized and is stuck in a local minimum on the energy landscape? In this case, kinetic morphologies are formed once the free Gibbs energy G cannot be minimized to its global minimum, but only to a kinetically stable local minimum. The main reason for a kinetically trapped morphology is a hindered phase separation of the materials inside the particle. Hindered phase separation can occur when high molecular weight polymers are employed in the SEED process. As diffusion of the chains is necessary for phase separation, one possibility to obtain kinetically trapped morphologies is to increase the viscosity of the polymeric emulsion droplets.[98] To control the viscosity inside the droplets of polymeric emulsions the molecular weight of the polymer can be varied. Additionally, both the kinetic factors of the evaporation temperature and the evaporation rate of the solvent are of high importance for the build-up of a thermodynamically stable morphology.[81,82,98] However, structures that resemble kinetically trapped morphologies can also be thermodynamically stable, for example if the phase separation occurs in the weak segregation limit.[51]

2.3.1.3. Resulting Morphologies of Nanoparticles

Possible morphologies of nanoparticles are depicted in Fig. 2.7. Most of these morphologies have been realized by phase separation in polymer blends or in block copolymers or by the use of a polymer and an oil. For obtaining a certain morphology, both thermodynamic and kinetic aspects as well as the amount and type of surfactant need to be controlled.

In addition to the aforementioned aspects, other factors such as the crystallization of polymers can also significantly influence the particle morphology.[51,100] Chen et al. showed that the viscosity of the liquids plays a significant role in the morphology of particles composed of poly(styrene) (PS) and PMMA.[101] Indeed, PMMA partially encapsulated PS for high molecular weight polymers whereas the opposite was observed for low molecular weight polymers. Okubo et al. investigated the effect of different stabilizers on the morphology of PS/PMMA particles.[76] Particles stabilized with poly(vinylalcohol) (PVA) displayed small dimples whereas acorn and spherical structures with increasing amount of sodium

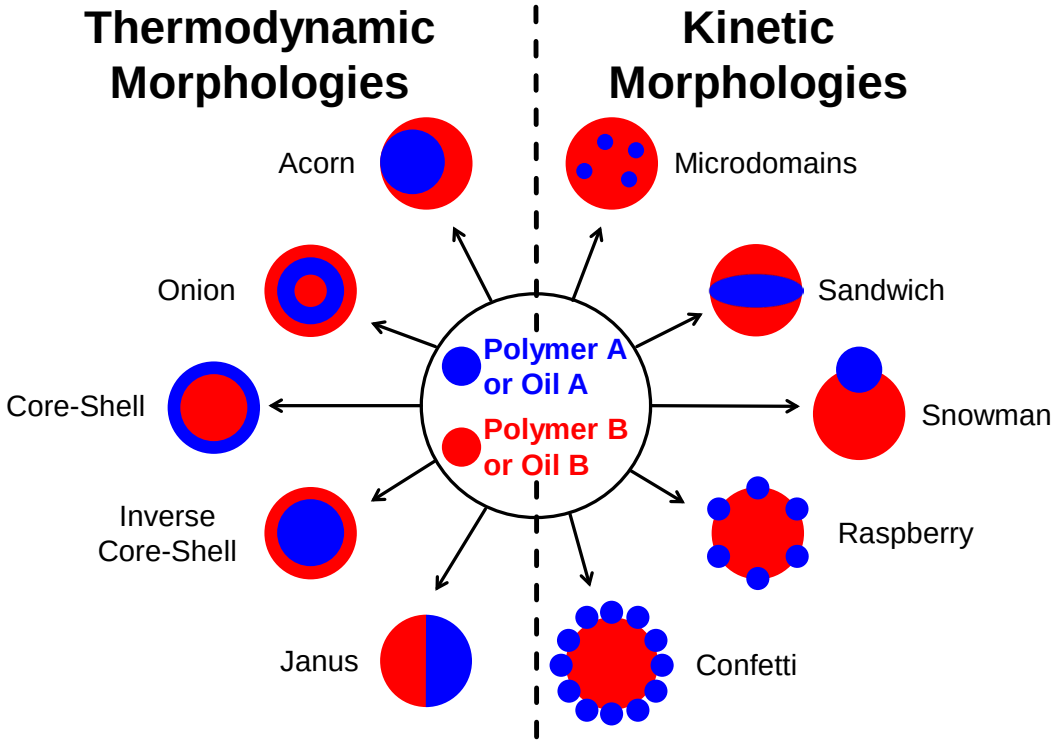

Fig. 2.7.: Depending on thermodynamic and kinetic factors, different morphologies of particles consisting of two polymers can be obtained.[99]

dodecylsulfate (SDS) were observed. Both phenomena were explained by the interplay of solvent evaporation and stabilization by the surfactant. While high amounts of SDS stabilized both the PS and the PMMA interfaces to water equally well, smaller amounts of SDS did not stabilize both interfaces equally. Therefore, bowl-like PMMA shells were formed, in which the PS slowly hardened upon further evaporation of the solvent. As the PS contracted because of the ongoing evaporation of solvent, bowl- or dimple-like structures were obtained. Such effects were not observed when dichloromethane was used instead of toluene as solvent to be evaporated, which was explained by the fact that toluene was preferentially partitioned in the PS phase, which is not the case for dichloromethane. The molecular weights of the PS and PMMA were also found to play a role on the morphology.[77] Whereas the interfacial tension of polymeric droplets against the aqueous phase was not depending on the molecular weight, the interfacial tension between PS and PMMA in the droplets increased with increasing molecular weight and snowman-like particles could be obtained for high molecular weight polymers. In the case of nanoparticles of a binary blend of a hole-transporting and an electron-transporting polymer, the composition of both phases, i.e. the distribution of one polymer in the other one in the two phases, followed the prediction of the Flory-Huggins theory.[102] The quantum efficiency of devices produced with the blend of nanoparticles were found to be improved compared to other methods.[103]

Besides the well-known core-shell and inverse core-shell morphologies,[104] acorn and Janus morphologies obtained with polymers with similar polarities,[76] other interesting structures

can be formed. Half-spherical structures are accessible by removing the liquid in acorn structures formed from a polymer and a liquid.[51,105] They can also be obtained by removing one polymer from a Janus particle consisting of two polymers.[106] Onion-like structures are created from block copolymers, for which the phase separation into lamellae causes layered structures that follow the curvature of the particle where they are confined[51,82,107]. The diameter of the particles is also very important in this case. Indeed, if the particle is small enough, core-shell or Janus structures can be obtained.[51] A large variety of different structures were predicted from simulations for diblock copolymer/homopolymer blends,[108] star-triblock copolymer assemblies in spherical nanopores,[109] or on diblock copolymer assemblies under different confinements.[110–112] Several of these assembly systems have already been prepared by the SEED process. However, these theoretical studies clearly show that many more interesting and highly complex morphologies can still be prepared.

Multicompartment morphologies[113] can easily be obtained by different methods. For example, crosslinking in the dispersed phase can lead to occluded structures, i.e. with multicores.[114] Multicompartment morphologies can also easily obtained by using block copolymers or polymer blends.[76,78,81–84,105,115–121] Such structures can be further compartmentalized by adding inorganic nanoparticles that preferentially migrate to one domain.[122,123] The obtained structures can be isotropic, i.e. the metal nanoparticles segregate in one type of lamellae in onion-like nanoparticles[123–125] or form isotropic surface structures.[126,127] Anisotropic structures with regard to the particle geometry based on metal nanoparticles/polymer assemblies[125] or similar assemblies but with a fluorescent dye instead of the metal nanoparticles were also prepared.[128] Isojima et al. also showed that by varying the ratio of metal nanoparticles to polymer matrix it was possible to obtain both isotropic and anisotropic morphologies.[129] Another way changing existing compartments is the removal of one compartment, for example by a selective solvent.[130,131]. Finally, swollen PMMA nanocapsules prepared by the SEED technique could be elongated to form core-shell ellipsoidal particles in an electrospinning jet.[132]

2.3.2. Janus Particles

Among the particle morphologies shown in Fig. 2.7, Janus particles are probably among the most prominent.[133–143] Named after the two-faced Roman god Janus, these particles have received widespread attention after their popularization by de Gennes in his Nobel Laureate speech in 1991.[144] A particle is usually called Janus particle if it consists of two different materials that are not homogeneously mixed but phase-separated in two distinct areas. A Janus particle can also consist of one material that is functionalized with another material or with other chemical groups on one side of the particle. In principle, three main groups of Janus particles can be differentiated, depending on the materials their faces consist of:

- both sides consist of inorganic materials such as metals or metal oxides
- one side consists of an inorganic material and the other side of an organic material, for example a polymer
- both sides consist of organic materials such as polymers

As the first two groups are not in the scope of this thesis, they will not be discussed here. The recent reviews by Hu et al.[137] and by Walther and Müller[143] are recommended for a detailed description of those Janus particles. For Janus particles in which both sides consists of polymers, there are several preparation procedures, which are introduced below.

2.3.2.1. Preparation of Janus Particles

Polymeric Janus particles can be generated by a wide variety of methods.[136,137] However, the main techniques used are microfluidics, toposelective surface modification after immobilization of particles, and phase separation of block copolymers or polymer blends.

Microfluidic methods have received widespread attention in recent years due to the relative ease with which Janus particles can be prepared. Droplets of two monomers are formed by joining two monomer streams in a water stream. The monomer droplets are then polymerized by UV-irradiation.[145] With this technique, not only classical Janus particles are accessible, but also ternary particles.[145] Janus particles can also be formed by merging two jets of polymer solutions and subsequent solvent evaporation by electrohydrodynamic jetting.[146–148] Here, the control of system parameters such as solution viscosity, concentration, or conductivity provides a wide variety of possible architectures. While microfluidics can be used to produce Janus particles in a highly controlled and continuous fashion, they are usually limited to particle diameters between 5 µm and 100 µm.[137]

Another process that is not limited to larger particle sizes is the toposelective surface modification after immobilization of the particles. The method is based on the protection of one particle side by masking it or by immobilizing it at an interface. The unprotected side can then be chemically modified. For example, Granick and coworkers immobilized particles on the surface of wax-droplets in water.[149] After redispersion of the wax-droplets in methanol, the protruding surface of the particles was chemically modified and the wax subsequently removed. Janus particles were obtained since a part of the surface was protected from the chemical modification by the wax. Liquid-liquid interfaces can also immobilize particles. For example, Suzuki et al. immobilized microgel particles at HD droplets dispersed in water.[150] After chemical modification and destabilization of the emulsion, the Janus particles were collected. Anisotropic Janus-like particles can also be generated by this method.[151] In general, the immobilization process allows for preparing Janus particles with different chemical functionalities and additional shape parameters, but it is rather complicated to perform and difficult to scale-up.[137]

Probably the most applied method to produce Janus particles is to use phase separation. Again, three main routes[137] can be differentiated:

1. Phase separation between a monomer and a preformed polymer in emulsion polymerizations[137,152–155] or as reaction-induced phase separation[156]
2. Phase separation between the two or more blocks of a block copolymer[51,137,142,143,157]
3. Phase separation between two homopolymers in blend systems[76–80,102,105,106,158]

As only the last method was used in this work, the other two will not be elucidated further and the cited literature may serve as further reading. Phase separation can occur if two immiscible polymers are present in a droplet of a common solvent in water and after the solvent is subsequently evaporated. The resulting Janus morphology depends on many aspects such as the hydrophobicity of the polymers and the type and amount of surfactant among others (also see Section 2.3.1). The phase separation method has been applied to several polymer blend systems. For example, PS was used in combination with poly(propylene carbonate) (PPC),[102] poly(isoprene) (PI),[158] and PMMA[76–80] to form Janus particles. Especially the latter system has been widely studied with respect to the influence of the molecular weight of the polymers[77,79] and to the type[76] and the amount of surfactant[76,79] used to prepare the Janus particles. By using a copolymer of methyl methacrylate (MMA) and a functional monomer[77] or by using a functional methacrylate,[78] Janus particles were prepared that could be subsequently used for an atom transfer radical polymerization (ATRP) on one side of the particles. By removing one side of the Janus particles after their preparation, it was also possible to obtain half-spherical particles. The resulting particles could be obtained either by removal of the liquid side of a polymer/oil Janus particle[105] or by removing one polymer from a polymer/polymer Janus particle.[106]

2.3.2.2. Applications of Janus Particles

Probably one of the most common applications of Janus particles is based on their potential amphiphilicity. Therefore, they can act as surfactant[159] and in addition they can stabilize droplets by the Pickering effect.[160] They can also act as compatibilizer[161] or even as water-repellent agent.[162] For further reading, the recent review by Kumar et al.[140] is recommended.

Another important field of research is the self-assembly or directed assembly of Janus particles.[133,134,163–172] Highly complex structures consisting of two or more Janus particles were obtained while the kinetic pathways leading to these structures were also studied.[168] Besides molecule-like structures consisting of Janus particles, both lattices[173] and tubes[169] of Janus particles have also been prepared. The assembly-properties of Janus particles

are also an interesting field for simulations.[174–178] Many of these simulations helped to explain old and elated to new findings in this field. Janus particles can also be applied to generate electronic paper: Nisiako et al. prepared Janus particles in which one side was loaded with black and the other side with withe pigments.[179] Since these pigments also carried opposite charges, they could be aligned in an electric field, resulting in a black and white pattern. Janus particles consisting of metals or metal-oxides also have a wide variety of potential applications such as drug-delivery,[180] catalysis,[181,182] autonomous motion,[183–187] sensors,[188] and others.[137]

3. Characterization Techniques

In this chapter, the characterization techniques used in this work are described. In some cases, the underlying theory is also mentioned. The experimental details can be found in Chapter 5.

3.1. Imaging Techniques

To resolve structures on the nano-scale, common optical microscopes are not sufficient because their resolution is not high enough due to the Abbe diffraction limit. Therefore, other methods such as scanning force microscopy or electron microscopy have to be employed. With electrons it is possible to resolve much smaller structures than with light since electrons have a smaller wavelength. Here, scanning and transmission electron microscopes are used, which are fundamentally different in their imaging technique. [189,190]

3.1.1. Scanning Electron Microscopy

With a scanning electron microscope (SEM) it is possible to resolve surface structures from several micrometers to a few nanometers. [189,191] In a SEM, electrons are accelerated to energies of 0.5 keV to 30 keV and are focused by electromagnetic lenses upon the sample (see Fig. 3.1a). The surface area of the sample is then scanned by the electron beam in a grid pattern. Since the electron beam interacts with the surface material, secondary electrons are generated, which in turn are recorded by a detector. As the number of detected electrons is proportional to the brightness of a specific point in the grid pattern, areas pointing in the direction of the electron beam appear brighter than areas that are adverted to the beam. In practice, this results in a "side-on" illumination which is responsible for the three-dimensional effect of SEM images.

In addition to imaging, a SEM can also be used for element-specific surface analysis, called scanning electron microscope energy-dispersive X-ray spectroscopy (SEM-EDX). The method is based on the fact that an electron from the electron beam can punch an electron from an atom in the sample out of its atomic orbit. The resulting hole is refilled very quickly by

an electron from an energetically higher orbital. During this process, X-rays are generated. X-rays are highly specific in energy for each atom and electron transition. It can therefore be used for element mapping. In this work, the SEM was primarily used to obtain images of the nanoparticles and nanocapsules prepared and to study the morphology of their surfaces. Furthermore, SEM-EDX was employed to check for the presence of specific elements.

3.1.2. Transmission Electron Microscopy

In principle, the transmission electron microscope (TEM) is similar to the SEM but here the transmitted and not the back-scattered electrons are used to image the sample.[190] Since the electrons are transmitted through the sample material, it must be sufficiently thin.[192] When the electrons hit a material, many of them are not transmitted but scattered to a certain angle out of the optical axis. Therefore, the observed intensity is depending on two factors: Firstly, thicker structures scatter more than thinner structures, therefore they appear darker. Secondly, heavy atoms scatter more strongly than lighter atoms, therefore areas containing a large amount of heavy atoms appear darker. The former can be used to differentiate between nanoparticles and nanocapsules because in top view the capsular wall appears darker than other parts of the capsule while in nanoparticles the center is most dark. The latter allows the selective visualization of different chemical structures, either by direct visualization or indirect visualization after staining certain parts of the sample with a staining agent containing heavy elements. In this work, TEM was primarily used to check if nanoparticles or nanocapsules were prepared. Furthermore, it was used to differentiate between different polymers in a blend after staining one polymer and for studying the morphology of block copolymers.

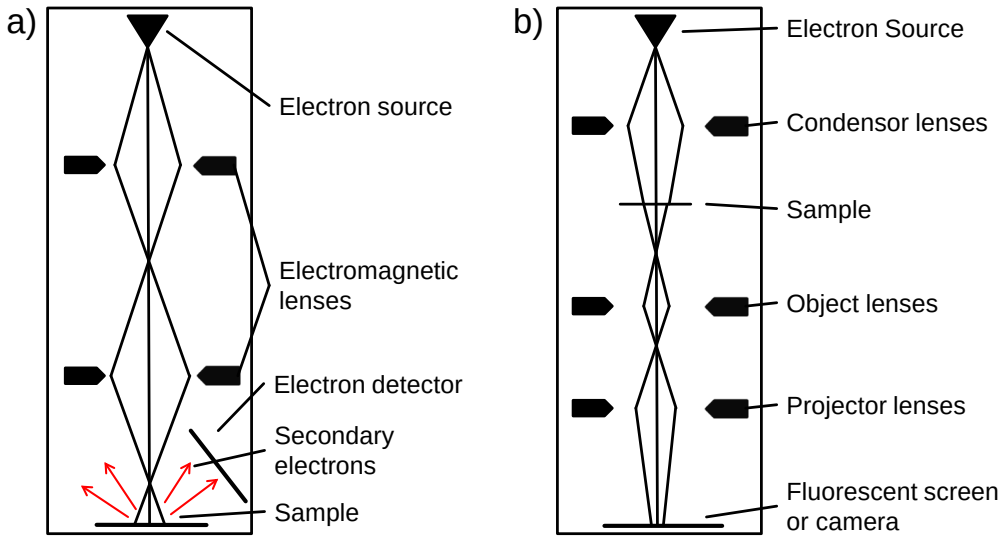

Fig. 3.1.: Schematic drawing of a SEM (a) and a TEM (b) based on Goldstein et al.[189]

3.1.3. Scanning Force Microscopy

Another method to resolve structures on the nano-scale is to employ a scanning force microscope (SFM).[20] The fundamental principle of this method is the measurement of forces between the sample's surface and an extremely sharp tip. The resolution is not limited by the diffraction limit because an SFM is not an optical microscope. Furthermore, opposed to the electron microscopy an SFM does not need a vacuum environment to operate in. Therefore, in many cases changes of the sample by the vacuum can be excluded. In an SFM, a cantilever is placed near or on the sample's surface. The sample is placed on a piezo-crystal, which can move the sample in x-, y- and z-direction by applying a current to it. The cantilever is moved by changes in the sample's topography as it is scanned. The movement of the cantilever is detected by the reflection of a laser beam that is focused on the back of the cantilever. The reflection information is then fed back into a feedback-loop to keep the z-position of the cantilever constant. Therefore, the z-position of the sample has to be changed by applying a current to the piezo. The impulses are then recalculated into a height-image of the sample.

In principle, there are two different operation modes in SFM: In contact-mode, the cantilever is in constant contact with the sample's surface. Therefore, the surface can be deformed by the cantilever quite easily, especially when the surface consists of soft matter such as polymers. In tapping-mode, the cantilever touches the surface only for short periods of time. Thus, the deformation problem significantly reduced. The vibration amplitude is measured in tapping mode. When the vibrating cantilever experiences a force from the surface, its vibration amplitude is changed. A feedback loop is then used to keep a constant vibration amplitude by regulating the tip's sample distance. The tapping mode also offers the possibility to image material composition in the sample's surface: Different materials have different adhesion constants with respect to the tip. Therefore, the time the cantilever rests on the surface is different which results in a change in the phase-lag between the exciting piezoelectric actuator and the cantilever vibration. In this work, a SFM was used to image the surface of nanoparticles and nanocapsules without subjecting them to harsh drying conditions.

3.2. Dynamic Light Scattering

DLS is a technique determining the size as well as the size distribution of droplets or solid particles in colloidal systems.[5,193,194] The technique is based on the random Brownian motion of the dispersed objects. Brownian motion is, among other factors, dependent on the size of the diffusing objects, which can be calculated from the diffusion coefficient D_z using

the Stokes-Einstein-equation assuming the dispersed objects to be hard (non-deformable), spherical particles by

$$D_z = \frac{k_B T}{6\pi r_h \eta} \qquad \text{Eq. 3.1}$$

Here, k_B is the Boltzmann constant, T the temperature, η the dynamic viscosity of the system and r_h the hydrodynamic radius of the dispersed objects. In DLS, a laser is employed as light emitter, which is necessary as only lasers produce light that is coherent in respect to time and space. The light is scattered by the particles and the intensity of the scattered light is detected and converted into an electric signal. Since the phase of the scattered light is dependent on the position of the particles, the measured intensity fluctuates with time. According to the Wiener-Khinchim-Theorem, this fluctuation can be described by an autocorrelation function such as

$$g_1(t) = \exp\left(-D_z q^2 t\right) \qquad \text{Eq. 3.2}$$

Here, q represents the wave vector and t the time. Therefore, the diffusion coefficient D_z can be calculated which in turn is used in Eq. 3.1 to calculate the hydrodynamic radius of the particles scattering the light. In this work, DLS was employed to measure the hydrodynamic diameter of droplets, nanoparticles and nanocapsules.

3.3. Techniques Based on Fluorescence

Many of the most abundantly used methods in chemical and biological systems are based on fluorescence.[195,196] Certain molecules, called fluorophores, have the ability to take up energy by absorbing photons. The energy is then released by emission of a photon with less energy and therefore higher wavelength than the absorbed one possessed. The details of this process are shown in Fig. 3.2a. A photon with the energy $h\nu_{abs}$ is absorbed by the fluorophore, which excites the molecule out of its electronic ground state S_0 to an excited vibrational state with a higher electronic state (S_1 or S_2). After non-radiating relaxation to the ground vibrational state of the higher electronic state, a photon with an energy $h\nu_{em}$ can be released. Subsequently the molecule reaches its electronic ground state again. Fluorescence competes with other processes within the same molecule such as inner conversion, intersystem crossing and phosphorescence. In addition, if other molecules are present, quenching of fluorescence or fluorescence resonance energy transfer (FRET) are possible (see Fig. 3.2b). To ensure a high fluorescence efficiency, the contribution of these alternative processes should be as low as possible. The emitted radiation is of lower energy than the absorbed one, hence fluorescence is shifted to larger wavelengths compared to the absorption (Stokes-Shift). In this work, fluorescence measurements were employed to measure the release of fluorescent dyes from nanocapsules and to quantify the amount of functional groups on a particle surface.

Furthermore, special, fluorescence-based techniques were employed which are described hereafter.

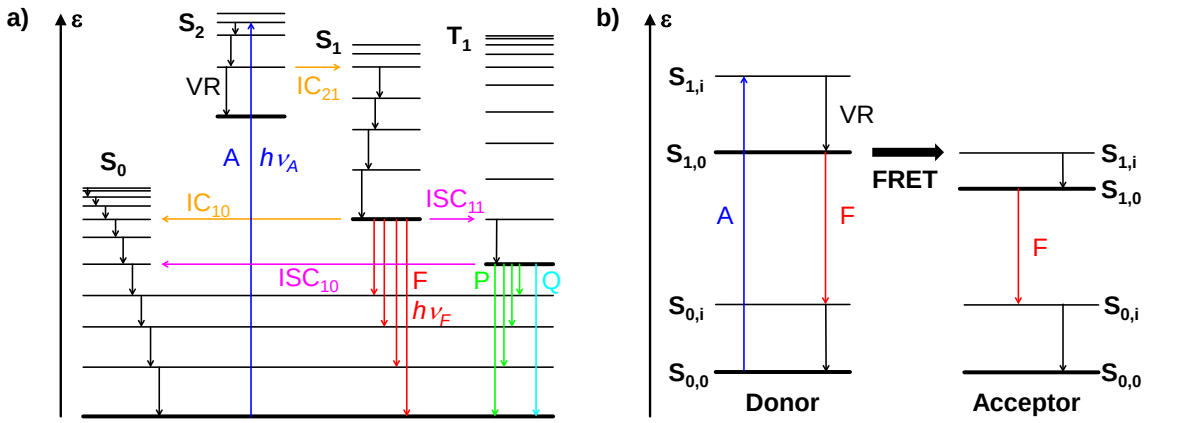

Fig. 3.2.: In the simplified Jablonski-diagram (a) the most important possibilities of energy reduction of a molecule after absorption (A) of a photon with an energy $h\nu_A$ in the vibrational ground state are displayed: The molecule can loose energy by vibrational relaxation (VR) without emission or by fluorescence (F) and phosphorescence (P) while sending out a photon with an energy of $h\nu_F$. Between two vibrational states with the same multiplicity, internal conversion (IC) can happen and intersystem crossing (ISC) occurs once the vibrational states do not have the same multiplicity. Furthermore, energy can also be dissipated by a quencher (Q). In the FRET-mechanism (b), energy is transferred without radiation from a donor to an acceptor. From the acceptor, it is then dissipated without radiation or by fluorescence.

3.3.1. Fluorescence Resonance Energy Transfer

The FRET mechanism is, in principle, a special case of quenching as energy is transferred without radiation from a donor to an acceptor (see Fig. 3.2b).[195,196] The acceptor quenches the fluorescence of the donor or fluoresces itself, albeit on a another wavelength than the acceptor. For the energy transfer, several criteria have to be fulfilled:

- The distance between donor and acceptor in space must be small, usually around a few nanometers.
- The absorption spectrum of the acceptor must overlap with the emission spectrum of the donor.
- The alignment of the transition dipoles of donor and acceptor must be free.

The efficiency Φ_{FRET} of the FRET-system is strongly dependent on the distance r_{FRET} of donor and acceptor according to

$$\Phi_{FRET} = \frac{1}{1 + \left(\frac{r_{FRET}}{R_{FRET}}\right)^6} \qquad \text{Eq. 3.3}$$

Here, the Förster radius R_{FRET} is defined as the distance of donor to acceptor at which the energy transfer works with 50 %. In this work, FRET was used to verify the presence or absence of two dyes in the same nanoparticle.

3.3.2. Fluorescence Spectroscopy

Most often, fluorescence is used to determine and possibly quantify the amount of a fluorophore. Therefore, an absolute value of fluorescence intensity at a certain time is measured. However, the fluctuation of the fluorescence intensity with time can also be measured, similar to the intensity fluctuations measured by DLS.[197,198] This is done in different fluorescence correlation spectroscopy techniques.

3.3.2.1. Fluorescence Correlation Spectroscopy

When the time-resolved absolute fluorescence intensity is measured, it is fluctuating because the fluorophores can diffuse.[197,198] The fluctuation can be modeled by an autocorrelation function, hence the technique is named fluorescence correlation spectroscopy (FCS). Ideally, the concentration of the fluorophore in the observation volume should be as low as possible to ascertain a very strong fluctuation of the fluorescence. This can be achieved by simply diluting the sample, but also by reducing the observation volume as it is done by combining fluorescence measurements and a confocal microscope.[199] Thus, observation volumes as small as 1×10^{-15} L are possible.[200]

Although initially developed and still predominantly used as a tool in molecular and cell biology,[201–204] FCS has also found many applications in polymer and colloid science in recent years. In particular, surface diffusion of adsorbed polymers,[205–209] or tracer diffusion in undiluted polymer solutions,[210–215] cross-linked networks,[216–219] and bulk polymers[220] were studied with the help of FCS. The formation of amphiphilic copolymer micelles and vesicles and their interaction with small molecules or nanoparticles were also investigated.[221–224] Furthermore, recently FCS was successfully applied to measure the size and polydispersity of microemulsion droplets.[225]

In practice, the temporal fluctuation of the fluorescence intensity $\delta F(t)$ can be used to calculate the probability of a fluorophore being in the same observation volume at the time $(t + \tau)$ as at the time t by applying the autocorrelation function

$$G(\tau) = 1 + \frac{\langle \delta F(t)\, \delta F(t+\tau) \rangle}{\langle F(t) \rangle^2} \qquad \text{Eq. 3.4}$$

If only free, three-dimensional diffusion is allowed, the autocorrelation function can be expressed by

$$G(\tau) = 1 + \frac{1}{N} \cdot \left(1 + \frac{\tau}{\tau_D}\right)^{-1} \cdot \left(1 + \frac{\tau}{S^2 \tau_D}\right)^{-\frac{1}{2}} \qquad \text{Eq. 3.5}$$

Here, N represents the average number of fluorophores in the observation volume V, τ_D is the lateral diffusion time though V and S stands for the ratio of axial to lateral dimension of V. If more than one species is present, the autocorrelation function has the following analytic form for an ensemble of m_d types of freely diffusing species:

$$G(\tau) = \sum_{i=1}^{m_d} \frac{f_i}{N} \cdot \left(1 + \frac{\tau}{\tau_{D_i}}\right)^{-1} \cdot \left(1 + \frac{\tau}{S^2 \tau_{D_i}}\right)^{-\frac{1}{2}} \qquad \text{Eq. 3.6}$$

where f_i is the fraction of species i ($0 \leq i \leq 1$) in the observation volume V. The observation volume V can be determined by reference measurements,[226] therefore the calculation of the absolute concentration c of the fluorophore by $c = N/V$ is possible. Furthermore, the diffusion coefficient D_z of each species present can be calculated by

$$D_z = \frac{r_0^2 + r_h^2}{4\tau_D} \qquad \text{Eq. 3.7}$$

Here, r_0 is the lateral dimension of the observation volume and r_h is the hydrodynamic radius of the fluorophore, which can be calculated using Eq. 3.1.[227] In this work, FCS was employed to measure the hydrodynamic radius of miniemulsion droplets and nanoparticles labeled with fluorophores.

3.3.2.2. Dual Color Fluorescence Cross Correlation Spectroscopy

An extension of the classical FCS is dual-color fluorescence cross-correlation spectroscopy (DC-FCCS). Here, instead of one laser as in FCS, two lasers and two different fluorophores are used (see Fig. 3.3). Two light beams from two lasers operating at different wavelengths, called "blue" (b) and "red" (r) for simplicity, are expanded, collinearized and focused to a diffraction limited spot (observation volume V) into the sample by an achromatic microscope objective with high numerical aperture. The created fluorescence light is collected by the same objective and delivered to two photon counting avalanche photo detectors (APD) after passing a confocal pinhole, dichroic mirrors, and emission filters. In this way, two sub-femtoliter observation volumes V_b and V_r are created. For an optimal experimental arrangement, they are perfectly overlapping in space (which was proved to be the case for the setup used), creating an efficient common observation volume V_{br}. When two types of fluorescent species excitable by the "blue" and the "red" laser are independently diffusing through the common observation volume V_{br}, the corresponding temporal fluctuations $\delta F_b(t)$

and $\delta F_r(t)$ of the fluorescent signals monitored in the "blue" and "red" detection channels will be random and not correlated. On the contrary, if "double-colored" species are formed and diffuse through V_{br}, the fluorescence fluctuations monitored in the two channels will be strongly correlated (see Fig. 3.3). Mathematically, this can be expressed by a cross-correlation function[228] such as

$$G_{br}(\tau) = 1 + \frac{\langle \delta F_b(t) \delta F_r(t+\tau) \rangle}{\langle F_b(t) \rangle \langle F_r(t) \rangle} \qquad \text{Eq. 3.8}$$

The amplitude $G_{br}(0)$ of the cross correlation function is directly proportional to the concentration of the double-labeled species, which is emphasized in Fig. 3.3. Additionally, the autocorrelation functions $G_b(\tau)$ and $G_r(\tau)$ can be also defined using equations analogous to Eq. 3.8. By fitting these experimentally acquired auto- and cross-correlation curves with appropriate model functions such as Eq. 3.5 for one diffusing species or Eq. 3.6 for more than one species, precise information about the average hydrodynamic radius of the diffusing species and the concentration and fraction of the double-labeled species can be obtained. In this work, DC-FCCS was employed to measure and quantify the degree of coalescence of droplets labeled with a polymeric fluorophore.

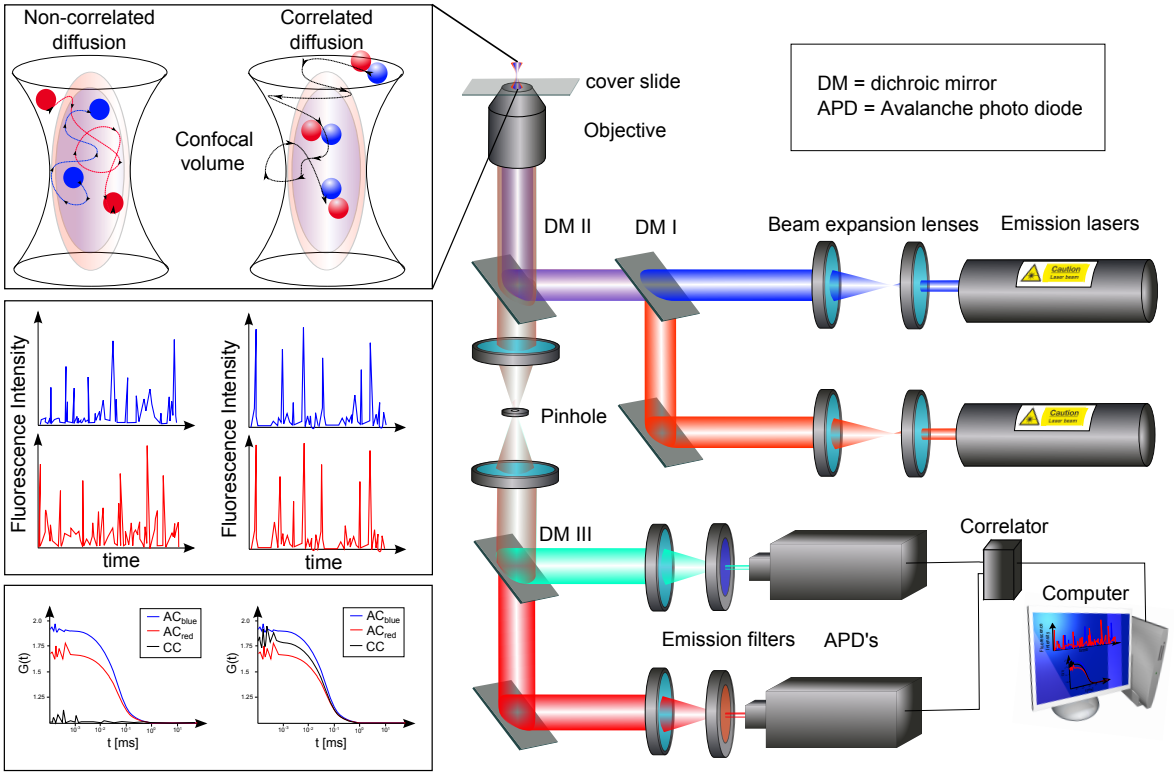

Fig. 3.3.: Schematic representation of a DC-FCCS-setup.[229] Two lasers with different wavelengths excite different fluorophores in the sample, the variation in fluorescence intensity is then measured for each laser and autocorrelated with the other laser. On the left side, the consequences of non-correlated or correlated diffusion of the fluorophores on the correlation of the fluorescence intensity and its consequence for the cross-correlation are shown. In case of non-correlated diffusion, the fluorescence signal in the red and in the blue channel are independent of each other, therefore their cross-correlation is negligible. On the other hand, if the diffusion of the red and blue particles is depending on each other, then there is a signal in the red channel at the same time as there is a signal in the blue channel. Hence, the fluorescence signals are strongly cross-correlated.

4. Results and Discussion

4.1. Mechanism of the Emulsion Solvent Evaporation Process[1]

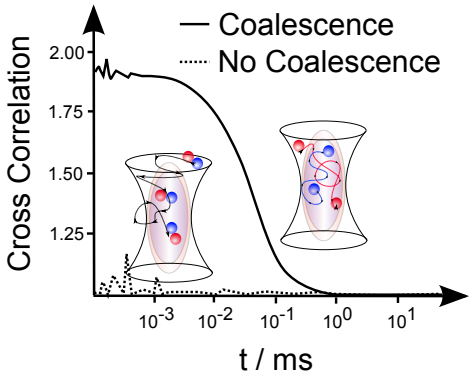

The mechanism of particle formation from submicrometer emulsion droplets by solvent evaporation, by miniemulsion polymerization, and by polycondensation of alkoxysilanes is revisited. A combination of different methods such as DLS, FCS, zeta potential, FRET and TEM measurements as well as DC-FCCS is used to analyze droplet coalescence during the evaporation process. It is shown that a combination of different methods yields reliable and quantitative data for describing the fate of the droplets. The results indicate that coalescence plays a minor role during the SEED process. The relatively large size distribution of the obtained polymer colloids can be explained by the droplet distribution after their formation.

4.1.1. Motivation

As it was shown in Section 2.2, the SEED process allows the fabrication of numerous colloids. However, the size distribution of the colloids obtained by this process is large compared to the particles prepared by heterophase polymerization. Therefore, a deep understanding of the mechanism of nanoparticle formation is needed to gain better control over the SEED process

[1]This section is based on the publication "Particle Formation in the Emulsion-Solvent Evaporation Process" by Roland H. Staff, David Schaeffel, Andrey Turshatov, Davide Donadio, Hans-Jürgen Butt, Katharina Landfester, Kaloian Koynov and Daniel Crespy published in 2013 in *Small*, volume 9 on pages 3514 to 3522,[230] as well as on the publication "Fluorescence Correlation Spectroscopy Directly Monitors Coalescence during Nanoparticle Preparation" by David Schaeffel, Roland H. Staff, Hans-Jürgen Butt, Katharina Landfester, Daniel Crespy and Kaloian Koynov, published in 2012 in *Nano Letters*, volume 12 on pages 6012 to 6017.[231] The publications are reprinted with permission. Copyright 2013 WILEY-VCH Verlag GmbH & Co. KGaA, Weinheim and Copyright 2012 American Chemical Society, respectively.

and the final particle properties. Indeed, the size and size distribution of the nanoparticles depend on many effects and parameters, for which each contribution cannot be easily isolated. For example, the temperature alone influences the evaporation speed of the solvent, the viscosity of the dispersed and continuous phase, the solubility of the different chemicals, the different interfacial tensions of the system, and the coefficient of diffusion of the droplets.

The coalescence between nanodroplets is another important effect that may strongly influence the polydispersity of the final nanoparticles. It can easily be imagined that the statistical merging of droplets will lead to a size distribution of different particle sizes after solvent evaporation. However, there are only a few studies on this topic. For example, the occurrence of coalescence during the formation of ethyl cellulose (EC) and poly(lactic acid) (PLA) nanoparticles by the SEED process was investigated by DLS.[50] In that work, the aggregation ratio A was defined as the average number of droplets necessary to form one polymer nanoparticle and A was evaluated by measuring the average droplet and particle sizes by DLS using

$$A = \frac{m_{polymer/nanoparticle}}{m_{polymer/droplet}} = \frac{\rho}{c\left(\frac{D_{droplet}}{D_{nanoparticle}}\right)^3} \qquad \text{Eq. 4.1}$$

Here, $m_{polymer/nanoparticle}$ is the mass of the polymer in the particles, $m_{polymer/droplet}$ the mass of the polymer in the droplets, ρ the density of the polymer in the nanoparticles, c the concentration of the polymer in the dispersed phase, $D_{droplet}$ the average diameter of the nanodroplets, and $D_{nanoparticle}$ the average diameter of the nanoparticles. Values of A between 9 and 32 were reported for EC nanoparticles depending on the viscosity of the dispersed phase, whereas a value of $A = 4$ for PLA was found independently on the viscosity.[50] On this basis, together with zeta potential measurements, the authors proposed that coalescence was significant in the case of EC and negligible for PLA. In another work, Loxley and Vincent assumed that coalescence of droplets was responsible for the broad size distribution of PMMA microcapsules prepared by the SEED process,[56] while Fryd and Mason studied the decrease of the average hydrodynamic diameters of emulsion droplets upon the SEED process with DLS.[232] They found a quadratic relationship between droplet shrinkage with time and the volume fraction of high molecular-weight oil. Although in some of the previous studies coalescence was assumed to occur during the SEED process, it was never evidenced by direct methods. Typically, DLS was used to measure the size of droplets and nanoparticles at different stages of the preparation process to retrieve information on coalescence. However, this information is often incomplete or questionable because some phenomena with opposite effects on droplets or particle sizes cannot be easily decoupled. For instance, in the SEED process, the solvent evaporation leads to a shrinking of the droplet size whereas the size is simultaneously increased by coalescence between droplets. Thus, new characterization methods that can provide direct information about the extent of coalescence during the SEED process are needed.

4.1.2. Tentative Monitoring of the SEED Process by DLS

Firstly, the average coefficients of diffusion of the droplets and their tentative conversion to hydrodynamic diameters were estimated by DLS directly after ultrasonication and in 30 min steps. The measurements were used to calculate the aggregation ratio A proportional to the ratio of the initial droplet diameter $D_{droplet}$ to the final particle diameter $D_{nanoparticle}$ according to Eq. 4.1.[50] The calculation requires to know the values of the concentration c of the polymer in the dispersed phase and the "true" density ρ of the polymer nanoparticles. The density of the polymer nanoparticles was assumed to be identical to the density of the polymer in bulk. This assumption is usually correct for particles without pores and was verified by other groups with gradient ultracentrifugation[233] and small-angle neutron scattering (SANS).[50] In this case, the same assumption was taken given the fact that no porous particles could be detected by TEM or SEM measurements. The measured hydrodynamic diameter in dependence on the evaporation time t is shown in Fig. 4.1 for a PS/chloroform-in-water miniemulsion. The first measurement ($t = 0$ min) was performed directly after ultrasonication and was taken as an estimation of the initial droplet diameter. As expected, a decrease of the diameter with time was observed until a plateau was reached after 3 h, similarly to results shown by others.[50] After several days, the nanoparticles still displayed the same diameter and therefore this value was taken as the final diameter of the nanoparticles. The A-value (see Eq. 4.1) for the measured system was calculated to be about 14, which indicated that on average 14 droplets merged to create one particle. This number is between the reported values of $A = 32$ and $A = 4$ for EC and PLA nanoparticles, respectively.[50]

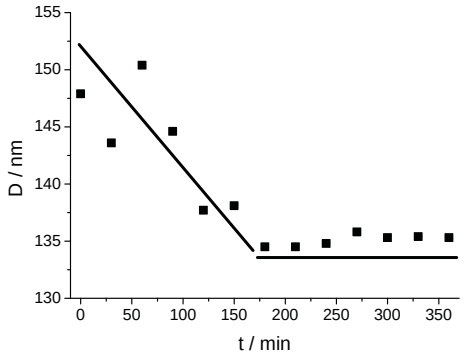

Fig. 4.1.: Temporal evolution of the hydrodynamic diameter of chloroform droplets containing PS during the SEED process. The lines are meant to guide the eye.

The concentration c is dependent on the amount of solvent left in the system after ultrasonication. Although the ultrasonication was performed under ice cooling, some chloroform was evaporated during the sonication step before the first DLS measurement at $t = 0$ min. The amount of chloroform in the emulsion after ultrasonication was determined by distillation.

Only 1.4 g of chloroform was recovered out of the 2.5 g chloroform initially added. The corrected aggregation number was hence refined to $A_{corrected} \approx 8$ instead of the $A \approx 14$ previously calculated.

The dilution of the emulsions or suspensions prior to the DLS measurements also need to be taken into account. Indeed, it is important to ascertain that there was no influence of the diluent and the dilution on the measured diameters. Prepared emulsions of PS in different solvents were diluted not only with water saturated with different solvents such as chloroform, toluene, and dichloromethane, but also with an aqueous solution of surfactant, and aqueous solutions of surfactant saturated with the different solvents. The emulsions were diluted at different concentrations with the different diluents and the hydrodynamic diameter was measured by DLS (see Fig. 4.2). Three main trends can be recognized for each graph. Firstly, the samples diluted with solvent-saturated water displayed a significantly larger diameter than the samples diluted with pure water or aqueous solution of SDS. Secondly, the hydrodynamic radii for the samples diluted with solvent-saturated water became smaller as the dilution was decreased; that is, high dilutions yielded larger particles than low dilutions with solvent-saturated water. Thirdly, the samples diluted with water or with an aqueous solution of SDS displayed roughly a constant diameter. The presence of species with a lower coefficient of diffusion upon diluting with solvent-saturated water was attributed to the swelling of the emulsion droplets. The interpretation of the results is delicate as the dilution can involve contradictory effects for which even a qualitative prediction is difficult to estimate. For instance, the dilution with water also dilutes the surfactant but allows a larger diffusion of the solvent in the continuous phase. A significant contribution of the dilution to the DLS results was also reported by Goddeeris et al.[234] They found that factors as diverse as droplet shape, droplet size distribution, angle of the incident laser beam and the potential presence of surfactant micelles all influence the measurement.

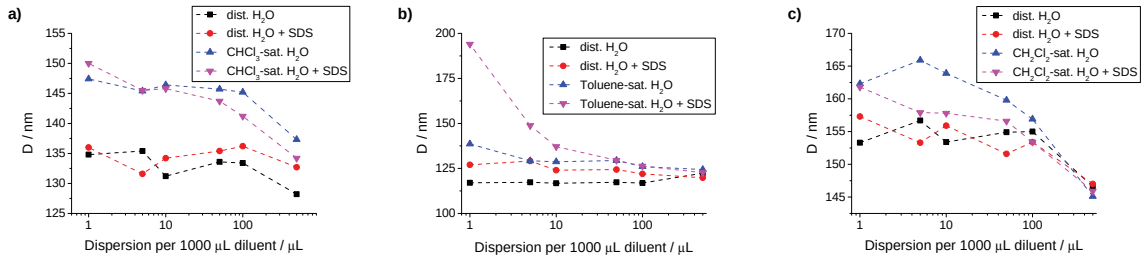

Fig. 4.2.: The hydrodynamic diameter of emulsions droplets is highly dependent on dilution and diluents such as chloroform (a), toluene (b) or dichloromethane (c).

In addition, the hydrodynamic boundary condition may introduce an uncertainty. The hydrodynamic radius of a droplet or a nanoparticle is calculated from the average coefficient of diffusion of the colloids by the Stokes-Einstein equation (see Section 3.2). The validity of this relationship for emulsions is assumed in most reports.[50,69,232] However, Hadamard[235]

and Rybczynski[236] introduced a viscosity-dependent boundary condition for describing a droplet in another liquid. Under full slip conditions (gas bubble), a 50 % higher velocity is obtained compared to the velocity under no slip conditions (solid sphere). Although these studies are related to gravity-induced and friction-retarded velocities, they may be considered in emulsions as well. If partial slip occurs, the droplet's size would be underestimated compared to the size of a hard sphere and would result in an overestimated value of A. Furthermore, the surface of the droplet is covered with surfactant molecules, thus resulting in a retardation of the droplet's motion by introduction of a surface tension gradient.[237] Such an effect has been observed in several studies,[238–240] with all results pointing to the occurrence of no slip once the surface of the droplet is covered by surfactant. However, a specific view on nanometer-sized droplets as well as the consideration of random Brownian motion is still missing. Additionally, the droplets in this study were not completely covered by surfactant due to the low surfactant concentration; thus, partial slip and therefore a higher diffusion coefficient and a resulting smaller diameter may have been obtained by tacitly assuming the utter validity of the Stokes-Einstein equation. In conclusion, there are too many conflicting factors, mainly diluent and theoretical considerations, to build a model for particle formation with DLS results as the sole basis under the reported experimental conditions.

4.1.3. Monitoring of the Zeta-Potential during Solvent Evaporation

The zeta potential of the PS-containing emulsions was measured directly after sonication and in 30 min steps during the SEED process. As shown in Fig. 4.3, the zeta potential did not change significantly with respect to the experimental error. Previous studies have demonstrated that the zeta potential could either decrease or increase/stagnate during the SEED process and the latter phenomenon was interpreted as a consequence of coalescence.[50] Indeed, the change of zeta potential was viewed as a temporary depletion of SDS at the droplet's surface induced by the coalescing droplets. However, as for DLS measurements, dilution was necessary to perform the zeta potential measurements. Hence, the partition of the surfactant as adsorbed species on the particle's surface or molecularly dissolved species were not the same for undiluted and diluted samples. Therefore, the zeta-potential measurements are probably as biased as the DLS measurements under the reported experimental conditions, because the influence of dilution is too significant to draw conclusions from these results.

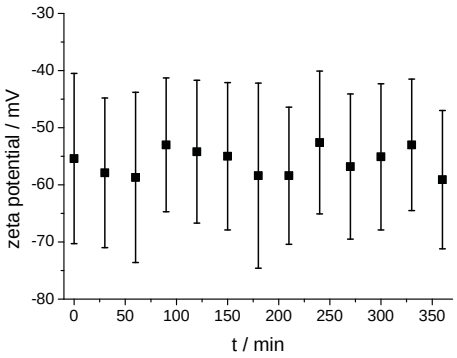

Fig. 4.3.: Zeta potential as a function of time of evaporation after ultrasonication.

4.1.4. Estimation of Nanoparticle Concentration by FCS

FCS can deliver information about the number of fluorescent diffusing species in a specific volume and thereby about the concentration of fluorescently labeled species as described in Section 3.3.2.1.[241–243] Almost no change in the concentration of fluorescent species was detected in the 240 min after sonication (see Fig. 4.4a), thus indicating that coalescence did not occur at a significant level. This observation was confirmed by measurements of the average particle brightness, which should increase upon coalescence but did not vary significantly with time (see Fig. 4.4b). In principle, the hydrodynamic radii of fluorescent species can also be extracted from the coefficient of diffusion measured by FCS. However, since diluting to a nanomolar concentration is required for a proper use of FCS,[200,244] the same problems as for DLS and zeta-potential measurements occurred, that is the results being dependent on dilution. Hence, more direct methods are necessary to study the coalescence of the droplets.

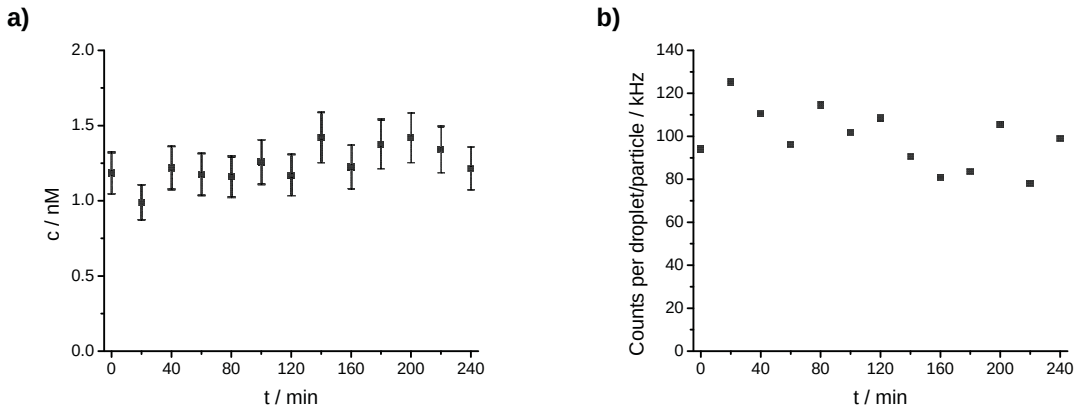

Fig. 4.4.: Temporal evolution of the concentration c of droplets or particles in the observation volume (a) and the photon counts per droplet/particle (b).

4.1.5. Determination of Coalescence by Other Methods

As the results obtained with DLS, FCS and zeta-potential measurements proved to be dependent on dilution, other methods are necessary to obtain information about coalescence. These methods should be versatile and should allow a quantitative determination of the amount of coalescence. A promising approach is to investigate the final dispersion. It should be possible to decipher the degree of coalescence of the emulsion droplets from the properties of the dispersion formed from the emulsion by deductive reasoning. For this, it is necessary to enclose the information about droplet coalescence in the particles of the dispersion in a way that by suitable methods of measurement the information is revealed.

This enclosing of information can be done by mixing two emulsions which contain polymers that have different properties and subsequently evaporating the solvent from this two-component emulsion. Doing so will lead to a sample that is henceforth called "actual sample". For the particles in this sample, there are two possibilities: Either coalescence did not occur at all, then all particles consist of only one polymer, or coalescence did occur, then the particles consist of both polymers. If coalescence occurred only to a certain amount, only a part of the particles consists of both polymers. Besides, if both polymers are mixed in solution, all particles will consist of both polymers after droplet generation and solvent evaporation. Therefore, this will be called "positive control sample". On the other hand, it is also possible to mix dispersions that were obtained by evaporating the solvent from single-component emulsions. A dispersion prepared in such a way will contain both polymers, but all particles consist of only one polymer or the other. It will hence be termed "negative control sample". The procedure for the generation of the three samples is depicted in Fig. 4.5.

Even with the aforementioned procedure, the coexistence of two polymers in the same particle still needs to be proved or disproved. Therefore, different methods were investigated with respect to their applicability and their ability to quantify coalescence. For this, it was also necessary to synthesize suitable polymers and to develop mathematical models as will be shown in the following section.

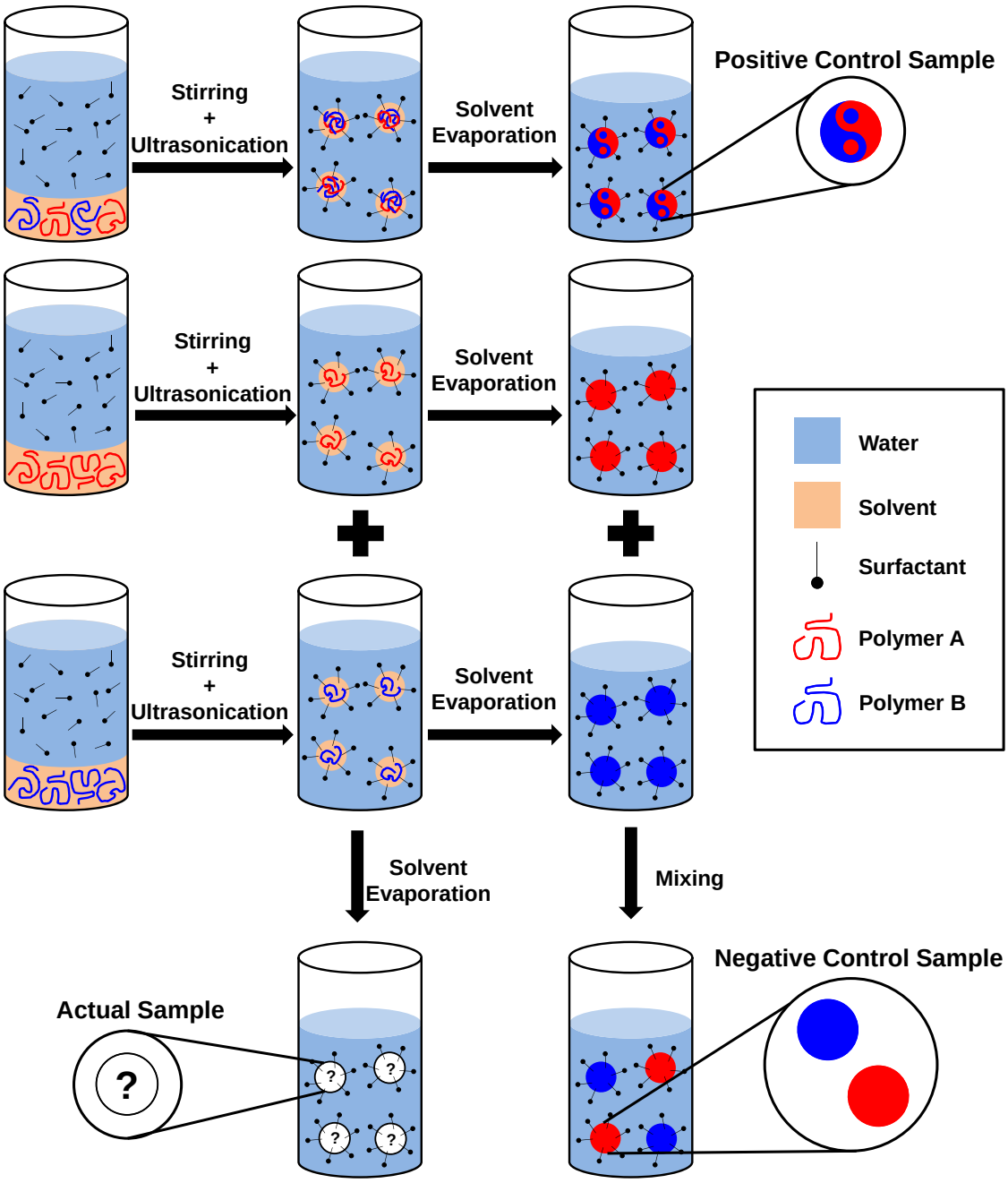

Fig. 4.5.: Scheme of the preparation of the samples for investigation of the occurrence of coalescence. Polymer A and polymer B can be two different polymers or two differently labeled polymers.

4.1.5.1. Determination of Coalescence by TEM

In order to differentiate between two polymers in the particles, the polymers were labeled with a suitable group and their co-presence was determined with a technique depending on the type of labeling. A labeling method can also induce a mass-thickness contrast for electron microscopy by staining a specific polymer or polymer block by heavy metals. In practice, this is realized by reacting the aromatic part of the PS chain with RuO_4. If the other polymer domain does not contain aromatic groups and if the polymers are immiscible, it is possible to selectively distinguish the domains in TEM measurements due to the high mass-thickness contrast given by the ruthenium. A system based on a mixture of emulsions of PS and PLLA was chosen for the coalescence studies with TEM because PS and PLLA are immiscible. Emulsions of dissolved PLLA and PS were prepared separately and mixed prior to solvent evaporation. As a positive control sample, both polymers were emulsified together, whereas the dispersions of nanoparticles of both polymers were mixed together after sonication as a negative control sample.

The positive control sample displayed particles with Janus morphologies with a dark PS and a bright PLLA domain (see Fig. 4.6a). The negative control sample showed both dark PS and bright PLLA particles (see Fig. 4.6b). The dark rings around the nanoparticles are due to the protective layer of carbon around the particles as PLLA is sensitive to the electron beam. As shown in Fig. 4.6, the PLLA particles are on average smaller (112 nm) than the PS particles (130 nm). The size difference was confirmed by DLS measurements. The size of the Janus particles of PS and PLLA (119 nm) was between the sizes of the particles of pure polymers. The sample prepared by mixing two emulsions of PS and PLLA after their respective sonication also showed distinct nanoparticles composed of either dark PS or bright PLLA (see Fig. 4.6c). The average particle size (129 nm) was comparable to the one of the negative control sample (127 nm).

The absence of Janus particles in the sample where emulsion droplets of PS and PLLA were mixed is indicative of an absence of coalescence. However, quantification is difficult in this case. Indeed, if small droplets of PLLA coalesce with large droplets of PS, the PLLA domain would be hardly detectable. Additionally, if one face of a Janus particle is placed on the grid, then it does not appear to be a Janus particle from top view (see Fig. 4.7). For these reasons, the study of coalescence by TEM gives evidence that none or not much coalescence is taking place, but is not quantifiable.

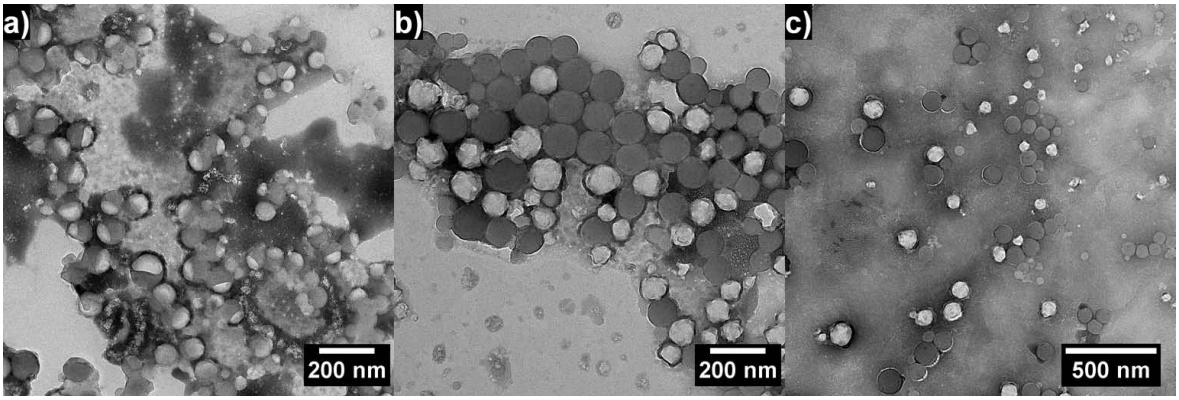

Fig. 4.6.: TEM-micrographs of the positive control sample (a) with Janus particles of PS and PLLA, of the negative control sample (b) with only separated PLLA or PS particles and of the sample from mixed emulsions (c). The small and dark rings around the particles are due to the protecting layer of carbon whereas the bright rings are probably focus artifacts.

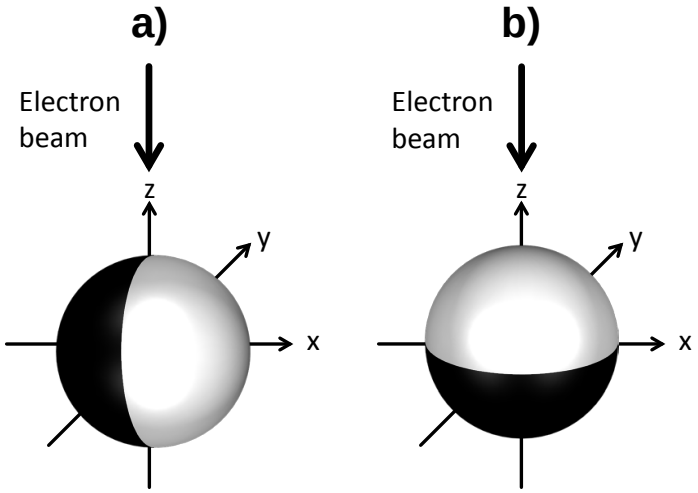

Fig. 4.7.: Because in TEM the electron beam is going though the sample, the Janus morphology can only be observed if the particle is located in a specific position (a) relative to the electron beam. If the particle is laying on the TEM grid as shown in (b), no Janus morphology can be observed.

4.1.5.2. Determination of Coalescence by FRET

In principle, the occurrence of coalescence can also be detected by the demonstration of the coexistence of two labeled species in the same particle when starting with separately labeled droplets. In the case of FRET measurements, the coexistence can be detected by a change of fluorescence decay of a donor fluorophore. Therefore, PS chains were labeled separately with the polymerizable dyes 9-vinylphenanthrene (VPA) as the FRET donor and [1-(4-nitrophenyl)-2-pyrrolidinmethyl] acrylate (NPP) as the FRET acceptor (see Fig. 4.8), which have already been used for FRET measurements.[245,246]

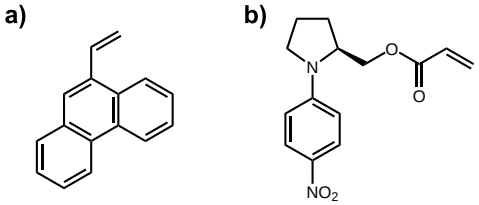

Fig. 4.8.: The FRET donor VPA (a) and the FRET acceptor NPP (b) were copolymerized with styrene in a miniemulsion polymerization.

Experimentally, the labeling was done by copolymerizing the dyes with styrene in miniemulsion. The dispersion was then freeze-dried and the obtained copolymers were purified by repeated reprecipitation. The apparent molecular weights of the copolymers PS-VPA and PS-NPP were 650 550 g/mol (PDI = 3.2) and 369 600 g/mol (PDI = 3.3), respectively, as determined by size exclusion chromatography (SEC). The purity of the copolymers was verified with high performance liquid chromatography (HPLC) by employing the free dye as reference. No free dye was detected in either copolymer after their purification (see Fig. 4.9). Absorption and emission measurements on the dyes and on the copolymers showed that there were no significant changes in absorption or fluorescence of the dyes upon their copolymerization (see Fig. 4.10).

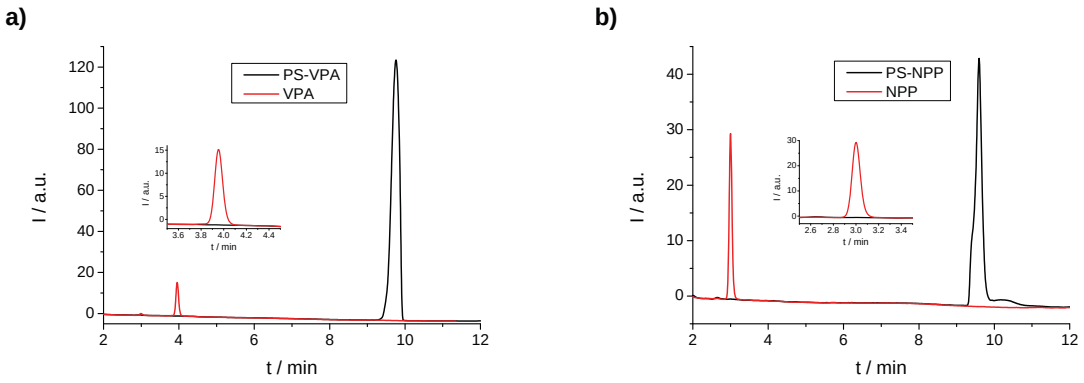

Fig. 4.9.: HPLC plots for PS-VPA (a) and PS-NPP (b). Both inlays show that there was no free dye present in the copolymers.

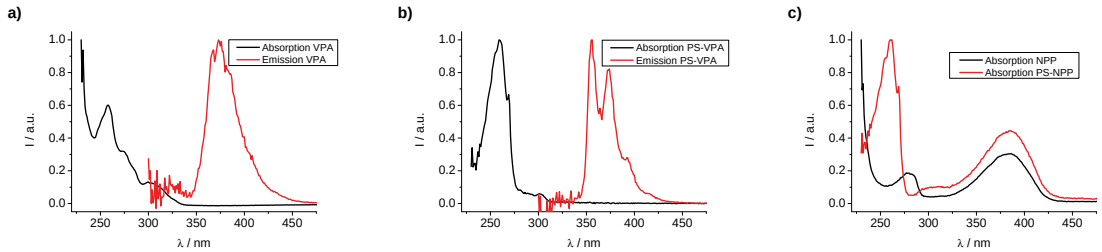

Fig. 4.10.: Absorption and emission spectra of VPA (a), PS-VPA (b) and the absorption spectra of NPP and PS-NPP (c). All spectra were corrected for background and solvent. NPP does not fluoresce.

Positive (FRET-P) and negative (FRET-N) samples were obtained by preparing particles from emulsions with the two labeled polymers in the same droplets and by mixing separately labeled dispersions of polymer particles, respectively (see Fig. 4.5). As expected, the positive control sample showed a fast decay of donor fluorescence, that is, a short lifetime, whereas the decay for the negative control sample was much slower (see Fig. 4.11). The actual sample (FRET-A) showed a behavior very close to that of the negative control sample (see Fig. 4.11). To obtain more quantitative information, the donor fluorescence decay curves for several possible scenarios by measuring defined mixtures of the FRET-P and FRET-N were detected. Decay 2 represents a possible situation when 80 % of all droplets coalesce but the process stops after coalescence of two droplets. If a larger number of droplets took part in the formation of a final "super droplet", the expected decay of FRET-A would become even shorter. Decay 4 (see Fig. 4.11) corresponds to a situation when approximately 20 % of all droplets coalesce in a binary manner. Thus, the decay of FRET-A revealed that only a very small fraction of all droplets is involved in coalescence.

However, as described in Section 3.3.1, the energy transfer occurs over short distances only, because the Förster radius R_{FRET} for the VPA-NPP donor-acceptor pair is (2.47 ± 0.03) nm.[245] In addition, the alignment of the transition dipoles of donor and acceptor must be free in order for FRET to occur. Therefore, even if two droplets coalesce, it is possible that the two differently labeled polymers are not mixed intimately and therefore the FRET measurements only indicate that the two fluorescently labeled species are not spatially close to each other.

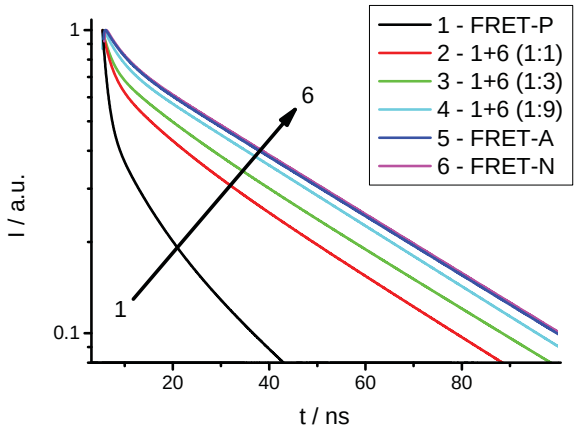

Fig. 4.11.: Fluorescence decay of the positive (FRET-P), negative (FRET-N), and actual (FRET-A) samples, and mixtures of FRET-P and FRET-A with different ratios.

4.1.5.3. Determination of Coalescence by DC-FCCS

On the contrary to FRET, DC-FCCS should retrieve information on the possible coexistence of two differently labeled polymers in the same nanoparticle or droplet even if they are spatially separated. That is why DC-FCCS was employed to further investigate the process of droplet coalescence.

In order to obtain fluorescent polymers suitable for DC-FCCS, Bodipy-based fluorescent monomers (see Fig. 4.12) were copolymerized with styrene. These fluorescent monomers, B504-MA and B612-MA, were selected because both had already been employed for the synthesis of fluorescent nanoparticles[132,247,248] and nanogels.[249] In addition, they have

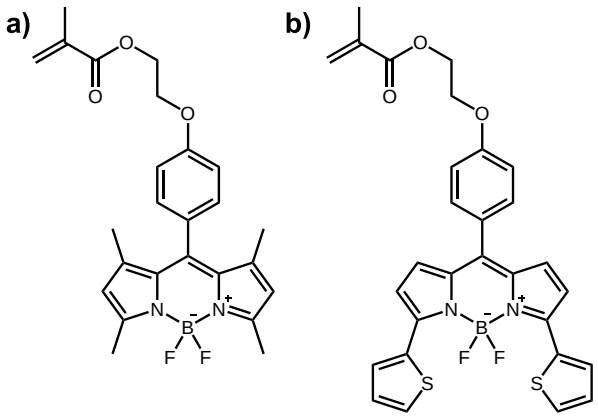

Fig. 4.12.: For DC-FCCS, the dyes B504-MA (a) and B612-MA (b) were copolymerized with styrene in solution.

relatively narrow absorption and emission bands which are necessary for DC-FCCS as shown in Fig. 4.14a and b. The apparent molecular weight of the copolymers PS-504 and PS-612 prepared with the dyes B504-MA and B612-MA were 44 700 g/mol (PDI = 1.9) and

29 000 g/mol (PDI = 2.2), respectively, as determined by SEC.

For DC-FCCS, it is also very important that the copolymers are free of residual dye. Therefore, HPLC measurements were conducted to verify the absence of free dye. Both copolymers did not contain any measurable residual dye after repeated precipitation from solution into methanol (see Fig. 4.13).

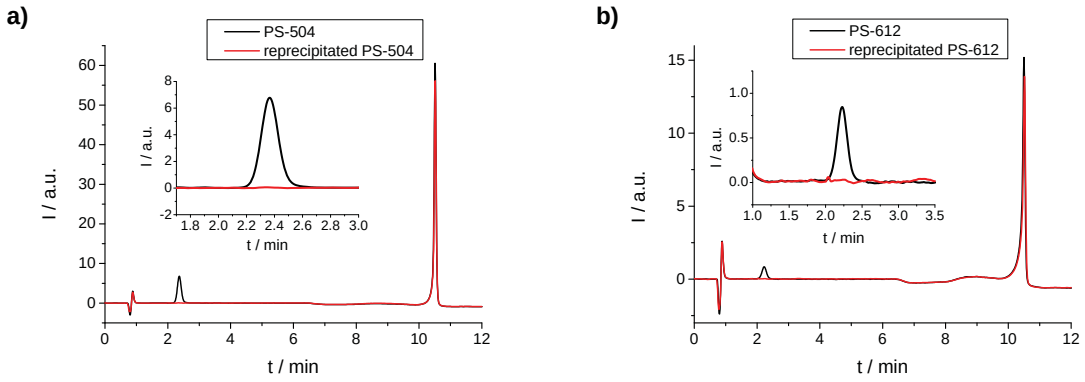

Fig. 4.13.: HPLC chromatograms for PS-504 (a) and PS-612 (b). Both inlays show that there is no free dye after repeated reprecipitation of the copolymers.

The fluorescent properties of the dyes (see Fig. 4.14a and b) were not lost upon copolymerization as can be seen in Fig. 4.14c and d. By measuring the intensity of fluorescence of the copolymers in solution and by establishing a reference curve by employing the free dye as a reference, it was also possible to quantify the amount of dye in the copolymer. The degree of labeling was 0.36 wt −% for PS-504 and 0.15 wt −% for PS-612 (see Fig. 4.15). In both cases, the amount of dye is in the linear region of the curve fit, i.e. it is not self-quenched, which is important for quantitative fluorescence measurements by DC-FCCS. At the same time, the amount of labeling is so low that the polymer will have in essence the same properties as pure PS.

Thus, these copolymers are suitable to be used in DC-FCCS studies. The positive, negative and the actual sample were prepared from the copolymers as shown in Fig. 4.5. These samples were subsequently used for investigations of coalescence with DC-FCCS.

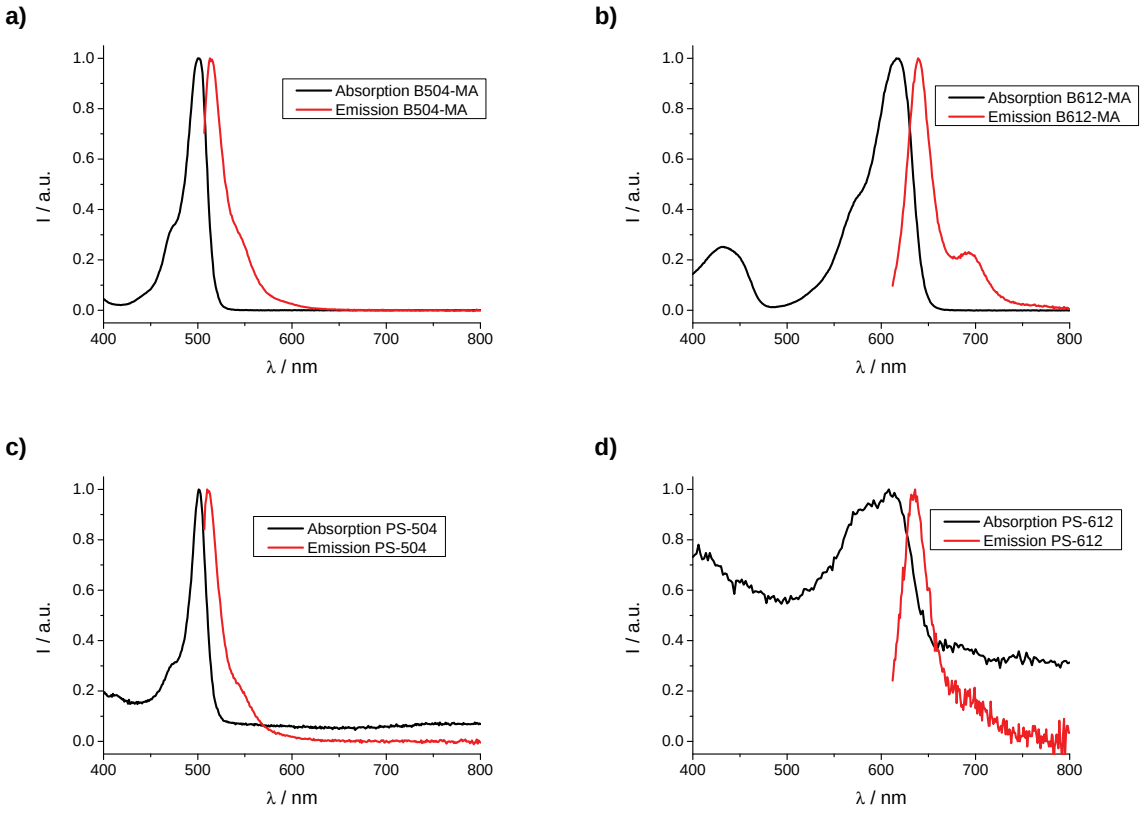

Fig. 4.14.: Absorption and emission spectra of B504-MA (a), B612-MA (b), PS-504 (c) and PS-612 (d). All spectra were corrected for background and solvent.

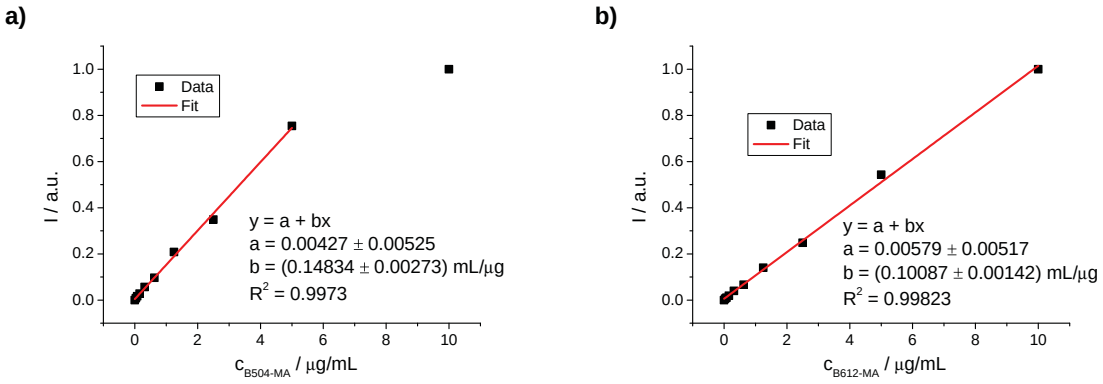

Fig. 4.15.: Plots for the quantification by fluorescence intensity measurements of the fluorescent labeling of the copolymers PS-504 (a) and PS-612 (b). For a), the highest concentration of B504-MA was not included into the fit due to apparent self-quenching of the fluorescence. The intensities of PS-504 and PS-612 in a 1 mg/mL solution in THF were 0.5371 and 0.1524, respectively, thereby being located in the linear region of both fits.

For each sample, the temporal fluorescence fluctuations $\delta F_x(t)$ monitored in the blue ($x = b$) and the red channel ($x = r$) of the DC-FCCS-setup shown in Fig. 3.3 were recorded independently. Subsequently, the cross-correlation function $G_{br}(\tau)$ was evaluated according to Eq. 3.8.[228] In addition, the autocorrelation functions from both channels were obtained. The experimental correlation curves were fitted with Eq. 3.5, yielding N and τ_D. Therefrom, the average concentration of the double labeled species c_{br} was computed through

$$c_{br} = (G_{br}(0) - 1) \cdot \frac{N_b N_r V_{br}}{V_b V_r} \qquad \text{Eq. 4.2}$$

Furthermore, the diffusion coefficient D and the hydrodynamic radius r_h of the species were evaluated from Eq. 3.7 and the Stokes-Einstein relationship.[227] In addition, the sample FCCS-1-PS-504 was used to quantify the cross-talk. A bleed through factor of 0.021 was obtained, which means that 2.1 % of the fluorescence emitted by the dye B504-MA was detected also in channel 2. All cross-correlation amplitudes were corrected by taking into account the cross-talk as described previously in other reports for other dyes.[250]

The experimentally measured correlation curves and their fits with Eq. 4.2 are shown in Fig. 4.16. The results of the fits are listed in Tab. 4.1. The positive control sample FCCS-1-P showed the expected strong cross-correlation, that is, a large value of $G_{br}(0)$ (see Fig. 4.16a). The almost identical values (see Tab. 4.1) for the concentration of the blue-, red-, and double-labeled nanoparticles obtained from the fits of the two autocorrelation and the cross-correlation curves indicate that all nanoparticles in this sample contain both blue- and red-labeled polymers. This finding is further supported by the values of the corresponding hydrodynamic radii (see Tab. 4.1), which were also found to be the same in the range of the computational errors. The negative control sample FCCS-1-N revealed a very low amplitude of cross-correlation (see Fig. 4.16b). Furthermore, when the cross-correlation function was corrected by taking cross-talk into account, its amplitude turned almost to one. The computed concentration of double-labeled particles c_{br} in Tab. 4.1 was negligible.

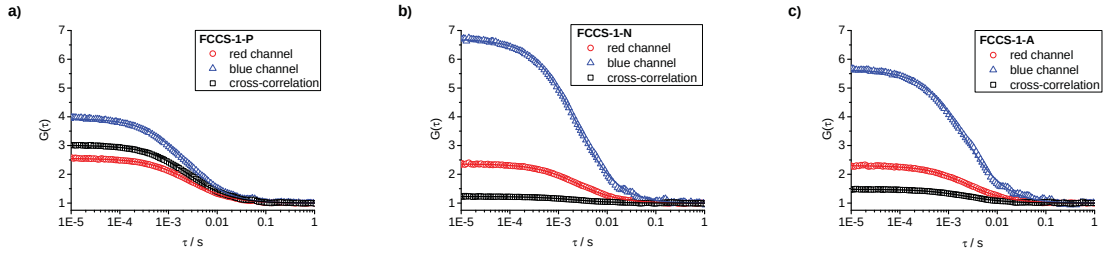

Fig. 4.16.: Correlation curves of the DC-FCCS samples FCCS-1-P (a), FCCS-1-N (b), and FCCS-1-A (c).

The sample FCCS-1-A displayed a non-negligible magnitude of cross-correlation even after the correction from cross-talk (see Fig. 4.16c). The computed concentration c_{br} also indicates

Tab. 4.1.: The channel colors, concentrations c and hydrodynamic radii r_h for the DC-FCCS experiments performed with samples FCCS-1-P, FCCS-1-N and FCCS-1-A are shown.

Sample	Channel	$c \pm \Delta c$ / nM	$r_h \pm \Delta r_h$ / nm
FCCS-1-P	r	1.70 ± 0.52	51.3 ± 4.0
	b	1.75 ± 0.21	49.6 ± 5.8
	br	1.71 ± 1.19	52.5 ± 5.2
FCCS-1-N	r	1.94 ± 0.60	46.3 ± 3.7
	b	0.91 ± 0.11	51.1 ± 5.7
	br	0.03 ± 0.02	44.4 ± 9.0
FCCS-1-A	r	2.02 ± 0.62	46.8 ± 3.8
	b	1.11 ± 0.13	47.6 ± 5.8
	br	0.23 ± 0.16	46.5 ± 6.9

that some coalescence occurred during the SEED process. The fraction of the blue-red particles f_{br} was estimated as

$$f_{br} = \frac{c_{br}}{c_r + c_b - c_{br}} \cdot 100\,\% = (8.0 \pm 6.3)\,\% \qquad \text{Eq. 4.3}$$

with c_{br} the concentration of double-labeled species detected by cross-correlation. To better quantify the extent of coalescence, a simple model based on the following assumptions was derived:

- Initially, the concentration of double-labeled species is zero.
- The probability of coalescence between the same and/or different colored droplets is equal.
- In each step $i+1$ of coalescence, all the droplets created in the previous step i coalesce in a binary manner to form new droplets.
- The number of droplets approaches infinity.

Taking these assumptions into consideration, it is possible to calculate the relative fraction of double-labeled droplets $f_{br}(i)$ after a particular coalescence "step" i from

$$f_{br}(i) = \frac{\left[(c_r + c_b)^{2i} - c_r^{2i} - c_b^{2i}\right]}{(c_r + c_b)^{2i}} \cdot 100\,\% \qquad \text{Eq. 4.4}$$

The model shows that already after a few steps almost all droplets should be dually labeled. The expected relative amount of double-labeled droplets N_{br} was calculated by $N_{br} = f_{br}/f_{br}(i = 1)$. Since $(8.0 \pm 6.3)\,\%$ of all droplets were found to be dually labeled, this means that $(17.4 \pm 13.7)\,\%$ of the initial droplets have coalesced assuming that only one "step" $(i = 1)$ has occurred. Please note that this number decreases even further when

further steps ($i > 1$) are considered.

It is concluded that on average slightly more than one droplet yields one nanoparticle during the entire SEED process. The A-value defined in Eq. 4.1 was calculated from the number of coalesced droplets N_{br} by

$$A = \frac{100\,\%}{100\,\% - \frac{N}{2}} \qquad \text{Eq. 4.5}$$

assuming that $i = 1$ coalescence steps occurred. The $(17.4 \pm 13.7)\,\%$ of initially present droplets undergoing coalescence mentioned before yield an A-value of only 1.10 ± 0.08, which means that 1.10 droplets form one final particle, which is much less than found previously.[50] As it was demonstrated that the zeta-potential and DLS measurements used by Vauthier et al. to obtain their values of A are strongly depending on dilution, these new results are of high importance as they unambiguously show that coalescence plays only a minor role during particle generation by solvent evaporation from miniemulsion droplets.

The DC-FCCS measurements were repeated with a different set of samples using the same procedure but with toluene instead of chloroform as solvent (FCCS-2). The results of the DC-FCCS experiments are listed in Tab. 4.2 and shown in Fig. 4.17a. The amount of double labeling was $(14.2 \pm 5.9)\,\%$, meaning that $(28.9 \pm 12.1)\,\%$ of the original droplets coalesced, yielding a value of $A = 1.17 \pm 0.08$. This value of A is slightly larger than in the case of chloroform. A possible explanation is the longer time needed to evaporate the less volatile toluene.

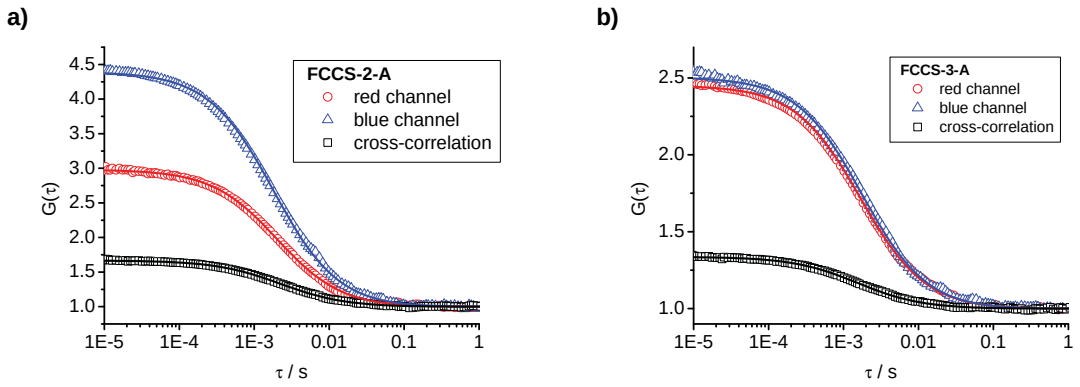

Fig. 4.17.: Correlation curves of the DC-FCCS samples FCCS-2-A (a) and FCCS3-A (b), which were prepared with toluene (a) or with chloroform with a low concentration of polymer in the droplets (b).

In another set of experiments, the amount of polymer in the chloroform was reduced by a factor of ten (FCCS-3). As expected, the obtained nanoparticles displayed smaller sizes than the nanoparticles formed from more concentrated polymer solutions (see Tab. 5.1). In this case, the amount of double labeling was $(11.4 \pm 6.5)\,\%$ (see Tab. 4.3 and Fig. 4.17b). Thus, $(24.4 \pm 13.9)\,\%$ of the original droplets coalesced during the solvent evaporation,

Tab. 4.2.: The channel colors, concentrations c and hydrodynamic radii r_h for the DC-FCCS experiments performed with samples FCCS-2-P, FCCS-2-N and FCCS-2-A are shown.

Sample	Channel	$c \pm \Delta c$ / nM	$r_h \pm \Delta r_h$ / nm
FCCS-2-P	r	2.11 ± 0.16	36.9 ± 2.3
	b	2.55 ± 0.36	33.9 ± 2.4
	br	2.15 ± 0.77	37.9 ± 2.5
FCCS-2-N	r	1.32 ± 0.10	39.3 ± 2.7
	b	1.61 ± 0.22	39.3 ± 2.8
	br	0.09 ± 0.03	48.8 ± 8.8
FCCS-2-A	r	1.95 ± 0.15	32.9 ± 2.0
	b	1.48 ± 0.21	39.3 ± 2.8
	br	0.43 ± 0.15	41.5 ± 3.2

which yields an A-value of 1.14 ± 0.09. The higher measured value for the magnitude of coalescence is the result of the larger initial content of solvent in the droplets. Indeed, the probability of coalescence between droplets is increased by lowering the viscosity of the dispersed phase and by increasing the evaporation time.

Tab. 4.3.: The channel colors, concentrations c and hydrodynamic radii r_h for the DC-FCCS experiments performed with samples FCCS-3-P, FCCS-3-N and FCCS-3-A are shown.

Sample	Channel	$c \pm \Delta c$ / nM	$r_h \pm \Delta r_h$ / nm
FCCS-3-P	red	4.51 ± 0.95	26.0 ± 2.4
	blue	3.78 ± 0.48	27.5 ± 3.0
	br	2.23 ± 1.17	31.3 ± 2.5
FCCS-3-N	red	1.32 ± 0.27	24.1 ± 1.7
	blue	1.62 ± 0.17	33.4 ± 2.7
	br	0.30 ± 0.15	26.7 ± 2.4
FCCS-3-A	red	2.02 ± 0.42	29.2 ± 2.0
	blue	3.39 ± 0.35	38.9 ± 2.8
	br	0.55 ± 0.28	30.2 ± 2.6

4.1.6. Simulations of Coalescence

To assess the importance of coalescence for the broadness of the size distribution, simulations were carried out to determine if coalescence alone could be responsible for the observed large distribution in size of the nanoparticles. As it is difficult to measure the size distribution of the droplets for the aforementioned reasons, the original emulsion was modeled by reverse

Monte Carlo simulations, based on the measured size distribution of the samples FCCS-1-A, FCCS-2-A, and FCCS-3-A. The effect of a broad range of different probabilities of coalescence from 5 % to 50 % was tested to check the influence of coalescence on the particle size distribution (see Fig. 4.18). The emulsions show an almost identical size distribution compared to the final nanoparticle dispersion at low degrees of coalescence, including the measured one. The peak position is shifted slightly to smaller diameters, but the overall shape remains, especially for larger droplet/particle sizes. Thus, the simulations show clearly that coalescence is not significantly responsible for the observed relatively broad size distribution.

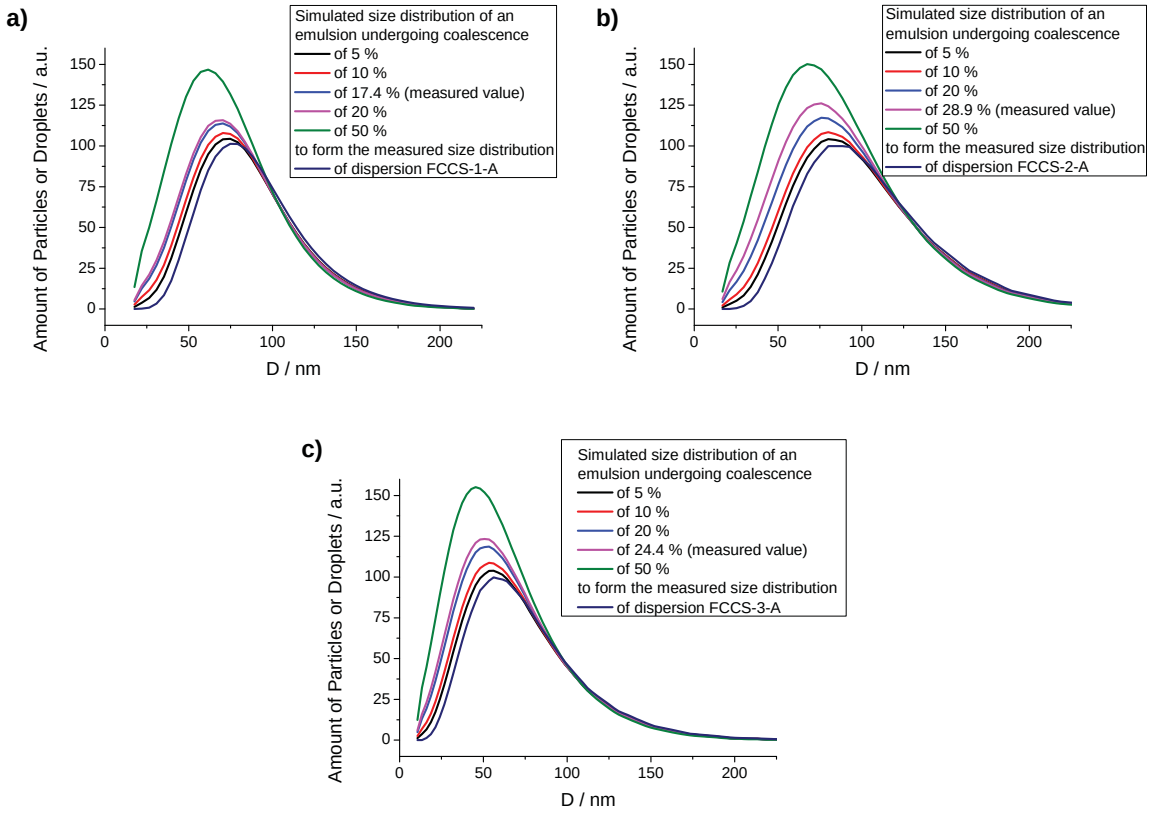

Fig. 4.18.: The distributions of hydrodynamic diameters of the nanoparticles measured by DLS were used to calculate the size distribution of the droplets in an emulsion by assuming different probabilities of coalescence below and above the measured value.

4.1.7. Influence of Ostwald Ripening

Although HD is usually employed as a hydrophobic agent to prevent Ostwald ripening of the droplets in miniemulsion polymerization,[25] the polymer itself can act as a hydrophobe for particles produced by the SEED process.[251] Indeed, it stabilizes the droplets kinetically, but not thermodynamically because the molar amount of polymer compared to solvent (1:62825) is usually not high enough to completely counterbalance the Laplace pressure.[25] To exclude

the influence of Ostwald ripening on the size distribution of the obtained nanoparticles, samples without (sample O-1) and with different amounts of HD were prepared, thereby keeping constant either the total dispersed mass (sample O-2) or the total dispersed volume (sample O-3). After solvent evaporation, the hydrodynamic diameter and the particle size distribution were measured by DLS. In all cases, the size distribution was almost identical, i.e. slightly larger than 30 % (see Tab. 5.1), although the molar ratio of HD/solvent was above the recommended ratio of 1:250,[25] that is, 1:162 and 1:119 for O-2 and O-3, respectively. Therefore, there is no influence of Ostwald ripening on the particle size distribution during the time of solvent evaporation. As coalescence was found not to be the cause of the observed particle size distribution, the observed large polydispersity most likely originates from the emulsification process itself, which has to be improved.

4.1.8. Droplet Coalescence in other Systems

Coalescence may not only occur during the SEED process but in any emulsion-based process. Therefore, the occurrence of coalescence during the synthesis of PS nanoparticles by radical miniemulsion polymerization (MEP) with an approach similar to the aforementioned one was examined. Small amounts of the fluorescently labeled polymers also used for the investigations on the SEED process were dissolved in the styrene monomer to label the miniemulsion consisting of styrene droplets dispersed in water. The positive control, negative control, and actual sample were prepared and studied by DC-FCCS. The normalized autocorrelation curves and the corresponding fits are shown in Fig. 4.19a, whereas the calculated values for the concentrations and hydrodynamic radii of "blue", "red", and "dual-colored" species are summarized in Tab. 4.4. The autocorrelation curves could be appropriately fitted utilizing Eq. 3.6 with a two-component decay ($m = 2$). The first component reflects the particles ($r_h > 60\,\text{nm}$) whereas the second consists of much smaller species ($r_h < 5\,\text{nm}$). The smaller species are probably single or small aggregates of labeled polymer chains, given that there was no detectable non-polymerized dye before the polymerizations. The amount of small species was significantly reduced by centrifugation. However, a small quantity still remained in the dispersions. Although the solubility of the labeled polymer is very low, some chains might be dissolved in the continuous phase. This hypothesis is supported by the fact that the measured fraction of small species f_i for the red dye (4 %) was lower than f_i for the blue dye (8 %), which can be correlated with the lower hydrophilicity of the red dye compared to the blue dye. Furthermore, as f_i is proportional to both the concentration and the squared molecular brightness of the particular observed species (see Eq. 3.6),[252] the absolute quantitative evaluation of their concentrations becomes more complex. As much lower amounts of labeled polymer were used in these experiments than in the ones conducted using the SEED process, it might be possible that some low-molecular weight chains dissolved in water or in some

kind of very small aggregates could be measured. This is especially true since the overall fluorescence brightness from the particles was much lower than the one of the nanoparticles present in the SEED investigations.

Tab. 4.4.: DC-FCCS results of the samples obtained from MEP. The concentrations c and the hydrodynamic radii r_h calculated from the autocorrelation curves are shown in contrast to the cross-correlation between the different channels.

Sample	Channel	$c \pm \Delta c$ / nM	Fraction $\pm\Delta$Fraction	$r_h \pm \Delta r_h$ / nm
MEP-P	r	0.54 ± 0.08	0.96 ± 0.02	82.9 ± 6.4
			0.04 ± 0.01	0.4 ± 0.5
	b	0.45 ± 0.06	0.93 ± 0.01	86.4 ± 10.7
			0.07 ± 0.01	1.5 ± 1.5
	br	0.38 ± 0.18	-	94.2 ± 10.7
MEP-N	r	0.33 ± 0.05	0.96 ± 0.02	88.8 ± 6.9
			0.04 ± 0.01	2.1 ± 1.5
	b	0.64 ± 0.09	0.80 ± 0.07	71.3 ± 8.8
			0.20 ± 0.02	5.4 ± 1.5
	br	0.09 ± 0.04	-	75.4 ± 9.9
MEP-A	r	0.16 ± 0.02	0.95 ± 0.01	76.4 ± 5.7
			0.05 ± 0.01	1.1 ± 0.7
	b	0.18 ± 0.02	0.82 ± 0.02	63.4 ± 8.0
			0.18 ± 0.01	4.5 ± 1.4
	br	0.04 ± 0.02	-	84.3 ± 10.6

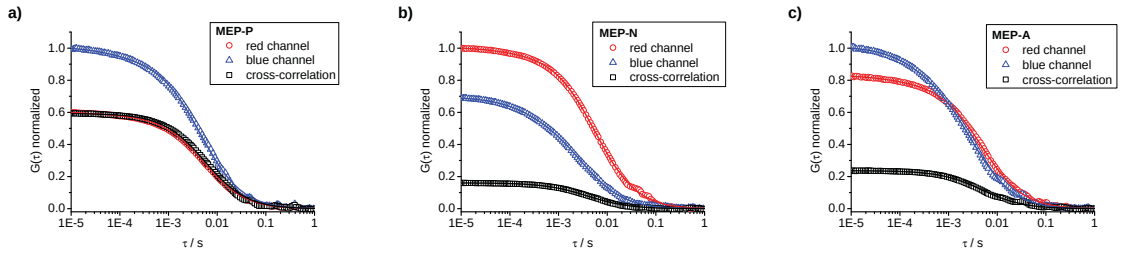

Fig. 4.19.: Correlation curves of the DC-FCCS samples prepared by MEP: MEP-P (a), MEP-N (b) and MEP-A (c).

The positive control sample MEP-P (see Fig. 4.19a) exhibited significant cross-correlation. Since the cross-correlation curve exclusively represents the dual-colored nanoparticles whereas the autocorrelation curves also show contributions from the small single-colored species, the value of the cross-correlation amplitude $G_{br}(0)$ is slightly lower than the "ideal" one which should lie between $G_b(0)$ and $G_r(0)$ as described above. In contrast, the negative control sample MEP-N (see Fig. 4.19b) showed only a very low amount of cross-correlation arising from the positive cross-talk of the DC-FCCS setup and from a low number of dual-colored nanoparticles aggregates most likely formed during the centrifugation. The negative

control sample MEP-N (see Fig. 4.19b) and the actual sample MEP-A (see Fig. 4.19c) displayed a similar behavior, which indicates that the coalescence of droplets does not occur significantly during the miniemulsion polymerization of styrene. This observation is consistent with previous SANS measurements on droplets of deuterated styrene before and after polymerization that indicated the absence of coalescence during polymerization.[31] However, a quantitative determination of the amount of coalescence was not feasible due to the presence of the second fraction.

Another process, the formation of silica nanocapsules by interfacial polycondensation of alkoxysilanes, was also investigated. For this purpose, small amounts of PS-504 and PS-612 were dissolved in a mixture of TEOS, toluene and HD.[10] After mixing with an aqueous solution of surfactant and ultrasonication, the monomer TEOS underwent hydrolysis and condensation, yielding silica nanocapsules.[10] The normalized correlation curves for the actual and control samples and their fits are shown in Fig. 4.20, while the obtained data are summarized in Tab. 4.5.

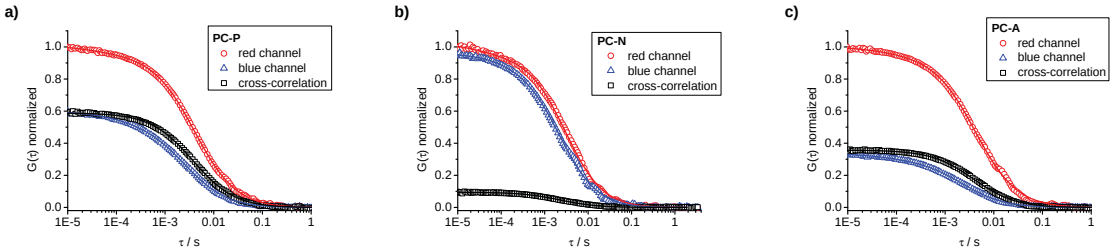

Fig. 4.20.: Correlation curves of the DC-FCCS samples prepared by interfacial polycondensation: PC-P (a), PC-N (b), and PC-A (c).

As in the miniemulsion polymerization, two-component fits were required to appropriately represent the autocorrelation curves with the model equation Eq. 3.6. The first component corresponds to the nanocapsules ($r_h > 49\,\text{nm}$) and the second component to a smaller species ($r_h < 3.5\,\text{nm}$), which are the aforementioned single-labeled polymer chains or their aggregates. Centrifugation of the samples to reduce the quantity of small species was not feasible since it caused aggregation of the nanocapsules. As expected, the positive control sample PC-P and the negative control sample PC-N displayed a high and negligible amount of cross-correlation, respectively (see Fig. 4.20a and b). On the other hand, the correlation curve for the actual sample PC-A is very similar to the correlation curve for the positive control sample PC-P (see Fig. 4.20c and a). Therefore, it is clearly demonstrated that coalescence between droplets of not fully reacted alkoxysilanes occurred during the preparation of the nanocapsules and yielded dual-colored species. This observation could explain the relatively large size distribution of similar silica nanocapsules measured by DLS.[10] As with the samples obtained from MEP, a quantitative determination of the amount of coalescence was not feasible due to the presence of the second fraction.

Tab. 4.5.: DC-FCCS results of the samples obtained by polycondensation of alkoxysilanes. The concentrations c and the hydrodynamic radii r_h calculated from the autocorrelation curves are shown in contrast to the cross-correlation between the different channels.

Sample	Channel	$c \pm \Delta c$ / nM	Fraction $\pm\Delta$Fraction	$r_h \pm \Delta r_h$ / nm
PC-P	r	2.90 ± 0.35	0.95 ± 0.01 0.05 ± 0.01	63.6 ± 4.4 0.49 ± 0.40
	b	8.07 ± 1.05	0.88 ± 0.02 0.12 ± 0.01	57.6 ± 10.7 3.1 ± 1.2
	br	3.73 ± 1.59	-	67.5 ± 6.6
PC-N	r	2.39 ± 0.32	0.93 ± 0.02 0.07 ± 0.02	49.4 ± 4.4 0.5 ± 0.5
	b	4.19 ± 0.55	0.92 ± 0.02 0.08 ± 0.01	51.4 ± 6.9 3.2 ± 2.6
	br	0.28 ± 0.12	-	42.6 ± 6.4
PC-A	r	1.29 ± 0.16	0.96 ± 0.01 0.04 ± 0.01	65.5 ± 5.4 0.9 ± 1.1
	b	6.32 ± 0.85	0.88 ± 0.01 0.12 ± 0.01	50.7 ± 6.1 1.7 ± 0.8
	br	1.82 ± 0.79	-	69.1 ± 7.5

4.1.9. Conclusions and Outlook

DLS was found not to be suitable to study coalescence in emulsion-based systems because the estimated diameters of the nanodroplets were influenced by the diluent and the dilution. FCS measurements showed that there was no change in nanodroplet concentration and fluorescence brightness while zeta-potential measurements did not show a change in the surface coverage of the nanodroplets. Both methods points to an absence of coalescence. DC-FCCS was used on a mixture of two emulsions, each of them containing polymer labeled with a different dye. By measuring the cross-correlation of the dyes, a quantification of the magnitude of coalescence was possible. The DC-FCCS measurements were supported by TEM and FRET measurements on labeled particles, which also showed nearly no coalescence. DC-FCCS was also applied to study coalescence occurring during different procedures for the preparation of organic or inorganic nanoparticles. The results unambiguously showed that coalescence did not play an important role in miniemulsion polymerization of styrene. However, coalescence was a major factor during the formation of inorganic silica nanocapsules by interfacial polycondensation of alkoxysilanes. Therefore, DC-FCCS was demonstrated to be suitable as a fast and versatile tool to study and quantify the coalescence of nanodroplets in emulsions or the aggregation of nanoparticles in suspensions.

Simulations were conducted to verify whether the measured amount of coalescence influenced the final particle size distribution. These simulations indicated that coalescence was not

responsible for the particle size distribution. Hence, the size distribution is very likely due to the process itself producing droplets with large size distribution. Thus, further efforts towards the preparation of monodisperse nanoparticles by the SEED process should focus on the step of emulsion droplet generation to obtain monodisperse droplets that then will form monodisperse nanoparticles.

4.2. Marrying Click-Chemistry to Janus Particles

Alkyne and azide functionalized polymeric Janus particles were prepared in water. The surface density of the functional groups could be changed by controlling the functional group density in the polymers used to generate the Janus particles. The control was achieved by the preparation of copolymers in which the percentage of the functional monomer was varied and by ATRP with functional initiators. Furthermore, reagents and methods were developed to quantify the alkyne and azide groups on the surface of the Janus particles. Thus, the clickability of the groups was also proven.

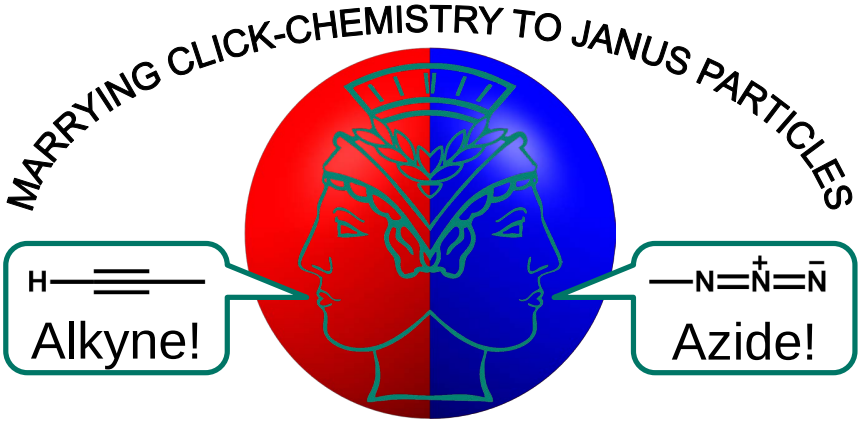

4.2.1. Motivation

In Chapter 1, the term "complex colloid" was defined as a colloid having some addressable functionality and being not homogeneous but heterogeneous in itself. Among the different colloidal morphologies introduced in Section 2.3, the Janus morphology has received widespread attention due to its anisotropy and potential multi-functionality.[133–143] Different possible preparation routes and applications of Janus particles were already introduced in Section 2.3.2.

The first part of the definition of "complex colloid" mentioned above is the presence of addressable functionality. For a colloidal chemist, addressable functionality often means the presence of hydroxyl, amino, carboxylic acid or other groups on the colloid. These groups can then either be used to react with other molecules or they can introduce stimuli-responsiveness to a colloid. However, due to the ubiquitous nature of the mentioned groups, they can be disadvantageous because they can undergo unwanted reactions in complex media such as biological systems. Therefore, bio-orthogonal groups that can undergo reactions in high yields and under mild conditions are needed. For this, click-chemistry is a promising

candidate. Especially the copper-catalyzed cycloaddition reactions between azides and alkynes, discovered by Sharpless et al.[253,254] and Meldal et al.[255] fulfill the criteria of reacting under mild conditions in high yield. Therefore, inspired by the title of Wegner's publication on the marriage of polymers and inorganics,[256] the marriage of click-chemistry to Janus particles in order to form complex colloids that are addressable by a bio-orthogonal reaction is an interesting and challenging aim.

4.2.2. Synthesis of the Polymers

The SEED process is quite common to form polymer-based Janus particles (see Section 2.3.2.1).[136–138] Phase separation between two polymers is necessary to form the Janus morphology, hence, different chemical structures of the polymers are needed to favor phase separation. The polymer pair PS/PMMA was used for the preparation of the Janus particles as a model system.

There are at least three possible routes for the functionalization of Janus particles with clickable alkyne or azide groups when the SEED process is used for particle generation. Firstly, the groups can be introduced by reacting suitable reagents onto the surface of pre-formed Janus particles. Secondly, a polymer can be prepared that carries an alkyne or an azide functionality directly by either using monomers that have one of these functionalities or by using initiators or terminating agents that are functionalized with an alkyne or an azide group. Thirdly, a polymer can be prepared and post-functionalized with the mentioned groups. The post-functionalization can occur at one or both ends of the polymer chain or in its backbone.

4.2.2.1. Synthesis of the Polymers by Radical Copolymerization

The post-functionalization approach was chosen since it allows a high variability in the introduction of the functional groups. Both the chemical nature of the functional group as well as its amount can be changed relatively easily. As a post-functionalizable monomer vinylbenzyl chloride (VBC) was chosen, since the chloride group can be substituted relatively easily by other groups.[257–260] Furthermore, it can be copolymerized with styrene or MMA in a solution polymerization (see Fig. 4.21).[261,262]

The prepared copolymers of styrene or MMA and VBC were characterized with SEC, NMR and infrared (IR) spectroscopy. The molar ratios of the copolymers and their molecular weights are shown in Tab. 4.6. All copolymers had a molecular weight between 30 000 g/mol and 40 000 g/mol and a polydispersity index (PDI) of roughly 2 as could be expected for a radical copolymerization in solution.

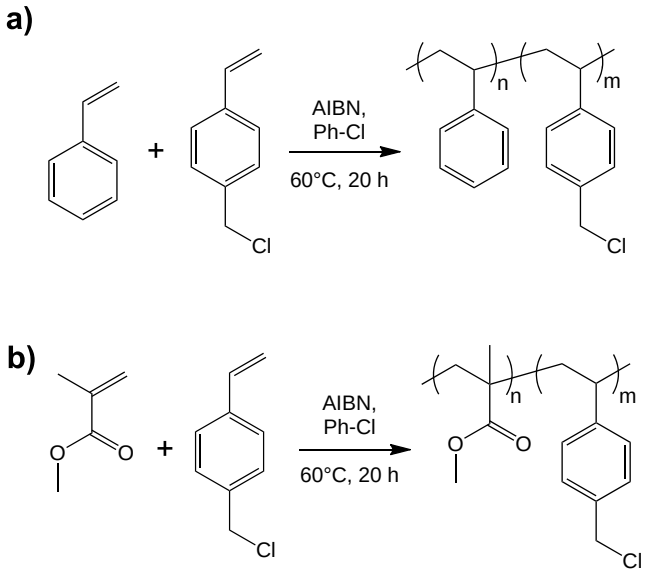

Fig. 4.21.: Copolymerization of VBC and styrene (a) or with MMA (b) in solution.

Tab. 4.6.: Theoretical and measured molar ratios n/m in the synthesized copolymers.

Copolymer	theo. molar ratio n/m			measured molar ratio n/m			M_n / g/mol	PDI
	Styrene	MMA	VBC	Styrene	MMA	VBC		
Co-1	89.8	-	10.2	88.9	-	11.1	30000	1.92
Co-2	-	89.8	10.2	-	86.5	13.5	37500	2.00
Co-3	94.9	-	5.1	94.4	-	5.6	30600	1.73
Co-4	-	94.9	5.1	-	92.9	7.1	35700	1.94
Co-5	97.4	-	2.6	97.0	-	3.0	32800	1.79
Co-6	-	97.4	2.6	-	96.0	4.0	34800	1.97

The IR spectra of the copolymers prepared from styrene and VBC showed the characteristic C-Cl-vibration at 1265 cm^{-1},[257,263] otherwise their spectra corresponded to the spectrum of pure PS (see Fig. 4.22a). In the copolymers of MMA and VBC, the C-Cl-vibration was not observed since it is overlapping with the broad and very intense vibration of the C-O-bond[264] of the ester (see Fig. 4.22b).

The ratio of the monomers n/m in the PS-*co*-PVBC copolymers was calculated from their NMR spectra (see Fig. 4.23a) by using the integral of the aromatic region I_{aromatic} from 6.0 ppm to 7.5 ppm and the integral of the benzylic protons I_{benzylic} from 4.3 ppm to 4.7 ppm in the formula

$$n/m = \frac{2 \cdot (I_{\text{aromatic}} - 2 \cdot I_{\text{benzylic}})}{5 \cdot I_{\text{benzylic}}} \qquad \text{Eq. 4.6}$$

In a similar manner, the ratio of the monomers in the PMMA-*co*-PVBC copolymers was calculated from their NMR spectra (see Fig. 4.23b). The integrals of the aromatic region I_{aromatic} from 6.0 ppm to 7.5 ppm and of the methyl group I_{methyl} from 3.1 ppm to 4.0 ppm

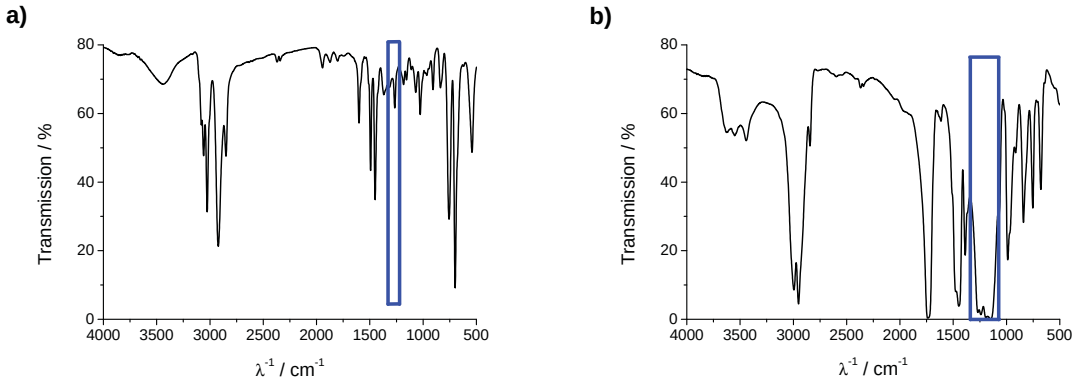

Fig. 4.22.: IR spectra of PS-*co*-PVBC (a) and PMMA-*co*-PVBC (b). The C-Cl-vibration is marked in (a), in (b) it is overlapping with the vibration of the C-O-bond.

were used in the formula

$$n/m = \frac{4 \cdot I_{\text{methyl}}}{3 \cdot I_{\text{aromatic}}} \qquad \text{Eq. 4.7}$$

The results of these calculations are shown in Tab. 4.6.

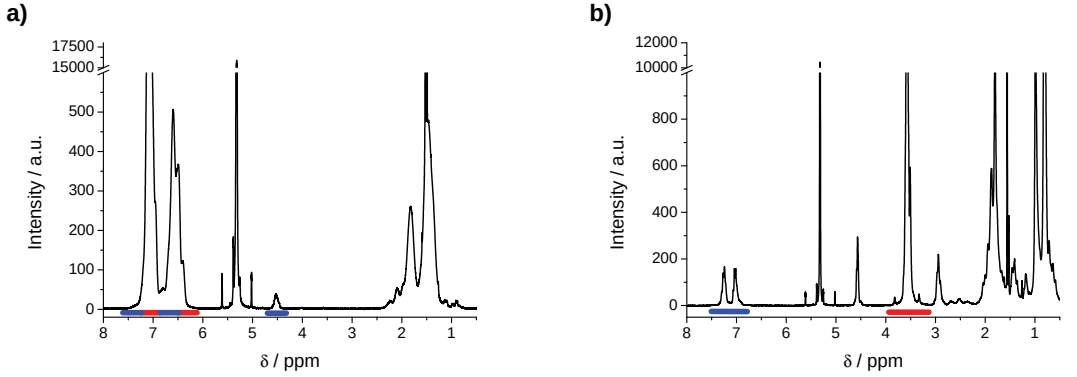

Fig. 4.23.: NMR spectra of PS-*co*-PVBC (a) and PMMA-*co*-PVBC (b). The signals used for the determination of the ratios of the monomers in the copolymer are marked in blue for PVBC and in red for PS (a) or PMMA (b).

A preferred incorporation of VBC into the copolymer in relation to its initial amount was observed in all copolymers. This trend was stronger with MMA than with styrene. The Mayo-Lewis copolymerization parameters of the system VBC/styrene are $r_{\text{VBC}} = 1.31$ and $r_{\text{styrene}} = 0.72$ and $r_{\text{VBC}} = 0.82$ and $r_{\text{MMA}} = 0.37$ for the system VBC/MMA.[261,262] As the copolymerization parameter of VBC is higher than that of the comonomer in both cases, it was incorporated preferentially into the copolymer which is also what was observed in the experiments. Even the relatively small difference in the copolymerization parameters was mirrored in the resulting copolymers. The relative difference is smaller in the system VBC/styrene than in the system VBC/MMA. Therefore, VBC is incorporated into the copolymer in a higher amount if the comonomer is MMA than if the comonomer is styrene.

Thus, the copolymers prepared from MMA showed a higher functional density than the copolymers prepared from styrene.

4.2.2.2. Post-Functionalization of the Copolymers

To remove the chloride group from the benzyl chloride, a nucleophilic substitution has to be performed. The substitution can be achieved easily by using other anions, since the chloride is a very good leaving group. The alkyne group was introduced when propargyl alcohol was deprotonated and subsequently left to react with the benzyl chloride. The deprotonation was achieved in DMF with sodium hydroxide as base.[265] Sodium azide was used to introduce the azide functionality, as the azide anion is a nucleophile strong enough to displace the chloride group if a polar solvent such as tetrahydrofuran (THF) or DMF is used.[257] The reactions are shown in Fig. 4.24.

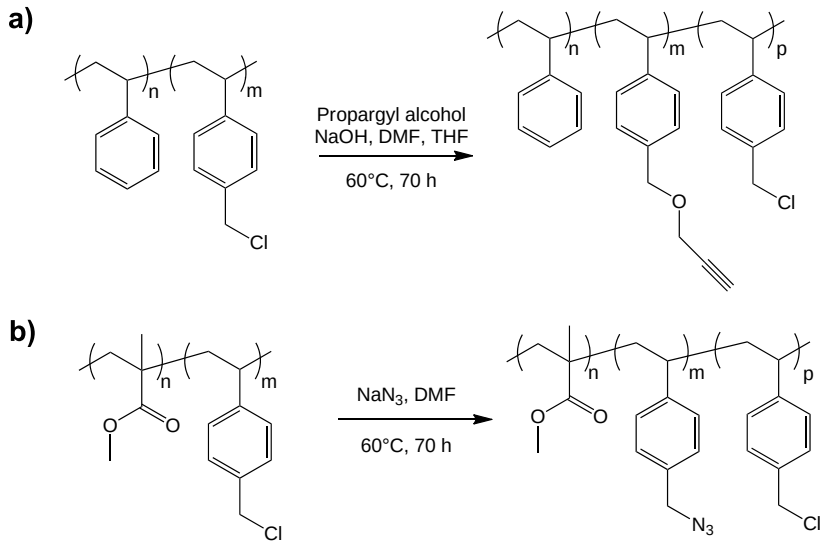

Fig. 4.24.: Post-functionalization of PS-*co*-PVBC with alkyne groups by nucleophilic substitution with propargyl alcohol (a) and of PMMA-*co*-PVBC with azide groups by nucleophilic substitution with sodium azide (b).

The post-functionalized copolymers of styrene or MMA and VBC were characterized with SEC, NMR, and IR spectroscopy, the results are shown in Tab. 4.7. The molecular weights of the copolymers were slightly higher after post-functionalization than before. This increase can be explained by two factors: Firstly, the introduced groups have a higher molecular weight than the leaving group and secondly some amount of copolymer is lost in every step of precipitation. As copolymer chains with a lower molecular weight have a higher solubility, the repeated precipitations led to an increased molecular weight. The same phenomenon was also observed in the PDI, which became slightly smaller. Additionally, it has to be considered that the SEC determines only a relative, PS-equivalent molecular weight. Because of the

post-functionalization, the interactions of the polymer with the material of the column may have changed, resulting in changes in the measured molecular weight.

Tab. 4.7.: Main monomer, type and degree of functionalization as well as molecular weight and PDI of the post-functionalized copolymers.

Copolymer	Monomer	Functionalization	func. Groups / %	M_n / g/mol	PDI
Co-1-f	styrene	alkyne	11.1	32600	1.67
Co-2-f	MMA	azide	13.5	39600	1.75
Co-3-f	styrene	alkyne	5.6	32600	1.63
Co-4-f	MMA	azide	7.1	39500	1.72
Co-5-f	styrene	alkyne	3.0	35300	1.63
Co-6-f	MMA	azide	4.0	37900	1.67

In the IR spectra of the PS-*co*-PVBC copolymers, the C-H vibration of the alkyne group was clearly visible at 3290 cm^{-1} (see Fig. 4.25a).[264] The weak C-C-vibration of the triple bond at 2120 cm^{-1} was also observed, but it is too weak for a definite identification.[264] The C-Cl vibration was not present anymore, which indicates a high degree of post-functionalization. In the post-functionalized PMMA-*co*-PVBC copolymers, the strong vibration of the azide group was clearly visible at 2100 cm^{-1} (see Fig. 4.25b).

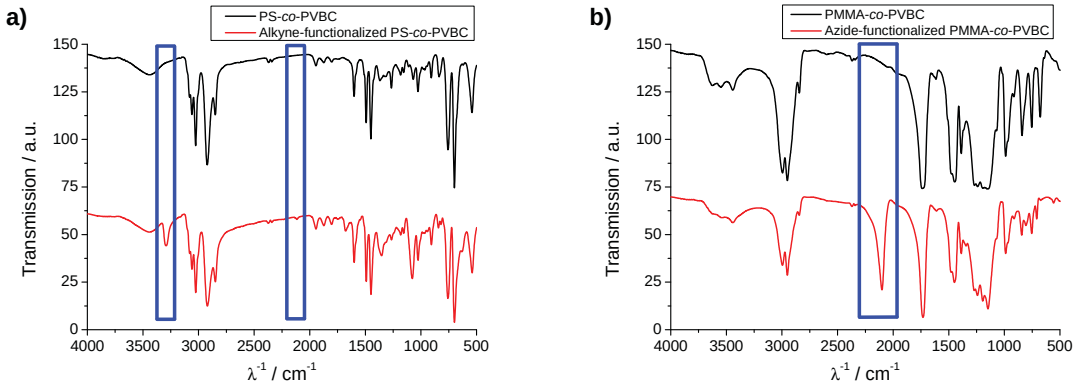

Fig. 4.25.: IR spectra of PS-*co*-PVBC before and after post-functionalization with alkyne groups (a) and of PMMA-*co*-PVBC before and after post-functionalization with azide groups (b). The vibrations belonging to the introduced groups are marked in boxes.

There was only a slight shift of the signal of the benzylic protons upon post-functionalization with propargyl alcohol in the NMR spectra of the PS-*co*-PVBC copolymers (see Fig. 4.26a). The degree of functionalization was easily determined by comparison of these two protons with the two protons of the CH_2-group of the propargyl alcohol. In all cases, the post-functionalization was complete, meaning that all groups had reacted. The signal at 4.6 ppm of the benzylic protons in the NMR spectra of post-functionalized PMMA-*co*-PVBC shifted strongly, as was also shown by Lang et al.[257] Because there is no remaining signal at

4.6 ppm, the post-functionalization also had a yield of 100 %, i.e. $p = 0$ in Fig. 4.24. The completeness of the post-functionalization was attributed to two factors: Firstly, the reactions were allowed to run for an extended period of time and secondly a large excess of propargyl alcohol or sodium azide was used. In conclusion, several copolymers of styrene or MMA and VBC were prepared which could be post-functionalized to have alkyne or azide functionality in the polymer backbone. The degree of functionality could be controlled by tuning the ratio of the monomers in the copolymerization. The prepared copolymers are listed in Tab. 4.7.

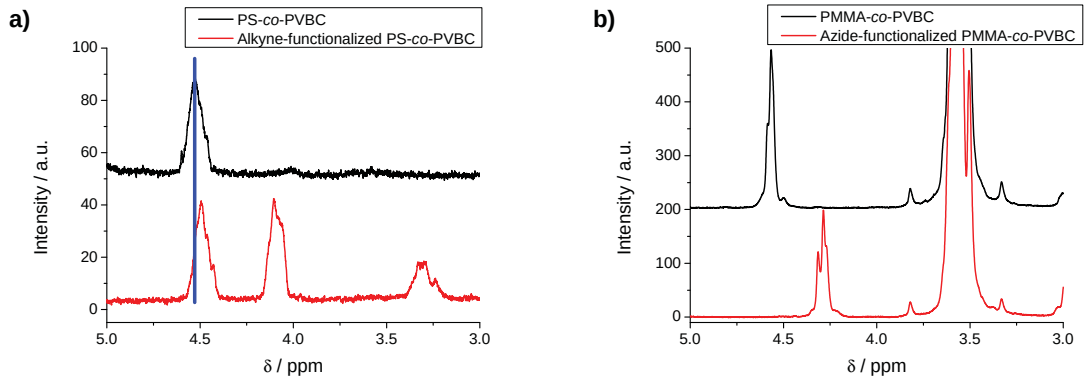

Fig. 4.26.: NMR spectra of PS-*co*-PVBC before and after post-functionalization with alkyne groups (a) and of PMMA-*co*-PVBC before and after post-functionalization with azide groups (b). In the case of alkyne groups, new signals and a very small shift of the protons belonging to the benzyl group can be observed (a). In case of the post-functionalization with azide groups, there is a stronger shift upfield (b).

4.2.2.3. Synthesis of the Polymers by ATRP

The alkyne and azide functionalized copolymers prepared by post-functionalization of copolymers present two drawbacks: Firstly, their molar mass disparity is large as the copolymers were prepared by free radical copolymerization in solution. Therefore, the degree of functionality is known only as an overall average, but not for a specific single chain. Secondly, the physico-chemical nature of the copolymers might be different from their homopolymers PS and PMMA as their properties might be significantly influenced by the comonomer. As VBC is a styrenic monomer, this point is more important in PMMA-*co*-PVBC copolymers than in PS-*co*-PVBC copolymers. Especially the phase separation of the copolymers might be influenced, which is of great importance for the formation of the Janus morphology during solvent evaporation. Polymers with just exactly one functionality per chain would phase separate without problems, but due to their low degree of functionality the surface functionalization would also be low. Therefore, the right balance between polymer functionality and the resulting polymer properties such as phase separation had to be found. Hence, polymers were prepared that have exactly one functionality per chain and are otherwise homopolymers.

To obtain exactly one functionality per polymer chain, functional initiators in an ATRP-reaction can be used. Therefore, ATRP-initiators bearing alkyne- and azide-functionality were synthesized.

The ATRP-initiator 3-(trimethylsilyl)prop-2-yn-1-yl 2-bromo-2-methylpropanoate was prepared according to a modified literature procedure reported by Opsteen and Hest (see Fig. 4.27).[266] In this initiator, the alkyne group is protected by a trimethylsilyl group as it would otherwise react during polymerization.[266]

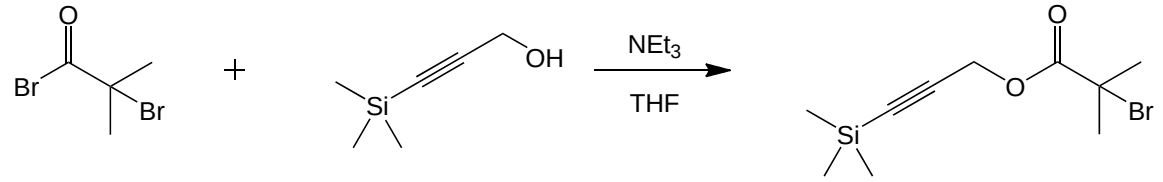

Fig. 4.27.: Synthesis of the ATRP-initiator 3-(trimethylsilyl)prop-2-yn-1-yl 2-bromo-2-methylpropanoate.

With this initiator and MMA as monomer, alkyne functionalized PMMA was prepared by ATRP (see Fig. 4.28). Subsequently, the trimethylsilyl group was removed by tetra-(*n*-butyl)-ammonium fluoride (TBAF) under mild conditions. The resulting polymer had a molecular weight of 29 000 g/mol and a PDI of 1.11. The calculated molar functional density was 0.3 %.

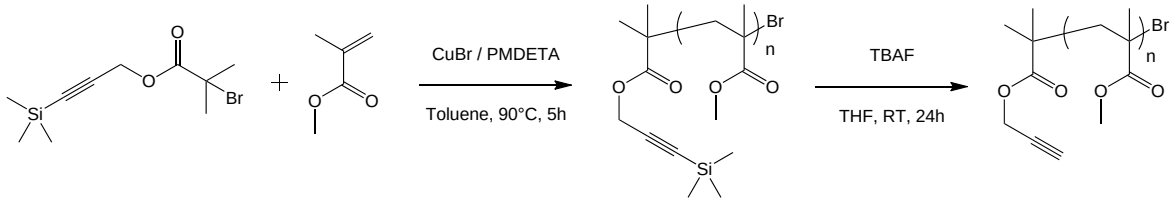

Fig. 4.28.: Synthesis and subsequent deprotection of alkyne end-functionalized PMMA.

To prepare the azide functionalized ATRP-initiator 2-azidoethyl 2-bromo-2-methylpropanoate, 2-azido ethanol was prepared following a procedure by Li et al. (see Fig. 4.29).[267] The esterification procedure by Opsteen and Hest[266] was then used again to synthesize 2-azidoethyl 2-bromo-2-methylpropanoate.

With the azide functionalized initiator and styrene as monomer, azide functionalized PS was prepared by ATRP (see Fig. 4.30). The resulting polymer had a molecular weight of 33 200 g/mol and a PDI of 1.17. The calculated molar functionality was 0.3 %.

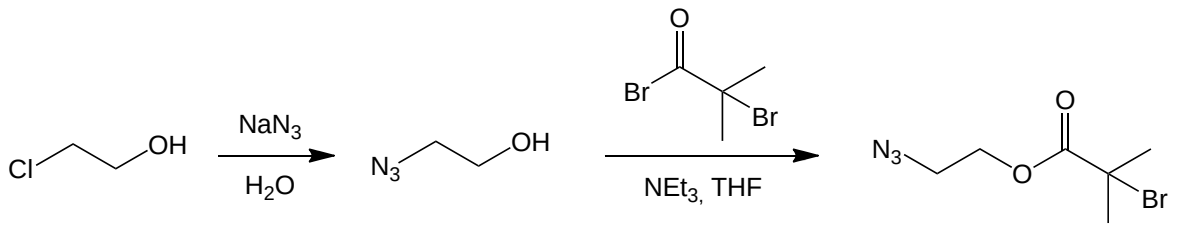

Fig. 4.29.: Synthesis of the ATRP-initiator 2-azidoethyl 2-bromo-2-methylpropanoate in two steps.

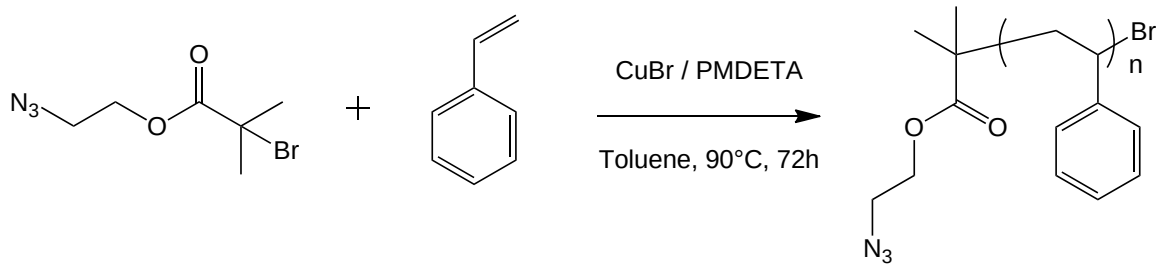

Fig. 4.30.: Synthesis of azide end-functionalized PS.

Eight different polymers bearing either alkyne or azide functionality have been synthesized either by post-functionalization of pre-synthesized polymers or by ATRP with functional initiators. Because of the different degrees of functionalization, a broad polymer library for the preparation of Janus particles was at hand (see Tab. 4.8).

Tab. 4.8.: Alkyne and azide functionalized polymers for the preparation of Janus particles.

Polymer	Monomer	Functionalization	Func. Groups / %	M_n / g/mol	PDI
Co-1-f	styrene	alkyne	11.1	32600	1.67
Co-2-f	MMA	azide	13.5	39600	1.75
Co-3-f	styrene	alkyne	5.6	32600	1.63
Co-4-f	MMA	azide	7.1	39500	1.72
Co-5-f	styrene	alkyne	3.0	35300	1.63
Co-6-f	MMA	azide	4.0	37900	1.67
ATRP-1	MMA	alkyne	0.3	29000	1.11
ATRP-2	styrene	azide	0.3	33200	1.17

4.2.3. Janus Particles

4.2.3.1. Non-functionalized Janus Particles

As reference samples, Janus particles were prepared from pure PS and pure PMMA by the SEED process from miniemulsion droplets (see Tab. 5.5). The amounts of polymers were chosen to have the same volume. In addition, the amount of surfactant was varied to

change the size of the miniemulsion droplets and hence the size of the particles.[51] TEM micrographs of the obtained Janus particles are shown in Fig. 4.31.

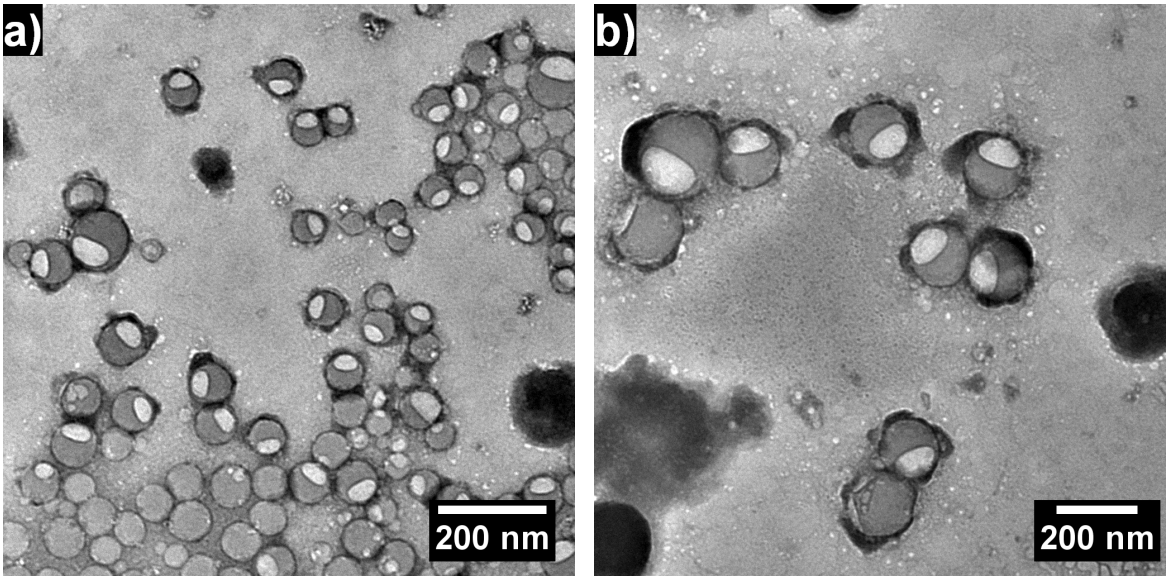

Fig. 4.31.: TEM micrographs of Janus particles prepared from pure PS and pure PMMA with amounts of 0.1 wt −% to 0.01 wt −% of surfactant.

Both polymers formed Janus particles under the experimental conditions and independently of the amount of surfactant. As expected, the particle size was controlled by the amount of surfactant.[51,85] Both faces of the Janus particles were almost equal in size, although the dark PS-face seemed to be slightly larger in the micrographs. A specific determination of the face's sizes is difficult for several reasons: The PS-face was enlarged by a layer of carbon, which was necessary to protect the particles from beam damage. Additionally, the way the particle is located on the TEM grid has pronounced effects on the determination of the morphology. As shown in Fig. 4.32, a classical Janus morphology is only observed if a particle is located in a very specific position. Once it is tilted relative to this position, one face will appear larger than the other one until no Janus morphology can be observed anymore at all. It is not clear whether the particles preferentially arrange with the PMMA side facing the TEM grid or whether there is no preference. As the evaporation of water from the droplet placed on the TEM grid is rather slow, a preferential orientation is likely. A preferential orientation also explains the relatively large amounts of purely "dark" particles in the lower part of Fig. 4.32a: When the PMMA face is orientated preferentially to the TEM grid, only the dark PS face is visible.

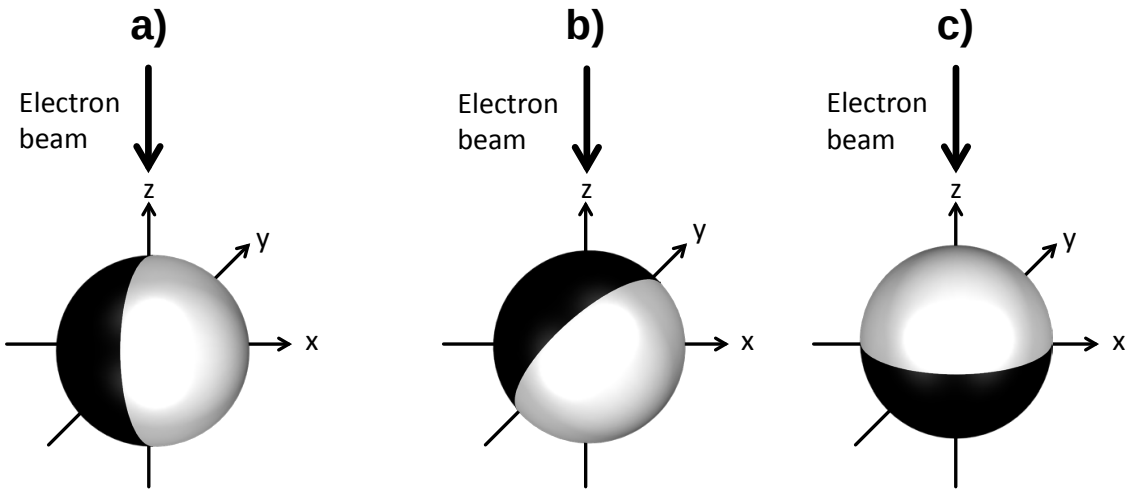

Fig. 4.32.: A Janus morphology can only be observed if the particle is located on the TEM grid as shown in (a). Once it is tilted (b), one face of the particle appears larger than the other one. If the particle is laying on the TEM grid with one face down (c), then no Janus morphology can be observed anymore.

4.2.3.2. Janus Particles Functionalized on Both Faces

The functional polymers prepared by post-functionalization and by ATRP were used to generate Janus particles, in which both faces were functionalized, i.e. one face was functionalized with alkyne groups and the other face with azide groups. In all cases, polymers with the same molar degree of functionality were used (see Tab. 5.5). TEM micrographs of the prepared particles are shown in Fig. 4.33. With the exception of the particles prepared from Co-f-1 and Co-f-2, all particles displayed a Janus morphology. The absence of the Janus morphology in the particles prepared from the mentioned copolymers is probably due to the high degree of functionalization of these copolymers. The copolymer Co-f-1 had a functionality of 11.1 % while the copolymer Co-f-2 had a functionality of 13.5 %. Apparently, this degree of functionalization was too high for phase separation in the droplets to occur during solvent evaporation, at least while both post-functionalized polymers were present in one droplet.

Changing the amount of surfactant from 0.1 wt −% to 0.01 wt −% had no significant effect on the particle morphology (see Fig. 4.34). However, as expected,[51,85] the particle diameter was significantly increased from roughly 100 nm to 200 nm. Again, all polymer pairs with the exception of Co-f-1 and Co-f-2 formed Janus particles which are functionalized with alkyne-groups on one face and azide-groups on the other face.

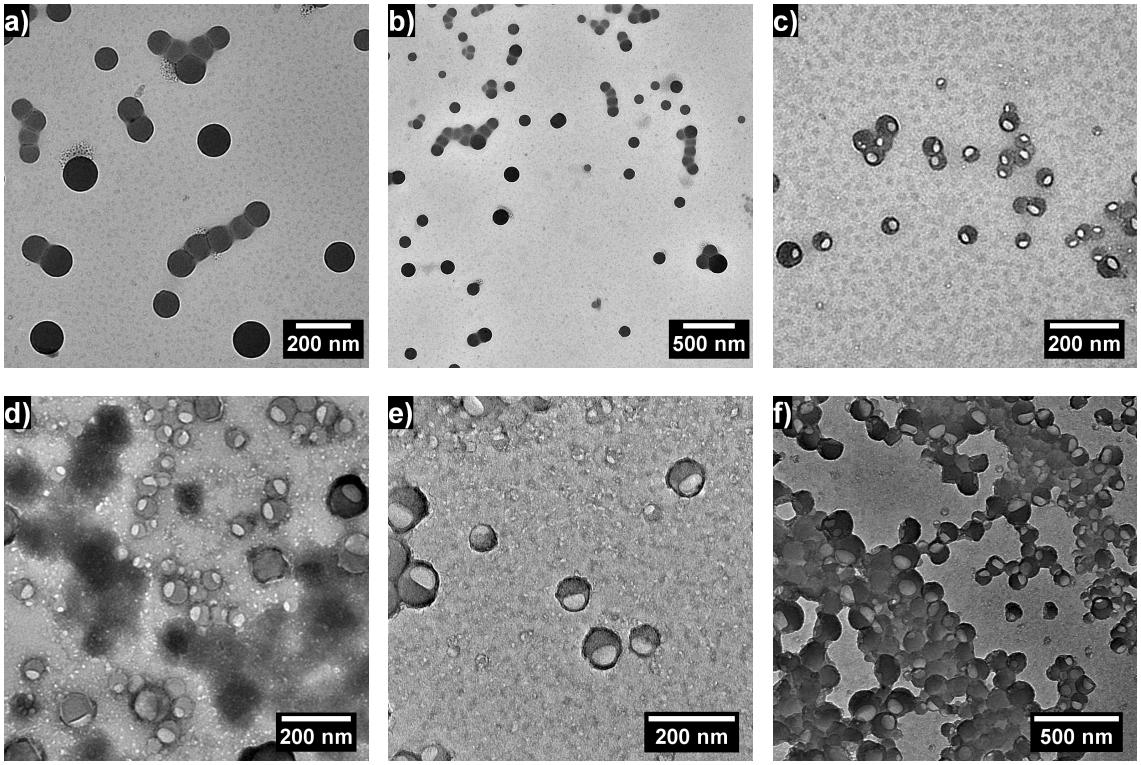

Fig. 4.33.: TEM micrographs of particles prepared from post-functionalized copolymers Co-f-1 and Co-f-2 (a, b), Co-f-3 and Co-f-4 (c), Co-f-5 and Co-f-6 (d) and from the polymers ATRP-1 und ATRP-2 (e, f) synthesized by ATRP. In all cases, a 0.1 wt −% solution of the surfactant was used. Only particles prepared from Co-f-1 and Co-f-2 did not show a Janus morphology.

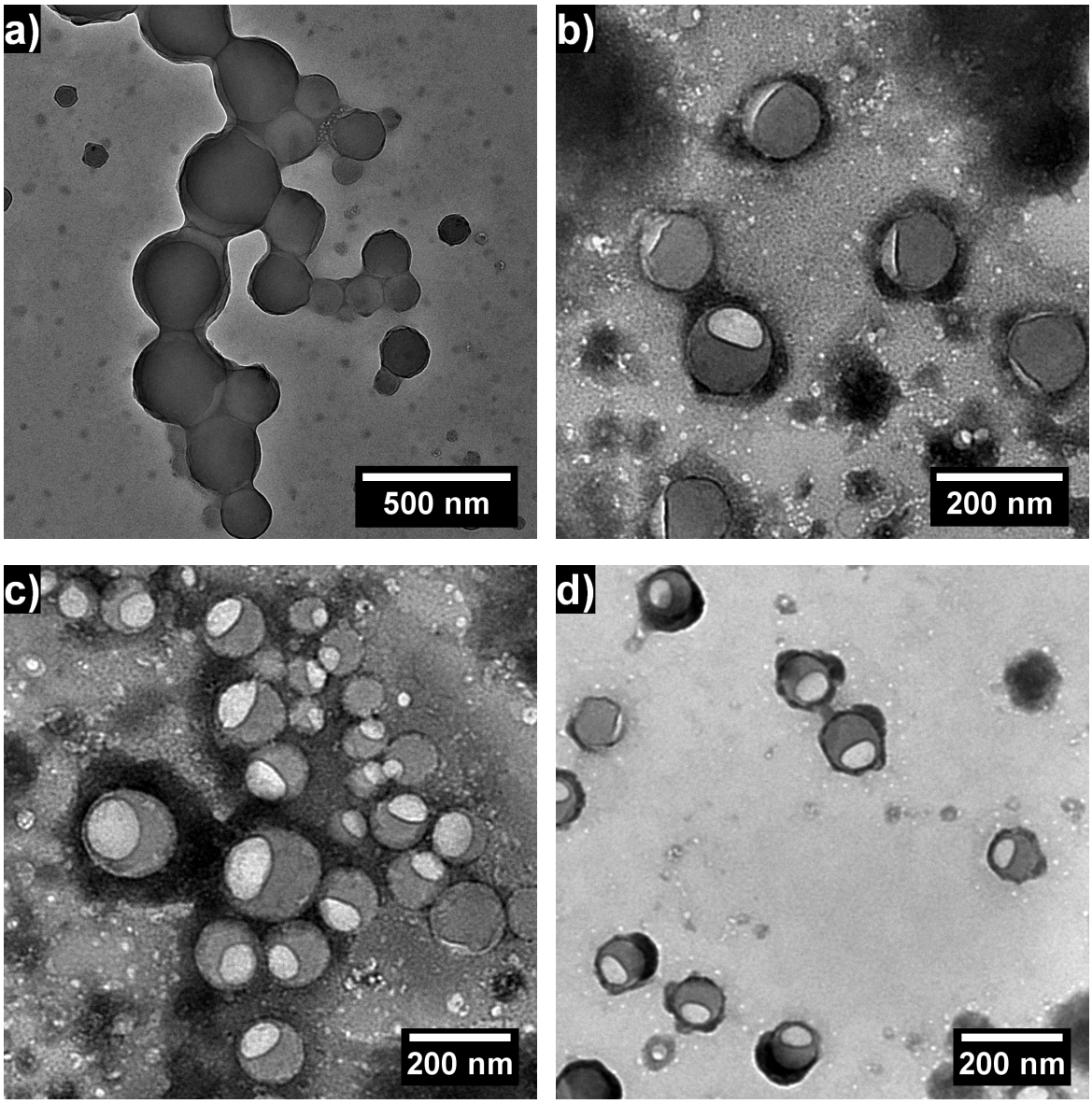

Fig. 4.34.: TEM micrographs of particles prepared from post-functionalized copolymers Co-f-1 and Co-f-2 (a), Co-f-3 and Co-f-4 (b), Co-f-5 and Co-f-6 (c) and from the polymers ATRP-1 and ATRP-2 (d) synthesized by ATRP. In all cases, a 0.01 wt −% solution of the surfactant was used. Only particles prepared from Co-f-1 and Co-f-2 did not show a Janus morphology.

4.2.3.3. Janus Particles Functionalized on one Face

Since not all functionalized copolymers formed Janus particles when mixed with another functionalized copolymer, the functionalized copolymers were also mixed with pure PS or pure PMMA to form Janus particles that are functionalized only on one face. As previously, the concentration of surfactant was varied from 0.1 wt −% to 0.01 wt −%. The obtained particles are shown in Fig. 4.35 and Fig. 4.36. In all cases, Janus particles were obtained. Therefore, it can be concluded that the phase separation was indeed hindered when two highly post-functionalized copolymers were used in previous samples.

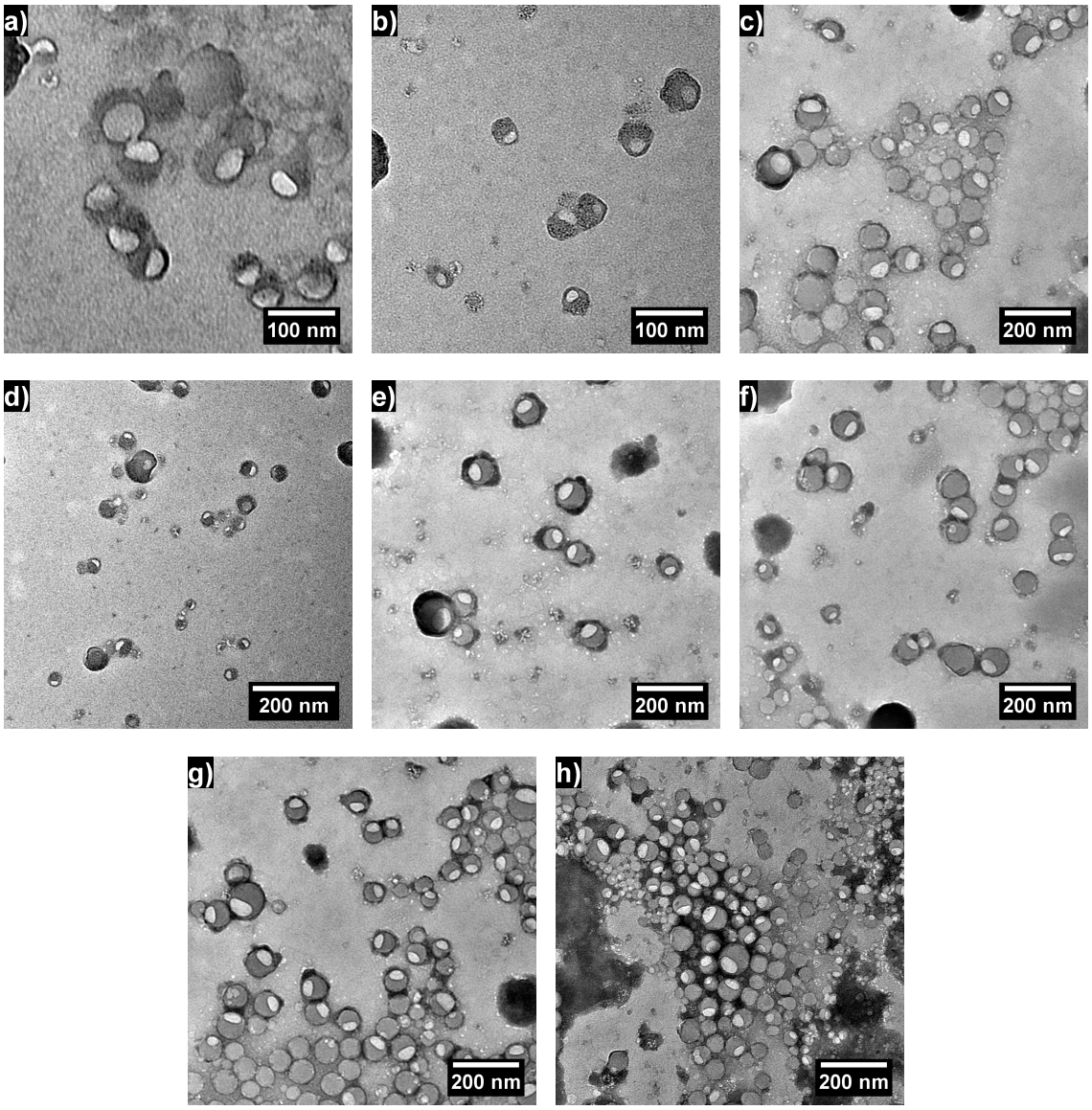

Fig. 4.35.: TEM micrographs of Janus particles functionalized on one face prepared from the post-functionalized copolymers Co-f-1 to Co-f-6 (a to f) or from the polymers ATRP-1 and ATRP-2 (g and h) prepared by ATRP and pure PS or PMMA. In all cases, a 0.1 wt −% solution of the surfactant was used. All particles showed a Janus morphology.

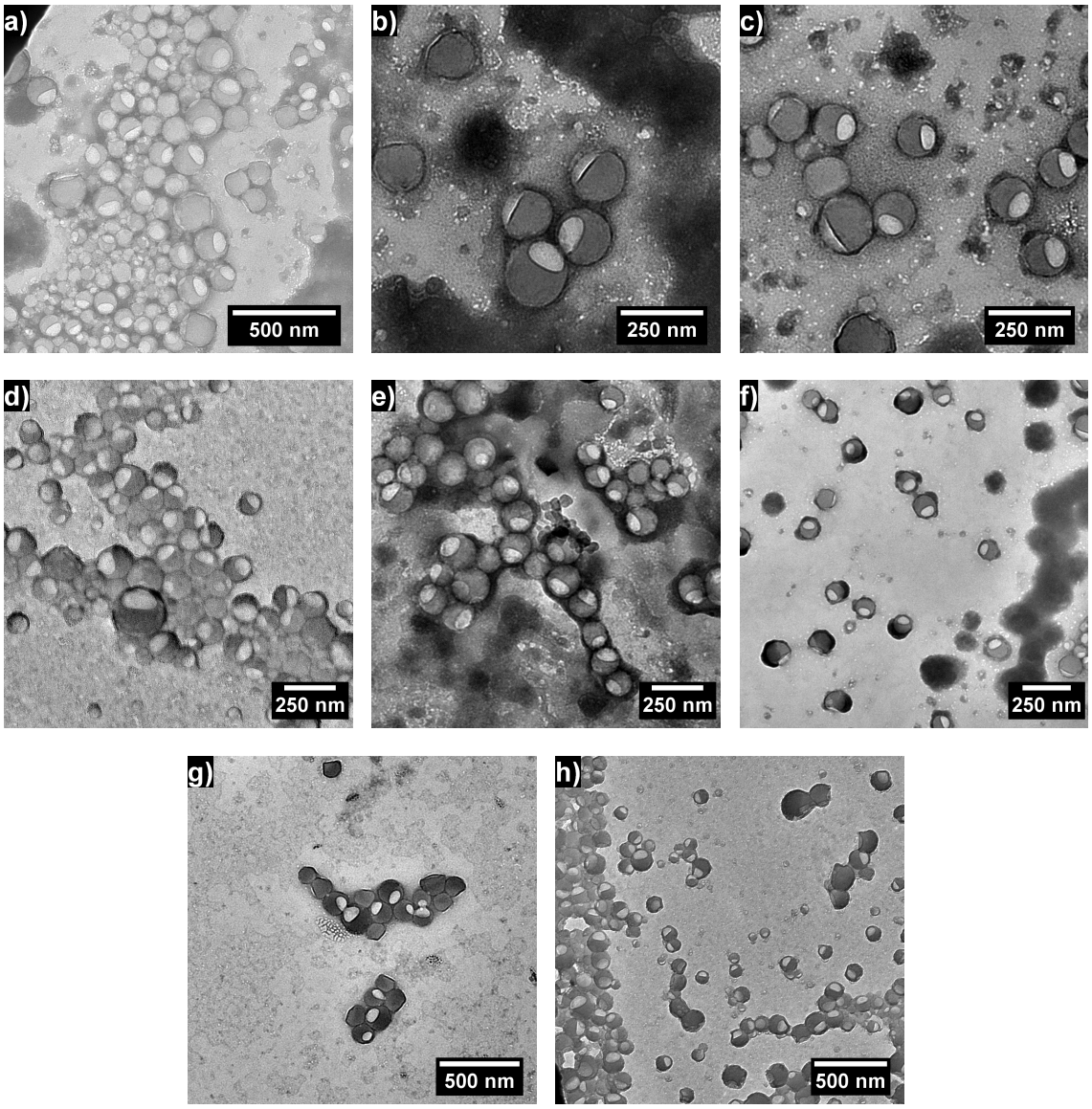

Fig. 4.36.: TEM micrographs of Janus particles functionalized on one face prepared from the post-functionalized copolymers Co-f-1 to Co-f-6 (a to f) or from the polymers ATRP-1 and ATRP-2 (g and h) prepared by ATRP and pure PS or PMMA. In all cases, a 0.01 wt −% solution of the surfactant was used. All particles showed a Janus morphology.

In conclusion, it was possible to generate a wide variety of Janus particles out of differently functionalized polymers. Both Janus particles in which one face was functionalized with alkyne and the other face with azide groups and particles in which just one face was functionalized with one of the mentioned groups were prepared. The size of the Janus particles could be varied by changing the amount of surfactant. However, the question whether the different degrees of functionality of the polymers are also transferred to the functionality of the Janus particles is still open. Therefore, it is necessary to quantify the functional groups on the surface of the Janus particles.

4.2.4. Determination of the Surface Functionalization

For the quantification of the functional groups on the surface of the Janus particles a suitable method needs to be found. Surface-sensitive techniques such as SEM-EDX or X-ray photoelectron spectroscopy (XPS) are neither accurate enough nor do they specifically detect only groups at the surface but also on the inside of the particles.[189,268] NMR and IR spectroscopy have a relatively low sensitivity,[264] which does not allow an accurate determination of the surface functionality. Therefore, an indirect method was chosen which is based on the reaction of the functional group with another molecule. After the reaction and appropriate cleaning procedures, the amount of the molecule bonded to the surface is quantified. In addition to the quantification, this method also allows to prove the activity of the functional groups for chemical reactions.

For the quantification of alkyne and azide groups on particle surfaces, two different methods have been established. The alkyne or azide groups can be reacted with carboxylic acids carrying azide or alkyne functionality by a click reaction. The amount of carboxylic acid can then be determined by particle charge detection (PCD) measurements.[269] The advantages of this method are the relatively easy sample preparation and the use of an established technique. However, the determination is also relatively slow, which prolongs the analysis of larger particle libraries. Additionally, the introduction of charges by the carboxylic acid can lead to aggregation and coagulation of the particles, thereby distorting the result. Another quantification method is the reaction of the clickable groups with fluorescent dyes. Subsequent to the reaction, the fluorescence can be measured to quantify the amount of functional groups. Both the presence of fluorescence by the attachment of a dye to the functional group as well as an enhancement of fluorescence due to a partaking of the triazole moiety in the chromophoric system can be used.[269,270] Fluorescence measurements have the advantage of being highly sensitive. In addition, the measurement is fast and can be automated. However, the price of suitable clickable fluorophores is relatively high and a suitable cleaning procedure after the reaction to remove any unreacted dye in order not to distort the quantification is needed.

4.2.4.1. Synthesis of Clickable Dyes

Because of the high price of commercially available clickable dyes and their limited solubility in water, clickable dyes were synthesized from rhodamine B (see Fig. 4.37). Rhodamine B was chosen as a starting material because it is soluble in water as well as in polar organic solvents such as THF, because it has a relatively high quantum yield of 0.31 in THF[271] and because it can be functionalized easily by reacting the carboxylic acid group with an alcohol.[269,272]

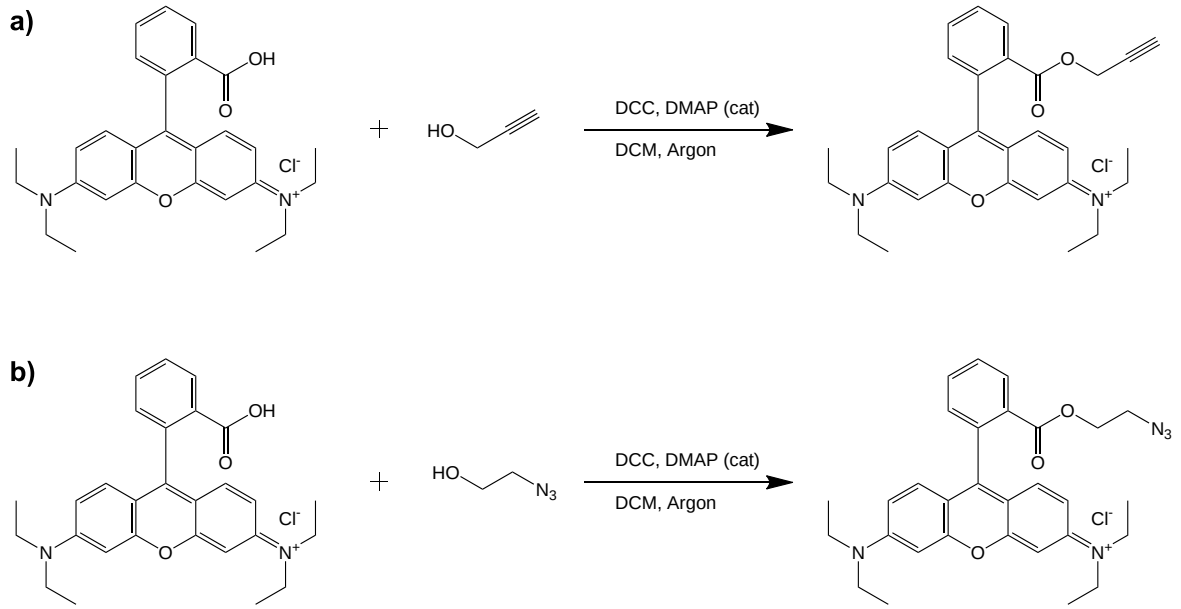

Fig. 4.37.: Synthesis of alkyne (b) and azide (b) functionalized rhodamine derivatives.

The synthesis was done by a Steglich esterification reaction with a functional alcohol in dry dichloromethane for both alkyne and azide functionality. *N*,*N*'-dicyclohexyl carbodiimide (DCC) was used as coupling reagent and the reaction was catalyzed with dimethyl aminopyridine (DMAP) to suppress the unwanted 1,3-rearrangement of the O-acyl intermediate to a N-acyl urea.[273] The yield of both reactions was approximately 50 % and the successful functionalization could be proven by NMR and IR spectroscopy. Neither the solubility in water nor the fluorescence properties of rhodamine B were changed by the reaction as can be seen in Fig. 4.38. Therefore, the prepared dyes are suitable to determine the amount of functional groups on Janus particles by fluorescence quantification.

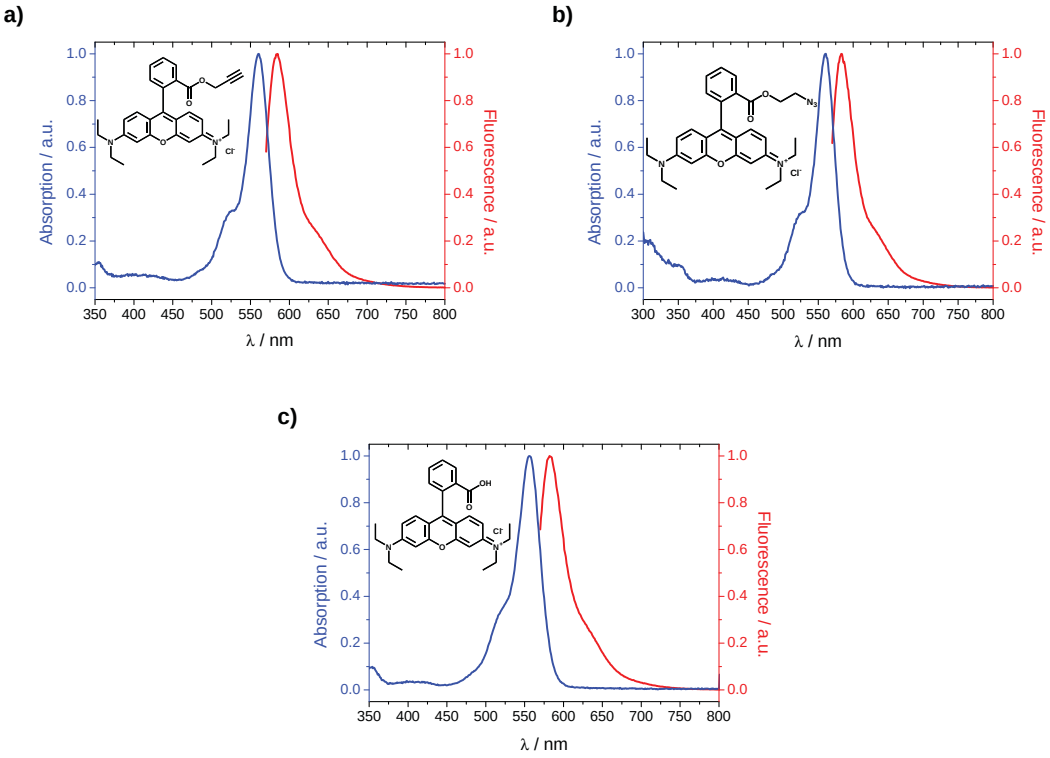

Fig. 4.38.: Absorption- and fluorescence spectra of alkyne- (a), azide- (b) and non-functionalized rhodamine B (c).

4.2.4.2. Quantification of the Clickable Groups

For the quantification of functional groups on the Janus particles by fluorescence detection, the azide-functionalized dye or the alkyne-functionalized dye was added to a dispersion of alkyne- or azide-functionalized Janus particles, respectively. Only particles that were functionalized on one face but not on the other one were used for two reasons. Firstly, they showed a Janus morphology independently of the copolymer. Secondly, by using particles with only one functionalized face, intra-molecular click reactions between particles and between the dye molecules could be excluded that would otherwise distort the quantification. To facilitate the click-reaction, copper sulfate and ascorbic acid were employed to obtain reactive copper(I)-species. The ligand *N*,*N*,*N*',*N*',*N*''-pentamethyl diethylenetriamine (PMDETA) was used to stabilize these species in the aqueous dispersion. After the reaction, the unreacted dye was removed by repeated centrifugation. The details of this process can be found in Section 5.2.4.2. Since the scattering of the particles might have influenced the fluorescence measurements and hence the quantification, the particles were dissolved. THF was used as solvent since it is a good solvent for both the polymers and the pure dyes. Furthermore, it was necessary to measure the fluorescence intensity of the pure dye at different concentrations to form a calibration curve. The calibration curves for both dyes are shown in Fig. 4.39. Both curves showed a linear trend over a wide range of concentrations. However, starting at

a concentration of over 2.5×10^{-5} mol/L the fluorescence intensity was not linear anymore. This observation is in excellent agreement with the data of Fikry et al.,[271] who showed that this behavior is based on energy transfer without radiation and due to the formation of dimers and higher aggregates. Therefore, the calibration was only valid for rhodamine-concentrations below 2.5×10^{-5} mol/L, which corresponded to an intensity of roughly 25 000 a.u. in the chosen experimental setup.

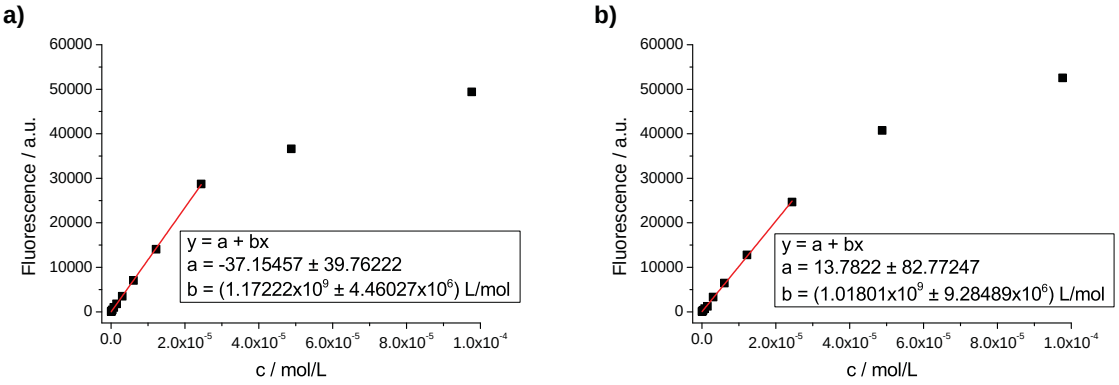

Fig. 4.39.: Calibration data for the quantification of the functional groups on the surface of the Janus particles. The fluorescence intensity in dependence of the concentration of alkyne-functionalized rhodamine B is shown in a) while the fluorescence intensity in dependence of the concentration of azide-functionalized rhodamine B is shown in b).

From the measured fluorescence intensity of the particles dissolved in THF and the fit data from the calibration curves, the average number of the alkyne- or azide groups N_{groups} on the surface of one particle was calculated with the formula

$$N_{groups} = \frac{\pi \cdot N_A \cdot D^3 \cdot (I_{measured} - a)\,(\rho_{PS} + \rho_{PMMA})}{12 \cdot b \cdot m_{Janusparticles}} \qquad \text{Eq. 4.8}$$

In this equation, N_A stands for the Avogadro constant, D for the average hydrodynamic diameter of the particles, $I_{measured}$ for the measured fluorescence intensity and $m_{Janusparticles}$ for the mass of the Janus particles obtained after the centrifugation steps used to remove unreacted dye. Furthermore, a and b are the fit parameters of the calibration curves and ρ_{PS} and ρ_{PMMA} are the densities of PS and PMMA, respectively. For these, values of 1.05 g/cm^3 for PS and of 1.19 g/cm^3 for PMMA were used.[274] In a similar manner, the density of alkyne and azide groups per surface unit on one face of one Janus particles was calculated by

$$\frac{N_{groups}}{surface\ unit} = \frac{N_A \cdot D \cdot (I_{measured} - a)\,(\rho_{PS} + \rho_{PMMA})}{6 \cdot b \cdot m_{Janusparticles}} \qquad \text{Eq. 4.9}$$

There are of course several assumptions that are used in these equations, which will be explained and rectified below:

- All functional groups on the surface have reacted with a dye.
    - Because of the relatively low functionality of the particles, the use of the dyes in excess and the long reaction time, all groups should have reacted. In the literature, similar reaction times were used at similar conditions.[269] Additionally, a sample measured after 24 h reaction time showed the same results as a sample measured after the regular reaction time of 48 h.
- The fluorescence properties of the dye were not changed by the reaction.
    - Neither the alkyne nor the azide groups are part of the chromophoric system before or after the click reaction because there are CH_2-spacers between the clickable groups and the chromophoric system. Therefore, the click-reaction should not have any influence on the fluorescence intensity. As the particles were dissolved in THF and the calibration was also done in THF, the environment of the dyes should not have any influence as well.
- The particles were "perfect" Janus particles, i.e. both faces have the same volume.
    - By using different amounts of polymer, equal volumes of the Janus faces should have been obtained, which was confirmed by the TEM micrographs in the limits of the technique (see Section 4.2.3).
- The densities of the copolymers in the particles were the densities of pure PS and pure PMMA.
    - Because of the relatively low degree of functionalization, the assumption of copolymers having the same density as their majority component homopolymers was a rather good assumption.
- The free non-reacted dye was removed completely by the purification.
    - Since the particles were centrifuged and redispersed until there was no fluorescence in the supernatant anymore, the free dye has been removed completely. To eliminate the possibility of adsorption of dye molecules on the particles or to quantify their amount, reference particles consisting of pure PS and PMMA were prepared.

The reference Janus particles prepared from pure PS and pure PMMA were treated as described in Section 5.2.4.2. Subsequently, the absolute number of adsorbed rhodamine molecules and therefore the number of "functional groups" as well as their density was determined. The results are shown in Tab. 4.9.

In all cases, only a small number of dye molecules were irreversibly adsorbed on the particle surface. While as expected, more dye molecules adsorbed on larger particles, the density of "functional groups" is similar on all particles. It is slightly higher in case of alkyne-functionalized rhodamine being used.

Tab. 4.9.: Absolute number of "functional groups" and the density per square nanometer of the "functional groups" calculated therefrom on non-functionalized Janus particles with particle diameter D.

Sample	tested for	D / nm	Groups per Particle	Groups / nm^{-2}
Quant-1	alkyne	96	9	6.51×10^{-4}
Quant-2	azide	96	14	9.83×10^{-4}
Quant-3	alkyne	220	28	3.71×10^{-4}
Quant-4	azide	220	68	9.02×10^{-4}

All samples of functionalized Janus particles showed a significantly higher fluorescence than the non-functionalized particles. The fluorescence increase already proved that the alkyne and azide groups on the surface can still undergo click reactions and could be used for further reactions. The number of functional groups on the functionalized Janus particles was calculated according to Eq. 4.8. The results are shown in Tab. 4.10. The particles contained 66 to 7497 functional groups on their surface. The large spread is also visible if the values for the different samples are plotted (see Fig. 4.40). Here, a trend can already be observed: The number of functional groups decreased with decreasing polymer functionality. Furthermore, the particle size was an extremely important factor in the number of groups per particle. Therefore, the absolute number of functional groups was not a good measure to compare and discuss the different trends.

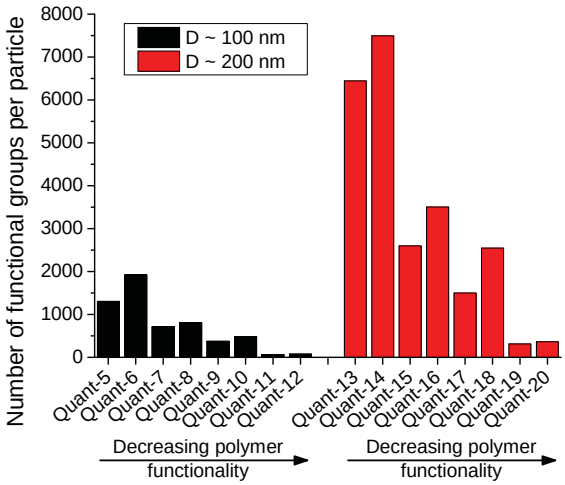

Fig. 4.40.: Absolute number of functional groups on the surface of the prepared Janus particles.

It is more useful to compare the density of the functional groups per surface unit calculated by Eq. 4.9. This number is independent on the particle size, hence its values are used for further discussions. The obtained values are shown in Tab. 4.10 and in Fig. 4.41. The density of functional groups per square nanometer was not dependent on the diameter. Indeed, it was about the same for particles with a diameter of roughly 100 nm (Quant-5 to Quant-12)

and for particles with a diameter of roughly 200 nm (Quant-13 to Quant-20). Because of the independence of the functional density on the diameter, each group had enough space to react with the relatively bulky dye molecule, which in turn implies that reactions to the surface were not limited by spatial restrictions.

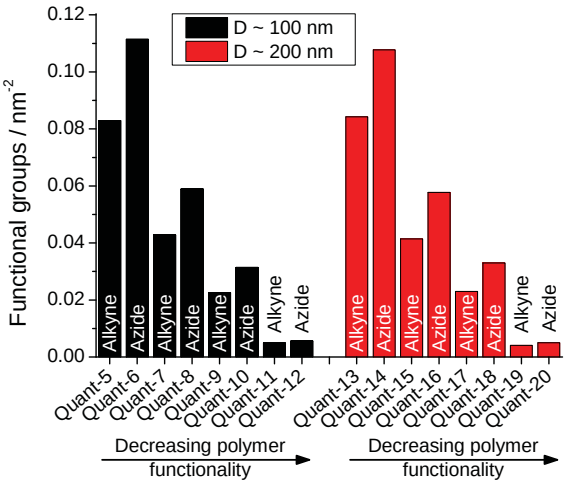

Fig. 4.41.: Amount of functional groups per square nanometer on one face of the prepared Janus particles.

Furthermore, there was a steady decrease of functionality of the particles with a decrease of the functionality of the polymers used. The number of functional groups per square nanometer for the samples prepared from the post-functionalized copolymers was reduced roughly by half, which corresponds very well with the decrease of functionalized groups in the different copolymers used to prepare the Janus particles. To study this more closely and to discover possible trends, the measured density of functional groups per square nanometer was normalized to the degree of functionality of the polymers used. The number of functional groups per square nanometer thus obtained is henceforth called Ψ. The obtained results are shown in Tab. 4.10 and displayed in Fig. 4.42.

The functional density on the surface of the particles was still independent on the particle size after normalization to the polymer functionality. Furthermore, the normalized density of the functional groups Ψ was almost constant for the Janus particles prepared from post-functionalized copolymers. Once the polymers prepared by ATRP were used, the normalized functional density was significantly increased. A possible explanation for this is the differences in the chemical structure of the functionalization of the copolymers and the ATRP-polymers. In the copolymers, the functional groups were attached to a non-polar benzyl group while in the ATRP-polymers the functionality was located at an ester group, which is much more polar. The ester groups could have oriented themselves preferentially to the surface of the droplets during solvent evaporation, leading to a higher surface functionalization. Such an effect was observed in nanoparticles consisting of poly(styrene)-*block*-poly(methyl

methacrylate) (PS-*b*-PMMA). Here, a preferential orientation of the PMMA-domains to the interface of the particles with the surrounding aqueous environment took place.[51] Possibly a similar effect was also responsible for the slightly higher normalized density of azide groups compared to alkyne groups, which could be found for all Janus particles prepared from the copolymers. The difference was quite small but present in all samples and could be attributed to the higher polarity of the azide group in comparison to the alkyne group.

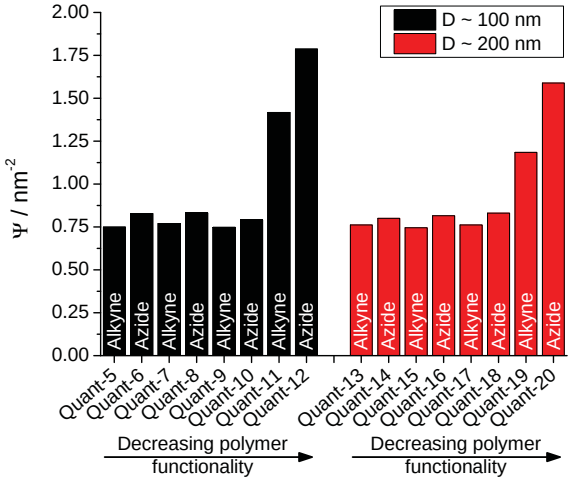

Fig. 4.42.: Amount of functional groups per square nanometer on one face of the prepared Janus particles normalized to the degree of polymer functionality.

Although both micro- and nano-sized particles with clickable groups on the surface have already been prepared,[269,270,275–281] there are only very few reports about the quantification of these groups. Kasuya et al. quantified azide groups on nanoparticles using a dansyl alkyne,[270] while Baier et al. quantified both alkyne and azide groups on nanocapsules by PCD and fluorescence measurements.[269] Although these systems are quite different from the one studied here, a comparison is useful for a qualitative evaluation of the quantification method applied here.

Kasuya et al. prepared azide functionalized nanoparticles by post-functionalizing nanoparticles bearing chloride groups with sodium azide.[270] They obtained azide groups densities of $0.21\,\mathrm{nm}^{-2}$ and $0.15\,\mathrm{nm}^{-2}$ while using 5.5 % and 5.3 % chloride functionalized monomer in respect to the comonomer styrene. Therefore, the normalized functional group density Ψ had values of $3.81\,\mathrm{nm}^{-2}$ and $2.83\,\mathrm{nm}^{-2}$. These values are significantly higher than those of the post-functionalized copolymers or the ATRP-polymers studied here, which is due to the polymerization technique used by Kasuya et al. They applied a "shot-growth"-technique for the particle generation, i.e. the functional monomer was added four hours after the initiation of the surfactant-free emulsion polymerization. As a result, a significantly higher functional group density than expected from the molar ratios of the reagents was obtained. Therefore, a comparison of the results presented here with the work by Kasuya et al. is impossible.

Tab. 4.10.: Absolute number and type of the functional groups as well as their absolute normalized density Ψ per square nanometer on one face of the prepared Janus particles.

Sample	Functionality	D / nm	Groups per Particle	Groups / nm^{-2}	Ψ / nm^{-2}
Quant-5	alkyne	100	1305	8.29×10^{-2}	0.75
Quant-6	azide	105	1919	1.11×10^{-1}	0.83
Quant-7	alkyne	103	709	4.28×10^{-2}	0.77
Quant-8	azide	93	807	5.89×10^{-2}	0.83
Quant-9	alkyne	103	373	2.26×10^{-2}	0.75
Quant-10	azide	99	479	3.15×10^{-2}	0.79
Quant-11	alkyne	93	66	4.91×10^{-3}	1.42
Quant-12	azide	93	76	5.62×10^{-3}	1.79
Quant-13	alkyne	221	6445	8.42×10^{-2}	0.76
Quant-14	azide	211	7497	1.08×10^{-1}	0.80
Quant-15	alkyne	200	2598	4.14×10^{-2}	0.75
Quant-16	azide	197	3506	5.77×10^{-2}	0.82
Quant-17	alkyne	204	1500	2.30×10^{-2}	0.76
Quant-18	azide	222	2546	3.30×10^{-2}	0.83
Quant-19	alkyne	221	315	4.10×10^{-3}	1.18
Quant-20	azide	216	366	5.00×10^{-3}	1.59

Baier et al. prepared azide functionalized nanocapsules by a polycondensation reaction on the interface of oil droplets dispersed in water. A diol functionalized with two azide groups was combined with toluene diisocyanate (TDI) to form a polyurethane nanocapsule. The amount of azide groups on the surface was subsequently quantified. From the ratio of the monomers and the dual azide functionality it can be concluded that every monomer unit is bearing one azide unit. Such a functionalization corresponds to a copolymer that has been functionalized to 100 %, e.g. to a much higher degree than it was done in this work. Azide group densities between $0.67\,nm^{-2}$ to $0.78\,nm^{-2}$ were measured, which would thus correspond to $\Psi = 0.67\,nm^{-2}$ to $\Psi = 0.78\,nm^{-2}$. These values are extremely close to the Ψ-values of the copolymers reported herein. Although this accordance of values must be viewed cautiously in view of the higher values for the ATRP-polymers and the simplified calculation, it can still be concluded that the results qualitatively agree with each other.

4.2.5. Conclusions and Outlook

Copolymers were synthesized and subsequently post-functionalized with azide or alkyne groups. Both groups were introduced quantitatively. By varying the amount of the post-functionalizable comonomer, the amount of alkyne and azide groups in the copolymers was varied. In addition, polymers bearing exactly one alkyne or azide group at the beginning of

the polymer chain were synthesized from functional initiators in an ATRP reaction. Thus, a large library of functional polymers was prepared.

Janus particles were prepared from the preformed polymers by the SEED process. If copolymers with a high degree of functionalization were used, no Janus particles were obtained due to insufficient phase separation between the polymers. However, once copolymers with lower degrees of functionalization were used, dually functionalized-particles were obtained. If pure PS or PMMA were used to form the other face of the Janus particle, the use of highly functionalized copolymers was also possible and hence Janus particles with one functionalized face were obtained.

The clickability of the surface was proven by the reaction with clickable rhodamine based dyes. These dyes were further used to quantify the amount of functional groups on the surface of the Janus particles. The degree of functionalization of the polymers used to prepare the Janus particles was found to be mirrored in the functionality of the surface. Moreover, the quantification results agreed well with results obtained by other groups, hence verifying the applicability of the quantification method. Thus, Janus particles with a controllable density of clickable groups on the surface could be prepared – click-chemistry was married to Janus particles.

The prepared Janus particles are an interesting platform for the subsequent functionalization with other molecules bearing azide- or alkyne groups. As the click-reaction is bio-orthogonal, bio molecules might also be selectively clicked to the surface without loss of bio-functionality. Further possible applications are the preparation of colloidal polymers[282] by inter-particular click reactions or the self-assembly of such particles by the click reaction.

4.3. Stimulus-Responsive Nanocapsules[1]

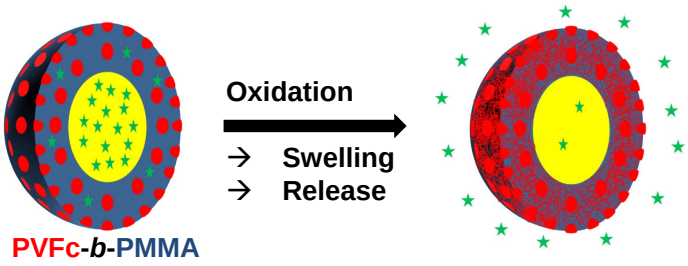

Redox-responsive block copolymer nanocapsules composed of a poly(vinylferrocene)-*block*-poly(methyl methacrylate) (PVFc-*b*-PMMA) shell and a hydrophobic liquid core were prepared in water. The shell of the nanocapsules displayed a patchy structure with poly(vinylferrocene) (PVFc) patches with sizes of (25 ± 3) nm surrounded by PMMA. The functional nanopatches were selectively oxidized, thereby influencing the colloidal morphology and introducing polar domains in the nanocapsule shell. The transition from hydrophobic to hydrophilic in the redox-responsive nanopatches was advantageously used to release a hydrophobic payload encapsulated in the core by an oxidation reaction.

4.3.1. Motivation

Besides Janus particles, capsules have received widespread attention in recent years due to their projected application as drug-delivery vehicle.[14–17] These capsules can be divided in micron-sized and nano-sized capsules. Micron-sized capsules are less interesting for applications in drug delivery because their cell uptake is rather non-existent, but they are very promising candidates for self-healing applications,[284] as are nanocapsules.[10–13] Independently of their use, nanocapsules are viewed as carrier system which should release their payload upon a certain stimulus. Therefore, the use of stimulus-responsive materials allows fabricating capsules that are also stimulus-responsive and hence are able to release their payload upon a trigger.

Each of the numerous different possible stimuli for different materials have their advantages and disadvantages. There are materials that are responsive to biological stimuli such as the presence of glucose[16,285–288] or enzymes.[285,289–295] Field-responsive materials can react to stimuli such diverse as ultrasound,[285,296–300] light,[285,301–304] electric fields,[285,305,305,306] or

[1] This section is based on the publication "Patchy Nanocapsules of Poly(vinylferrocene)-Based Block Copolymers for Redox-Responsive Release" by Roland H. Staff, Markus Gallei, Markus Mazurowski, Matthias Rehahn, Rüdiger Berger, Katharina Landfester and Daniel Crespy, published in 2012 in *ACS Nano*, volume 6 on pages 9042 to 9049.[283] Reprinted with permission. Copyright 2012 American Chemical Society.

magnetic fields.[285,307,308] Other important stimuli are the pH[17,309] and the temperature[310] of the surrounding medium as well as the oxidation potential of a material.

The oxidation potential is crucial for some reactions in nature to happen.[311,312] A balanced concentration of redox-active species is necessary in plants and animals since these species can be both beneficial, such as for redox signaling[313] and detrimental, such as for oxidative stress in cells.[314,315] The disulfide bond can be cleaved by a reduction and this reversible reaction plays an important role in the conformation, and therefore the activity, of many proteins. This principle was transferred to synthetic materials with disulfide bonds to yield mesoporous silica,[316,317] hollow particles,[318] or liposomes[319] with redox-responsive release. Other approaches for the preparation of redox-responsive materials based on quinone derivatives,[320] supramolecular chemistry[321] or the transition from sulfides to sulfoxides and sulfones upon oxidation in polymers were also proposed.[322]

Another interesting redox couple is the ferrocene/ferrocenium pair, as it was already well explored for biosensor applications[323–328] and for redox-responsive self-healing in host-guest polymers.[329] Furthermore, ferrocene-containing polymers attracted a lot of attention in the past decade due to their promising combination of redox, mechanical, semi-conductive, photophysical, optoelectronic and magnetic properties.[330–336] Since Manner's discovery of the living ring-opening polymerization of ansa-metallocenophanes[337–339] leading to polymers with ferrocenes in the polymer main chain, and the improved anionic polymerization of vinylferrocene and ferrocenyl methyl methacrylates leading to laterally bonded ferrocene polymers,[340,341] well-defined and high molecular weight ferrocene polymers with interesting properties were synthesized. However, there is up to now no report on functional nanocapsules based on a material with ferrocene units.

Compared to non-crosslinked micelles that are subjected to unimer/micelle equilibrium, nanocapsules have the advantage of keeping their structural integrity. A redox-responsive nanocapsule should allow the triggered diffusion of substances encapsulated in the core upon a redox stimulus. Such a system represents one of the most challenging tasks in colloid science since the triggered release must be coupled with the maintenance of the structural integrity and colloidal stability of the nano-containers. One promising answer to overcome this issue is the preparation of patchy nanocapsules with responsive patches located in the nanocapsule shell. Patches present in the capsule shells could act as channels for the diffusion of substances encapsulated in the core while keeping the structural integrity of the shell. Whereas patchy nanocapsules from block copolymers were reported in the literature, they presented neither functionality nor responsive behavior.[51] Therefore, the preparation of patchy nanocapsules from a redox-responsive block copolymer with control of the release of guest-encapsulated substances from their cores upon selective oxidation of the nanopatches is a challenging and intriguing task. In addition, such a nanocapsule is a highly complex colloid in terms of the definition given in Chapter 1.

4.3.2. Preparation of Patchy Colloids

For the preparation of nanocapsules and nanoparticles by the SEED process, the redox-responsive PVFc-*b*-PMMA block copolymer (see Fig. 4.43) prepared by the group of Dr. Markus Gallei at the TU Darmstadt was employed. The block copolymer was dissolved in dichloromethane containing a small amount of HD which is a non-solvent for the copolymer and mixed with an aqueous solution of SDS by stirring and ultrasonication. For the preparation of nanoparticles, no HD was added. After evaporation of the dichloromethane, opaque yellowish dispersions of nanocapsules were obtained. These dispersions were used later for the oxidation experiments.

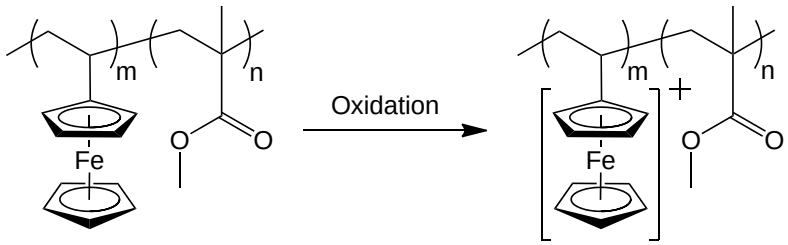

Fig. 4.43.: Nanocapsules consisting of the oxidizable block copolymer PVFc-*b*-PMMA were prepared by the SEED process.

The average diameter of the nanocapsules was about (236 ± 110) nm, as measured by DLS. It is well known that the size of the colloids can be adjusted by the amount of surfactant in the system.[51,85] However, in the case of nanocapsules, great care has to be taken in order not to induce acorn-like or hemispherical morphologies (also see Section 2.3). The absence of these morphologies can be ensured by limiting the amount of surfactant in the emulsions to avoid the stabilization of the HD/aqueous interface.[51] The SEM and TEM micrographs evidenced the core-shell structure of the nanocapsules (see Fig. 4.44): In the SEM pictures some capsules appeared to be collapsed under the preparation or the observation conditions. The nanocapsules were found to display a patchy structure (see Fig. 4.44) that could be clearly detected by TEM. The presence of nanopatches is verified by the SEM micrographs which revealed heterogeneities on the nano-scale on the nanocapsule's surface (see Fig. 4.44a-c). Here, no treatment with metal oxide vapors was needed due to the inherent contrast between the PMMA and the PVFc phases caused by the presence of iron in the latter, darker phase. The patches with a size of (25 ± 3) nm originated from the microphase separation between the PVFc and PMMA building blocks in the polymer shell. Similar structures in nanoparticles have been obtained for weakly phase-separating PS-*b*-PMMA,[51] poly(styrene)-*block*-poly(4-vinylpyridine) (PS-*b*-P4VP) block copolymers,[126,130] blends of poly(styrene)-*block*-poly(butadiene) (PS-*b*-PBD) with PS,[116] and poly(styrene)-*block*-poly(ferrocenylethylmethylsilane) (PS-*b*-PFEMS) block copolymers,[342] but in monolithic nanoparticles. Remarkably, the patches of PVFc presented

herein were created in the shell of the nanocapsules, which is an unprecedented case of patchy colloids.

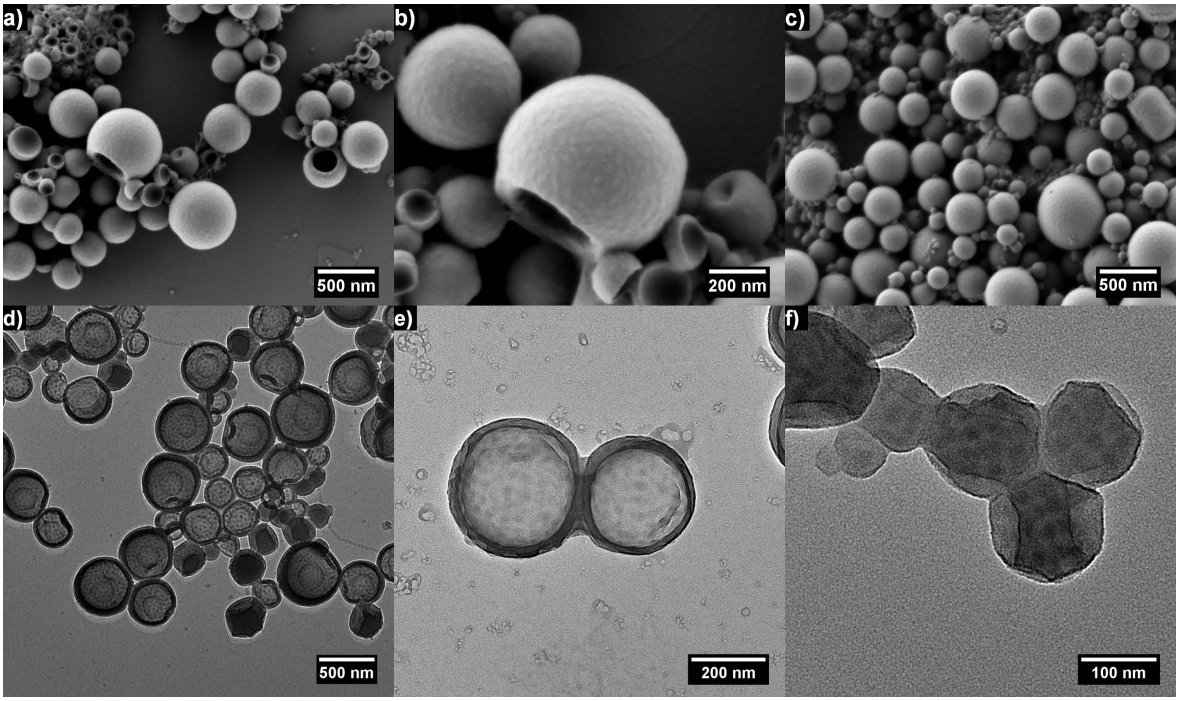

Fig. 4.44.: SEM micrographs of dialyzed nanocapsules (a-b), of nanoparticles (c) and TEM micrographs of nanocapsules (d-e) and nanoparticles (f). In TEM, the microphase separation is evidenced by the presence of dark domains (PVFc block) in the PMMA surrounding matrix. The TEM micrographs of dialyzed nanoparticles showed the same patchy structure as for nanocapsules. Conversely to the nanocapsule's case, the PVFc domains can only be observed on smaller particles, as the mass-contrast outweighs the thickness-contrast for smaller nanoparticles but not for larger nanoparticles.

XPS measurements were employed to verify that the vinylferrocene moieties remained stable upon preparation of the nanocapsules. As the amount of iron in the nanocapsules is rather low, only signals with very low intensities appeared in the survey spectrum (see Fig. 4.45a). The XPS measurements of the Fe2p photoelectron emissions were hence performed for 24 h. The shape of the Fe2p area (see Fig. 4.45b) indicated the presence of ferrocene (Fe^{II} at 707.5 eV) and a weak signal for ferricenium (Fe^{III} at 710.5 eV).[343,344] The ferricenium in the capsules probably appeared during the measurement. Because of the presence of ferrocene units in the functional nanopatches, the nanocapsules are a promising candidate for oxidation reactions.

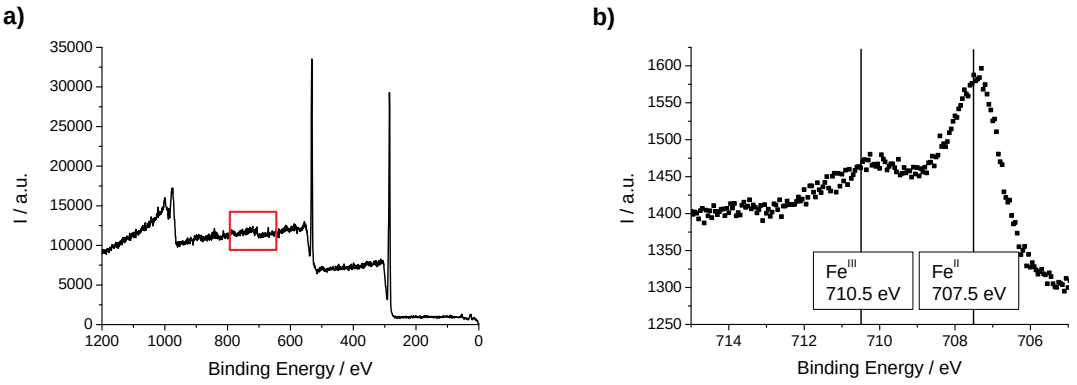

Fig. 4.45.: XPS survey spectrum of nanocapsules (a), in which the Fe2p area enlarged in (b) is shown in red.

4.3.3. Selective Oxidation of the PVFc Nanopatches

It is well known that PVFc can be oxidized to poly(vinylferrocenium) ($PVFc^+$) by a variety of oxidants.[345,346] As oxidants H_2O_2 and $KMnO_4$ were employed because they are water-soluble and did not influence the colloidal stability of the dispersions. $KMnO_4$ offers the additional advantage of allowing visual monitoring of the reaction by the control of the color. Indeed, the color of the dispersion changed from purple to brown in the first hour after addition of the oxidant solution. After oxidation, the average hydrodynamic diameter of the nanocapsules measured by DLS increased from 236 nm to 310 nm when treated with H_2O_2 and to 282 nm upon oxidation with $KMnO_4$ (see Fig. 4.46a). The increase of the hydrodynamic diameter is attributed to the oxidation reaction: upon oxidation, the PVFc domains are converted to $PVFc^+$ domains that are hydrophilic and therefore swollen in water. HPLC was employed to follow the change of polarity of the block copolymer upon oxidation. A shift to lower elution volume was observed after oxidation of the nanocapsules (see Fig. 4.46b) and can be attributed to the higher polarity of the block copolymer with ferrocenium units compared to the original block copolymer. As expected, the shift is irrespective of the oxidant.

In parallel, significant structural changes appeared on the surface of the nanocapsules after the oxidation (see Fig. 4.47 for nanocapsules and Fig. 4.48 for nanoparticles). In order to verify that the structural changes are not introduced by the vacuum of the SEM or by drying effects, SFM experiments[347] under atmospheric conditions (50 % humidity, room temperature) were performed (see Fig. 4.47). Whereas the untreated nanocapsules displayed only weak surface irregularities with length scales comparable to the size of the block copolymer domains, the surface of the capsules oxidized with H_2O_2 displayed indents smaller than 10 nm in depth after oxidation (see Fig. 4.47b). Both size and distances between the indents corresponded to the size and distance between the PVFc domains were observed before oxidation. When the nanocapsules were oxidized with $KMnO_4$, there were no holes but patches presenting outgrowths of 10 nm to 20 nm in height on the surface (see Fig. 4.47c).

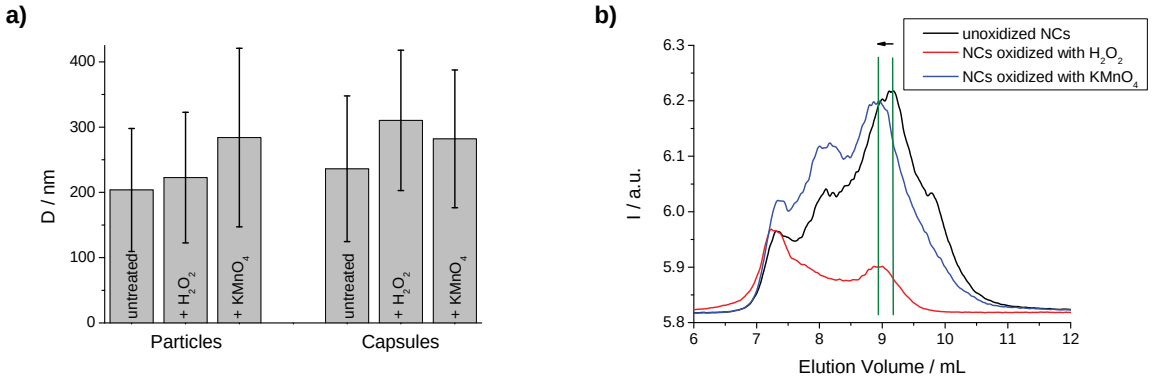

Fig. 4.46.: Upon oxidation, there was a significant increase in size of both nanoparticles and nanocapsules as measured by DLS (a). The HPLC measurements showed that the elution volume of the oxidized block copolymer nanocapsules is shifted to a more polar regimen (b), indicating an oxidation of the PVFc side groups to $PVFc^+$ side groups.

The distribution of size of such outgrown patches was broader than the distribution of size of the indents, as were the distances between them. However, it is still fairly comparable with the size and distances between the initially non-oxidized PVFc domains.

The proposed mechanisms to explain the structural difference of the patches after oxidation depend on the ability of the oxidant to diffuse in the shell. Upon oxidation, the PVFc domains swelled more or less, depending on the oxidant used. Firstly, due to its ionic character, MnO_4^- is expected to diffuse less rapidly than H_2O_2 in the shell. The $PVFc^+$ is therefore mainly created on the surface. Since the PVFc that is buried in the patches cannot react anymore, the $PVFc^+$ chains swell in water pushing the polymer shell outward. The volume is only locally extended and outgrowths are observed after drying the sample. On the contrary, H_2O_2 diffuses faster in the shell, thus allowing a spatial rearrangement of the $PVFc^+$ chains. As a spherical shape is thermodynamically favored compared to the formation of outgrowths, the rearrangement of the $PVFc^+$ chains leads to a slight increase of the whole diameter of the nanocapsules. Upon drying, the $PVFc^+$ chains collapse, leaving empty spaces in the previously swollen channels that appear as holes in the SEM micrographs. Secondly, the MnO_4^- may interact with the $PVFc^+$ domains after the initial oxidation has taken place, preferably oxidizing ferrocene units spatially very close to $PVFc^+$ side groups, and thus enhancing the local charge density. In contrast, H_2O_2 as an non-polar molecule may oxidize the PVFc side groups more evenly, yielding more uniform and less pronounced surface structures. Conversely, the enhanced charge density after oxidation with $KMnO_4$ may result in locally highly swollen $PVFc^+$ domains, yielding outgrowths. In addition, it is also known that the counter-ion can has a significant impact on the morphology and volume of poly(ferrocenyl dimethyl silane) (PFDMS) thin films upon oxidation,[348] therefore, a similar mechanism might be present here. Control experiments were performed by synthesizing monolithic nanoparticles

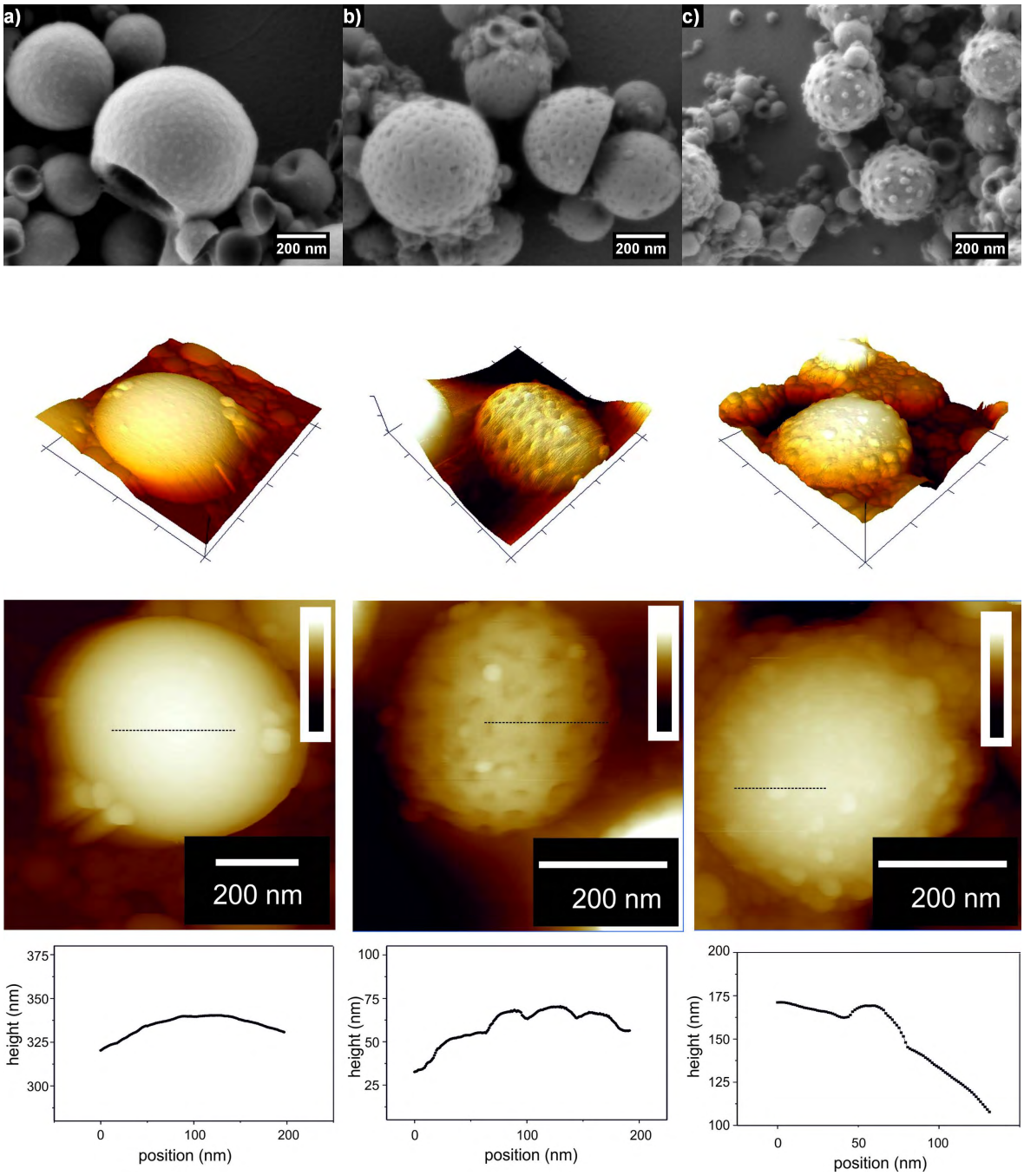

Fig. 4.47.: The surface morphology of dialyzed PVFc-*b*-PMMA nanocapsules changed from slightly rough before oxidation (a) to surfaces presenting indents (b) or outgrowths (c) after oxidation with H_2O_2 or $KMnO_4$, respectively. For clarity, the SFM height images are displayed twice: first row in 3D perspective view with back-light illumination and in the second row as standard color-scale images. The *z*-scale bar is 750 nm (untreated), 200 nm (H_2O_2 treated), and 500 nm ($KMnO_4$ treated), respectively. In these images, the black dotted line highlights the topography profiles, which are presented in the bottom row. The untreated sample showed a much smoother surface compared to the oxidated nanocapsules. From such profiles, the range of the depths of the indents and the outgrowths were determined.

instead of nanocapsules of PVFc-*b*-PMMA. The nanoparticles showed similar changes of their morphology upon oxidation (see Fig. 4.48), indicating no significant differences in the oxidation ability of the two morphologies. To further verify the proposed mechanism for the occurrence of outgrowths and indents, $FeCl_3$ was also used as oxidant. As expected, outgrowths but no indents were detected by SEM and SFM (see Fig. 4.49), as in the case of the oxidation with $KMnO_4$.

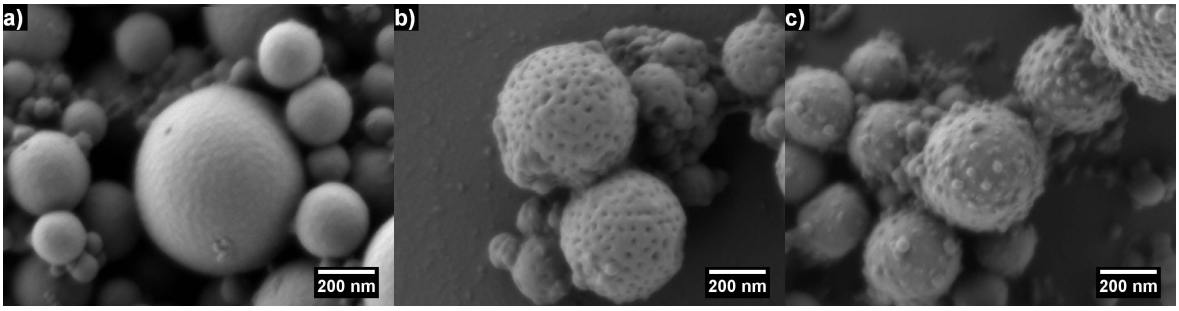

Fig. 4.48.: Before oxidation, the dialyzed PVFc-*b*-PMMA nanoparticles had a relatively smooth surface (a). After oxidation with H_2O_2, their morphology presented indents (b) whereas outgrowths appeared on the surface upon oxidation with $KMnO_4$ (c), very similar to those observed on nanocapsules.

As MnO_2 is produced by the oxidation reaction with $KMnO_4$, the outgrowths could also consist of precipitated nano-crystals of MnO_2. Therefore, it was necessary to verify that the metal oxide was not present in the outgrowths. The surface composition of the nanocapsules was analyzed with SEM-EDX (see Fig. 4.50a). No peaks for manganese could be detected even when various voltages were applied, and the spectra of the materials before and after oxidation were very similar. Thus, MnO_2 is not present in the outgrowths of the nanocapsules oxidized with $KMnO_4$, either because it was removed during the dialysis or because the low quantities produced are not enough to form nano-crystals.

Finally, reference samples with nanocapsules and nanoparticles of PMMA homopolymer were prepared by the same procedure to verify the stability of PMMA against oxidation. As expected, no increase in the hydrodynamic diameter was observed for the PMMA colloids after oxidation (see Fig. 4.50b). Furthermore, SEM micrographs showed no changes of the morphology on nanocapsules or nanoparticles (see Fig. 4.51). Therefore, the observed changes in the PVFc-*b*-PMMA nanocapsules and nanoparticles are not caused by a partial oxidation or degradation of the PMMA matrix. They occurred solely by the conversion of the ferrocene moiety to the ferrocenium moiety upon oxidation and the resulting change in polarity of the polymer. The hydrophobic to hydrophilic transition of the patches upon oxidation therefore represents a promising strategy to fabricate hydrophilic patches on a hydrophobic colloid surface.

To investigate the reversibility of the transition, the nanoparticles and nanocapsules were reduced by the addition of ascorbic acid after oxidation by H_2O_2, $KMnO_4$, and $FeCl_3$. The

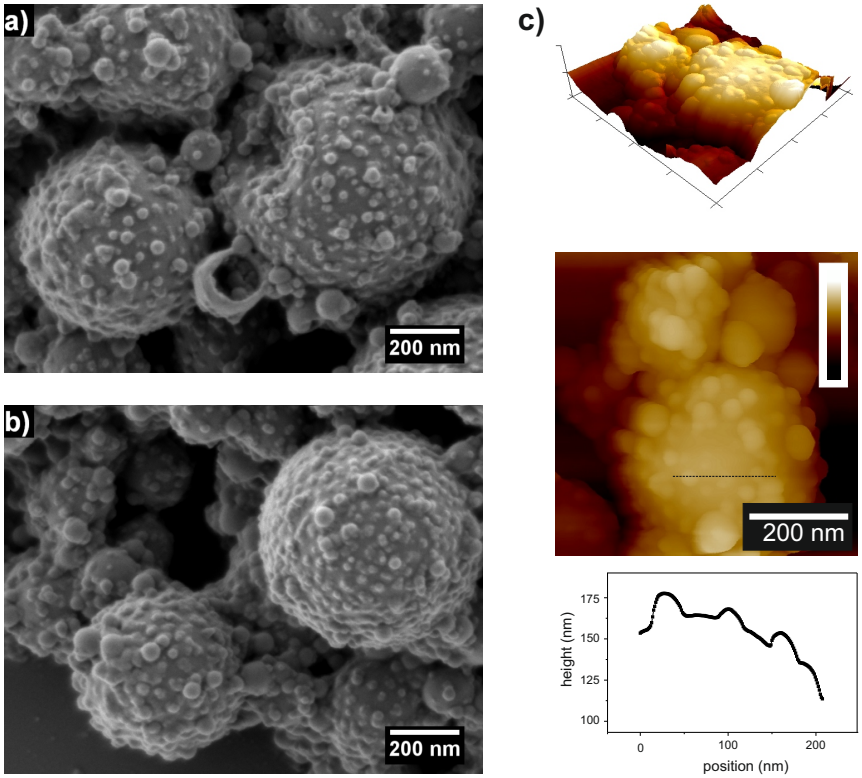

Fig. 4.49.: Both nanocapsules (a) and nanoparticles (b) displayed outgrowth-structures after oxidation with $FeCl_3$ in SEM micrographs. These outgrowths were also visible in the SFM height images (c): 3D perspective view with back-light illumination, standard color-scale images, and topography profile of the nanocapsules measured by SFM after oxidation with $FeCl_3$.

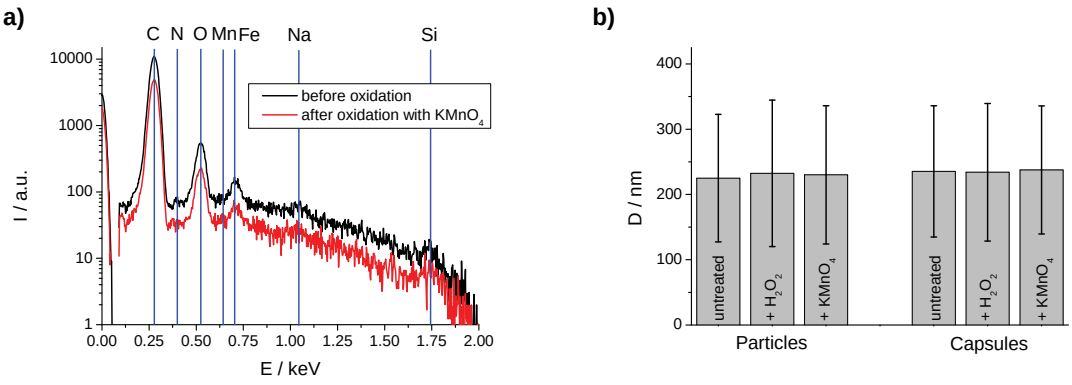

Fig. 4.50.: SEM-EDX spectra of a single dialyzed nanocapsule before and after oxidation with $KMnO_4$ (a). There were no traces of manganese in the spectrum, indicating that the observed outgrowths are not due to deposited MnO_2. Nanocapsules and nanoparticles of PMMA show no increase in diameter upon oxidation (b).

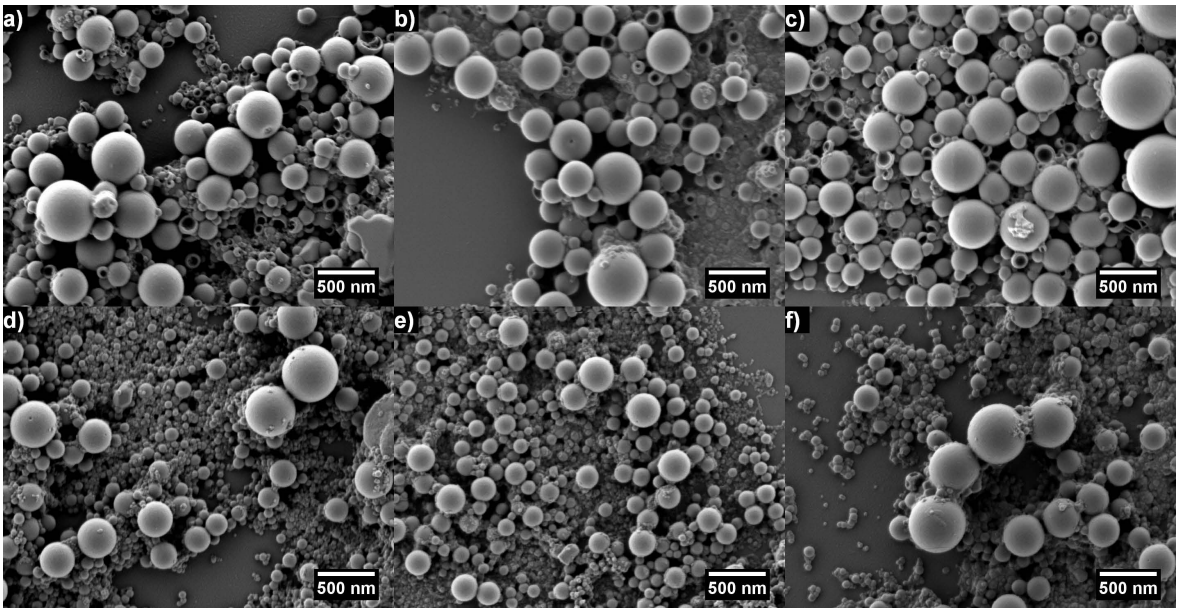

Fig. 4.51.: SEM micrographs of dialyzed PMMA nanocapsules (first row) and nanoparticles (second row) before (a, d) and after oxidation with H_2O_2 (b, e) and $KMnO_4$ (c, f). There are no changes in morphology.

color of the dispersions changed back to their original states; from brown to orange with $KMnO_4$ and from slightly greenish to orange with $FeCl_3$; indicating that reduction had taken place at least to some extent. However, no significant changes in the diameter or in the morphology of the nanocapsules or nanoparticles could be detected after the reduction with ascorbic acid, as shown by SEM micrographs (see Fig. 4.52).

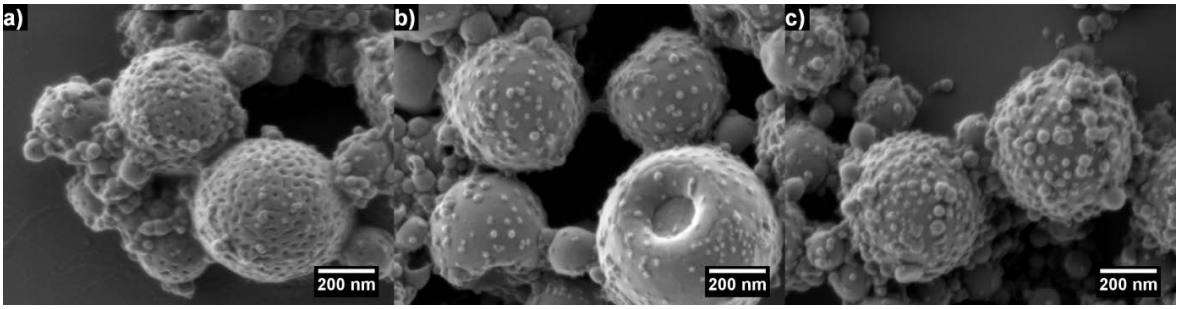

Fig. 4.52.: The indents and outgrowths observed after oxidation with H_2O_2 (a), $KMnO_4$ (b), and $FeCl_3$ (c) remained identical after a subsequent reduction of the nanoparticles and nanocapsules by ascorbic acid in SEM micrographs.

Theses observations were confirmed by cyclic voltammetry (CV) measurements on nanocapsules consisting of PVFc-*b*-PMMA deposited on an indium tin oxide (ITO) slice, which were conducted by Dr. Markus Gallei at the TU Darmstadt. Indeed, the asymmetric shape of the curves (see Fig. 4.53) indicated that the oxidation of the PVFc block was possible, but the reduction was partially hindered. Thus, the oxidized ferrocene moieties in a dense confinement could not be fully reduced again. After several cycles the signal intensity decreased due to

better solubility of the PVFc block copolymer in acetonitrile and the formation of a film on the electrode surface.

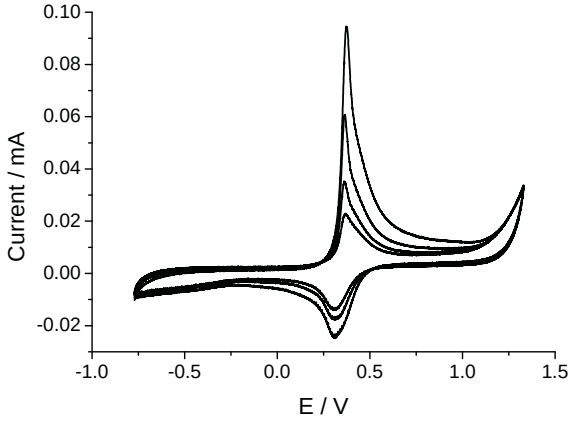

Fig. 4.53.: Cyclic voltamogram of PVFc-*b*-PMMA nanocapsules deposited on an ITO slice.

4.3.4. Redox-Responsive Release of Pyrene

As demonstrated before, accessible responsive patches are present in the nanocapsule shells. This unique feature could be advantageously used to release a molecule present in the core of the nanocapsules upon an oxidation stimulus. Pyrene was chosen as a model for a hydrophobic substance since it is commonly employed as a fluorophore to monitor the release kinetics from compartmentalized objects.[349] Since the colloids scatter light strongly and the strong absorption of light by $KMnO_4$, the release of pyrene was not measured in the dispersion. Instead, the colloids were mixed with a solvent used to extract the pyrene released after oxidation. Cyclohexane was chosen because it is a good solvent for pyrene, it has no significant influence on the morphology of the polymer shell and it is immiscible with the nanocapsule dispersion, thus allowing a fast separation. The chosen extraction method is milder than centrifugation, which can damage the nanocapsules, thereby artificially increasing the amount of released pyrene. Samples were withdrawn from the reaction mixture at certain intervals of time t after addition of the oxidation reagents at $t = 0\,\text{min}$. A significant increase in fluorescence intensity with oxidation time of the nanocapsules with H_2O_2 or $KMnO_4$ was observed (see Fig. 4.54a). The increase is indicative for a release of pyrene from the nanocapsules, in contrast to the almost constant intensity detected for the non-oxidized sample. The non-absence of a fluorescence signal for the untreated sample is due to pyrene absorbed on the surface of the nanocapsules and/or to slow leaking from the nanocapsules. However, the stimulus-responsive behavior of the release is evidenced by the large increase in intensity upon addition of the oxidants as schematized in Fig. 4.55. The release upon oxidation with H_2O_2 is more significant than the release upon oxidation

with $KMnO_4$. The difference is related to the aforementioned remarks about the different diffusion of the oxidants and hence different loci of oxidation. A larger number of ferrocene units converted to ferrocenium (H_2O_2) allows an enhanced diffusion of pyrene outside the nanocapsules, whereas a more local oxidation ($KMnO_4$) causes a less pronounced release of pyrene. Control experiments performed with nanoparticles instead of nanocapsules showed an overall much lower release (see Fig. 4.54b). In addition, in this case the release upon oxidation with $KMnO_4$ is more pronounced than the release with H_2O_2. This difference could be due to different oxidation depths of $KMnO_4$ and H_2O_2, which are not important in nanocapsules as the capsule shell is relatively thin. However, in monolithic particles, the oxidation depth might be an important factor in the release kinetics. Thus, the results indicated a morphology-, time-, and oxidant-dependent release of pyrene from the patchy nanocapsules and nanoparticles.

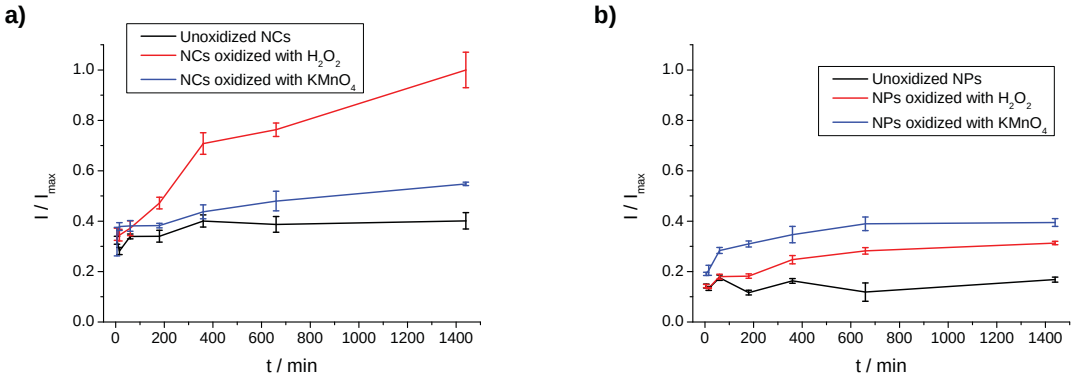

Fig. 4.54.: Release kinetics of pyrene from PVFc-*b*-PMMA patchy nanocapsules (a). The fluorescence intensity of the oxidized nanocapsules increased with time, indicating a release of pyrene, whereas the intensity of the non-oxidized nanocapsules remained almost constant. The release behavior of nanoparticles is similar to the one observed for nanocapsules, only with a far lower magnitude (b).

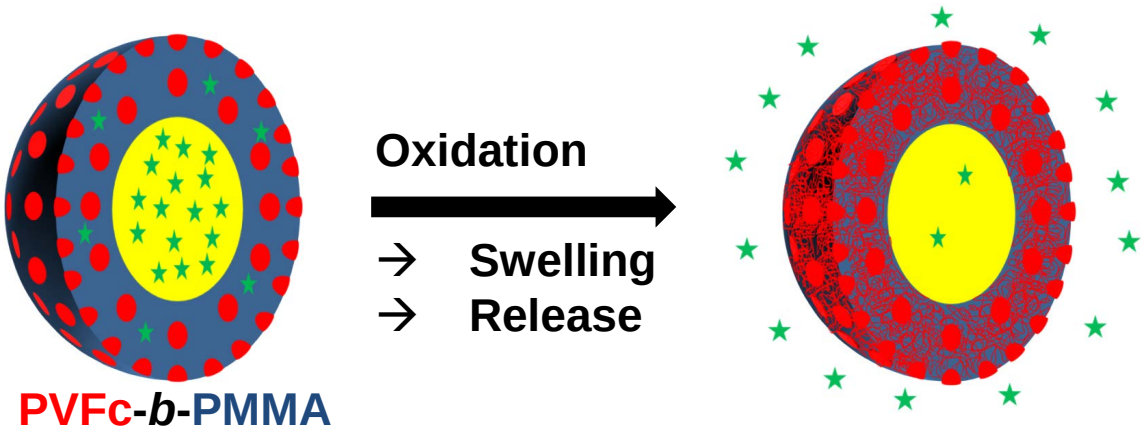

Fig. 4.55.: Schematic showing the oxidation-responsive release of the hydrophobic payload from the PVFc-*b*-PMMA patchy nanocapsules.

4.3.5. Conclusions and Outlook

Patchy nanocapsules with the functional block copolymer PVFc-*b*-PMMA as shell were prepared from droplet templates of aqueous emulsions. The nanopatches were composed of PVFc blocks distributed in the PMMA matrix as the result of a microphase separation between both polymer blocks. The PVFc nanopatches could be selectively oxidized, thereby inducing a transition from a purely hydrophobic patchy object to a hydrophobic object with swollen hydrophilic nanopatches. The topography of the nanocapsules surface after oxidation was dependent on the nature of the oxidizing agent. The hydrophobic to hydrophilic transition of the PVFc nanopatches was advantageously utilized to release a hydrophobic payload upon selective oxidation of the nanopatches.

Driven by the early concept of multicompartment polymer micelles envisioned by Ringsdorf,[350,351] the self-assembly of multicompartment objects is currently the object of intensive research because of the possibility to create unprecedented structures.[352–355] In this respect, the hydrophobic nano-objects with hydrophilic patches are also promising building blocks for the self-assembly of patchy structures.

In addition, the reported synthetic procedure represents a unique strategy to prepare functional patchy nano-objects. Various functional block copolymers could also be employed to target other types of stimulus-responsive release. Here, the use of more than one stimulus is an ambitious goal since having two or even more possible stimuli in one material significantly enhances its complexity. Therefore, the following section will deal with stimuli-responsive capsules capable of release.

4.4. Stimuli-Responsive Nanocapsules

Nanocapsules not only responsive to one but also to two stimuli were prepared by the SEED process. The capsules displayed a response to acidification and to oxidation or temperature changes depending on the chemical composition of the block copolymers constituting the capsular shell. The double responsiveness was advantageously used to release an encapsulated payload from the capsules or to hinder the release. In addition, it was possible to selectively release a material upon one stimulus but not upon the other stimulus.

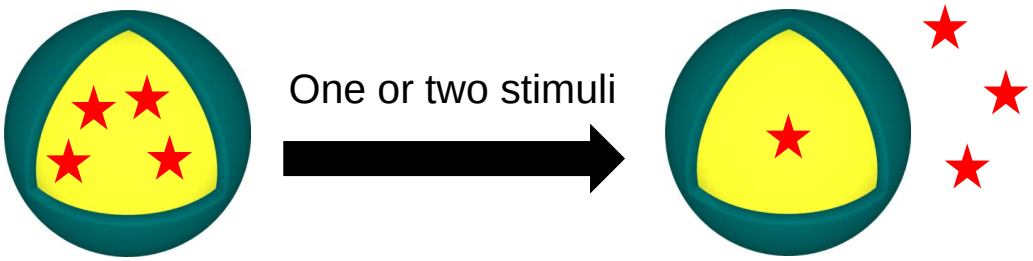

Release behavior upon stimulus application										
PVFc-*b*-P2VP		oxidation		pH		PS-*b*-PDMAEMA		pH		
		no	yes	basic	acidic			basic	neutral	acidic
core responsiveness	inert	☹	😐	☹	🙂	temperature	low	☹	😐	🙂
	pH	☹	☹	☹	🙂		interm.	☹	😐	🙂
	Oxid.	☹	😐	☹	☹		high	☹	☹	🙂

🙂 strong release

😐 intermediate release

☹ weak release

4.4.1. Motivation

Polymer-based drug-delivery systems have attracted much attention and research efforts since the pioneering work of Ringsdorf et al.[356,357] Soon, complex and multicompartmentalized materials arose as this extremely complex and demanding topic was studied in more detail.[350,358] While these materials are often responsive to one stimulus,[14–17,309,359–363] materials with more than one stimulus are also of great interest as they allow for a finer tuning of the material response and additional properties of the system.[364,365] Most of the time, soft and non-crosslinked micellar systems are employed for drug delivery applications. Compared to these systems, nanocapsules have the advantage of having a higher structural integrity. In addition, hydrophobic polymers such as PS or PVFc can be used to build the shell of the nanocapsules. In contrast to hydrogels[360,366,367] that usually release a hydrophilic compound upon one or two stimuli,[303,304] hydrophobic nanocapsules can release hydrophobic drugs or self-healing materials, for example.

Although numerous dual- or multi-responsive materials have been synthesized,[364,365] there are relatively few capsular systems that are capable of releasing their payload upon application of more than one stimulus. Microcapsules responsive to pH-change and to reduction were prepared by Gu et al. on the basis of *tert*-butyl methacrylate and bis(2-methacryloyloxyethyl) disulfide.[368] However, no release was shown for these capsules. Soft microcapsules responsive to pH-change and to reduction were also prepared by Gao et al. from a polysaccharide alginate dialdehyde derivative and cystamine dihydrochloride,[369] while Basset et al. synthesized polyelectrolyte capsules responsive to pH-change and to temperature.[370] Polyelectrolytes also formed the basis of the soft microcapsules prepared by Shi et al. which showed release upon pH-change or temperature increase.[371] Finally, hollow nano-gels responsive to pH and temperature changes were prepared by Chiang et al.[372] and by Xing et al.[373,374] who both demonstrated release from these systems.

Another interesting feature of polymer nanocapsules would be a stimuli-selective dual release. The release of two encapsulated components can be more beneficial than the release of just one component as shown by Richardson et al.[375] by delivering two growth factors in the same nanocontainer instead of just one. Due to the interplay of the growth factors, the growth effect was enhanced compared to the delivery of the growth factors by different nanocontainers. The release of just one encapsulated component upon one stimulus and of another encapsulated component upon another stimulus is a very challenging task. The concept of stimuli-selective release is shown schematically in Fig. 4.56 and was realized by Wijaya et al. who released two different DNA oligonucleotides from two different gold nanorods by using two different laser wavelengths.[376] Another approach based on double emulsions was taken by Hu et al. who liberated one hydrophilic and one hydrophobic component from the same capsule upon heating the capsule by a magnetic field.[377]

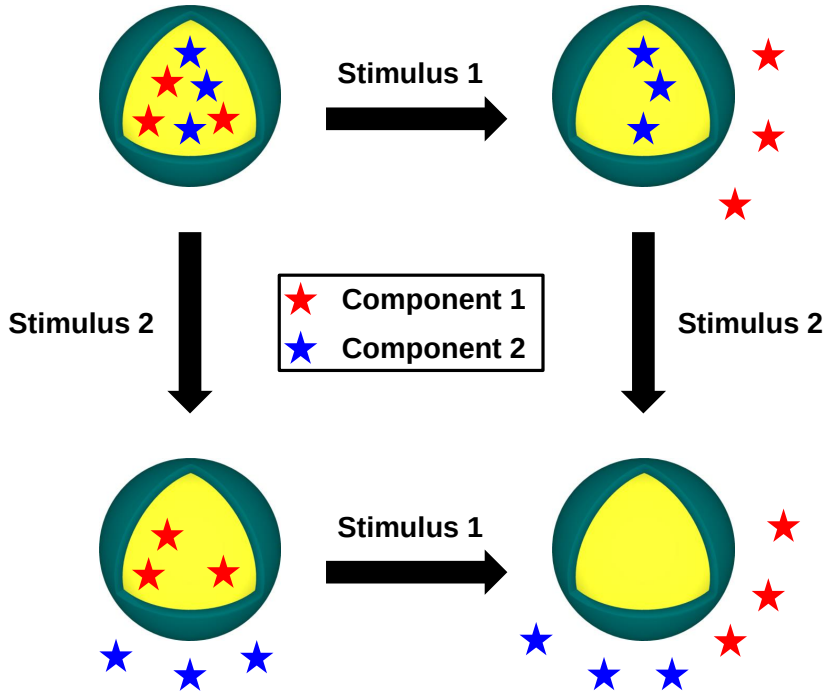

Fig. 4.56.: By stimuli-selective release it is understood that the capsules release one encapsulated component upon one stimulus and another encapsulated component upon another stimulus, but not vice versa.

Therefore, it is the aim of this project to prepare complex nanocapsules from stimuli-responsive block copolymers that are able to release an encapsulated payload upon application of one or both stimuli. Furthermore, these nanocapsules should show stimuli-selective release.

4.4.2. Preparation of the Nanocapsules

Suitable stimuli-responsive materials had to be synthesized for the preparation of stimuli-responsive nanocapsules. Since block copolymers fulfill the criteria for complex materials outlined in Chapter 1 and also because of the experience gained in the study of the PVFc-*b*-PMMA system, the use of block copolymers and in particular the use of PVFc suggests itself. As the PVFc block is responsive to oxidation, the other block should be responsive to another stimulus. Here, a pH-responsive material was chosen because the pH can be varied over a wide range, it is an ubiquitous stimulus, and does neither hinder nor aid the oxidation-responsiveness. The polymer of choice was poly(vinylferrocene)-*block*-poly(2-vinylpyridine) (PVFc-*b*-P2VP) (see Fig. 4.57a), as poly(2-vinylpyridine) (P2VP) is hydrophobic at high pH but becomes hydrophilic at low pH.

In the block copolymer PVFc-*b*-P2VP, each block constitutes one responsive unit. Therefore, it is expected that the capsular morphology disappear upon application of both stimuli. Hence, another block copolymer responsive to two stimuli but that carries the stimuli-responsiveness

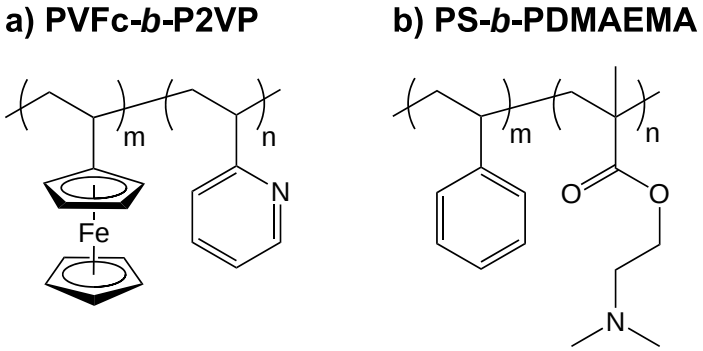

Fig. 4.57.: The stimuli-responsive polymers PVFc-*b*-P2VP (a) and PS-*b*-PDMAEMA (b) have been used.

in just one block would be useful to obtain capsules that maintain their morphology even after the application of both stimuli. For this, the block copolymer PS-*b*-PDMAEMA was chosen (see Fig. 4.57b). In this block copolymer, the PS block is not responsive. However, the poly(2-dimethylaminoethyl methacrylate) (PDMAEMA) block is responsive to acidic pH-values and to temperature, as PDMAEMA copolymers often possess a lower critical solution temperature (LCST). The block copolymer PS-*b*-PDMAEMA was already successfully applied by Schacher et al. to form stimuli-responsive membranes, in which the permeability of the membranes could be tuned by the pH and by the temperature.[378,379] Very recently, PS-*b*-PDMAEMA nanoparticles were prepared by a reversible addition-fragmentation chain transfer (RAFT) polymerization in miniemulsion.[380] It was demonstrated that N_2- and CO_2-bubbling through the dispersion of these nanoparticles could be advantageously used to both aggregate and re-disperse them. In addition, the release behavior upon CO_2-stimulation was studied and it was shown that the release could be varied by the on-set of CO_2-bubbling.

Hence, both block copolymers are promising candidates to form stimuli-responsive nanocapsules. They were synthesized by the group of Dr. Markus Gallei (AK Rehahn) at the TU Darmstadt. The molecular weights and the different stimuli are summarized in Tab. 4.11. In addition, the homopolymers of the block copolymers were also prepared by the group of Dr. Markus Gallei as references, their molecular weights are shown in Tab. 4.11 as well.

Tab. 4.11.: Molecular weights of the block copolymers and their homopolymers used in the study of stimuli-responsive capsules. The molecular weights were determined by different methods, see Section 5.4.

Polymer	Block	M_n / g/mol	M_w / g/mol	PDI	Stimuli
PVFc-*b*-P2VP	PVFc	14200	22000	1.54	Ox
	P2VP	204000	-	-	pH
	PVFc-*b*-P2VP	218200	232300	1.06	Ox, pH
PS-*b*-PDMAEMA	PS	73900	76800	1.03	-
	PDMAEMA	11200	-	-	pH, T
	PS-*b*-PDMAEMA	85100	-	-	pH, T
PS	-	198900	206600	1.04	-
PVFc	-	11900	12800	1.08	Ox
PDMAEMA	-	25000	-	-	pH, T
P2VP	-	25800	25900	1.004	pH

Complex polymer nanocapsules consisting of PVFc-*b*-P2VP as well as of PS-*b*-PDMAEMA were prepared by using the SEED process.[51,115] In order not to protonate the pH-responsive blocks, the capsules were prepared under basic conditions (pH $\approx$ 10). As a core material, the hydrophobic oil HD was employed. The capsules resulting from this process are shown in Fig. 4.58. Both block copolymers formed capsules with a hydrodynamic diameter around 250 nm. There was no apparent phase separation between the two blocks, neither in PVFc-*b*-P2VP capsules nor in PS-*b*-PDMAEMA capsules. However, the block copolymers did show phase separation in bulk.[381] Three possible reasons were assigned to explain the different observations in the nanocapsules and in bulk. Firstly, as it was impossible to evaporate the polymer solvent completely at 0 °C and there was no phase separation at an evaporation temperature of 20 °C, there might not have been enough time for phase separation to occur during the formation of the capsules. Secondly, the apparent absence of phase separation might also be due to confinement restrictions as the capsular wall is quite thin. Thirdly, phase separation may have occurred but is not visible in the capsules. Even in the thin films, the determination of the morphology is quite difficult.[381] The curvature induced by the spherical nanocapsules even adds to this difficulty.

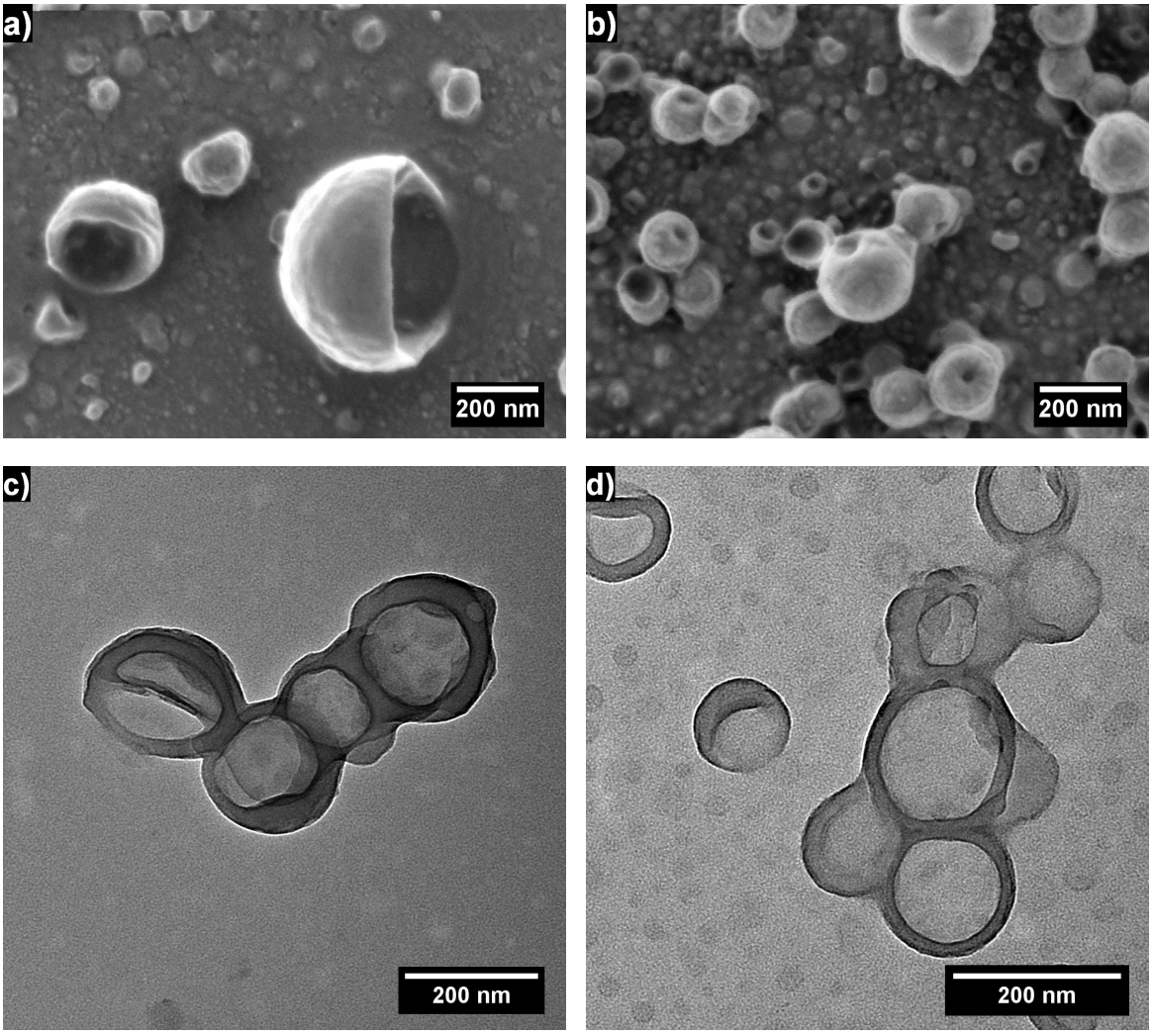

Fig. 4.58.: Capsules prepared from PVFc-*b*-P2VP (a, c) and PS-*b*-PDMAEMA (b, d).

The homopolymers of the block copolymers were also used to fabricate nanocapsules as references. However, with the exception of P2VP, no capsules were formed under the same experimental conditions that were used for the block copolymer nanocapsules (see Fig. 4.59). For PVFc and PS, half-spherical particles were obtained (see Fig. 4.59a and c). The half-spheres are the remains of Janus particles consisting of the polymer and HD as it was also observed previously for PS-*b*-PMMA and HD.[51] It is known that for capsule formation, a careful balance of the different interfacial tensions has to be respected in order to form core-shell structures (see Section 2.3).[75,96] Apparently, this balance was not fulfilled when the very hydrophobic polymers PVFc and PS are employed. On the other hand, PDMAEMA is a very hydrophilic polymer. Due to its hydrophilicity, it formed films upon drying (see Fig. 4.59d). The absence of defined capsular morphologies clearly showed the benefit of using block copolymers for the formation of complex nanocapsules.

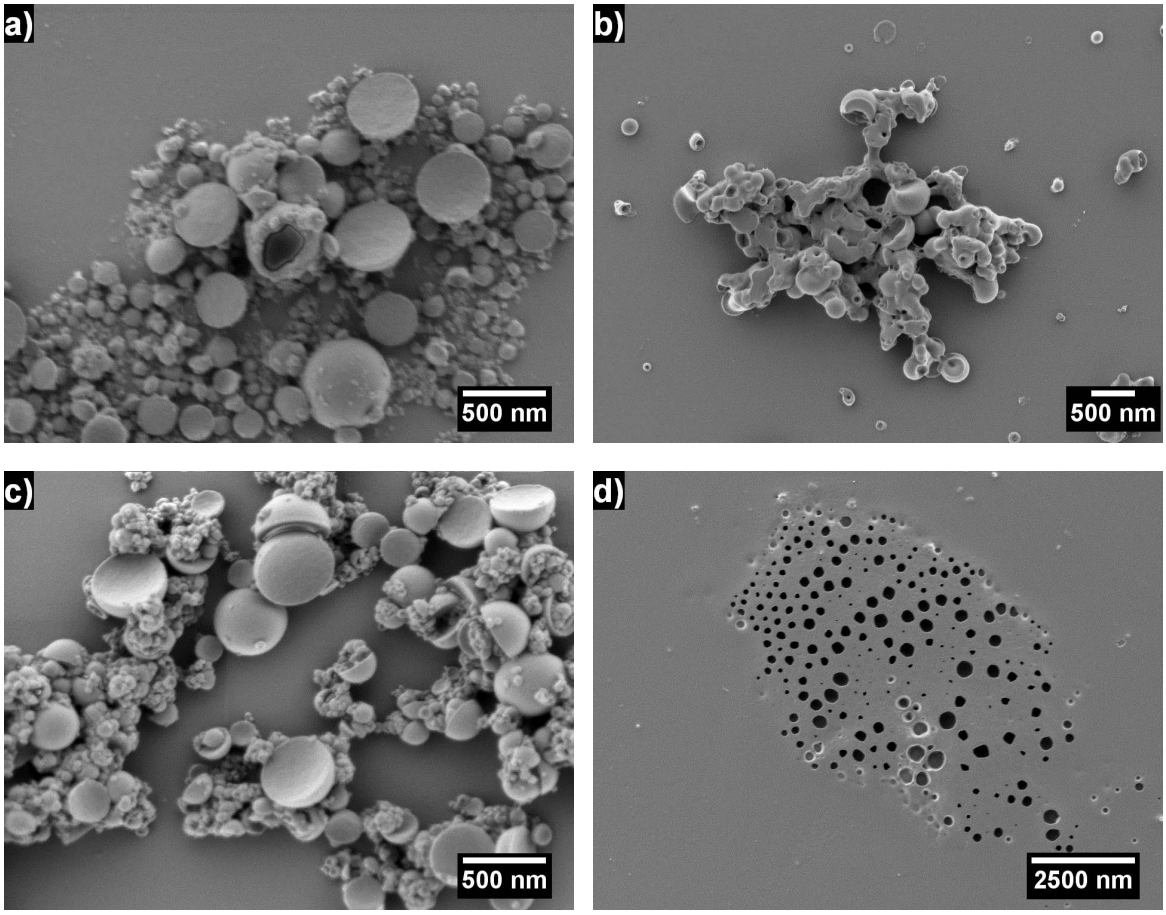

Fig. 4.59.: Control samples prepared from PVFc (a), P2VP (b), PS (c) and PDMAEMA (d). The irregular structure of the colloids prepared from homopolymers shows the benefit of using block copolymers which yielded capsules.

4.4.3. Stimuli-Responsiveness of the Nanocapsules

Upon acidifying the dispersions of nanocapsules from each block copolymer, an increase in capsule diameter was detected by DLS (see Fig. 4.60). The increase was significantly more pronounced for PVFc-*b*-P2VP than for PS-*b*-PDMAEMA. The change in diameter was ascribed to the swelling of the pH-responsive blocks that become protonated and hence more hydrophilic. The reason for the stronger increase in diameter of capsules of PVFc-*b*-P2VP than of PS-*b*-PDMAEMA was the relative amount of the pH-responsive block in each copolymer. In PVFc-*b*-P2VP, the P2VP-block constituted roughly 93 % of the copolymer while the PDMAEMA constituted only 13 % of the PS-*b*-PDMAEMA copolymer. The same behavior, i.e. swelling, was also observed after oxidation of PVFc-*b*-P2VP nanocapsules. Here, the capsule size increased from (277 ± 101) nm to (354 ± 135) nm, which agrees well with previous results from nanocapsules prepared from PVFc-*b*-PMMA in Section 4.3. It is worthwhile to mention that in all cases, the dispersions stayed stable and that no agglomeration was observed. Therefore, the non-responsive block held the capsule together and prevented dissolution.

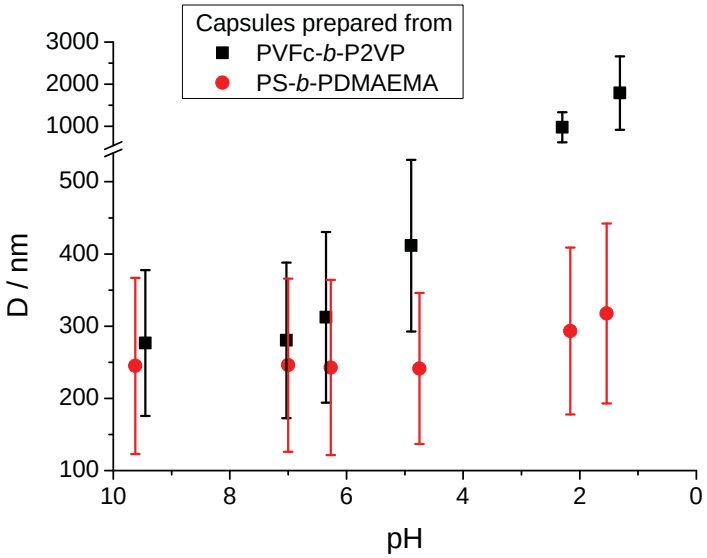

Fig. 4.60.: Upon acidification, both capsules of PVFc-*b*-P2VP and PS-*b*-PDMAEMA increased in size, the former more strongly than the latter because of the higher content of pH-responsive groups in the PVFc-*b*-P2VP block copolymer.

Apart from the increase in diameter, there were also changes in the topography of the nanocapsules detectable by electron microscopy (see Fig. 4.61). Upon oxidation, the surface of PVFc-*b*-P2VP capsules roughened considerably and outgrowths similar to the ones detected on PVFc-*b*-PMMA nanocapsules were observed (see Section 4.3.3 for comparison). However, in the case of PVFc-*b*-P2VP they were less regular, which was probably due to the incomplete phase separation of the polymer blocks. Upon acidification there were pronounced

differences between PVFc-*b*-P2VP and PS-*b*-PDMAEMA. The capsules of PVFc-*b*-P2VP became disformed and seemed to slowly converge on another upon drying. In contrast, the capsules of PS-*b*-PDMAEMA only showed surface roughening under complete preservation of capsule identity. The difference between the morphology changes of the nanocapsules prepared from two block copolymers was again attributed to the different amounts of stimuli-responsive blocks in each block copolymer.

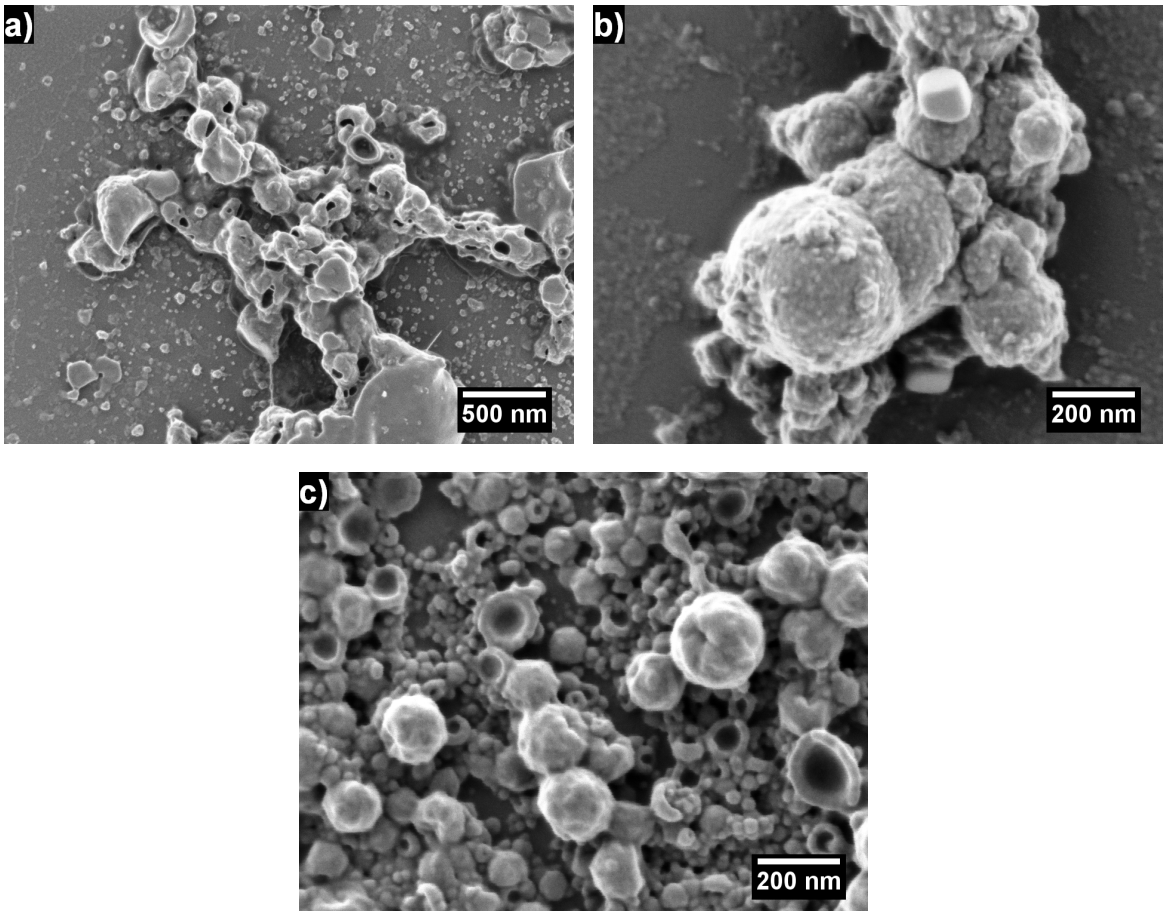

Fig. 4.61.: Response of the capsules prepared from PVFc-*b*-P2VP to a lowering of the pH (a) and to oxidation (b) as well as of capsules prepared from PS-*b*-PDMAEMA to a lowering of the pH (c).

4.4.4. Release Behavior

Nile red was incorporated into the nanocapsules to study their release behavior. The fluorescence of Nile red is known to be strongly dependent on its surrounding: the more polar the environment of the molecule the less it fluoresces.[302,382,383] Therefore, the determination of the release behavior was based on a probe that did not necessarily need to diffuse out of the capsule. This diffusion out of the capsule is classically termed release. The fluorescence of the dye will be lessened upon changing its local environment to a more polar state. Although

the change of local environment is not the same as classical release, the term "release" will be used in this thesis for the sake of clarity and conciseness. In addition, Nile red has already been used for the purpose of determining release as it was just defined quite often.[302,384–387] The use of Nile red offered the advantage of measuring the fluorescence directly in the dispersion, i.e. no centrifugation step was necessary that could destroy the capsules and thereby lead to an artificially increased release. The capsule dispersions were dialyzed before acidifying or oxidizing them in their continuous phase to remove non-encapsulated dye.

Firstly, the release behavior of both capsule types upon acidification was studied. For this, the capsule dispersions were mixed with hydrochloric acid solutions of different concentrations. The fluorescence intensity of Nile red was measured after certain time intervals, its decrease was taken as a measure of release. For capsules prepared from PVFc-*b*-P2VP, a pH-dependent release was observed (see Fig. 4.62a). There was hardly an observable release at basic pH. However, there was already a decrease of fluorescence intensity of about 40 % at intermediate pH-values between 5 and 7 corresponding to a release of about 40 %. Upon further lowering of the pH below 2, there was no dependence of the absolute release on the pH anymore, which means that at these values the maximum possible release had occurred. The remaining fluorescence is possibly due to Nile red located inside the non-pH-responsive parts of the capsules. There was no strong influence of the time between addition of the hydrochloric acid and the time of measurement. At least two minutes passed between addition of the acid and the measurement, which was apparently sufficient for the release, especially at low pH-values. Therefore, the release is very fast. This was to be expected as the protonation reaction allowing the capsule to swell and subsequently to release its payload is usually fast.

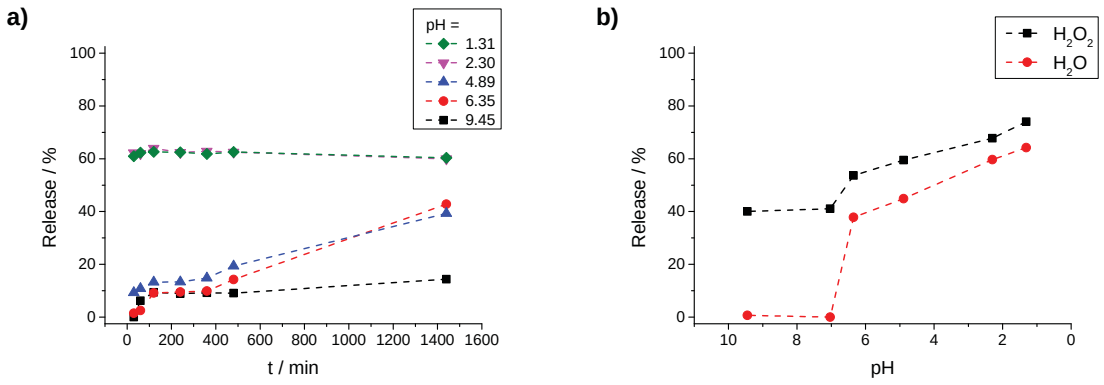

Fig. 4.62.: The nanocapsules prepared from the block copolymer PVFc-*b*-P2VP show release upon acidification (a) and oxidation (b).

To study the release from PVFc-*b*-P2VP capsules upon oxidation and upon oxidation in dependence of the pH, dispersions of the capsules were treated with H_2O_2 and hydrochloric acid. Even at basic or neutral pH, there was a significant drop of fluorescence intensity indicating a release of about 40 % upon oxidation (see Fig. 4.62b). Upon acidifying the

dispersion, the release from the oxidized nanocapsules was more pronounced than the release from the non-oxidized nanocapsules. This release behavior is schematically shown in Fig. 4.63.

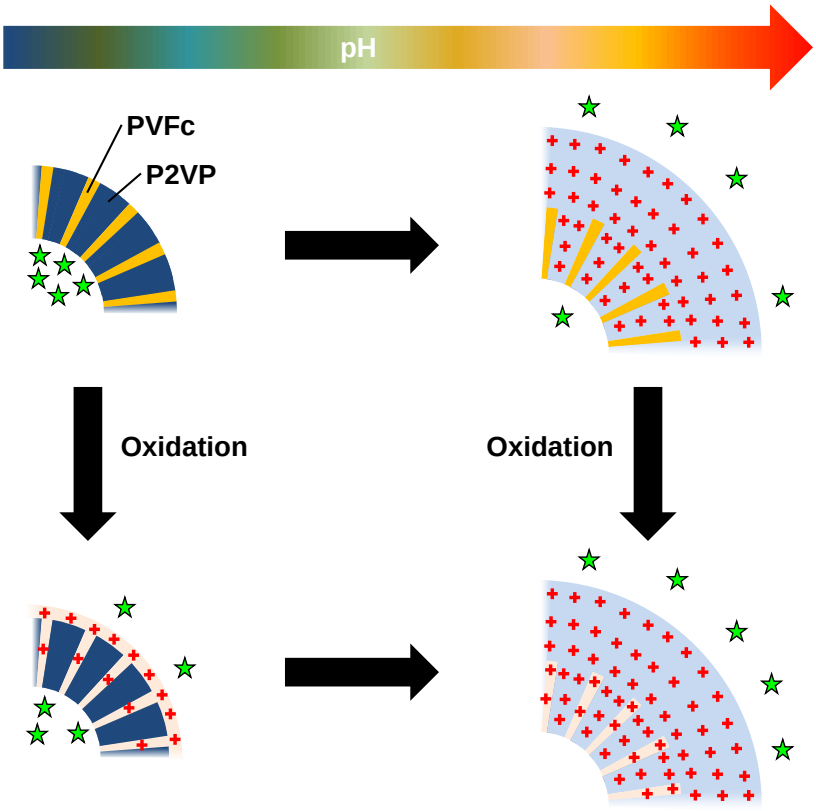

Fig. 4.63.: Scheme showing the release behavior and swelling of PVFc-*b*-P2VP capsules upon acidification and oxidation.

The release behavior of PS-*b*-PDMAEMA capsules upon acidification was studied in the same way as for PVFc-*b*-P2VP capsules. Again, a pH-dependent release was observed (see Fig. 4.64a). A release of up to 80 % was reached upon acidification, the amount released being strongly dependent on the pH of the dispersion. While there was no release occurring at basic pH, a slight release occurred at neutral pH. Upon lowering the pH to 4.75, an already significant release was observed which was further intensified by decreasing the pH-value to 2 or to 1.5. Thus, the release was controlled by the pH of the dispersion.

As in the PVFc-*b*-P2VP-system, the release was very fast. Upon addition of the acid solution, a decoloring of the dispersion was observed, which is mirrored in the release being almost complete once the fluorescence intensity was measured. After this initial "burst"-release, there was a slow release with time, the release being more significant the less acidic the dispersion was. The speed of the release points to a very fast initial protonation reaction and swelling. Then more protonation occurred, which allowed the release to slowly reach its final value.

In contrast to PVFc-*b*-P2VP nanocapsules, there are not two but only one stimulus-responsive block in PS-*b*-PDMAEMA nanocapsules. However, the PDMAEMA-block is not only re-

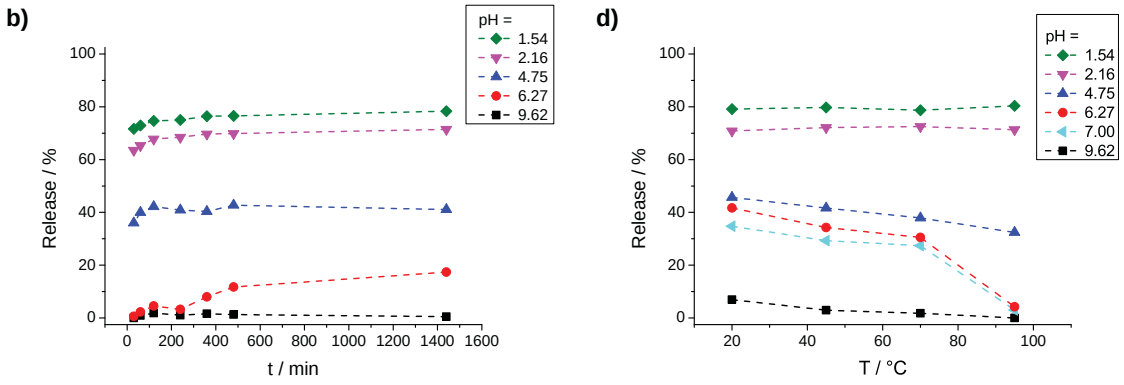

Fig. 4.64.: Release behavior of capsules prepared from the block copolymer PS-*b*-PDMAEMA. The capsules show release upon acidification (a) while the release at intermediate pH-values is hindered at elevated temperatures (b).

sponsive to pH-changes, but also to temperature as PDMAEMA-copolymers often display a LCST in water below 100 °C. To check for the influence of the LCST, the nanocapsule dispersions were kept at elevated temperature, the pH was changed and the release was measured. No effects were observed for basic and very acidic pH-values, i.e. the LCST did not influence the release under these conditions (see Fig. 4.64b). However, at intermediate pH-values, increasing the temperature of the dispersion above 75 °C led to a loss of the release behavior. This hindrance of the release was attributed to the PDMAEMA-chains being not able to swell; hence no release is possible as schematically shown in Fig. 4.65. Indeed, a very similar behavior was observed by Schacher et al. who studied the flow behavior of water through PS-*b*-PDMAEMA porous membranes at elevated temperatures under different pH-conditions.[378,379] Here, an increase of the flow through the membrane was observed if the membrane was kept at elevated temperatures and intermediate pH-values. When the pH was changed to very high or low values, no significant differences between the different temperatures were observed.

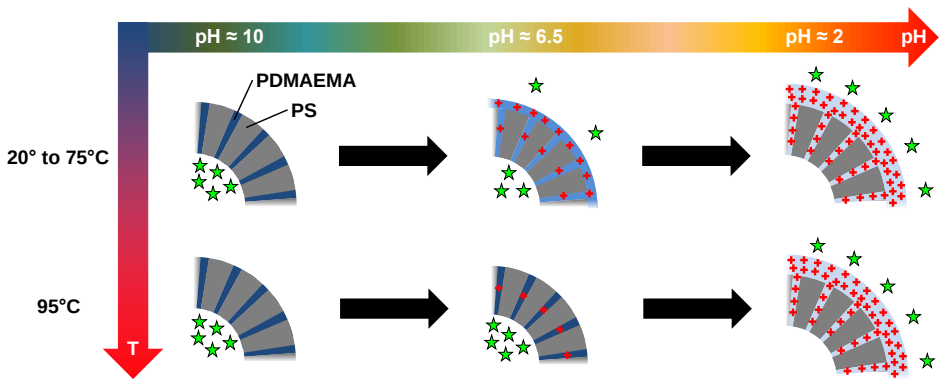

Fig. 4.65.: Scheme of the release behavior and swelling of PS-*b*-PDMAEMA capsules. At high pH, there is no release independent of temperature, whereas release occurs only below the LCST at intermediate pH. At low pH, the release behavior is again independent of temperature.

Finally, the release behavior of control samples prepared from the homopolymers of the block copolymers was studied (see Fig. 4.66). In the case of PVFc, aggregation and sedimentation took place in the dispersion upon acidification, making the release measurements meaningless. For P2VP capsules, a similar release behavior as for the block copolymer was observed. Considering that P2VP constitutes the main part of the block copolymer, this was to be expected. However, the absence of the stabilizing PVFc-block is noticeable, as the capsules did show a slow release even at high pH. Probably the dilution by the addition of the continuous phase before the fluorescence measurement was already enough to soften the capsules and to cause release. The continuous phase had to be added to the dispersion to keep the total volume comparable to the dispersions treated with acid. The release from the PS control sample was negligible. Finally, the dispersion of PDMAEMA demonstrated a release behavior very similar to that of PS-*b*-PDMAEMA. Therefore, capsules were probably formed but did not keep their structural integrity upon drying.

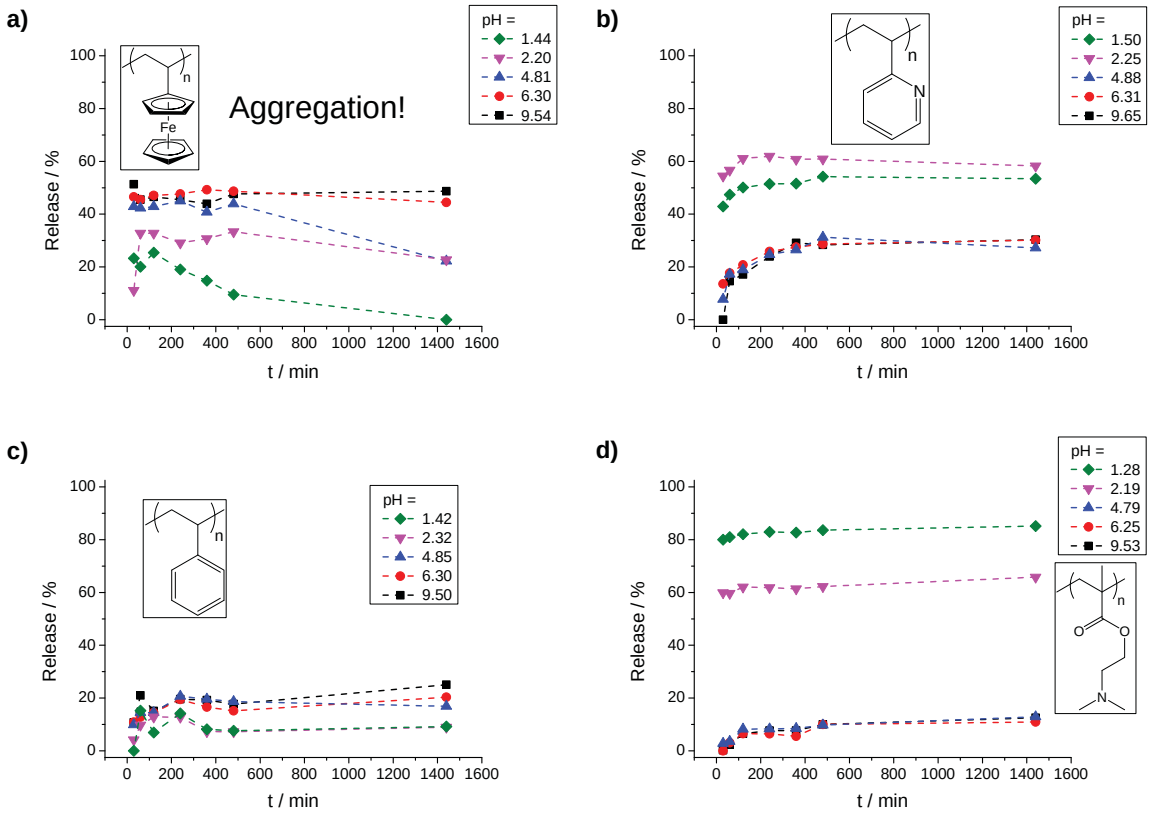

Fig. 4.66.: The release from the control samples prepared of homopolymers was similar to the samples prepared from block copolymers. However, aggregation did occur in the case of PVFc, hence its apparent "release behavior".

4.4.5. Stimuli-Selective Release

It is of interest to selectively release an encapsulated component upon one stimulus, but not upon the other one for several applications. A possible scenario are self-healing materials,[11,12] where a monomer is released upon one stimulus and the catalyst needed to polymerize the monomer upon the other stimulus. This concept was realized in the capsules composed of PVFc-*b*-P2VP by introducing stimuli-responsive encapsulated components. For pH-responsiveness, dimethyldodecylamine (DDA) was chosen since it is very hydrophobic at basic pH but becomes hydrophilic upon protonation. The NMR signal of the protons on the methyl groups changes from 2.10 ppm in the deprotonated state to 2.85 ppm in the protonated state,[87] thereby enabling detection of the release by NMR. Thus, DDA was encapsulated into PVFc-*b*-P2VP and the capsule dispersion was subsequently treated with acid or oxidant. As shown in Fig. 4.67a, DDA was released from PVFc-*b*-P2VP capsules upon protonation, but not upon oxidation. Therefore, selective release was indeed taking place as DDA is only released upon one stimulus, but not upon the other one.

To achieve stimuli-selective release by oxidizing the nanocapsules, an oxidation-responsive material was encapsulated. For this, diphenyl disulfide (DPDS) was chosen as disulfides can be oxidized to sulfoxides, disulfoxides or sulfones.[388,389] These species are much more polar than the disulfide. Therefore, they can be released from the hydrophobic capsule interior into the aqueous environment, where they can be detected by NMR. After encapsulation of DPDS the dispersion was treated with an acid or with an oxidant. The release can be seen in the NMR spectra in Fig. 4.67b. Again, stimuli-selective release was achieved because there was no release upon a pH-change but on oxidation. Thus, the stimuli-selective release from PVFc-*b*-P2VP capsules by both a pH-change and oxidation was demonstrated.

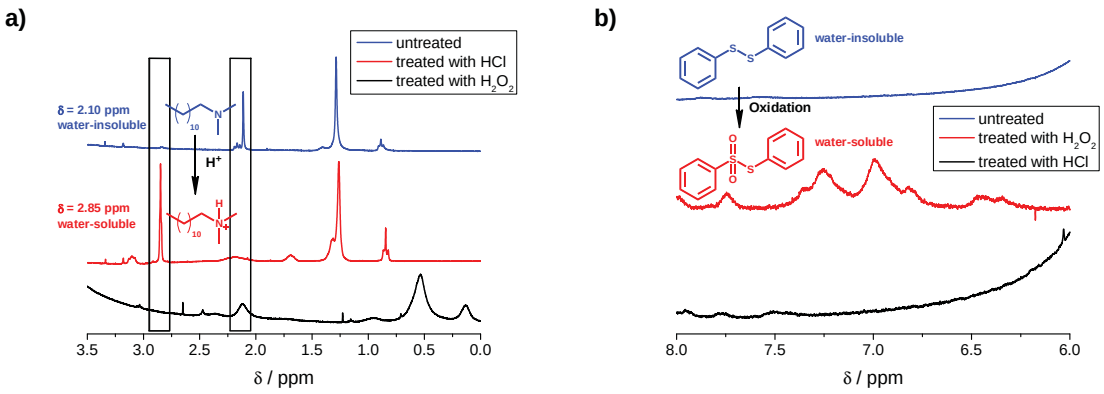

Fig. 4.67.: The release of DDA occurred upon a pH-change and not upon an oxidation (a) while the release of DPDS occurred upon an oxidation and not upon a pH-change (b).

4.4.6. Conclusions and Outlook

In conclusion, dual-stimuli-responsive nanocapsules were prepared by the SEED process using block copolymers as shell material. Either both blocks were responsive to one stimulus each or to two stimuli at once. Upon addressing the stimuli of the block polymers, i.e. lowering the pH or oxidizing the pendant side-group, the capsules swelled and changed their morphology, which was shown with DLS and electron microscopy, respectively. The swelling was used to release an incorporated model substance. Control was achieved by the control of the pH and the presence or absence of an oxidizing species. In addition, the pH-responsive release was hindered by increasing the temperature above the LCST of one of the polymer blocks. Furthermore, it was also possible to encapsulate stimuli-switchable substances into the capsules, which were released upon one stimulus, but not upon the other one. Hence, it was possible to prepare stimuli-selective nanocapsules. In conclusion, a general strategy for the synthesis of dual-responsive nanocapsules for selective dual-release was developed, which will open the path to highly functional, addressable polymer-based nano-carrier systems with unprecedented properties. In addition, this concept will also prove useful for the preparation of triple- or multi-stimuli-responsive nanocapsules.

5. Experimental Part

5.1. Experimental Details for Section 4.1

5.1.1. Materials

Polystyrene (PS, M_w = 300 000 g/mol, PDI = 2.38, Acros), poly(L-lactic acid) (PLLA, M_w = 90 000 g/mol, PDI = 4.42, Biomer L9000), sodium dodecylsulfate (SDS, Alfa Aesar, 99 %), *N*-(2,6-diisopropylphenyl)-perylene-3,4-dicarbonacidimide (PMI, BASF), cetyltrimethylammonium chloride (CTMA-Cl, Acros, 99 %), toluene (Sigma-Aldrich, 99.7 %), tetrahydrofuran (THF, Sigma-Aldrich, 99.9 %), methanol (Fluka, 99.99 %), dichloromethane (Fluka, 99.99 %), chloroform (Acros, 99 %), V59 (Wako), tetraethoxysilane (TEOS, Alfa Aesar, 98 %), and hexadecane (HD, Merck, 99 %) were used as received. The monomers 9-vinylphenanthrene (VPA, Toronto Research Chemicals) and [1-(4-nitrophenyl)-2-pyrrolidinmethyl] acrylate (NPP, Sigma-Aldrich) were also used as received. Styrene (Merck, 99 %) was purified on a column packed with neutral aluminum oxide (Merck) before use. The initiator 2,2'-azobis(2-methylpropionitrile) (AIBN, Fluka, 98 %) was recrystallized from methanol prior to use. The synthesis of the fluorescent dyes B504-MA and B612-MA was based on the ones reported in literature.[390,391] Distilled water was used throughout the work.

5.1.2. Synthesis of Labeled Polymers for FRET Measurements

Copolymers of styrene and VPA or NPP were prepared by free-radical polymerization in miniemulsion. To this end, 100 mg AIBN, 250 mg HD and 6 g styrene were added to 30 mg VPA or 60 mg NPP to build the dispersed phase and were added subsequently to a solution of 72 mg SDS in 24 g water. The mixtures were emulsified for 1 h at 1250 rpm and submitted to ultrasonication for 2 min at 90 % amplitude under ice cooling to a Branson W450-D sonifier with a 1/2-inch tip. Afterwards, the polymerizations were carried out in a closed 50 mL round-bottom flask at 72 °C for 12 h. The obtained dispersions were freeze-dried, dissolved in THF and reprecipitated three times into methanol.

5.1.3. Synthesis of Labeled Polymers for DC-FCCS Measurements

Copolymers of styrene and the dyes B504-MA or B612-MA were prepared by radical polymerization in solution. 12.5 mg AIBN, 7 mg of one dye and 2.5 g styrene were dissolved in 20 g THF. The solution was degassed three times by the freeze-thaw-technique and the polymerization was carried out at 80 °C in an oil bath for 40 h. The copolymer was precipitated into 200 mL of a water:methanol mixture (20:80) and filtered. The solid copolymer was dissolved in 15 mL THF and reprecipitated three times to remove any unreacted dye and monomer. Afterwards, the copolymer was dried in vacuo. The copolymers of styrene and B504-MA or styrene and B612-MA were named PS-504 and PS-612, respectively.

5.1.4. Preparation of Nanoparticles by Emulsion Solvent Evaporation

A certain amount of polymer (PS, PLLA, PS-504, PS-612, PS-VPA, PS-NPP, (see Tab. 5.1)) was dissolved in 2.5 g solvent and added to an aqueous solution of SDS (20 g, 1 g/L). A macroemulsion was obtained by stirring at 1250 rpm for 1 h. The macroemulsion was sonicated using a Branson W450-D sonifier with a 1/2-inch tip at 70 % amplitude in a pulsed regime (30 s sonication, 10 s pause) under ice cooling. The obtained emulsions were then either treated directly (see Section 5.1.7) or transferred into a 50 mL reaction flask and stirred at 500 rpm and 40 °C for 12 h. In the case of further treatment, the emulsions were transferred to the reaction flask directly after the treatment. Spherical nanoparticles were obtained as shown by the exemplary SEM images in Fig. 5.1 and 5.2a.

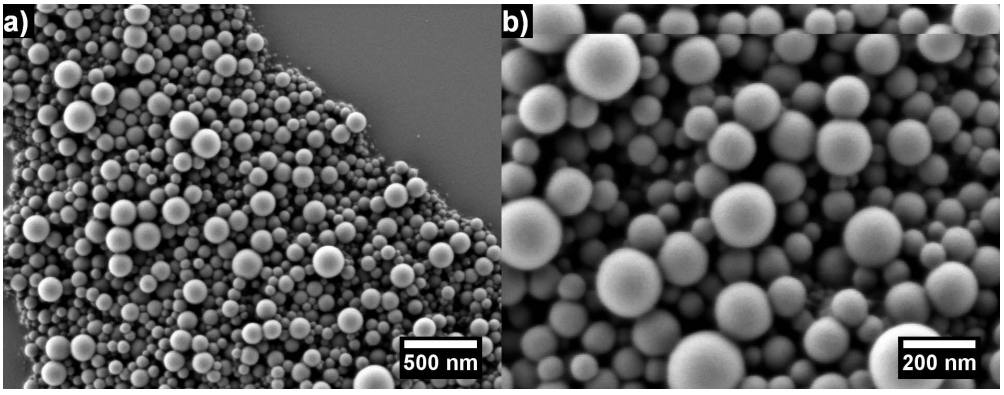

Fig. 5.1.: SEM micrographs of the sample "Time" at two different magnifications. Dense, spherical nanoparticles were obtained.

5.1.5. Preparation of Nanoparticles by Miniemulsion Polymerization

To synthesize nanoparticles by direct miniemulsion polymerization, 1.6 mg V59, 4 mg HD and 9955 mg styrene were added to 5 mg of PS-504 or PS-612 to build the dispersed phase. A solution of 2 mg SDS in 20 g of water was subsequently added to the monomer solution. The mixture was emulsified for 1 h at 1250 rpm and submitted to ultrasonication for 2 min at 90 % amplitude under ice-cooling to a Branson W450-D sonifier with a 1/2-inch tip. Afterwards, the polymerization was carried out in a closed 50 mL round bottom flask at 72 °C for 16 h under stirring. For the positive control sample, 2.5 mg of each polymer was used. Dense, solid nanoparticles were obtained (see Fig. 5.2b).

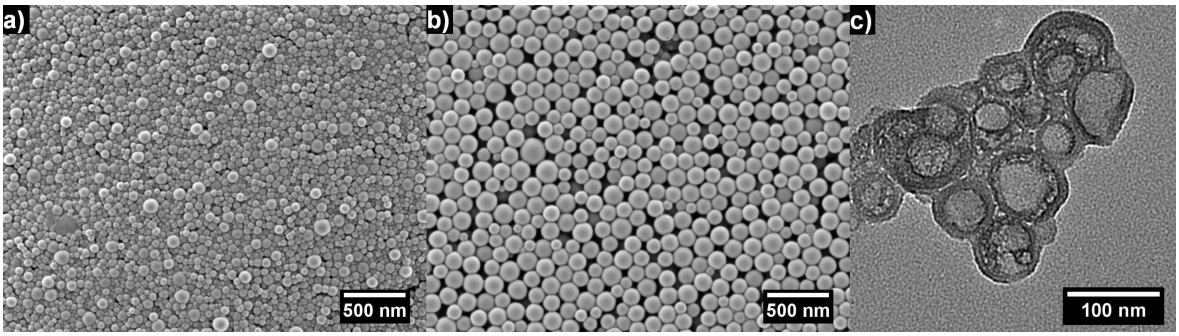

Fig. 5.2.: SEM micrographs of PS nanoparticles prepared by the SEED process (a) and miniemulsion polymerization (b). In (c), a TEM-micrograph of silica nanocapsules prepared by polycondensation of an alkoxysilane is shown.

5.1.6. Preparation of Nanocapsules by Polycondensation of Alkoxysilanes

To synthesize nanoparticles by the interfacial reaction of TEOS, 5 mg of PS-504 or PS612 were dissolved in 1 g TEOS, 62.6 mg HD and 500 mg toluene. Subsequently, a solution of 11.5 mg CTMA-Cl in 15 g water was added. The mixture was preemulsified for 5 min at 1000 rpm and subjected to ultrasonication for 2 min at 70 % amplitude under ice-cooling in a pulse / pause regime of 30 s and 10 s at a Branson W450-D sonifier with a 1/2-inch tip. Afterwards, the polycondensation was carried out at room temperature by stirring the miniemulsion at 1000 rpm in a closed vial for 48 h. For the positive control sample, 2.5 mg of each polymer was used. Capsules were obtained in all cases (see Fig. 5.2c).

Tab. 5.1.: Entry names, polymers and solvents used in the experiments. Starred entries are depending on diluent and dilution.

Entry	m_{PS} / mg	m_{PLLA} / mg	m_{PS-504} / mg	m_{PS-612} / mg	m_{PS-VPA} / mg	m_{PS-NPP} / mg	m_{PMI} / mg	m_{HD} / mg	Solvent	D / nm	σ / %
Time	100	-	-	-	-	-	-	-	$CHCl_3$	*	*
Dil-1	100	-	-	-	-	-	-	-	$CHCl_3$	*	*
Dil-2	100	-	-	-	-	-	-	-	toluene	*	*
Dil-3	100	-	-	-	-	-	-	-	CH_2Cl_2	*	*
O-1	100	-	-	-	-	-	-	0	$CHCl_3$	141	31
O-2	60	-	-	-	-	-	-	40.0	$CHCl_3$	101	35
O-3	60	-	-	-	-	-	-	29.3	$CHCl_3$	97	32
FCS-1	100	-	-	-	-	-	0.01	-	$CHCl_3$	*	*
TEM-PS	100	-	-	-	-	-	-	-	$CHCl_3$	130	31
TEM-PLLA	-	100	-	-	-	-	-	-	$CHCl_3$	112	39
TEM-P	50	50	-	-	-	-	-	-	$CHCl_3$	119	30
TEM-N	prepared by mixing equal volumes of **particles** from the samples TEM-PS and TEM-PLLA									127	30
TEM-A	prepared by mixing equal volumes of **droplets** from the samples TEM-PS and TEM-PLLA									129	31
FCCS-1-PS-504	-	-	100	-	-	-	-	-	$CHCl_3$	98	33
FCCS-1-PS-612	-	-	-	100	-	-	-	-	$CHCl_3$	91	35
FCCS-1-P	-	-	50	50	-	-	-	-	$CHCl_3$	96	34
FCCS-1-N	prepared by mixing equal volumes of **particles** from the samples FCCS-1-PS-504 and FCCS-1-PS-612									95	31
FCCS-1-A	prepared by mixing equal volumes of **droplets** from the samples FCCS-1-PS-504 and FCCS-1-PS-612									92	35
FCCS-2-PS-504	-	-	100	-	-	-	-	-	toluene	85	39
FCCS-2-PS-612	-	-	-	100	-	-	-	-	toluene	83	37
FCCS-2-P	-	-	50	50	-	-	-	-	toluene	87	33
FCCS-2-N	prepared by mixing equal volumes of **particles** from the samples FCCS-2-PS-504 and FCCS-2-PS-612									83	32
FCCS-2-A	prepared by mixing equal volumes of **droplets** from the samples FCCS-2-PS-504 and FCCS-2-PS-612									83	38
FCCS-3-PS-504	-	-	10	-	-	-	-	-	$CHCl_3$	70	43
FCCS-3-PS-612	-	-	-	10	-	-	-	-	$CHCl_3$	68	44
FCCS-3-P	-	-	5	5	-	-	-	-	$CHCl_3$	69	31
FCCS-3-N	prepared by mixing equal volumes of **particles** from the samples FCCS-3-PS-504 and FCCS-3-PS-612									71	46
FCCS-3-A	prepared by mixing equal volumes of **droplets** from the samples FCCS-3-PS-504 and FCCS-3-PS-612									72	44
FRET-PS-VPA	-	-	-	-	100	-	-	-	$CHCl_3$	124	35
FRET-PS-NPP	-	-	-	-	-	100	-	-	$CHCl_3$	114	28
FRET-P	-	-	-	-	50	50	-	-	$CHCl_3$	123	27
FRET-N	prepared by mixing equal volumes of **particles** from the samples FRET-PS-VPA and FRET-PS-NPP									121	29
FRET-A	prepared by mixing equal volumes of **droplets** from the samples FRET-PS-VPA and FRET-PS-NPP									120	25

*depending on diluent and dilution

Tab. 5.2.: Entry names, monomers, labeling polymers and solvents used in the polymerization experiments.

Entry	$m_{styrene}$ / mg	m_{TEOS} / mg	m_{HD} / mg	m_{V59} / mg	m_{PS-504} / mg	m_{PS-612} / mg	$m_{toluene}$ / mg
MEP-PS-504	9955	-	4	1.6	5	-	-
MEP-PS-612	9955	-	4	1.6	-	5	-
MEP-P	9955	-	4	1.6	2.5	2.5	-
MEP-N	prepared by mixing equal volumes of **particles** from the samples MEP-PS-504 and MEP-PS-612						
MEP-A	prepared by mixing equal volumes of **droplets** from the samples MEP-PS-504 and MEP-PS-612						
PC-PS-504	-	1000	62.6	-	5	-	500
PC-PS-612	-	1000	62.6	-	-	5	500
PC-P	-	1000	62.6	-	2.5	2.5	500
PC-N	prepared by mixing equal volumes of **particles** from the samples PC-PS-504 and PC-PS-612						
PC-A	prepared by mixing equal volumes of **droplets** from the samples PC-PS-504 and PC-PS-612						

5.1.7. Preparation of Samples for TEM, DC-FCCS and FRET Experiments

Positive and negative control samples were prepared for comparison with the actual samples. For positive control samples (denoted "P"), the two labeled polymers were miniemulsified together (see Tab. 5.1). Negative control samples (denoted "N") were prepared by mixing equal volumes of the differently labeled dispersions obtained after solvent evaporation. For the actual samples (denoted "A"), equal volumes of the differently labeled emulsions were combined directly after ultrasonication and before solvent evaporation. The description of the preparation of the three different kinds of samples is summarized and explained in Fig. 4.5. In the case of the miniemulsion polymerization in droplets or polycondesation polymerization on droplets, the same procedure was applied (see Tab. 5.2).

5.1.8. Analytical Tools

5.1.8.1. DLS Measurements

The hydrodynamic diameters of the nanoparticles were measured with a Nicomp 380 Submicron Particle Sizer (PSS-Nicomp) at an angle of 90° for 300 s. 10 µL of the latexes were diluted in 1000 µL of either distilled water, an aqueous solution of 1 g/L SDS, distilled water saturated with a solvent (toluene, chloroform, dichloromethane), or distilled water saturated with a solvent (toluene, chloroform, dichloromethane) and containing 1 g/L SDS. The averages of two independent measurements as well as their standard deviations are reported.

5.1.8.2. Zeta-Potential Measurements

The zeta potential of the emulsion droplets was measured at 25 °C in potassium chloride solution (10×10^{-3} mol/L, 50 µL sample per 1000 µL diluent) with a Zetasizer ZEN2600 from Malvern Instruments. The average of at least ten runs is reported herein.

5.1.8.3. FRET Measurements

FRET was recorded with the time-correlated single photon counting technique (FluoTime 200, PicoQuant GmbH). The diluted dispersion was excited inside a cuvette (thickness 10 mm) by a light emitting source PLS 280 (spectral width < 20 nm, repetition rate 2 MHz, power 1 µW, and pulse duration ≈ 900 ps; PicoQuant GmbH). Right-angle geometry of detection was chosen for fluorescence collection. Glan-Thompson polarizers (for excitation and detection)

were arranged under magic angle conditions. An additional long-pass filter (Brightline 300/LP, Semrock Inc.) was placed in front of a Sciencetech Model 9030 monochromator for better separation of scattered light and fluorescence signal. A counting photomultiplier PMA 165 (PicoQuant GmbH) was used as detector. The FRET measurements were carried out by Dr. Andrey Turshatov at the Max Planck Institute for Polymer Research in Mainz.

5.1.8.4. FCS and DC-FCCS Measurements

FCS and DC-FCCS experiments were performed on an inverted microscope Olympus IX70 combined with the FluoView300 confocal laser scanning unit (Olympus) fiber-coupled to a PicoQuant FCS unit that included two separate avalanche photodiodes τ-SPAD (PicoQuant GmbH) and the respective emission filters. An Olympus UPLSAPO 60XW 60x/1.2 water immersion objective was used. In the FCS experiments, the labeled nanoparticles were excited with an argon-ion laser at 488 nm, whereas emission was collected after filtering with an LP488R RazorEdge filter. In the DC-FCCS experiments, argon-ion (488 nm) and helium-neon (633 nm) lasers were used simultaneously to excite the B504-MA and B612-MA dye-labeled polymers, respectively. The collected fluorescence was divided into two channels by a dichroic mirror and filtered further with an LP635 long-pass (635 nm) filter in channel 1 and a BP525/50 band-pass filter (500 nm to 550 nm) in channel 2. Each channel contained an emission filter, a confocal pinhole and a single photon counting avalanche photodiode detector. These arrangements resulted in the formation of two perfectly overlapping confocal observation volumes V_b and V_r that superimpose to a common observation volume V_{br}.[197] Calibration of the confocal detection volumes was achieved by performing reference measurements with Alexa Fluor 488® and Alexa Fluor 647® (Invitrogen) dyes using the reported values of their diffusion coefficients.[226] Throughout all measurements, an eight-well, polystyrene-chambered cover glass (Nalge Nunc International) was used as sample cell. The FCS- and DC-FCCS measurements were carried out by David Schäffel at the Max Planck Institute for Polymer Research in Mainz.

5.1.8.5. Simulations

To evaluate the effect of coalescence during evaporation on the size distribution of the precipitated nanoparticles, a model was set up to reconstruct the size distribution of the droplets in the emulsion. To this aim, a reverse Monte Carlo procedure was implemented which took as input parameters the probability of coalescence in solution. The process was assumed to occur in a single step and the number of coalescence events per particle was assumed to be at most one. A minimum size of the particles in the emulsion, equivalent to the smallest particles detected in the precipitate, was set as a boundary condition and

particle diameters were rescaled according to the different density between nanodroplets in emulsions and precipitated nanoparticles. The reverse Monte Carlo loop was iterated a sufficient number of times to achieve a statistical uncertainty two decades smaller than the scale of the distributions. The simulations were carried out by Dr. Davide Donadio at the Max Planck Institute for Polymer Research in Mainz.

5.1.8.6. SEC Measurements

SEC was used to estimate the average molecular weights of the polymers and their PDI. The dried polymers were dissolved in THF (PLLA: chloroform) at a concentration of 5 mg/mL and filtered through a 0.45 µm Teflon filter. An elution rate of 1.0 mL/min and UV- (254 nm) and RI-detectors were used. PLLA was measured with an elution rate of 1.0 mL/min and a RI-detector only. The apparent molecular weights of the polymers were calculated using PS standards.

5.1.8.7. HPLC Measurements

For PS-VPA and PS-NPP, HPLC measurements were conducted on the polymer and the free dye to check the absence of free dye in the polymer. The measurements were performed with a gradient of THF and water starting from a ratio of 50 to 50 up to 100 to 0 in 10 min. The flow was 1 mL/min employing a RP8e-column (Merck) on a 1200 HPLC from Agilent Technologies. For detection, a DAD-Detector at a wavelength of 310 nm for PS-VPA and at 380 nm for PS-NPP was used.

For PS-504 and PS-612, HPLC measurements were conducted before and after repeated precipitation in order to ascertain the purity of the polymer and the absence of free dye. HPLC measurements were performed with a gradient of THF + 0.1 % trifluoroacetic acid (TFA) in water starting from a ratio of 60 to 40 up to 100 to 0 in 5 min. The flow was 1 mL/min employing a reversed phase AB C18-column (Macherey-Nagel) on a 1200 HPLC from Agilent Technologies. For detection, a DAD-Detector at a wavelength of 500 nm for PS-504 and at 600 nm for PS-612 was used.

5.1.8.8. Absorption and Emission Spectroscopy

Absorption and fluorescence emission spectroscopy on the dyes and the polymers was performed in chloroform (VPA, NPP and their polymers) or THF solutions (B504-MA, B612-MA and their polymers) at concentrations of 0.1 mg/mL respectively 1 mg/mL on a Tecan Plate Reader Infinite M1000. For the quantification of labeling, the fluorescence emission of a concentration series of both dyes was measured. The obtained intensities were corrected for background and solvent.

5.1.8.9. Electron Microscopy

For electron microscopy, 10 µL of the dispersions of the nanoparticles or nanocapsules were diluted with 1 mL of distilled water. Droplets of 10 µL were then placed on small silica platelets for SEM and on carbon-coated copper grids for TEM measurements. For TEM measurements on the PS/PLLA-system, the nanoparticles were stained with vapor of RuO_4 for 30 min prior to investigation. Both samples for SEM and TEM measurements were sputtered with carbon on a BALZERS BAE250 for five seconds to prevent beam damage. TEM observations were carried out on a JEOL 1400 at a voltage of 120 kV and images were taken with a GATAN Ultrascan 1000 CCD-camera. SEM-images were taken on a Zeiss 1530 Gemini Leo at varying voltages.

5.2. Experimental Details for Section 4.2

5.2.1. Materials

Polystyrene (PS, M_w = 300 000 g/mol, PDI = 2.38, Acros), poly(methyl methacrylate) (PMMA, M_w = 88 000 g/mol, PDI = 2.29, Acros), copper(II) sulfate (Sigma-Aldrich, 99 %), sodium azide (Sigma-Aldrich, 99.5 %), sodium hydroxide (Riedel-de Haën, 99 %), propargyl alcohol (Alfa Aesar, 99 %), triethylamine (Sigma-Aldrich, 99.5 %), 3-(trimethylsilyl)prop-2-yn-1-ol (Sigma-Aldrich, 99 %), 2-bromo-2-methylpropanoyl bromide (Sigma-Aldrich, 98 %), ammonium chloride (Roth, 99.5 %), magnesium sulfate (Sigma-Aldrich, 99 %), rhodamine B (Acros, 99 %), dimethyl aminopyridine (DMAP, Sigma-Aldrich, 99 %), *N,N'*-dicyclohexyl carbodiimide (DCC, Sigma-Aldrich, 99 %), sodium hydrogen carbonate (Fisher, 99.8 %), sodium chloride (VWR, 99.9 %), 2-chloroethanol (Sigma-Aldrich, 99 %), copper(I) bromide (Sigma-Aldrich, 99.999 %), tetra-*n*-butylammonium fluoride (TBAF, Sigma-Aldrich, 1 mol/L in THF), L-(+)-ascorbic acid (ABCR, 99 %) and sodium dodecylsulfate (SDS, Alfa Aesar, 99 %) were used as received. The solvents pentane (Sigma-Aldrich, 99 %), hexane (Fluka, 98.5 %), ethyl acetate (Sigma-Aldrich, 99.9 %), chlorobenzene (Sigma-Aldrich, 99.5 %), dimethyl formamide (DMF, Sigma-Aldrich, 99.8 %), acetonitrile (VWR, 99.9 %), diethyl ether (Sigma-Aldrich, 99.8 %), toluene (Sigma-Aldrich, 99.7 %), tetrahydrofuran (THF, Sigma-Aldrich, 99.9 %), methanol (Fluka, 99.99 %) and dichloromethane (Fluka, 99.99 %) were also used as received. Styrene (Merck, 99 %), methyl methacrylate (MMA, Sigma-Aldrich 98.5 % and vinylbenzyl chloride (VBC, Sigma-Aldrich, 97 %) were purified on a column packed with neutral aluminum oxide (Merck) before use. The initiator 2,2'-azobis(2-methylpropionitrile) (AIBN, Fluka, 98 %) was recrystallized from methanol prior to use while the ligand *N,N,N',N',N''*-pentamethyl diethylenetriamine (PMDETA, Sigma-Aldrich, 99 %) was distilled under reduced pressure. Distilled water was used throughout the work.

5.2.2. Synthesis of the Polymers

5.2.2.1. Synthesis of the Polymers by Radical Copolymerization

Copolymers of styrene or MMA and VBC were prepared according to an altered preparation procedure by Lee et al (see Fig. 5.3).[263] The monomers (for amounts see Tab. 5.3) and 164.2 mg AIBN (100 mmol) were dissolved in 20 mL (in case of MMA in 100 mL) of chlorobenzene and degassed by bubbling argon through the solution for 30 min. Afterwards the polymerization was started by heating the solution to 60 °C for 20 h. The solution was then added dropwise into methanol and the precipitated copolymer PS-*co*-PVBC or PMMA-*co*-PVBC was recovered by filtration and dried in a vacuum oven at 60 °C. After the

first drying, the polymers were dissolved in THF and reprecipitated in the same manner as before and dried in vacuo. Afterwards, the obtained polymers were analyzed by SEC, NMR, and IR spectroscopy and used for subsequent post-functionalization reactions.

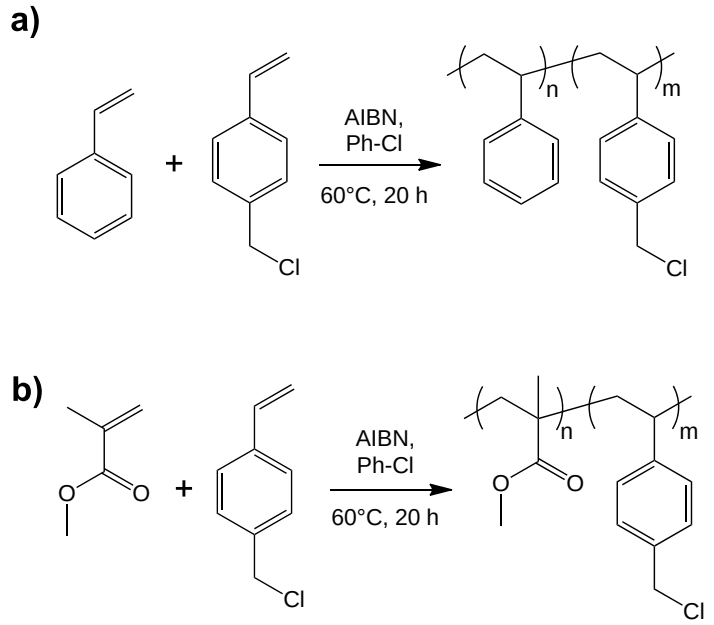

Fig. 5.3.: Copolymerization of VBC and styrene (a) or of VBC and MMA (b) in solution.

Tab. 5.3.: Amounts used for the preparation of copolymers from styrene, MMA and VBC.

Copolymer	Amounts used			Yield / g
	styrene / g	VBC / g	MMA / g	
Co-1	18.747	3.132	-	9.375
Co-2	-	3.132	18.022	9.422
Co-3	19.789	1.565	-	8.998
Co-4	-	1.566	19.023	9.062
Co-5	20.310	0.783	-	7.849
Co-6	-	0.783	19.523	9.408

5.2.2.2. Post-Functionalization of the Copolymers

For the post-functionalization of PS-*co*-PVBC with alkyne groups (see Fig. 5.4a), a solution containing 1.5 g NaOH per gram copolymer in 100 mL DMF was prepared. Subsequently, 1 mL propargyl alcohol per gram copolymer was added slowly to the solution. Afterwards, a solution of the copolymer in 150 mL THF was added, the amounts are given in Tab. 5.4. The solution was stirred for 70 h at 60 °C. Subsequently, the copolymer was purified as described above and characterized with SEC, NMR, and IR spectroscopy.

For the post-functionalization of PMMA-*co*-PVBC with azide groups (see Fig. 5.4b), a certain amount of the copolymer was dissolved in 100 mL DMF together with 250 mg NaN_3

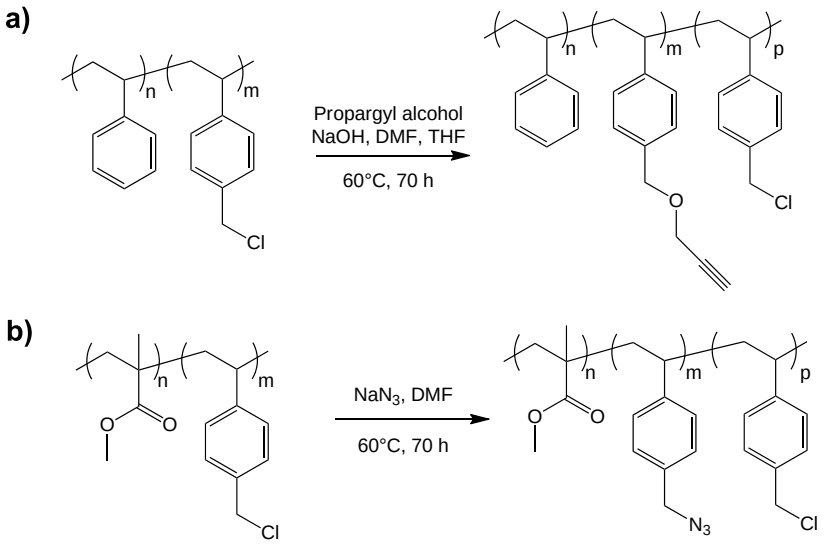

Fig. 5.4.: Post-functionalization of PS-*co*-PVBC with alkyne groups by nucleophilic substitution with propargyl alcohol (a) and of PMMA-*co*-PVBC with azide groups by use of sodium azide (b).

per gram copolymer. The amounts of the copolymer used are listed in Tab. 5.4. Argon was bubbled through the solution for 30 min. Subsequently, the temperature was increased to 60 °C and the solution was stirred for 70 h. Afterwards, the copolymer was purified as described above and characterized with SEC, NMR, and IR spectroscopy.

Tab. 5.4.: Prepared post-functionalized copolymers.

Functional Copolymer	Prepared from	$m_{Copolymer}$ / g	Functionalization	Yield / g
Co-1-f	Co-1	8.000	alkyne	4.576
Co-2-f	Co-2	9.000	azide	5.163
Co-3-f	Co-3	8.490	alkyne	4.336
Co-4-f	Co-4	8.601	azide	6.005
Co-5-f	Co-5	7.350	alkyne	5.975
Co-6-f	Co-6	8.905	azide	5.696

5.2.2.3. Synthesis of the Polymers by ATRP

The ATRP-initiator 3-(trimethylsilyl)prop-2-yn-1-yl 2-bromo-2-methylpropanoate was prepared according to a procedure by Opsteen and Hest[266] with some small alterations (see Fig. 5.5). To a solution of triethylamine (2.515 mL, 17.9 mmol) and 3-(trimethylsilyl)prop-2-yn-1-ol (1.796 mL, 17.86 mmol) in 80 mL of THF, a solution of 2-bromo-2-methylpropanoyl bromide (2.2 mL, 17.86 mmol) in 40 mL of THF was added dropwise at 0 °C. The solution was stirred at room temperature for 1 h after which 10 mL of methanol were added. After removal of the precipitated Et_3NHBr, the solvent was removed by distillation. The residue

was dissolved in 20 mL of dichloromethane and washed twice with saturated ammonium chloride solution (20 mL) and water (20 mL) after which it was dried with magnesium sulfate. The dichloromethane was removed by distillation and the residue was purified by column chromatography with hexane/ethyl acetate (20:1). A colorless oil was obtained.

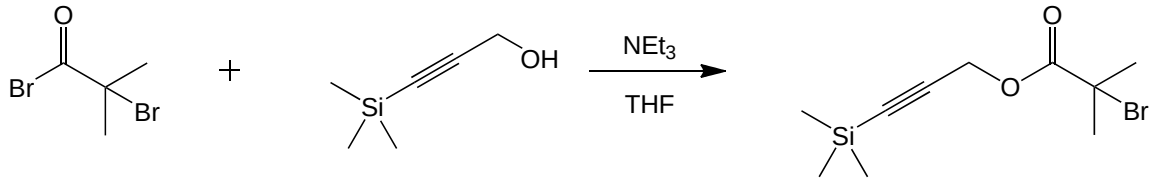

Fig. 5.5.: Synthesis of the ATRP-initiator 3-(trimethylsilyl)prop-2-yn-1-yl 2-bromo-2-methylpropanoate.

Yield: 2.2 g, 7.6 mmol, 43 %
^{1}H-NMR (300 MHz, CD_2Cl_2, δ in ppm): 4.75 (s, 2H); 1.93 (s, 6H); 0.18 (s, 9H)
^{13}C-NMR (300 MHz, CD_2Cl_2, δ in ppm): 171.32; 98.86; 93.09; 56.05; 54.72; 31.06; 0.11
FT-IR (λ^{-1} in cm^{-1}): 2962 (CH_3); 2182 (alkyne); 1744 (ester); 642 (C−Br)

The azide-containing ATRP-initiator 2-azidoethyl 2-bromo-2-methylpropanoate was prepared in two steps (see Fig. 5.6). To a solution of 2-chloroethanol (13.4 mL, 200 mmol) in 150 mL of NaOH (1 mol/L), NaN_3 (51.2 g, 800 mmol) was added. This mixture was stirred for 1 h at room temperature and for 24 h at 50 °C. After cooling the solution to room temperature, 20 g NaCl was added. Subsequently, the solution was extracted with CH_2Cl_2 five times. The organic phase was washed, dried with $MgSO_4$ and the organic solvent was removed. A clear liquid was obtained.

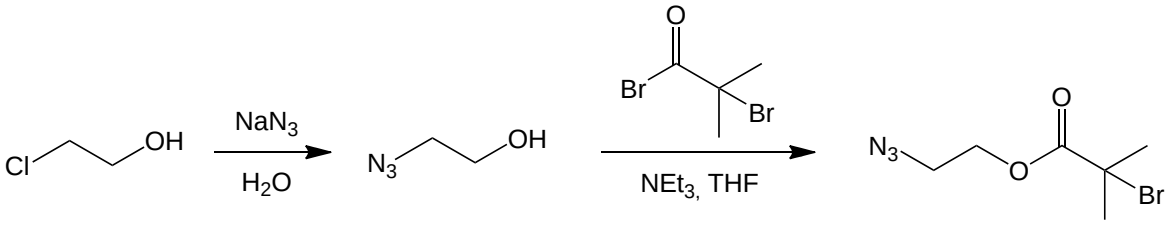

Fig. 5.6.: Synthesis of the ATRP-initiator 2-azidoethyl 2-bromo-2-methylpropanoate in two steps.

Yield: 12.4 g, 142 mmol, 71 %
^{1}H-NMR (300 MHz, CD_2Cl_2, δ in ppm): 3.72 (t, 2H, J = 6 Hz); 3.39 (t, 2H, J = 6 Hz)
^{13}C-NMR (300 MHz, CD_2Cl_2, δ in ppm): 62.05; 54.18
FT-IR (λ^{-1} in cm^{-1}): 3372 (OH); 2877 (CH_2); 2104 (N_3)

For the second step, a solution of triethylamine (3.77 mL, 26.85 mmol) and 2-azidoethanol (1.055 g, 18.18 mmol) in 120 mL of THF was added dropwise to a solution of 2-bromo-2-methylpropanoyl bromide (3.3 mL, 26.85 mmol) in 60 mL of THF at 0 °C. The solution

was stirred at room temperature for 1 h after which 15 mL of methanol were added. After removal of the precipitated Et_3NHBr, the solvent was removed by distillation. The residue was dissolved in 30 mL of dichloromethane and washed three times with saturated ammonium chloride solution (30 mL) and twice with water (30 mL) after which it was dried with magnesium sulfate. The dichloromethane was removed by distillation and the residue was purified by column chromatography with hexane/ethyl acetate (15:1). A slightly yellow oil was obtained.

Yield: 1.8 g, 7.6 mmol, 28 %
^{1}H-NMR (300 MHz, CD_2Cl_2, δ in ppm): 4.32 (t, 2H, J = 6 Hz); 3.52 (t, 2H, J = 6 Hz); 1.94 (s, 6H)
^{13}C-NMR (300 MHz, CD_2Cl_2, δ in ppm): 171.88; 65.16; 56.22; 50.30; 31.06
FT-IR (λ^{-1} in cm^{-1}): 2929 (CH_2); 2103 (N_3); 1739 (ester)

To prepare azide-functionalized PS (also see Fig. 5.7), dry copper(I) bromide (28.0 mg, 0.206 mmol), freshly distilled PMDETA (0.042 mL, 0.206 mmol), 2-azidoethyl 2-bromo-2-methylpropanoate (47.0 mg, 0.206 mmol) and styrene (11.4 mL, 103 mmol) were added to a dried Schlenk-flask in a steady stream of argon and then dissolved in 35 mL of dry toluene. The solution was subsequently degassed by freezing it with liquid nitrogen, degassing by vacuum and warming to room temperature. This process was performed three times. Afterwards, the flask was immersed into a preheated oil bath (90 °C) in which the solution was stirred for 72 h. The polymerization was stopped by removal of the oil bath and opening of the flask to air. For purification, the polymer solution was passed over a short column packed with aluminum oxide and precipitated as described before. Subsequently, the polymer was purified by repeated reprecipitation and analyzed by SEC, NMR, and IR spectroscopy.

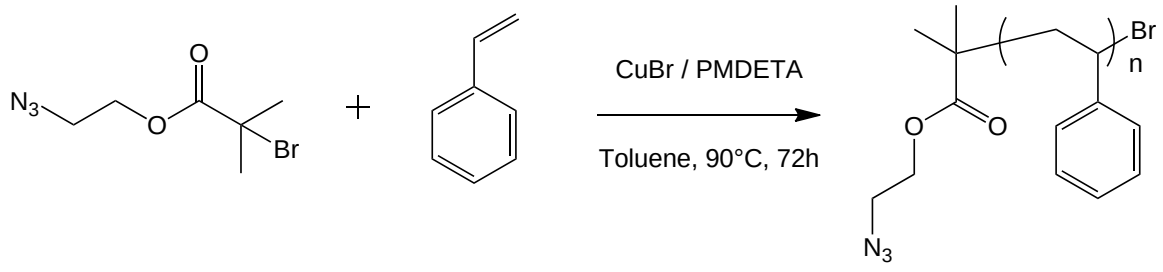

Fig. 5.7.: Synthesis of azide end-functionalized PS.

Yield: 5.0 g, M_n = 33 200 g/mol, PDI = 1.17
^{1}H-NMR (300 MHz, CD_2Cl_2, δ in ppm): 7.06 (m); 6.57 (m); 4.46 (m); 3.53 (m); 1.82 (m); 1.52 (m)
FT-IR (λ^{-1} in cm^{-1}): 3434 (aryl-H); 3023 (CH_2); 2920 (CH)

To prepare alkyne-functionalized PMMA (see Fig. 5.8), dry copper(I) bromide (31.0 mg, 0.206 mmol), freshly distilled PMDETA (0.045 mL, 0.206 mmol), 3-(trimethylsilyl)prop-2-yn-1-yl 2-bromo-2-methylpropanoate (63.0 mg, 0.206 mmol) and methyl methacrylate (11.5 mL,

103 mmol) were added to a dried Schlenk-flask in a steady stream of argon and then dissolved in 35 mL of dry toluene. The solution was subsequently degassed by freezing it with liquid nitrogen, degassing by vacuum and warming to room temperature. This process was performed three times. Afterwards, the flask was immersed into a preheated oil bath (90 °C) in which the solution was stirred for 5 h. The polymerization was stopped by removal of the oil bath and opening of the flask to air. For purification, the polymer solution was passed over a short column packed with aluminum oxide and precipitated as described above. Subsequently, the polymer was purified by repeated reprecipitation and analyzed by SEC, NMR, and IR spectroscopy.

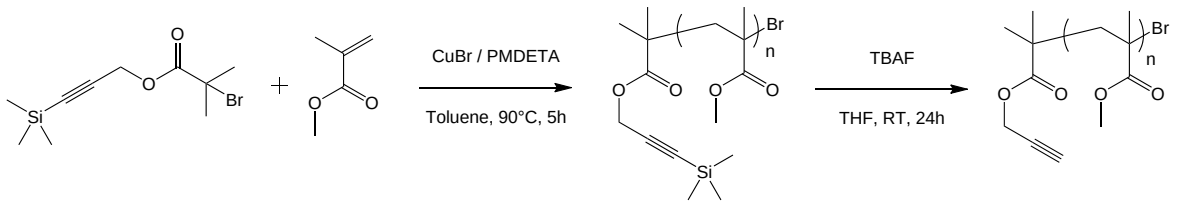

Fig. 5.8.: Synthesis and subsequent deprotection of alkyne end-functionalized PMMA.

Yield: 2.8 g, $M_n = 26\,400$ g/mol, PDI = 1.12
^{1}H-NMR (300 MHz, CD_2Cl_2, δ in ppm): 4.61 (s); 3.57 (s); 1.80-0.81 (m); 0.17 (s)
FT-IR (λ^{-1} in cm^{-1}): 2952 (CH_3); 1731 (ester)

To remove the protecting trimethylsilane-group from the polymer, 1.25 mL of a TBAF-solution (1 mol/L in dry THF) was added to a solution of 2.5 g polymer in 12.5 mL dry THF. The solution was stirred for 24 h at room temperature and the polymer was obtained as described above. Subsequently, the polymer was purified by repeated reprecipitation and analyzed by SEC, NMR, and IR spectroscopy.

Yield: 2.1 g, $M_n = 29\,000$ g/mol, PDI = 1.11
^{1}H-NMR (300 MHz, CD_2Cl_2, δ in ppm): 4.64 (s); 3.58 (s); 2.52 (s); 1.80-0.81 (m)
FT-IR (λ^{-1} in cm^{-1}): 2952 (CH_3); 1731 (ester)

5.2.3. Preparation of Janus Particles

For the preparation of particles, 46.9 mg of the PS-component and 53.1 mg of the PMMA-component were dissolved in 2.5 g CH_2Cl_2 (see Tab. 5.5). An aqueous solution of SDS with a volume of 20 mL was added. Subsequently, a pre-emulsion was formed by stirring at 1250 rpm for 1 h. Afterwards, the pre-emulsion was subjected to ultrasonication for 2 min at 70 % amplitude in a pulse-pause-program of 30 s pulse and 10 s pause all the while it was cooled in an ice-bath. The solvent was evaporated from the miniemulsion by stirring it for 16 h at 500 rpm and room temperature. The obtained particles were characterized by DLS and TEM.

Tab. 5.5.: Polymers and their amounts used for the preparation of Janus particles. The hydrodynamic diameter D of the prepared particles is also given.

Probe	m_{PS} / mg	m_{PMMA} / mg	$m_{Co\text{-}1\text{-}f}$ / mg	$m_{Co\text{-}2\text{-}f}$ / mg	$m_{Co\text{-}3\text{-}f}$ / mg	$m_{Co\text{-}4\text{-}f}$ / mg	$m_{Co\text{-}5\text{-}f}$ / mg	$m_{Co\text{-}6\text{-}f}$ / mg	$m_{ATRP\text{-}1}$ / mg	$m_{ATRP\text{-}2}$ / mg	m_{SDS} / mg	tested for	D / nm
Double-1	-	-	46.9	53.1	-	-	-	-	-	-	20	-	96
Double-2	-	-	-	-	46.9	53.1	-	-	-	-	20	-	100
Double-3	-	-	-	-	-	-	46.9	53.1	-	-	20	-	104
Double-4	-	-	-	-	-	-	-	-	53.1	46.9	20	-	107
Double-5	-	-	46.9	53.1	-	-	-	-	-	-	2	-	208
Double-6	-	-	-	-	46.9	53.1	-	-	-	-	2	-	214
Double-7	-	-	-	-	-	-	46.9	53.1	-	-	2	-	199
Double-8	-	-	-	-	-	-	-	-	53.1	46.9	2	-	210
Quant-1	46.9	53.1	-	-	-	-	-	-	-	-	20	alkyne	96
Quant-2	46.9	53.1	-	-	-	-	-	-	-	-	20	azide	96
Quant-3	46.9	53.1	-	-	-	-	-	-	-	-	2	alkyne	220
Quant-4	46.9	53.1	-	-	-	-	-	-	-	-	2	azide	220
Quant-5	-	53.1	46.9	-	-	-	-	-	-	-	20	alkyne	100
Quant-6	46.9	-	-	53.1	-	-	-	-	-	-	20	azide	105
Quant-7	-	53.1	-	-	46.9	-	-	-	-	-	20	alkyne	103
Quant-8	46.9	-	-	-	-	53.1	-	-	-	-	20	azide	93
Quant-9	-	53.1	-	-	-	-	46.9	-	-	-	20	alkyne	103
Quant-10	46.9	-	-	-	-	-	-	53.1	-	-	20	azide	99
Quant-11	46.9	-	-	-	-	-	-	-	53.1	-	20	alkyne	93
Quant-12	-	53.1	-	-	-	-	-	-	-	46.9	20	azide	93
Quant-13	-	53.1	46.9	-	-	-	-	-	-	-	2	alkyne	221
Quant-14	46.9	-	-	53.1	-	-	-	-	-	-	2	azide	211
Quant-15	-	53.1	-	-	46.9	-	-	-	-	-	2	alkyne	200
Quant-16	46.9	-	-	-	-	53.1	-	-	-	-	2	azide	197
Quant-17	-	53.1	-	-	-	-	46.9	-	-	-	2	alkyne	204
Quant-18	46.9	-	-	-	-	-	-	53.1	-	-	2	azide	222
Quant-19	46.9	-	-	-	-	-	-	-	53.1	-	2	alkyne	221
Quant-20	-	53.1	-	-	-	-	-	-	-	46.9	2	azide	216

5.2.4. Determination of the Surface Functionalization

5.2.4.1. Synthesis of Clickable Dyes

For the preparation of alkyne-functionalized rhodamine B, which is shown in Fig. 5.9a, 9.58 g (1 eq, 0.020 mol) of rhodamine B and 24 mg (0.0002 mol) of DMAP were introduced in a dried Schlenk-flask. The air was removed from the flask by application of a vacuum and argon was added. This step was repeated twice. Afterwards, 1.27 mL (1.1 eq, 0.022 mol) of propargyl alcohol and 100 mL of dry dichloromethane were added with a syringe. The flask was cooled to 0 °C and 8.3 g (2 eq, 0.04 mol) of DCC were added under a steady stream of argon. The solution was stirred for 30 min at 0 °C and for another 24 h at room temperature. The colorless precipitate was removed by filtration and 100 mL of dichloromethane were added. The solution was washed with 200 mL saturated $NaHCO_3$ solution twice and once with 200 mL of water. The organic phase was dried with magnesium sulfate and the dichloromethane was removed by distillation. The solid residue was dissolved in acetonitrile and precipitated in ether. This step was repeated twice. After filtration, the residue was washed multiple times with ether and dried in vacuo. A deeply golden powder was obtained.

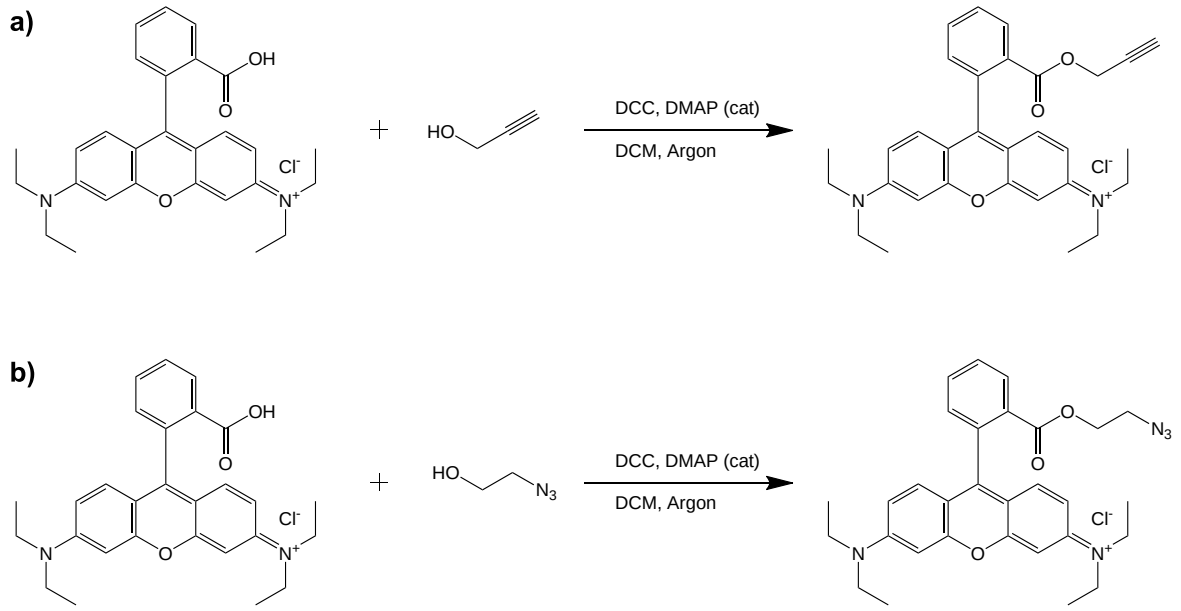

Fig. 5.9.: Synthesis of alkyne (b) and azide (b) functionalized rhodamine derivatives.

Yield: 5.149 g, 0.010 mol, 49.8 %
^{1}H-NMR (300 MHz, CD_2Cl_2, δ in ppm): 8.11 (d, 1H, $J = 7.3$ Hz); 7.76 (m, 2H); 7.25 (d, 1H, $J = 7.5$ Hz); 6.83 (d, 2H, $J = 9.3$ Hz); 6.68 (d, 2H, $J = 9.6$ Hz); 4.26 (s, 2H); 3.51 (q, 8H, $J = 3.4$ Hz); 2.56 (s, 1H); 1.14 (t, 12H, $J = 7.0$ Hz)
^{13}C-NMR (300 MHz, CD_2Cl_2, δ in ppm): 163.91; 157.37; 157.15; 155.11; 133.54; 133.40; 130.84; 130.55; 128.77; 114.58; 112.88; 95.89; 77.97; 77.36; 52.80; 45.32; 12.42
FT-IR (λ^{-1} in cm^{-1}): 2115 (alkyne)

For the preparation of azide-functionalized rhodamine B, which is shown in Fig. 5.9b, 9.58 g (1 eq, 0.020 mol) of rhodamine B and 24 mg (0.0002 mol) of DMAP were added into a dried Schlenk-flask. The air was removed from the flask by application of a vacuum and argon was added. This step was repeated twice. Afterwards, 1.92 g (1.1 eq, 0.022 mol) of azidoethanol and 100 mL of dry dichloromethane were added with a syringe. Afterwards, the same procedure as for alkyne-functionalized rhodamine dye was used.

Yield: 5.976 g, 0.011 mol, 54.5 %
^{1}H-NMR (300 MHz, CD_2Cl_2, δ in ppm): 8.21 (d, 1H, $J = 7.3$ Hz); 7.82 (m, 2H); 7.34 (d, 1H, $J = 7.5$ Hz); 6.96 (d, 2H, $J = 9.5$ Hz); 6.77 (d, 2H, $J = 9.3$ Hz); 3.87 (t, 2H, $J = 4.7$ Hz); 3.50 (q, 8H, $J = 3.4$ Hz), 3.06 (t, 2H, $J = 4.7$ Hz); 1.16 (t, 12H, $J = 7.1$ Hz)
^{13}C-NMR (300 MHz, CD_2Cl_2, δ in ppm): 164.55; 157.44; 157.20; 155.11; 133.38; 133.22; 130.86; 130.53; 129.19; 114.54; 112.91; 95.79; 63.64; 48.96; 45.31; 12.38
FT-IR (λ^{-1} in cm^{-1}): 2100 (azide)

5.2.4.2. Quantification Procedure

To quantify the amount of alkyne or azide groups on the surface of Janus particles, 400 µL of the particle dispersion was mixed with 400 µL of an aqueous solution containing 1×10^{-5} mol/L of one of the rhodamine derivatives. Additionally, 2.1 µL of freshly distilled PMDETA und 100 µL of a freshly prepared solution of $CuSO_4$ with the concentration 0.05 mol/L was added. The mixture was degassed by bubbling argon through the solution for 3 min and the click-reaction was initiated by adding 100 µL of 0.05 mol/L ascorbic acid. The mixture was left standing under shaking for 48 h in the dark. Afterwards, the dispersion was centrifuged and the residue redispersed in 1 mL of water. The centrifugation and redispersion was repeated until the supernatant did not show any fluorescence. Subsequently, the residue was dried and dissolved in 250 µL of THF. This solution was used for fluorescence measurements.

5.2.5. Analytical Tools

5.2.5.1. DLS Measurements

The hydrodynamic diameter of the particles was measured with a Nicomp 380 Submicron Particle Sizer (PSS-Nicomp) at an angle of 90° for 300 s. The latexes (10 µL) were diluted in 1000 µL of distilled water. The average of two independent measurements as well as their standard deviations is reported.

5.2.5.2. NMR Measurements

NMR-experiments were carried out on solutions of 10 mg of the substances in CD_2Cl_2 on a Bruker Avance 300. For ^{1}H-measurement, 128 scans were used while for ^{13}C-measurements 1024 scans were performed.

5.2.5.3. IR Spectroscopy

IR spectroscopy was performed on a IFS 113v Bruker spectrometer in a range of 4000 cm^{-1} to 400 cm^{-1}. Solid samples were prepared by mixing 3 mg of the substance with KBr. This mixture was pressed and subsequently measured. Liquid samples were analyzed by putting a drop of the sample between transparent NaCl-plates. The IR measurements were performed by Elke Muth at the Max Planck Institute for Polymer Research in Mainz.

5.2.5.4. SEC Measurements

SEC was used to estimate the average molecular weights of the polymers and their polydispersity index. The dried polymers were dissolved in THF at a concentration of 5 mg/mL and filtered through a 0.45 µm Teflon filter. An elution rate of 1.0 mL/min and both UV- (254 nm) and RI-detectors were used. The apparent molecular weights of the polymers were calculated using PS standards from Polymer Standard Service (PSS).

5.2.5.5. TEM Measurements

For TEM, 10 µL of the dispersions of the nanoparticles were diluted with 1 mL of distilled water. Droplets of 10 µL were then placed on carbon-coated copper grids. Subsequently, the nanoparticles were stained with vapor of RuO_4 for 30 min. Afterwards, the grids were sputtered with carbon on a BALZERS BAE250 for five seconds to prevent beam damage. TEM observations were carried out on a JEOL 1400 at a voltage of 120 kV and images were taken with a GATAN Ultrascan 1000 CCD-camera.

5.2.5.6. Absorption and Fluorescence Measurements

Absorption and fluorescence measurements on the prepared dyes were done in THF solutions on a Tecan Plate Reader Infinite M1000. For the quantification of the functional groups on the surface of Janus particles, the Janus particles were also dissolved in THF. An excitation wavelength of 560 nm and an emission wavelength of 584 nm were used. The obtained intensities were corrected for background and solvent.

5.3. Experimental Details for Section 4.3

5.3.1. Materials

The block copolymer PVFc-*b*-PMMA was prepared by living anionic polymerization as described previously[340] in the group of Dr. Markus Gallei at the TU Darmstadt. The molecular weight of PVFc was determined via SEC against PVFc standards and with size exclusion chromatography with multi angle light scattering detection (SEC-MALLS) (M_n = 9600 g/mol, M_w = 11 000 g/mol, PDI = 1.14). The molecular weight of PVFc-*b*-PMMA was measured via SEC in THF against PS standards (M_n = 139 700 g/mol, M_w = 142 500 g/mol, PDI = 1.02). Poly(methyl methacrylate) (PMMA, Acros, M_w = 88 000 g/mol, PDI = 2.29), hexadecane (HD, Acros, 99.8 %), sodium dodecylsulfate (SDS, Alfa Aesar, 99 %), dichloromethane (Fisher, 99.99 %), cyclohexane (VWR, HPLC-grade), $FeCl_3$ (Sigma-Aldrich, 97 %), L-(+)-ascorbic acid (ABCR, 99 %), H_2O_2 (Sigma-Aldrich, 35 % in water), and $KMnO_4$ (Sigma-Aldrich, 99 %) were used as received. Distilled water was used throughout the work.

5.3.2. Preparation of the Nanoparticles and Nanocapsules

To prepare the nanoparticles, 100 mg of the polymer PVFc-*b*-PMMA or PMMA was dissolved in 2.5 g of CH_2Cl_2 to which a solution of 2 mg of SDS in 20 g of water was added. The mixture was stirred at 1250 rpm in a closed glass vial to obtain a macroemulsion. The emulsion was then subjected to ultrasonication under ice-cooling for 2 min in a pulse-pause-regimen of 30 s and 10 s, respectively (Branson W450-D sonifier with a 1/2-inch tip). Afterwards, the CH_2Cl_2 was evaporated at 40 °C while stirring at 500 rpm overnight. For the preparation of nanocapsules, 60 mg of polymer and 40 mg of HD were dissolved in 2.5 g CH_2Cl_2, and the aforementioned procedure was followed.

5.3.3. Oxidation of the Nanoparticles and Nanocapsules

For oxidation experiments, the dispersions were diluted to reach a total volume of 24 mL. The diluted dispersions of nanoparticles were then divided in three equal parts, which were further treated either with 1 mL of 35 % H_2O_2 solution, 1 mL of a freshly prepared $KMnO_4$ solution (158 mg $KMnO_4$ in 100 mL water), 1 mL of 0.0053 mol/L $FeCl_3$ aqueous solution or 1 mL of distilled water. The oxidants were in slight molar excess compared to the vinylferrocene units in the copolymer. For nanocapsules, the volume of added solutions of oxidants was reduced to 0.6 mL to keep the reaction ratios constant. Afterwards, the sealed dispersions were stirred for 24 h and dialyzed against distilled water for 48 h with a Visking 27/32 dialysis

tube (Roth, cut-off of 14 000 g/mol). The nanoparticles and nanocapsules oxidized by H_2O_2 and $KMnO_4$ were reduced by the addition of 0.5 mL of a 0.1 mol/L solution of ascorbic acid and stirred for 24 h at room temperature.

5.3.4. Release experiments

For the release experiments, a solution of 1 mg pyrene in 2.5 g of CH_2Cl_2 was used to dissolve the polymer. After the preparation of the nanocapsules or nanoparticles, the dispersions were dialyzed as described above and treated with the different oxidizing reagents. A 0.75 mL portion of the dispersion was withdrawn from the vial at certain time intervals. Then 1.5 mL of cyclohexane was added to the dispersion and the mixture was shaken for a short time. After rapid phase separation, 0.75 mL of the upper phase was removed and 0.75 mL of cyclohexane was added again. After shaking and phase separation, the upper phase was removed again. This procedure was repeated one more time; therefore the total volume of cyclohexane amounted to 2.25 mL, from which the fluorescence intensity was measured.

5.3.5. Analytical tools

5.3.5.1. SEC Measurements

SEC was performed with THF as the mobile phase (flow rate 1 mL/min) on a Mixed Gel column set from PL (PL Mixed Gel B, PL Mixed Gel C, PL Mixed Gel D) or an SDV column set from PSS, Mainz (SDV 1000, SDV 100 000, SDV 1 000 000) at 30 °C. Calibration was carried out using PS from PSS and PVFc (synthesized) calibration standards.

For the SEC-MALLS experiments, a system composed of a Waters 515 pump (Waters, Milford, CT), a TSP AS100 auto sampler, a Waters column oven, a Waters 486 UV detector operating at 254 nm, a Waters 410 RI-detector, and a DAWN DSP light scattering detector (Wyatt Technology, Santa Barbara, CA) was used. For data acquisition and evaluation of the light scattering experiments, Astra version 4.73 (Wyatt Technology, Santa Barbara, CA) was employed. The light scattering instrument was calibrated using pure toluene, assuming a Rayleigh ratio of $9.78 \times 10^{-6}\,cm^{-1}$ at 690 nm. An injection volume of 118 µL, a sample concentration between 1 g/L and 2 g/L, a column temperature of 35 °C and a THF flow rate of 1 mL/min was used and SEC analysis was performed on a high resolution column set from PSS (SDV 5 µm, 106 Å, SDV 5 µm, 105 Å, SDV 5 µm, 1000 Å). The SEC-MALLS-experiments were carried out in the group of Dr. Markus Gallei at the TU Darmstadt.

5.3.5.2. Fluorescence Measurements

To measure the amount of pyrene released from the nanoparticles and nanocapsules, its fluorescence intensity was measured on a Tecan Plate Reader Infinite M1000 at an excitation wavelength of 335 nm in cyclohexane. All measurements were performed in quadruplet.

5.3.5.3. HPLC Measurements

HPLC measurements were conducted to check the polarity of the polymer. Dispersions of oxidized and non-oxidized nanocapsules were freeze-dried. HPLC measurements were performed with a gradient of THF + 0.1 % TFA in water starting from a ratio of 60 to 40 up to 100 to 0 in 20 min. The flow was 1 mL/min employing a Thermo PFP column on a 1200 HPLC from Agilent Technologies equipped with a Varian 385-LC light scattering detector.

5.3.5.4. Electron Microscopy

For electron microscopy, 10 µL of the dispersions of the nanoparticles and nanocapsules were diluted with 1 mL of distilled water. Dispersion droplets of 3 µL were then placed on small silica platelets for SEM and on copper grids for TEM measurements. Both sample types were sputtered with carbon on a BALZERS BAE250 for 5 s to prevent beam damage during the SEM and TEM measurements. TEM observations were carried out on a JEOL 1400 at a voltage of 120 kV and images were taken with a GATAN Ultrascan 1000 CCD-camera. Due to the inherent phase contrast between PMMA and PVFc, no further contrasting was needed. SEM images were taken on a Zeiss 1530 Gemini Leo at varying voltages, while SEM-EDX scans were taken on a Hitachi SU8000 at 2 kV.

5.3.5.5. XPS Measurements

XPS investigations were performed in a PHI 5000 spectrometer with a monochromatic Al-K_α radiation ($h\nu = 1486.6$ eV). The diameter of the X-ray illuminated area was 200 µm. The photoelectron spectra were collected at a pass energy of $E = 11.75$ eV and an electron escape angle of $\theta = 45°$. The binding energies were calibrated with respect to the $Ag3d_{5/2}$ photoelectron line and the Fermi level of a sputtered Ag foil. As the samples were not well electronically conductive, a neutralizer equipped with a low voltage electron gun and a floating ion gun generating a low energy ion beam to compensate the sample charge was employed. Additionally, the measured photoelectron spectra were referred to the C1s photoelectron emission of the C-C bond ($E = 284.5$ eV). The nanocapsules dispersions were dropped on a silicon wafer and left in a desiccator for 48 h and the sample was subsequently dried under vacuum. The XPS measurements were carried out at the TU Darmstadt.

5.3.5.6. SFM Measurements

SFM imaging was were carried out with a Dimension 3100 and Environmental Scope (Bruker) at a controlled humidity of 50 % at room temperature.[392] An Olympus OMCL-AC160TS cantilever in tapping mode (nominal spring constant $K = 42\,\mathrm{N/m}$ and nominal resonance frequency $F_0 = 300\,\mathrm{kHz}$) was used. The dispersions were diluted by a factor of 100 and placed on silicon wafers to dry. The SFM measurements were conducted by Helma Burg and Dr. Rüdiger Berger at the Max Planck Institute for Polymer Research in Mainz.

5.3.5.7. CV Measurements

CV measurements were conducted in acetonitrile with tetra-(*n*-butyl)-ammonium hexafluorophosphate (TBAHFP) as electrolyte ($c = 0.1\,\mathrm{M}$). An $Ag/AgNO_3$ reference electrode and Pt counter electrodes were chosen and scan rates from 60 mV/s to 90 mV/s in a range of $-1.0\,\mathrm{V}$ to $1.7\,\mathrm{V}$ were applied. Calibration was carried out using Fc/Fc^+ as standard. The nanocapsules were deposited on an ITO slide. The CV measurements were carried out in the group of Dr. Markus Gallei at the TU Darmstadt.

5.3.5.8. DLS Measurements

The hydrodynamic diameter of the nanoparticles and nanocapsules was measured by DLS on diluted dispersions with a Nicomp™ 380 Submicron Particle Sizer (PSS-Nicomp) at an angle of 90° for 300 s.

5.4. Experimental Details for Section 4.4

5.4.1. Materials

Dichloromethane (Fisher, 99.99 %), hexadecane (HD, Acros, 99.8 %), cetyltrimethylammonium chloride (CTMA-Cl, Acros, 99 %), Nile red (Sigma-Aldrich), hydrogen peroxide (H_2O_2, Sigma-Aldrich, 35 %), deuterated water (D_2O, Sigma-Aldrich, 99.9 %), dimethyldodecylamine (DDA, Fluka, 99.9 %) and diphenyl disulfide (DPDS, Sigma-Aldrich, 99 %) were used as received. Sodium hydroxide and hydrochloric acid solutions were prepared by diluting stock solutions (both from VWR, 1 mol/L) to the desired value. Distilled water was used for the preparation of all solutions. The stimuli-responsive polymers PVFc-*b*-P2VP and PS-*b*-PDMAEMA (see Fig. 4.57) as well as the homopolymers of these block copolymers, that is PVFc, PDMAEMA, P2VP and PS were prepared by the group of Dr. Markus Gallei at the TU Darmstadt. The characterization data of the polymers as well as their responsiveness to different stimuli are provided in Tab. 5.6.

5.4.2. Preparation of Nanocapsules

To prepare the nanocapsules, 50 mg of the respective polymer and 50 mg HD were dissolved in 2.5 g of dichloromethane containing Nile red at a concentration of 1 mg per 2.5 g dichloromethane. Then a solution of 1 mg CTMA-Cl in 20 mL of water having a NaOH-concentration of 0.0001 mol/L was added. The mixture was stirred at 1250 rpm for 1 h in a closed glass vial to obtain a macroemulsion. The emulsion was then subjected to ultrasonication under ice-cooling for 2 min in a pulse-pause regimen of 30 s and 10 s, respectively, with a Branson W450-D sonifier equipped with a 1/2 inch tip. Afterwards, the dichloromethane was evaporated at room temperature while stirring at 500 rpm for 16 h. Subsequently, the dispersions were dialyzed against their continuous phase for two days to remove non-encapsulated dye molecules. For the release experiments with DDA and DPDS, deuterated water was used instead of water. When DDA was used as a core material, 50 mg of DDA were used instead of HD. When DPDS was present in the capsules, 20 mg of DPDS was dissolved together with HD and the polymer.

Tab. 5.6.: Molecular weights of the block copolymers and their homopolymers used in this study as well as their method of determination.

Polymer	Block	M_n / g/mol	M_w / g/mol	PDI	Stimulus	Method of Determination
PVFc-*b*-P2VP	PVFc	14200	22000	1.54	Ox	SEC-MALLS
	P2VP	204000	-	-	pH	Difference of PVFc-precursor and block copolymer
	PVFc-*b*-P2VP	218200	232300	1.06	Ox, pH	Block copolymer SEC vs. PS
PS-*b*-PDMAEMA	PS	73900	76800	1.03	-	SEC vs. PS
	PDMAEMA	11200	-	-	pH, T	Difference of PS-precursor and block copolymer
	PS-*b*-PDMAEMA	85100	-	-	pH, T	Calculated from ^{1}H-NMR
PS	-	198900	206600	1.04	-	SEC vs. PS
PVFc	-	11900	12800	1.08	Ox	SEC-MALLS
PDMAEMA	-	25000	-	-	pH, T	Calculated from ^{1}H-NMR (rough value)
P2VP	-	25800	25900	1.004	pH	SEC-MALLS
		15900	16500	1.04	pH	SEC vs. PS

5.4.3. Further Treatment of the Nanocapsules

In order to elucidate the pH-responsiveness of the nanocapsules, equal volumes of the dispersion and hydrochloric acid at different concentrations (0.000 01 mol/L to 1 mol/L) which also contained 1 mg CTMA-Cl per 20 mL were mixed. The dispersions were then stirred for 24 h. Equal volumes of dispersion and a freshly prepared hydrogen peroxide solution containing 1 mg CTMA-Cl per 20 mL were mixed and stirred for 24 h to oxidize the PVFc-*b*-P2VP nanocapsules. To prove the temperature-responsiveness of PS-*b*-PDMAEMA, the dispersions were put into preheated oil baths at different temperatures and treated with hydrochloric acid as described above. The dispersions were then subsequently stirred for 24 h. Samples of the dispersions were also diluted with their continuous phase without addition of acid or oxidant to obtain control samples. Otherwise, they were handled the same way as the samples with added acid or oxidant.

5.4.4. Analytical Tools

5.4.4.1. DLS Measurements

The hydrodynamic diameter of the nanocapsules was measured by DLS on the dispersions with a Nicomp™ 380 Submicron Particle Sizer (PSS-Nicomp) at an angle of 90° for 300 s.

5.4.4.2. NMR Measurements

NMR spectra were recorded on a Bruker DRX 500 NMR operating at 500 MHz for the determination of the molecular weights. These experiments were performed in the group of Dr. Markus Gallei at the TU Darmstadt. The stimuli-selective release from the block copolymer nanocapsules was measured on a Bruker DRX 300 spectrometer working at 300 MHz.

5.4.4.3. SEC Measurements

Standard SEC was performed with THF as the mobile phase (flow rate 1 mL/min) on a SDV column set from PSS, Mainz (SDV 1000, SDV 100000, SDV 1000000) at 30 °C. The calibration was carried out using PS standards from PSS, Mainz. For the SEC-MALLS experiments, a system composed of a Waters 515 pump (Waters, Milford, CT), a TSP AS100 autosampler, a Waters column oven, a Waters 486 UV-detector operating at 254 nm, a Waters 410 RI-detector, and a DAWN DSP light scattering detector (Wyatt Technology,

Santa Barbara, CA) was used. For the data acquisition and the evaluation of the light-scattering experiments, Astra version 4.73 (Wyatt Technology, Santa Barbara, CA) was used. The light-scattering instrument was calibrated using pure toluene, assuming a Rayleigh ratio of $9.78 \times 10^{-6}\,\mathrm{cm}^{-1}$ at 690 nm. An injection volume of 118 µL, a sample concentration of 1 g/L to 2 g/L, a column temperature of 35 °C, and a THF flow rate of 1 mL/min were applied. SEC analysis was performed on a high resolution column set from PSS (SDV 5 µm, 106 Å, SDV 5 µm, 105 Å, SDV 5 µm, 1000 Å). The SEC measurements were performed in the group of Dr. Markus Gallei at the TU Darmstadt.

5.4.4.4. Absorption and Emission Spectroscopy

The fluorescence intensity at the emission wavelength of 624 nm of the treated dispersion was measured on a Tecan Plate Reader Infinite M1000 at an excitation wavelength of 520 nm in all release experiments.

5.4.4.5. Electron Microscopy

Droplets of 3 µL of the dispersions were placed on small silica platelets for SEM measurements and on copper grids for TEM measurements. Both sample types were sputtered with carbon on a BALZERS BAE250 for 5 s to prevent beam damage during the measurements. TEM observations were carried out on a JEOL 1400 at a voltage of 120 kV and images were taken with a GATAN Ultrascan 1000 CCD-camera. SEM images were carried out on a Zeiss 1530 Gemini Leo at 0.4 kV.

6. Conclusions

In this thesis, different complex colloids were prepared. The term "complex" is used to include both an addressable functionality as well as the heterogeneous nature of the colloids.

Firstly, the mechanism of the SEED process especially in regard to coalescence was investigated, as the process was used throughout the thesis. A wide variety of different techniques was employed to study the coalescence of nanodroplets during the evaporation of the solvent. DLS turned out not to be a suitable method to determine droplet coalescence as the evaluation of the hydrodynamic diameter of the droplets was highly dependent on the diluent and on the dilution. Neither FCS nor zeta-potential measurements showed a change in the nanodroplet concentration and fluorescence brightness or a change in the zeta-potential of the nanodroplets, respectively. While these results point to an absence of coalescence, the data are also dependent on dilution. Thus, other methods were developed. TEM measurements were conducted on mixed polymeric emulsions with the results pointing to an absence of coalescence. However, these results were not quantifiable. FRET measurements on mixed polymeric emulsions also indicated an absence of coalescence. However, again the results were not quantifiable. The amount of coalescence taking place was then quantified by the application of DC-FCCS. This method also allowed for measuring coalescence in other processes such as the miniemulsion polymerization or the polycondensation reaction on the interface of the droplets. Simulations were performed to estimate the effect of the measured amount of coalescence on the final particle size distribution. It was shown that coalescence is not responsible for the usually observed broad size distribution. Therefore, the process itself, especially the emulsification step, needs to be improved to generate monodisperse colloids.

The Janus morphology is probably the best known among the different complex morphologies of nanoparticles. With the help of functional polymers, it was possible to marry click-chemistry to Janus particles. The marriage was achieved by the synthesis and subsequent post-functionalization of copolymers with alkyne and azide groups. By varying the ratio of the monomers, it was possible to obtain copolymers with different degrees of functionalization. In addition, polymers with exactly one alkyne or azide functional group per chain were synthesized by ATRP using functional initiators. The large library of functional polymers prepared was then used to generate Janus particles by the SEED process. Both dually

functionalized Janus particles and particles with one functionalized face could be obtained. The latter were used for the quantification of functional groups on the surface of the Janus particles. For this, clickable fluorescent dyes were synthesized. The degree of functionality of the polymers was found to be closely mirrored in the degree of functionality of the surface. Thus, the marriage of click-chemistry to Janus particles was successful.

Another complex morphology besides Janus particles are nanocapsules. Stimulus-responsive nanocapsules that show triggered release are a highly demanding and interesting system, as nanocapsules have promising applications in drug delivery and in self-healing materials. To achieve heterogeneity in the polymer shell, the stimulus-responsive block copolymer PVFc-*b*-PMMA was employed for the preparation of the capsules. The phase separation of the two blocks in the shell of the capsule led to a patchy morphology. These patches could then be oxidized with ionic or non-ionic oxidants. The oxidations resulted in different morphology changes such as outgrowths and indents. In addition, swelling occurred because of the hydrophobic to hydrophilic transition of the patches induced by the oxidation. Because of the swelling, an encapsulated payload could diffuse out of the capsules, hence release was achieved.

The concept of using block copolymers responsive to one stimulus for the preparation of stimulus-responsive capsules was extended to block copolymers responsive to more than one stimulus. Here, a block copolymer responsive to oxidation and a pH change as well as a block copolymer responsive to a pH change and temperature were studied in detail. The capsule preparation process was extended to work under basic conditions, as both block copolymers were sensitive to neutral or acidic pH values. Subsequently, the effect of the different stimuli on the morphology and the release behavior of the capsules was studied. The release from the nanocapsules could be regulated by tuning the different stimuli. In addition, by encapsulating stimuli-responsive payloads it was possible to selectively release a payload upon one stimulus but not upon the other one.

In conclusion, the approaches taken in the course of this thesis demonstrate the broad applicability and usefulness of the SEED process to generate complex colloids. In addition, the experimental techniques established such as DC-FCCS will provide further insight into other research areas as well.

7. Zusammenfassung

In dieser Arbeit wurden verschiedene komplexe Kolloide hergestellt. Hierbei beinhaltet der Begriff „komplex“ sowohl die adressierbare Funktionalität als auch die heterogene Natur der Kolloide. Da zur Herstellung der Kolloide das Lösemittelverdampfungsverfahren aus Emulsionströpfchen eingesetzt wurde, wurde zunächst dessen Mechanismus untersucht. Hierbei wurde ein besonderes Augenmerk auf die eventuell stattfindende Koaleszenz der Tröpfchen gelegt.

Verschiedenste Messmethoden wurden eingesetzt, um die Koaleszenz von Emulsionströpfchen während der Verdampfung des Lösemittels aus den Tröpfchen zu untersuchen. Aufgrund der Abhängigkeit der Messergebnisse vom Verdünnungsmittel und der Stärke der Verdünnung wurde DLS als Messmethode verworfen. Während FCS-Messungen keine Änderungen in der Konzentration der Nanotröpfchen und ihrer Helligkeit zeigten, wurde mit zeta-Potential-Messungen keine Änderung der Oberflächenbedeckung der Tröpfchen mit Tensid festgestellt. Obgleich diese Ergebnisse auf die Abwesenheit von Koaleszenz hindeuten, waren sie doch durch Verdünnung beeinflusst sein. Daher wurden neue Methoden entwickelt. Zunächst wurden TEM-Messungen durchgeführt, die ebenfalls auf das Nichtvorhandensein von Koaleszenz hindeuteten. Allerdings waren diese Ergebnisse nicht quantifizierbar. Dies galt auch für FRET-Messungen, die ebenso die Anwesenheit von Koaleszenz negierten. Mittels des Einsatzes von DC-FCCS konnte schließlich nachgewiesen werden, dass Koaleszenz nur zu einem geringen Umfang stattfindet. Im Folgenden wurden mit DC-FCCS auch andere Systeme wie die Miniemulsionspolymerisation und die Polykondensation an Tropfengrenzflächen auf Koaleszenz untersucht. Durch die erfolgte Quantifizierung der Koaleszenz konnten Simulationen durchgeführt werden, die nachwiesen, dass Koaleszenz nur einen zu vernachlässigenden Einfluss auf die Größenverteilung der Partikel hat. Somit muss der Lösemittelverdampfungsprozess und hier insbesonders der Emulsifikationsschritt weiter optimiert werden, um monodisperse Partikel zu erhalten.

Unter den vielen komplexen Morphologien von Nanopartikeln ist die Janus-Morphologie eine der bekanntesten. In Kombination mit funktionellen Polymeren konnte Klick-Chemie mit Janus-Partikeln kombiniert werden. Klickbare Polymere wurden durch die Synthese von Copolymeren und ihrer anschließenden Postfunktionalisierung mit Alkin- und Azid-Gruppen hergestellt. Durch die Variation des Verhältnisses der Comonomere wurden unterschiedlich

stark funktionalisierte Copolymere erhalten. Weiterhin konnten durch Einsatz von ATRP Polymere hergestellt werden, die exakt eine Alkin- oder Azid-Gruppe trugen. Diese breite Polymerbibliothek wurde dann eingesetzt, um Janus-Partikel über das Lösemittelverdampfungsverfahren aus Emulsionströpfchen herzustellen. Sowohl beidseitig als auch einseitig funktionalisierte Janus-Partikel wurden präpariert. Letztere wurden verwendet, um die Dichte der funktionellen Gruppen auf der Oberfläche zu quantifizieren und die Möglichkeit der Reaktion von Molekülen mit der Oberfläche nachzuweisen. Hierfür wurden klickbare Farbstoffe hergestellt. Die Funktionalität der Oberfläche entsprach sehr gut der Funktionalität der verwendeten Polymere, wodurch unterschiedlich stark funktionalisierte, klickbare Janus-Partikel zugänglich waren.

Eine andere komplexe Morphologie sind Nanokapseln. Diese haben vielversprechende Anwendungsfelder wie z.B. den gezielten Transport und die Freisetzung von Arzneistoffen oder von Selbstheilungsreagenzien. Um heterogene Strukturen innerhalb der Polymerschale zu erzeugen, wurden das stimulus-responsive Blockcopolymer PVFc-*b*-PMMA eingesetzt. Die Phasenseparation der beiden Blöcke führte zur Ausbildung von sphärischen PVFc-Domänen in der PMMA-Matrix der Wand der Nanokapseln. Diese Domänen konnten gezielt oxidiert werden, was je nach Oxidationsmittel zu Auswächsen oder Einbuchtungen führte. Zudem quollen die Kapseln in Wasser, da durch die Oxidation die vormals hydrophoben Domänen hydrophil wurden. Durch die Quellung konnte dann eingekapseltes Material aus der Kapsel diffundieren.

Das Konzept der Nutzung stimulus-responsiver Blockcopolymere für die Herstellung von stimulus-responsiven Nanokapseln wurde im Folgenden auch auf stimuli-responsive Blockcopolymere ausgedehnt. Sowohl ein Blockcopolymer, das auf eine Änderung des pH-Wertes und auf Oxidation reagiert, als auch ein Blockcopolymer mit den Stimuli der pH-Wert-Änderung und der Temperatur wurden verwendet. Hier wurde vor allem der Effekt der verschiedenen Stimuli auf die Morphologie der Nanokapseln und auf das Freisetzungsverhalten untersucht. Es wurde gezeigt, dass die Freisetzung aus den Nanokapseln durch die Einstellung der verschiedenen Parameter reguliert werden kann. Zusätzlich war es möglich, durch die Verkapselung von stimuli-responsiven Materialien den Kapselinhalt nur bei Einsatz eines Stimulus, nicht aber bei Einsatz des anderen Stimulus freizusetzen. Insbesondere das generelle Konzept des Einsatzes stimuli-responsiver Blockcopolymere für stimuli-responsive Kapseln wird das Forschungsfeld über die hier gezeigten Beispiele hinaus bereichern.

Der Lösemittelverdampfungsprozess aus Miniemulsionströpfchen bietet also, wie in dieser Arbeit exemplarisch gezeigt, die Möglichkeit, eine große Bandbreite an komplexen Kolloiden herzustellen. Zusätzlich wurden im Rahmen dieser Arbeit experimentelle Techniken entwickelt, die auch Fragen aus anderen Wissenschaftsfeldern beantworten werden.

Literature

[1] G. Yu, **2004**, in course syllabus for "Algorithm Design and Implementations" (2004) on mccombs.utexas.edu.

[2] G. C. Pimentel, J. A. Coonrod, *Opportunities in Chemistry:Today and Tomorrow*, The National Academies Press, Washington, **1987**.

[3] Taken from "Opportunities in Chemistry" by the National Academy of Sciences, *J. Chem. Educ.* **1986**, *63*, 743.

[4] G. Odian, *Principles of Polymerization*, 4. ed., Wiley, Hoboken, New Jersey, **2004**.

[5] M. D. Lechner, K. Gehrke, E. H. Nordmeier, *Makromolekulare Chemie*, 4. ed., Birkhäuser, Basel, **2010**.

[6] F. S. Bates, G. H. Fredrickson, *Annu. Rev. Phys. Chem.* **1990**, *41*, 525–557.

[7] F. S. Bates, *Science* **1991**, *251*, 898–905.

[8] R. H. Staff, K. Landfester, D. Crespy, *Adv. Polym. Sci.* **2013**, DOI: 10.1007/12_2013_233.

[9] E. V. Skorb, H. Möhwald, *Adv. Mater.* **2013**, *25*, 5029–5043.

[10] J. Fickert, P. Rupper, R. Graf, K. Landfester, D. Crespy, *J. Mater. Chem.* **2012**, *22*, 2286–2291.

[11] Y. Zhao, J. Fickert, K. Landfester, D. Crespy, *Small* **2012**, *8*, 2954–2958.

[12] J. Fickert, M. Makowski, M. Kappl, K. Landfester, D. Crespy, *Macromolecules* **2012**, *45*, 6324–6332.

[13] J. Fickert, Nanocapsules for self-healing materials, PhD thesis, Johannes Gutenberg University Mainz, **2013**.

[14] Y. L. Colson, M. W. Grinstaff, *Adv. Mater.* **2012**, *24*, 1521–4095.

[15] S. Ganta, H. Devalapally, A. Shahiwala, M. Amiji, *J. Controlled Release* **2008**, *126*, 187–204.

[16] P. Bawa, V. Pillay, Y. E. Choonara, L. C. du Toit, *Biomed. Mater.* **2009**, *4*, 022001.

[17] D. Schmaljohann, *Adv. Drug Delivery Rev.* **2006**, *58*, 1655–1670.

[18] G. Lagaly, O. Schulz, R. Zimehl, *Dispersionen und Emulsionen*, Steinkopf, Darmstadt, **1997**.

[19] H.-D. Dörfler, *Grenzflächen und kolloid-disperse Systeme*, Springer, Berlin, **2002**.

[20] H.-J. Butt, K. Graf, M. Kappl, *Physics and Chemistry of Interfaces*, 2. ed., Wiley, Weinheim, **2006**.

[21] K. Landfester, M. Willert, M. Antonietti, *Macromolecules* **2000**, *33*, 2370–2376.

[22] K. Landfester, *Macromol. Symp.* **2000**, *150*, 171–178.

[23] K. Landfester, *Macromol. Rapid Commun.* **2001**, *22*, 896–936.

[24] K. Landfester, *Angew. Chem., Int. Ed.* **2009**, *48*, 4488–4507.

[25] K. Landfester, *Annu. Rev. Mater. Res.* **2006**, *36*, 231–279.

[26] S. Tesch, H. Schubert, *J. Food Eng.* **2002**, *52*, 305–312.

[27] S. Asakura, F. Oosawa, *J. Polym. Sci.* **1958**, *33*, 183–192.

[28] K. Landfester, N. Bechthold, F. Tiarks, M. Antonietti, *Macromolecules* **1999**, *32*, 5222–5228.

[29] W. Ostwald, *Zeitschrift für Physikalische Chemie* **1900**, *34*, 495.

[30] K. Tauer, in *Colloids and Colloids Assemblies*, (Edited by F. Caruso), Wiley, Weinheim, Chap. Latex Particles, **2004**, Pages 1–51.

[31] K. Landfester, N. Bechthold, S. Förster, M. Antonietti, *Macromol. Rapid Commun.* **1999**, *20*, 81–84.

[32] F. Tiarks, K. Landfester, M. Antonietti, *Langmuir* **2001**, *17*, 908–918.

[33] J. M. Asua, *J. Polym. Sci. A Polym. Chem.* **2004**, *42*, 1025–1041.

[34] C. Chern, *Prog. Polym. Sci.* **2006**, *31*, 443–486.

[35] D. Crespy, K. Landfester, *Beilstein J. Org. Chem.* **2010**, *6*, 1132–1148.

[36] F. M. Pavel, *J. Dispersion Sci. Technol.* **2004**, *25*, 1–16.

[37] P. Y. Chow, L. M. Gan, in *Advances in Polymer Science*, Vol. 175, (Edited by M. Okubo), Springer Berlin Heidelberg, **2005**, Pages 257–298.

[38] S. A. Vitale, J. L. Katz, *Langmuir* **2003**, *19*, 4105–4110.

[39] F. Ganachaud, J. L. Katz, *Chem. Eur. J. of Chem. Phys.* **2005**, *6*, 209–216.

[40] S. Schubert, J. T. Delaney, Jr, U. S. Schubert, *Soft Matter* **2011**, *7*, 1581–1588.

[41] G. W. Burton, C. P. O'Farrell, *J. Elastomers and Plastics* **1977**, *9*, 94–101.

[42] J. P. Rao, K. E. Geckeler, *Prog. Polym. Sci.* **2011**, *36*, 887–913.

[43] J. W. Vanderhoff, M. S. El-Aasser, J. Ugelstad, Polymer Emulsification Process, **1979**.

[44] D. Quintanar-Guerrero, E. Allémann, H. Fessi, E. Doelker, *Drug Dev. Ind. Pharm.* **1998**, *24*, 1113–1128.

[45] S. Freiberg, X. Zhu, *Int. J. Pharm.* **2004**, *282*, 1–18.

[46] P. B. O'Donnell, J. W. McGinity, *Adv. Drug Delivery Rev.* **1997**, *28*, 25–42.

[47] N. Anton, J.-P. Benoit, P. Saulnier, *J. Controlled Release* **2008**, *128*, 185–199.

[48] J. Wang, S. P. Schwendeman, *J. Pharm. Sci.* **1999**, *88*, 1090–1099.

[49] Y. Zhao, R. Berger, K. Landfester, D. Crespy, *Polym. Chem.* **2014**, DOI: 10.1039/C3PY01096A.

[50] S. Desgouilles, C. Vauthier, D. Bazile, J. Vacus, J.-L. Grossiord, M. Veillard, P. Couvreur, *Langmuir* **2003**, *19*, 9504–9510.

[51] R. H. Staff, P. Rupper, I. Lieberwirth, K. Landfester, D. Crespy, *Soft Matter* **2011**, *7*, 10219–10226.

[52] R. M. Mainardes, R. C. Evangelista, *J. Microencapsul.* **2005**, *22*, 13–24.

[53] P. Sansdrap, Moës, *Int. J. Pharm.* **1993**, *98*, 157–164.

[54] W. I. Higuchi, J. Misra, *J. Pharm. Sci.* **1962**, *51*, 459–466.

[55] C. M. Miller, P. J. Blythe, E. D. Sudol, C. A. Silebi, M. S. El-Aasser, *J. Polym. Sci. A Polym. Chem.* **1994**, *32*, 2365–2376.

[56] A. Loxley, B. Vincent, *J. Colloid Interface Sci.* **1998**, *208*, 49–62.

[57] A. Taden, K. Landfester, *Macromolecules* **2003**, *36*, 4037–4041.

[58] R. Atkin, P. Davies, J. Hardy, B. Vincent, *Macromolecules* **2004**, *37*, 7979–7985.

[59] D. Crespy, K. Landfester, *Soft Matter* **2011**, *7*, 11054–11064.

[60] J. Fujiyama, Y. Nakase, K. Osaki, C. Sakakura, H. Yamagishi, A. Hagiwara, *J. Controlled Release* **2003**, *89*, 397–408.

[61] Z. Mana, Y. Pellequer, A. Lamprecht, *Int. J. Pharm.* **2007**, *338*, 231–237.

[62] D. Crespy, K. Landfester, *Macromol. Chem. Phys.* **2007**, *208*, 457–466.

[63] T. Kietzke, D. Neher, K. Landfester, R. Montenegro, R. Guntner, U. Scherf, *Nat. Mater.* **2003**, *2*, 408–412.

[64] C. Nouvel, J. Raynaud, E. Marie, E. Dellacherie, J.-L. Six, A. Durand, *J. Colloid Interface Sci.* **2009**, *330*, 337–343.

[65] C.-H. Chu, Y.-C. Wang, H.-Y. Huang, L.-C. Wu, C.-S. Yang, *Nanotechnology* **2011**, *22*, 185601.

[66] A. Musyanovych, J. Schmitz-Wienke, V. Mailänder, P. Walther, K. Landfester, *Macromol. Biosci.* **2008**, *8*, 127–139.

[67] M. M. Abdel-Mottaleb, B. Moulari, A. Beduneau, Y. Pellequer, A. Lamprecht, *Eur. J. Pharm. Biopharm.* **2012**, *82*, 151–157.

[68] M. Urban, A. Musyanovych, K. Landfester, *Macromol. Chem. Phys.* **2009**, *210*, 961–970.

[69] G. Mistlberger, A. L. Medina-Castillo, S. M. Borisov, T. Mayr, A. Fernández-Gutiérrez, J. F. Fernandez-Sanchez, I. Klimant, *Microchim. Acta* **2011**, *172*, 299–308.

[70] C. Perez, A. Sanchez, D. Putnam, D. Ting, R. Langer, M. Alonso, *J. Controlled Release* **2001**, *75*, 211–224.

[71] E. Pisani, N. Tsapis, J. Paris, V. Nicolas, L. Cattel, E. Fattal, *Langmuir* **2006**, *22*, 4397–4402.

[72] E. Pisani, N. Tsapis, B. Galaz, M. Santin, R. Berti, N. Taulier, E. Kurtisovski, O. Lucidarme, M. Ourevitch, B. T. Doan, J. C. Beloeil, B. Gillet, W. Urbach, S. L. Bridal, E. Fattal, *Adv. Funct. Mater.* **2008**, *18*, 2963–2971.

[73] C. Wohnhaas, K. Friedemann, D. Busko, K. Landfester, S. Baluschev, D. Crespy, A. Turshatov, *ACS Macro Lett.* **2013**, *2*, 446–450.

[74] C. Herrmann, M. B. Bannwarth, K. Landfester, D. Crespy, *Macromol. Chem. Phys.* **2012**, *213*, 829–838.

[75] J. Fickert, C. Wohnhaas, A. Turshatov, K. Landfester, D. Crespy, *Macromolecules* **2013**, *46*, 573–579.

[76] N. Saito, Y. Kagari, M. Okubo, *Langmuir* **2006**, *22*, 9397–9402.

[77] T. Tanaka, R. Nakatsuru, Y. Kagari, N. Saito, M. Okubo, *Langmuir* **2008**, *24*, 12267–12271.

[78] T. Tanaka, M. Okayama, Y. Kitayama, Y. Kagawa, M. Okubo, *Langmuir* **2010**, *26*, 7843–7847.

[79] X. Ge, M. Wang, X. Ji, X. Ge, H. Liu, *Colloid Polym. Sci.* **2009**, *287*, 819–827.

[80] N. Virgilio, B. D. Favis, *Macromolecules* **2011**, *44*, 5850–5856.

[81] T. Higuchi, K. Motoyoshi, H. Sugimori, H. Jinnai, H. Yabu, M. Shimomura, *Macromol. Rapid Commun.* **2010**, *31*, 1773–1778.

[82] M. Okubo, N. Saito, R. Takekoh, H. Kobayashi, *Polymer* **2005**, *46*, 1151–1156.

[83] T. Tanaka, N. Saito, M. Okubo, *Macromolecules* **2009**, *42*, 7423–7429.

[84] S.-J. Jeon, G.-R. Yi, C. M. Koo, S.-M. Yang, *Macromolecules* **2007**, *40*, 8430–8439.

[85] R. H. Staff, I. Lieberwirth, K. Landfester, D. Crespy, *Macromol. Chem. Phys.* **2012**, *213*, 351–358.

[86] J. Fickert, K. Landfester, D. Crespy, **2013**, submitted.

[87] Y. Zhao, K. Landfester, D. Crespy, *Soft Matter* **2012**, *8*, 11687–11696.

[88] D. Crespy, K. Landfester, *Macromolecules* **2005**, *38*, 6882–6887.

[89] M. G. Schwab, D. Crespy, X. Feng, K. Landfester, K. Müllen, *Macromol. Rapid Commun.* **2011**, *32*, 1798–1803.

[90] D. Crespy, K. Landfester, U. S. Schubert, A. Schiller, *Chem. Commun.* **2010**, *46*, 6651–6662.

[91] F. Bai, D. Wang, Z. Huo, W. Chen, L. Liu, X. Liang, C. Chen, X. Wang, Q. Peng, Y. Li, *Angew. Chem., Int. Ed.* **2007**, *46*, 6650–6653.

[92] Z. Lu, Y. Yin, *Chem. Soc. Rev.* **2012**, *41*, 6874–6887.

[93] E. Peng, E. S. G. Choo, P. Chandrasekharan, C.-T. Yang, J. Ding, K.-H. Chuang, J. M. Xue, *Small* **2012**, *8*, 3620–3630.

[94] J. W. Park, K. H. Bae, C. Kim, T. G. Park, *Biomacromolecules* **2011**, *12*, 457–465.

[95] L. H. Sullivan, *Lippincott's Magazine* **1896**, *57*, 403–409.

[96] S. Torza, S. G. Mason, *J. Colloid Interface Sci.* **1970**, *33*, 67–83.

[97] J. Berg, D. Sundberg, B. Kronberg, in *Polymeric Materials Science and Engineering*, Vol. 54, Proceedings of the ACS Division of Polymeric Material, **1986**, Pages 367–369.

[98] M. R. Muscato, D. C. Sundberg, *J. Polym. Sci. B Polym. Phys.* **1991**, *29*, 1021–1024.

[99] A. Musyanovych, K. Landfester, in *Macromolecular Engineering: Precise Synthesis, Materials Properties, Applications*, Vol. 2, (Edited by K. Matyjaszewski, Y. Gnanou, L. Leibler), Wiley, Chap. Core-Shell Particles, **2007**, Pages 1209–1249.

[100] F. S. Romanski, J. S. Winkler, R. C. Riccobene, M. S. Tomassone, *Langmuir* **2012**, *28*, 3756–3765.

[101] Y.-C. Chen, V. Dimonie, M. S. El-Aasser, *J. Appl. Polym. Sci.* **1992**, *46*, 691–706.

[102] T. Kietzke, D. Neher, M. Kumke, O. Ghazy, U. Ziener, K. Landfester, *Small* **2007**, *3*, 1041–1048.

[103] T. Kietzke, D. Neher, M. Kumke, R. Montenegro, K. Landfester, U. Scherf, *Macromolecules* **2004**, *37*, 4882–4890.

[104] S. Muroi, H. Hashimoto, K. Hosoi, *J. Polym. Sci. Polym. Chem. Ed.* **1984**, *22*, 1365–1372.

[105] T. Tanaka, T. Yamagami, T. Nogami, H. Minami, M. Okubo, *Polym. J.* **2012**, *44*, 1112–1116.

[106] N. Yamashita, N. Konishi, T. Tanaka, M. Okubo, *Langmuir* **2012**, *28*, 12886–12892.

[107] N. Saito, R. Takekoh, R. Nakatsuru, M. Okubo, *Langmuir* **2007**, *23*, 5978–5983.

[108] R. Yang, B. Li, A.-C. Shi, *Langmuir* **2011**, *28*, 1569–1578.

[109] S. Li, Y. Jiang, J. Z. Y. Chen, *Soft Matter* **2013**, *9*, 4843–4584.

[110] B. Yu, B. Li, Q. Jin, D. Ding, A.-C. Shi, *Soft Matter* **2011**, *7*, 10227–10240.

[111] B. Yu, B. Li, Q. Jin, D. Ding, A.-C. Shi, *Macromolecules* **2007**, *40*, 9133–9142.

[112] A.-C. Shi, B. Li, *Soft Matter* **2013**, *9*, 1398–1413.

[113] C. L. Winzor, D. C. Sundberg, *Polymer* **1992**, *33*, 4269–4279.

[114] D. C. Sundberg, Y. G. Durant, *Polym. React. Eng.* **2003**, *11*, 379–432.

[115] D. Crespy, R. H. Staff, T. Becker, K. Landfester, *Macromol. Chem. Phys.* **2012**, *213*, 1183–1189.

[116] S.-J. Jeon, G.-R. Yi, S.-M. Yang, *Adv. Mater.* **2008**, *20*, 4103–4108.

[117] L. Li, K. Matsunaga, J. Zhu, T. Higuchi, H. Yabu, M. Shimomura, H. Jinnai, R. C. Hayward, T. P. Russell, *Macromolecules* **2010**, *43*, 7807–7812.

[118] K. Hales, Z. Chen, K. L. Wooley, D. J. Pochan, *Nano Lett.* **2008**, *8*, 2023–2026.

[119] I. Wyman, G. Njikang, G. Liu, *Prog. Polym. Sci.* **2011**, *36*, 1152–1183.

[120] T. Higuchi, K. Motoyoshi, H. Sugimori, H. Jinnai, H. Yabu, M. Shimomura, *Soft Matter* **2012**, *8*, 3791–3797.

[121] H. Yabu, S. Sato, T. Higuchi, H. Jinnai, M. Shimomura, *J. Mater. Chem.* **2012**, *22*, 7672–7675.

[122] S. G. Jang, D. J. Audus, D. Klinger, D. V. Krogstad, B. J. Kim, A. Cameron, S.-W. Kim, K. T. Delaney, S.-M. Hur, K. L. Killops, G. H. Fredrickson, E. J. Kramer, C. J. Hawker, *J. Am. Chem. Soc.* **2013**, *135*, 6649–6657.

[123] S.-J. Jeon, S.-M. Yang, B. J. Kim, J. D. Petrie, S. G. Jang, E. J. Kramer, D. J. Pine, G.-R. Yi, *Chem. Mater.* **2009**, *21*, 3739–3741.

[124] K. Zhang, L. Gao, Y. Chen, Z. Yang, *Chem. Mater.* **2008**, *20*, 23–25.

[125] P. Qiu, C. Jensen, N. Charity, R. Towner, C. Mao, *J. Am. Chem. Soc.* **2010**, *132*, 17724–17732.

[126] M. P. Kim, D. J. Kang, D.-W. Jung, A. G. Kannan, K.-H. Kim, K. H. Ku, S. G. Jang, W.-S. Chae, G.-R. Yi, B. J. Kim, *ACS Nano* **2012**, *6*, 2750–2757.

[127] S.-H. Hu, X. Gao, *J. Am. Chem. Soc.* **2010**, *132*, 7234–7237.

[128] J. Geng, K. Li, W. Qin, L. Ma, G. G. Gurzadyan, B. Z. Tang, B. Liu, *Small* **2013**, *9*, 2012–2019.

[129] T. Isojima, S. K. Suh, J. B. Vander Sande, T. A. Hatton, *Langmuir* **2009**, *25*, 8292–8298.

[130] R. Deng, S. Liu, J. Li, Y. Liao, J. Tao, J. Zhu, *Adv. Mater.* **2012**, *24*, 1889–1893.

[131] R. Deng, F. Liang, W. Li, S. Liu, R. Liang, M. Cai, Z. Yang, J. Zhu, *Small* **2013**, DOI: 10.1002/smll.201300271.

[132] C. Herrmann, A. Turshatov, D. Crespy, *ACS Macro Lett.* **2012**, *1*, 907–909.

[133] S. Jiang, Q. Chen, M. Tripathy, E. Luijten, K. S. Schweizer, S. Granick, *Adv. Mater.* **2010**, *22*, 1060–1071.

[134] Q. Chen, J. Yan, J. Zhang, S. C. Bae, S. Granick, *Langmuir* **2012**, *28*, 13555–13561.

[135] A. Perro, S. Reculusa, S. Ravaine, E. Bourgeat-Lami, E. Duguet, *J. Mater. Chem.* **2005**, *15*, 3745–3760.

[136] F. Wurm, A. F. M. Kilbinger, *Angew. Chem., Int. Ed.* **2009**, *48*, 8412–8421.

[137] J. Hu, S. Zhou, Y. Sun, X. Fang, L. Wu, *Chem. Soc. Rev.* **2012**, *41*, 4356–4378.

[138] G. Loget, A. Kuhn, *J. Mater. Chem.* **2012**, *22*, 15457–15474.

[139] J. Du, R. K. O'Reilly, *Chem. Soc. Rev.* **2011**, *40*, 2402–2416.

[140] A. Kumar, B. J. Park, F. Tu, D. Lee, *Soft Matter* **2013**, *9*, 6604–6617.

[141] A. Synytska, L. Ionov, *Part. Part. Syst. Charact.* **2013**, *30*, 922–930.

[142] A. Walther, A. H. E. Müller, *Soft Matter* **2008**, *4*, 663–668.

[143] A. Walther, A. H. E. Müller, *Chem. Rev.* **2013**, *113*, 5194–5261.

[144] P.-G. de Gennes, *Angew. Chem., Int. Ed.* **1992**, *31*, 842–845.

[145] Z. Nie, W. Li, M. Seo, S. Xu, E. Kumacheva, *J. Am. Chem. Soc.* **2006**, *128*, 9408–9412.

[146] K.-H. Roh, D. C. Martin, J. Lahann, *Nat. Mater.* **2005**, *4*, 759–763.

[147] K.-H. Roh, M. Yoshida, J. Lahann, *Mat.-wiss. u. Werkstofftech.* **2007**, *38*, 1008–1011.

[148] J. Lahann, *Small* **2011**, *7*, 1149–1156.

[149] L. Hong, S. Jiang, S. Granick, *Langmuir* **2006**, *22*, 9495–9499.

[150] D. Suzuki, S. Tsuji, H. Kawaguchi, *J. Am. Chem. Soc.* **2007**, *129*, 8088–8089.

[151] Y. Wang, C. Zhang, C. Tang, J. Li, K. Shen, J. Liu, X. Qu, J. Li, Q. Wang, Z. Yang, *Macromolecules* **2011**, *44*, 3787–3794.

[152] H. R. Sheu, M. S. El-Aasser, J. W. Vanderhoff, *J. Polym. Sci. A Polym. Chem.* **1990**, *28*, 629–651.

[153] J.-W. Kim, R. J. Larsen, D. A. Weitz, *J. Am. Chem. Soc.* **2006**, *128*, 14374–14377.

[154] A. Misra, M. W. Urban, *Macromol. Rapid Commun.* **2010**, *31*, 119–127.

[155] H. Ahmad, N. Saito, Y. Kagawa, M. Okubo, *Langmuir* **2008**, *24*, 688–691.

[156] B. Liu, H. Möhwald, D. Wang, *Chem. Commun.* **2013**, *49*, 9746–9748.

[157] R. Erhardt, M. Zhang, A. Böker, H. Zettl, C. Abetz, P. Frederik, G. Krausch, V. Abetz, A. H. E. Müller, *J. Am. Chem. Soc.* **2003**, *125*, 3260–3267.

[158] T. Higuchi, A. Tajima, H. Yabu, M. Shimomura, *Soft Matter* **2008**, *4*, 1302–1305.

[159] J.-W. Kim, D. Lee, H. C. Shum, D. A. Weitz, *Adv. Mater.* **2008**, *20*, 3239–3243.

[160] A. Walther, M. Hoffmann, A. H. E. Müller, *Angew. Chem., Int. Ed.* **2008**, *47*, 711–714.

[161] A. Walther, K. Matussek, A. H. E. Mueller, *ACS Nano* **2008**, *2*, 1167–1178.

[162] A. Synytska, R. Khanum, L. Ionov, C. Cherif, C. Bellmann, *ACS Appl. Mater. Interfaces* **2011**, *3*, 1216–1220.

[163] S. C. Glotzer, M. J. Solomon, *Nat. Mater.* **2007**, *6*, 557–562.

[164] L. Hong, A. Cacciuto, E. Luijten, S. Granick, *Nano Lett.* **2006**, *6*, 2510–2514.

[165] L. Cheng, G. Zhang, L. Zhu, D. Chen, M. Jiang, *Angew. Chem., Int. Ed.* **2008**, *47*, 10171–10174.

[166] H. Xing, Z. Wang, Z. Xu, N. Y. Wong, Y. Xiang, G. L. Liu, Y. Lu, *ACS Nano* **2011**, *6*, 802–809.

[167] Z. Nie, D. Fava, E. Kumacheva, S. Zou, G. C. Walker, M. Rubinstein, *Nat. Mater* **2007**, *6*, 609–614.

[168] Q. Chen, J. K. Whitmer, S. Jiang, S. C. Bae, E. Luijten, S. Granick, *Science* **2011**, *331*, 199–202.

[169] J. Yan, M. Bloom, S. C. Bae, E. Luijten, S. Granick, *Nature* **2012**, *491*, 578–581.

[170] S. Sacanna, D. J. Pine, G.-R. Yi, *Soft Matter* **2013**, *9*, 8096–8106.

[171] G.-R. Yi, D. J. Pine, S. Sacanna, *J. Phys.: Condens. Matter* **2013**, *25*, 193101–193114.

[172] H. Ejima, J. J. Richardson, F. Caruso, *Angew. Chem., Int. Ed.* **2013**, *52*, 3314–3316.

[173] Q. Chen, S. C. Bae, S. Granick, *Nature* **2011**, *469*, 381–384.

[174] A. G. Vanakaras, *Langmuir* **2005**, *22*, 88–93.

[175] F. Sciortino, A. Giacometti, G. Pastore, *Phys. Rev. Lett.* **2009**, *103*, 237801–237804.

[176] Y. Liu, W. Li, T. Perez, J. D. Gunton, G. Brett, *Langmuir* **2011**, *28*, 3–9.

[177] G. Rosenthal, K. E. Gubbins, S. H. L. Klapp, *J. Chem. Phys.* **2012**, *136*, 174901–174910.

[178] H. Shin, K. S. Schweizer, *Soft Matter* **2014**, DOI: 10.1039/C3SM52094C.

[179] T. Nisisako, T. Torii, T. Takahashi, Y. Takizawa, *Adv. Mater.* **2006**, *18*, 1152–1156.

[180] C. Xu, B. Wang, S. Sun, *J. Am. Chem. Soc.* **2009**, *131*, 4216–4217.

[181] Z. W. Seh, S. Liu, S.-Y. Zhang, M. S. Bharathi, H. Ramanarayan, M. Low, K. W. Shah, Y.-W. Zhang, M.-Y. Han, *Angew. Chem., Int. Ed.* **2011**, *50*, 10140–10143.

[182] S. Pradhan, D. Ghosh, S. Chen, *ACS Appl. Mater. Interfaces* **2009**, *1*, 2060–2065.

[183] S. J. Ebbens, J. R. Howse, *Langmuir* **2011**, *27*, 12293–12296.

[184] P. M. Wheat, N. A. Marine, J. L. Moran, J. D. Posner, *Langmuir* **2010**, *26*, 13052–13055.

[185] J. R. Howse, R. A. L. Jones, A. J. Ryan, T. Gough, R. Vafabakhsh, R. Golestanian, *Phys. Rev. Lett.* **2007**, *99*, 48102–48105.

[186] L. Baraban, D. Makarov, R. Streubel, I. Mönch, D. Grimm, S. Sanchez, O. G. Schmidt, *ACS Nano* **2012**, *6*, 3383–3389.

[187] L. Baraban, M. Tasinkevych, M. N. Popescu, S. Sanchez, S. Dietrich, O. G. Schmidt, *Soft Matter* **2012**, *8*, 48–52.

[188] J. N. Anker, C. J. Behrend, H. Huang, R. Kopelman, *J. Magn. Magn. Mater.* **2005**, *293*, 655–662.

[189] J. Goldstein, D. E. Newbury, D. C. Joy, J. R. Michael, P. Echlin, E. Lifshin, L. Sawyer, C. E. Lyman, *Scanning electron microscopy and x-ray microanalysis*, 3. ed., Springer, New York, **2002**.

[190] D. B. Williams, C. B. Carter, *Transmission Electron Microscopy*, 6. ed., Plenum Press, New York, **1996**.

[191] G. Binnig, C. F. Quate, C. Gerber, *Phys. Rev. Lett.* **1986**, *56*, 930–933.

[192] A. R. West, *Grundlagen der Festkörperchemie*, Wiley, Weinheim, **1992**.

[193] W. Schärtl, *Light Scattering from Polymer Solutions and Nanoparticle Dispersions*, Springer, Berlin, **2007**.

[194] B. Tieke, *Makromolekulare Chemie*, 2. ed., Wiley, Weinheim, **2005**.

[195] J. R. Lakowicz, *Principles of Fluorescence Spectroscopy*, 3. ed., Springer, New York, **2010**.

[196] B. Valeur, J.-C. Brochon, *New Trends in Fluorescence Spectroscopy: Applications to Chemical and Life Sciences*, Springer, Heidelberg, **2001**.

[197] P. Schwille, *Fluorescence Correlation Spectroscopy: Theory and Applications*, Springer, Berlin, **2001**.

[198] K. Koynov, H.-J. Butt, *Curr. Opin. Colloid Interface Sci.* **2012**, *17*, 377–387.

[199] R. Rigler, Ü. Mets, J. Widengren, P. Kask, *Eur. Biophys. J.* **1993**, *22*, 169–175.

[200] P. Schwille, *Cell Biochem. Biophys.* **2001**, *34*, 383–408.

[201] P. Schwille, J. Bieschke, F. Oehlenschläger, *Biophys. Chem.* **1997**, *66*, 211–228.

[202] M. Börsch, P. Turina, C. Eggeling, J. R. Fries, C. A. Seidel, A. Labahn, P. Gräber, *FEBS Lett.* **1998**, *437*, 251–254.

[203] J. Ries, P. Schwille, *Phys. Chem. Chem. Phys.* **2008**, *10*, 3487–3497.

[204] R. Kohler, P. Schwille, W. Webb, M. Hanson, *J. Cell Sci.* **2000**, *113*, 3921–3930.

[205] S. A. Sukhishvili, Y. Chen, J. D. Müller, E. Gratton, K. S. Schweizer, S. Granick, *Macromolecules* **2002**, *35*, 1776–1784.

[206] J. Enderlein, *Phys. Rev. Lett.* **2012**, *108*, 108101–108104.

[207] J. Zhao, S. Granick, *J. Am. Chem. Soc.* **2004**, *126*, 6242–6243.

[208] J. S. S. Wong, L. Hong, S. C. Bae, S. Granick, *Macromolecules* **2011**, *44*, 3073–3076.

[209] Q. Yang, J. Zhao, *Langmuir* **2011**, *27*, 11757–11760.

[210] C. A. Grabowski, A. Mukhopadhyay, *Macromolecules* **2008**, *41*, 6191–6194.

[211] R. Liu, X. Gao, J. Adams, W. Oppermann, *Macromolecules* **2005**, *38*, 8845–8849.

[212] D. Wöll, H. Uji-i, T. Schnitzler, J.-i. Hotta, P. Dedecker, A. Herrmann, F. C. De Schryver, K. Müllen, J. Hofkens, *Angew. Chem., Int. Ed.* **2008**, *47*, 783–787.

[213] U. Zettl, S. T. Hoffmann, F. Koberling, G. Krausch, J. Enderlein, L. Harnau, M. Ballauff, *Macromolecules* **2009**, *42*, 9537–9547.

[214] T. Cherdhirankorn, A. Best, K. Koynov, K. Peneva, K. Müllen, G. Fytas, *J. Phys. Chem. B* **2009**, *113*, 3355–3359.

[215] T. Kalwarczyk, N. Ziębacz, A. Bielejewska, E. Zaboklicka, K. Koynov, J. Szymański, A. Wilk, A. Patkowski, J. Gapiński, H.-J. Butt, R. Hołyst, *Nano Lett.* **2011**, *11*, 2157–2163.

[216] A. Michelman-Ribeiro, H. Boukari, R. Nossal, F. Horkay, *Macromolecules* **2004**, *37*, 10212–10214.

[217] M. Gianneli, P. W. Beines, R. F. Roskamp, K. Koynov, G. Fytas, W. Knoll, *J. Phys. Chem. C* **2007**, *111*, 13205–13211.

[218] G. Modesti, B. Zimmermann, M. Börsch, A. Herrmann, K. Saalwächter, *Macromolecules* **2009**, *42*, 4681–4689.

[219] R. Raccis, R. Roskamp, I. Hopp, B. Menges, K. Koynov, U. Jonas, W. Knoll, H.-J. Butt, G. Fytas, *Soft Matter* **2011**, *7*, 7042–7053.

[220] T. Cherdhirankorn, V. Harmandaris, A. Juhari, P. Voudouris, G. Fytas, K. Kremer, K. Koynov, *Macromolecules* **2009**, *42*, 4858–4866.

[221] T. B. Bonné, K. Lüdtke, R. Jordan, P. Štěpánek, C. M. Papadakis, *Colloid Polym. Sci.* **2004**, *282*, 833–843.

[222] T. B. Bonné, K. Lüdtke, R. Jordan, C. M. Papadakis, *Macromol. Chem. Phys.* **2007**, *208*, 1402–1408.

[223] K. Jaskiewicz, A. Larsen, I. Lieberwirth, K. Koynov, W. Meier, G. Fytas, A. Kroeger, K. Landfester, *Angew. Chem., Int. Ed.* **2012**, *51*, 4613–4617.

[224] W. Mueller, K. Koynov, K. Fischer, S. Hartmann, S. Pierrat, T. Basché, M. Maskos, *Macromolecules* **2008**, *42*, 357–361.

[225] K. Starchev, J. Buffle, E. Pérez, *J. Colloid Interface Sci.* **1999**, *213*, 479–487.

[226] Z. Petrášek, P. Schwille, *Biophys. J.* **2008**, *94*, 1437–1448.

[227] C. Zander, J. Enderlein, R. A. Keller, *Single Molecule Detection in Solution - Methods and Applications*, Wiley-VCH, **2002**.

[228] P. Schwille, F. Meyer-Almes, R. Rigler, *Biophys. J.* **1997**, *72*, 1878–1886.

[229] Based on a drawing by David Schäffel, with friendly permission.

[230] R. H. Staff, D. Schaeffel, A. Turshatov, D. Donadio, H. J. Butt, K. Landfester, K. Koynov, D. Crespy, *Small* **2013**, *9*, 3514–3522.

[231] D. Schaeffel, R. H. Staff, H.-J. Butt, K. Landfester, D. Crespy, K. Koynov, *Nano Lett.* **2012**, *12*, 6012–6017.

[232] M. M. Fryd, T. G. Mason, *J. Phys. Chem. Lett.* **2010**, *1*, 3349–3353.

[233] C. Vauthier, C. Schmidt, P. Couvreur, *J. Nanopart. Res.* **1999**, *1*, 411–418.

[234] C. Goddeeris, F. Cuppo, H. Reynaers, W. Bouwman, G. Van den Mooter, *Int. J. Pharm.* **2006**, *312*, 187–195.

[235] J. S. Hadamard, *CR Acad. Sci.* **1911**, *152*, 1735.

[236] W. Rybczynski, *Bull. Int. Acad. Sci. Cracovie, Ser. A* **1911**, *1*, 40–46.

[237] S. S. Sadhal, R. E. Johnson, *J. Fluid Mech.* **1983**, *126*, 237–250.

[238] J. Lowndes, *J. Fluid Mech.* **1980**, *101*, 631–646.

[239] S. L. Carnie, D. Y. C. Chan, C. Lewis, R. Manica, R. R. Dagastine, *Langmuir* **2005**, *21*, 2912–2922.

[240] R. R. Dagastine, R. Manica, S. L. Carnie, D. Y. C. Chan, G. W. Stevens, F. Grieser, *Science* **2006**, *313*, 210–213.

[241] M. Eigen, R. Rigler, *Proc. Natl. Acad. Sci. USA* **1994**, *91*, 5740–5747.

[242] J. Eastoe, K. J. Hetherington, D. Sharpe, D. C. Steytler, S. Egelhaaf, R. K. Heenan, *Langmuir* **1997**, *13*, 2490–2493.

[243] A. Di Venere, E. Nicolai, N. Rosato, A. Rossi, A. Finazzi Agrò, G. Mei, *FEBS J.* **2011**, *278*, 1585–1593.

[244] T. Cherdhirankorn, M. Retsch, U. Jonas, H.-J. Butt, K. Koynov, *Langmuir* **2010**, *26*, 10141–10146.

[245] A. Turshatov, J. Adams, *Polymer* **2007**, *48*, 7444–7448.

[246] A. Turshatov, J. Adams, D. Johannsmann, *Macromolecules* **2008**, *41*, 5365–5372.

[247] K. Friedemann, A. Turshatov, K. Landfester, D. Crespy, *Langmuir* **2011**, *27*, 7132–7139.

[248] D. Busko, S. Baluschev, D. Crespy, A. Turshatov, K. Landfester, *Micron* **2012**, *43*, 583–588.

[249] D. Crespy, S. Zuber, A. Turshatov, K. Landfester, A.-M. Popa, *J. Polym. Sci. A Polym. Chem.* **2012**, *50*, 1043–1048.

[250] K. Bacia, P. Schwille, *Nat. Protocols* **2007**, *2*, 2842–2856.

[251] K. Landfester, R. Montenegro, U. Scherf, R. Güntner, U. Asawapirom, S. Patil, D. Neher, T. Kietzke, *Adv. Mater.* **2002**, *14*, 651–655.

[252] R. Riegler, E. S. Elson, *Fluorescence correlation spectroscopy: theory and applications*, Springer, New York, **2001**.

[253] H. C. Kolb, M. G. Finn, K. B. Sharpless, *Angew. Chem., Int. Ed.* **2001**, *40*, 2004–2021.

[254] Z. P. Demko, K. B. Sharpless, *Angew. Chem., Int. Ed.* **2002**, *114*, 2214–2217.

[255] C. W. Tornœ, C. Christensen, M. Meldal, *J. Org. Chem.* **2002**, *67*, 3057–3064.

[256] G. Wegner, M. M. Demir, M. Faatz, K. Gorna, R. Munoz-Espi, B. Guillemet, F. Gröhn, *Macromol. Res.* **2007**, *15*, 95–99.

[257] C. Lang, C. Kiefer, E. Lejeune, A. S. Goldmann, F. Breher, P. W. Roesky, C. Barner-Kowollik, *Polym. Chem.* **2012**, *3*, 2413–2420.

[258] J. Y. Dong, E. Manias, T. C. Chung, *Macromolecules* **2002**, *35*, 3439–3447.

[259] W. H. Yu, E. T. Kang, K. G. Neoh, *Ind. Eng. Chem. Res.* **2004**, *43*, 5194–5202.

[260] P. Krajnc, J. F. Brown, N. R. Cameron, *Org. Lett.* **2002**, *4*, 2497–2500.

[261] M. Negre, M. Bartholin, A. Guyot, *Angew. Makromol. Chem.* **1979**, *80*, 19–30.

[262] S. Kondo, T. Ohtsuka, K. Ogura, K. Tsuda, *J. Macromol. Sci., Part A: Chem.* **1979**, *13*, 767–775.

[263] Y.-S. Lee, Y.-S. Byoun, *Bull. Korean Chem. Soc.* **2002**, *23*, 1833–1835.

[264] M. Hesse, H. Meier, B. Zeeh, *Spektroskopische Methoden in der organischen Chemie*, 7. ed., Thieme, Stuttgart, **2005**.

[265] C. N. Urbani, C. A. Bell, D. E. Lonsdale, M. R. Whittaker, M. J. Monteiro, *Macromolecules* **2007**, *40*, 7056–7059.

[266] J. A. Opsteen, J. C. M. van Hest, *Chem. Commun.* **2005**, *0*, 57–59.

[267] Y. Li, J. Yang, B. C. Benicewicz, *J. Polym. Sci. A Polym. Chem.* **2007**, *45*, 4300–4308.

[268] D. Briggs, J. T. Grant, *Surface Analysis by Auger and X-Ray Photoelectron Spectroscopy*, IM Publications LLP, Chichester, **2003**.

[269] G. Baier, J. M. Siebert, K. Landfester, A. Musyanovych, *Macromolecules* **2012**, *45*, 3419–3427.

[270] M. Kasuya, T. Taniguchi, R. Motokawa, M. Kohri, K. Kishikawa, T. Nakahira, *J. Polym. Sci. Part A: Polym. Chem.* **2013**, *51*, 4042–4051.

[271] M. Fikry, M. M. Omar, L. Z. Ismail, *J. Fluoresc.* **2009**, *19*, 741–746.

[272] J. M. G. E. Siebert, Abbaubare Polymere und Kupfer-katalysierte Reaktionen in Miniemulsion zum Aufbau funktioneller Nanopartikel und -kapseln, PhD thesis, Johannes Gutenberg University Mainz, **2011**.

[273] B. Neises, W. Steglich, *Angew. Chem., Int. Ed.* **1978**, *17*, 522–524.

[274] CRC Handbook of Chemistry and Physics, **2013**, Internet Version 2013.

[275] J. M. Siebert, G. Baier, A. Musyanovych, K. Landfester, *Chem. Commun.* **2012**, *48*, 5470–5472.

[276] R. Roux, L. Sallet, P. Alcouffe, S. Chambert, N. Sintes-Zydowicz, E. Fleury, J. Bernard, *ACS Macro Lett.* **2012**, *1*, 1074–1078.

[277] N. Li, W. H. Binder, *J. Mater. Chem.* **2011**, *21*, 16717–16734.

[278] D. R. Breed, R. Thibault, F. Xie, Q. Wang, C. J. Hawker, D. J. Pine, *Langmuir* **2009**, *25*, 4370–4376.

[279] A. S. Goldmann, L. Barner, M. Kaupp, A. P. Vogt, C. Barner-Kowollik, *Prog. Polym. Sci.* **2012**, *37*, 975–984.

[280] A. S. Goldmann, A. Walther, L. Nebhani, R. Joso, D. Ernst, K. Loos, C. Barner-Kowollik, L. Barner, A. H. E. Müller, *Macromolecules* **2009**, *42*, 3707–3714.

[281] S. A. Krovi, D. Smith, S. T. Nguyen, *Chem. Commun.* **2010**, *46*, 5277–5279.

[282] M. B. Bannwarth, S. W. Kazer, S. Ulrich, G. Glasser, D. Crespy, K. Landfester, *Angew. Chem., Int. Ed.* **2013**, *52*, 10107–10111.

[283] R. H. Staff, M. Gallei, M. Mazurowski, M. Rehahn, R. Berger, K. Landfester, D. Crespy, *ACS Nano* **2012**, *6*, 9042–9049.

[284] S. R. White, N. R. Sottos, P. H. Geubelle, J. S. Moore, M. R. Kessler, S. R. Sriram, E. N. Brown, S. Viswanathan, *Nature* **2001**, *409*, 794–797.

[285] D. Roy, J. N. Cambre, B. S. Sumerlin, *Progress in Polymer Science* **2010**, *35*, 278–301.

[286] T. Traitel, Y. Cohen, J. Kost, *Biomaterials* **2000**, *21*, 1679–1687.

[287] A. Guiseppi-Elie, S. Brahim, D. Narinesingh, *Adv. Mater.* **2002**, *14*, 743–746.

[288] T. Uchiyama, Y. Kiritoshi, J. Watanabe, K. Ishihara, *Biomaterials* **2003**, *24*, 5183–5190.

[289] M. Maier, N. Kotman, C. Friedrichs, J. Andrieu, M. Wagner, R. Graf, W. S. L. Strauss, V. Mailänder, C. K. Weiss, K. Landfester, *Macromolecules* **2011**, *44*, 6258–6267.

[290] J. Andrieu, N. Kotman, M. Maier, V. Mailänder, W. S. L. Strauss, C. K. Weiss, K. Landfester, *Macromol. Rapid Commun.* **2012**, *33*, 248–253.

[291] D. Klinger, E. M. Aschenbrenner, C. K. Weiss, K. Landfester, *Polym. Chem.* **2012**, *3*, 204–216.

[292] Z.-R. Lu, P. Kopečková, J. Kopeček, *Macromol. Biosci.* **2003**, *3*, 296–300.

[293] T. Miyata, N. Asami, T. Uragami, *Macromolecules* **1999**, *32*, 2082–2084.

[294] T. Miyata, N. Asami, T. Uragami, *Nature* **1999**, *399*, 766–769.

[295] R. Zhang, A. Bowyer, R. Eisenthal, J. Hubble, *Biotechnol. Bioeng.* **2007**, *97*, 976–984.

[296] J. Kost, R. Langer, *Trends Biotechnol.* **1992**, *10*, 127–131.

[297] P. Norris, M. Noble, I. Francolini, A. M. Vinogradov, P. S. Stewart, B. D. Ratner, J. W. Costerton, P. Stoodley, *Antimicrob. Agents Chemother.* **2005**, *49*, 4272–4279.

[298] S. Mitragotri, *Nat. Rev. Drug Discov.* **2005**, *4*, 255–260.

[299] S. Miyazaki, C. Yokouchi, M. Takada, *J. Pharm. Pharmacol.* **1988**, *40*, 716–717.

[300] G. A. Husseini, G. D. Myrup, W. G. Pitt, D. A. Christensen, N. Y. Rapoport, *J. Control. Release* **2000**, *69*, 43–52.

[301] D. Klinger, K. Landfester, *Soft Matter* **2011**, *7*, 1426–1440.

[302] D. Klinger, K. Landfester, *Macromol. Rapid Commun.* **2011**, *32*, 1979–1985.

[303] D. Klinger, K. Landfester, *Macromolecules* **2011**, *44*, 9758–9772.

[304] D. Klinger, K. Landfester, *J. Polym. Sci. A Polym. Chem.* **2012**, *50*, 1062–1075.

[305] G. Filipcsei, J. Fehér, M. Zrínyi, *J. Mol. Struct.* **2000**, *554*, 109–117.

[306] T. Shiga, in *Advances in Polymer Science*, Vol. 134, Springer Berlin Heidelberg, **1997**, Pages 131–163.

[307] M. Zrínyi, *Colloid Polym. Sci.* **2000**, *278*, 98–103.

[308] P. M. Xulu, G. Filipcsei, M. Zrínyi, *Macromolecules* **2000**, *33*, 1716–1719.

[309] M. A. C. Stuart, W. T. S. Huck, J. Genzer, M. Müller, C. Ober, M. Stamm, G. B. Sukhorukov, I. Szleifer, V. V. Tsukruk, M. Urban, F. Winnik, S. Zauscher, I. Luzinov, S. Minko, *Nat. Mater.* **2010**, *9*, 101–113.

[310] J. Seuring, S. Agarwal, *Macromol. Rapid Commun.* **2012**, *33*, 1898–1920.

[311] C. C. Page, C. C. Moser, X. Chen, P. L. Dutton, *Nature* **1999**, *402*, 47–52.

[312] W. Dröge, *Physiol. Rev.* **2002**, *82*, 47–95.

[313] J. S. Stamler, *Cell* **1994**, *78*, 931–936.

[314] J. T. Coyle, P. Puttfarcken, *Science* **1993**, *262*, 689–695.

[315] T. Finkel, N. J. Holbrook, *Nature* **2000**, *408*, 239–247.

[316] R. Liu, X. Zhao, T. Wu, P. Feng, *J. Am. Chem. Soc.* **2008**, *130*, 14418–14419.

[317] X. Wan, D. Wang, S. Liu, *Langmuir* **2010**, *26*, 15574–15579.

[318] R. Bird, T. J. Freemont, B. R. Saunders, *Chem. Commun.* **2011**, *47*, 1443–1445.

[319] B. Goldenbogen, N. Brodersen, A. Gramatica, M. Loew, J. Liebscher, A. Herrmann, H. Egger, B. Budde, A. Arbuzova, *Langmuir* **2011**, *27*, 10820–10829.

[320] W. Ong, Y. Yang, A. C. Cruciano, R. L. McCarley, *J. Am. Chem. Soc.* **2008**, *130*, 14739–14744.

[321] C. Wang, Y. Guo, Y. Wang, H. Xu, X. Zhang, *Chem. Commun.* **2009**, *36*, 5380–5382.

[322] A. Napoli, M. Valentini, N. Tirelli, M. Müller, J. A. Hubbell, *Nat. Mater.* **2004**, *3*, 183–189.

[323] T. Tatsuma, K. Saito, N. Oyama, *Anal. Chem.* **1994**, *66*, 1002–1006.

[324] T. Saito, M. Watanabe, *React. Funct. Polym.* **1998**, *37*, 263–269.

[325] T. Saito, M. Watanabe, *Polymer Journal* **1999**, *31*, 1149–1154.

[326] H. Patel, X. Li, H. Karan, *Biosensors and Bioelectronics* **2003**, *18*, 1073–1076.

[327] A. Gülce, H. Gülce, *J. Biochem. Biophys. Methods* **2005**, *62*, 81–92.

[328] A. E. G. Cass, G. Davis, G. D. Francis, H. A. O. Hill, W. J. Aston, I. J. Higgins, E. V. Plotkin, L. D. L. Scott, A. P. F. Turner, *Anal. Chem.* **1984**, *56*, 667–671.

[329] M. Nakahata, Y. Takashima, H. Yamaguchi, A. Harada, *Nat. Commun.* **2011**, *2*, 511.

[330] G. R. Whittell, I. Manners, *Adv. Mater.* **2007**, *19*, 3439–3468.

[331] A. S. Abd-El-Aziz, I. Manners, *Frontiers in Transition Metal-Containing Polymers*, Wiley-Interscience, Hoboken, NJ, **1997**.

[332] I. Manners, *Synthetic Metal-Containing Polymers*, VCH, Weinheim, **2004**.

[333] D. Wöhrle, A. D. Pomogailo, *Metal Complexes and Metals in Macromolecules: Synthesis, Structure and Properties*, Wiley-VCH, Weinheim, Germany, **2003**.

[334] C. E. Carraher, A. S. Abd-El-Aziz, C. Pittman, J. Sheats, M. Zeldin, *A Half Century of Metal and Metalloid Containing Polymers*, Wiley, New York, **2003**.

[335] M. Rehahn, *Organic-Inorganic Hybrid Polymers*, Wiley-VCH, Weinheim, Germany, **1999**.

[336] T. M. Smith, G. L. Nelson, *Polym. Adv. Technol.* **2006**, *17*, 746–753.

[337] D. A. Foucher, B. Z. Tang, I. Manners, *J. Am. Chem. Soc.* **1992**, *114*, 6246–6248.

[338] I. Manners, *Can. J. Chem.* **1998**, *76*, 371–381.

[339] V. Bellas, M. Rehahn, *Angew. Chem., Int. Ed.* **2007**, *46*, 5082–5104.

[340] M. Gallei, R. Klein, M. Rehahn, *Macromolecules* **2010**, *43*, 1844–1854.

[341] M. Gallei, B. V. K. J. Schmidt, R. Klein, M. Rehahn, *Macromol. Rapid Commun.* **2009**, *30*, 1463–1469.

[342] D. A. Rider, J. I. L. Chen, J.-C. Eloi, A. C. Arsenault, T. P. Russell, G. A. Ozin, I. Manners, *Macromolecules* **2008**, *41*, 2250–2259.

[343] M. Umana, D. R. Rolison, R. Nowak, P. Daum, R. W. Murray, *Surface Science* **1980**, *101*, 295–309.

[344] L. M. Han, K. Rajeshwar, R. B. Timmons, *Langmuir* **1997**, *13*, 5941–5950.

[345] H. Ritter, B. E. Mondrzik, M. Rehahn, M. Gallei, *Beilstein J. Org. Chem.* **2010**, DOI: 10.3762/bjoc.6.60.

[346] C. D'Silva, S. Afeworki, O. L. Parri, P. K. Baker, A. E. Underhill, *J. Mater. Chem.* **1992**, *2*, 225–230.

[347] H.-J. Butt, R. Berger, E. Bonaccurso, Y. Chen, J. Wang, *Adv. Colloid Interface Sci.* **2007**, *133*, 91–104.

[348] M. Péter, M. A. Hempenius, E. S. Kooij, T. A. Jenkins, S. J. Roser, W. Knoll, G. J. Vancso, *Langmuir* **2004**, *20*, 891–897.

[349] C. Schatz, E. G. Smith, S. P. Armes, E. J. Wanless, *Langmuir* **2008**, *24*, 8325–8331.

[350] H. Ringsdorf, P. Lehmann, R. Weberskirch, Multicompartmentation - a Concept for the Molecular Architecture of Life, **1999**, Anaheim, CA.

[351] A. Laschewsky, *Curr. Opin. Colloid Interface Sci.* **2003**, *8*, 274–281.

[352] Z. Li, E. Kesselman, Y. Talmon, M. A. Hillmyer, T. P. Lodge, *Science* **2004**, *306*, 98–101.

[353] H. Cui, Z. Chen, S. Zhong, K. L. Wooley, D. J. Pochan, *Science* **2007**, *317*, 647–650.

[354] A. B. Ebrahim Attia, Z. Y. Ong, J. L. Hedrick, P. P. Lee, P. L. R. Ee, P. T. Hammond, Y.-Y. Yang, *Curr. Opin. Colloid Interface Sci.* **2011**, *16*, 182–194.

[355] A. H. Gröschel, F. H. Schacher, H. Schmalz, O. V. Borisov, E. B. Zhulina, A. Walther, A. H. Müller, *Nat. Commun.* **2012**, *3*, 710.

[356] H. Ringsdorf, *J. Polym. Sci., C Polym. Symp.* **1975**, *51*, 135–153.

[357] L. Gros, H. Ringsdorf, H. Schupp, *Angew. Chem., Int. Ed.* **1981**, *20*, 305–325.

[358] R. Haag, *Angew. Chem., Int. Ed.* **2004**, *43*, 278–282.

[359] M. Motornov, Y. Roiter, I. Tokarev, S. Minko, *Prog. Polym. Sci.* **2010**, *35*, 174–211.

[360] I. Tokarev, S. Minko, *Soft Matter* **2009**, *5*, 511–524.

[361] B. Jeong, A. Gutowska, *Trends Biotechnol.* **2002**, *20*, 305–311.

[362] C. d. l. H. Alarcón, S. Pennadam, C. Alexander, *Chem. Soc. Rev.* **2005**, *34*, 276–285.

[363] O. J. Cayre, N. Chagneux, S. Biggs, *Soft Matter* **2011**, *7*, 2211–2234.

[364] R. Cheng, F. Meng, C. Deng, H.-A. Klok, Z. Zhong, *Biomaterials* **2013**, *34*, 3647–3657.

[365] P. Schattling, F. Jochum, P. Theato, *Polym. Chem.* **2013**, DOI: 10.1039/C3PY–00880K.

[366] A. Doring, W. Birnbaum, D. Kuckling, *Chem. Soc. Rev.* **2013**, *42*, 7391–7420.

[367] D. Klinger, K. Landfester, *Polymer* **2012**, *53*, 5209–5231.

[368] W. Gu, S. S. Ting, M. H. Stenzel, *Polymer* **2013**, *54*, 1010–1017.

[369] L. Gao, J. Fei, J. Zhao, W. Cui, Y. Cui, J. Li, *Chem. Eur. J.* **2012**, *18*, 3185–3192.

[370] C. Basset, C. Harder, C. Vidaud, C. Déjugnat, *Biomacromolecules* **2010**, *11*, 806–814.

[371] J. Shi, C. Du, J. Shi, Y. Wang, S. Cao, *Macromol. Biosci.* **2013**, *13*, 494–502.

[372] W.-H. Chiang, V. T. Ho, W.-C. Huang, Y.-F. Huang, C.-S. Chern, H.-C. Chiu, *Langmuir* **2012**, *28*, 15056–15064.

[373] Z. Xing, C. Wang, J. Yan, L. Zhang, L. Li, L. Zha, *Colloid Polym. Sci.* **2010**, *288*, 1723–1729.

[374] Z. Xing, C. Wang, J. Yan, L. Zhang, L. Li, L. Zha, *Soft Matter* **2011**, *7*, 7992–7997.

[375] T. P. Richardson, M. C. Peters, A. B. Ennett, D. J. Mooney, *Nat. Biotech* **2001**, *19*, 1029–1034.

[376] A. Wijaya, S. B. Schaffer, I. G. Pallares, K. Hamad-Schifferli, *ACS Nano* **2008**, *3*, 80–86.

[377] S.-H. Hu, S.-Y. Chen, X. Gao, *ACS Nano* **2012**, *6*, 2558–2565.

[378] F. Schacher, M. Ulbricht, A. H. E. Müller, *Adv. Funct. Mater.* **2009**, *19*, 1040–1045.

[379] F. Schacher, T. Rudolph, F. Wieberger, M. Ulbricht, A. H. E. Müller, *ACS Appl. Mater. Interfaces* **2009**, *1*, 1492–1503.

[380] X. Wang, G. Jiang, Z. Wei, X. Li, B. Tang, *Eur. Polym. J.* **2013**, *49*, 3165–3170.

[381] C. Schmidt, Synthese amphiphiler Blockcopolymere und Untersuchung der Strukturbildung in Substanz und in selektiven Lösungsmitteln, Diploma thesis, Technische Universität Darmstadt, **2013**, This diploma thesis was subject to a non-disclosure agreement at the time this thesis was prepared. The information about the block copolymer morphology was a personal communication with Dr. Markus Gallei, TU Darmstadt.

[382] J. F. Deye, T. A. Berger, A. G. Anderson, *Anal. Chem.* **1990**, *62*, 615–622.

[383] A. K. Dutta, K. Kamada, K. Ohta, *J. Photochem. Photobiol. A* **1996**, *93*, 57–64.

[384] R. Chen, F. Chu, C. Gauthier, L. Chazeau, I. Chaduc, E. Bourgeat-Lami, M. Lansalot, *J. Polym. Sci. A Polym. Chem.* **2010**, *48*, 2329–2339.

[385] N. Vij, T. Min, R. Marasigan, C. Belcher, S. Mazur, H. Ding, K.-T. Yong, I. Roy, *J. Nanobiotechnology* **2010**, *8*, 22.

[386] T. Delmas, A. Fraichard, P.-A. Bayle, I. Texier, M. Bardet, J. Baudry, J. Bibette, A.-C. Couffin, *J. Colloid Sci. Biotechnol.* **2012**, *1*, 16–25, DOI 10.1166/jcsb.2012.1010.

[387] N. Uehara, O. Yoshida, *Anal. Sci.* **2012**, *28*, 1125–1132.

[388] K. Jeyakumar, D. K. Chand, *Tetrahedron Lett.* **2006**, *47*, 4573–4576.

[389] G. I. Giles, K. M. Tasker, C. Jacob, *Free Radic. Biol. Med.* **2001**, *31*, 1279–1283.

[390] I. Nikiforow, J. Adams, A. M. König, A. Langhoff, K. Pohl, A. Turshatov, D. Johannsmann, *Langmuir* **2010**, *26*, 13162–13167.

[391] I. García-Moreno, A. Costela, L. Campo, R. Sastre, F. Amat-Guerri, M. Liras, F. López Arbeloa, J. Bañuelos Prieto, I. López Arbeloa, *J. Phys. Chem. A* **2004**, *108*, 3315–3323.

[392] T. Liu, S. Pihan, M. Roth, M. Retsch, U. Jonas, J. S. Gutmann, K. Koynov, H.-J. Butt, R. Berger, *Macromolecules* **2011**, *45*, 862–871.

Appendix

A. List of Abbreviations

AIBN	2,2'-azobis(2-methylpropionitrile)
APD	avalanche photo detectors
ATRP	atom transfer radical polymerization
CTMA-Cl	cetyltrimethylammonium chloride
CV	cyclic voltammetry
DCC	*N*,*N*'-dicyclohexyl carbodiimide
DC-FCCS	dual-color fluorescence cross-correlation spectroscopy
DDA	dimethyldodecylamine
DLS	dynamic light scattering
DMAP	dimethyl aminopyridine
DMF	dimethyl formamide
DMSO	dimethyl sulfoxide
DPDS	diphenyl disulfide
EC	ethyl cellulose
FCS	fluorescence correlation spectroscopy
FRET	fluorescence resonance energy transfer
GC	gas chromatography
HD	hexadecane
HFIP	hexafluoroisopropanol
HPLC	high performance liquid chromatography
IR	infrared
ITO	indium tin oxide
LCST	lower critical solution temperature
MEP	miniemulsion polymerization
MMA	methyl methacrylate
NMR	nuclear magnetic resonance spectroscopy
NPP	[1-(4-nitrophenyl)-2-pyrrolidinmethyl] acrylate
P2VP	poly(2-vinylpyridine)
PCD	particle charge detection
PDI	polydispersity index
PDMAEMA	poly(2-dimethylaminoethyl methacrylate)
PET	poly(ethylene terephtalate)
PFDMS	poly(ferrocenyl dimethyl silane)
PI	poly(isoprene)
PLA	poly(lactic acid)
PLLA	poly(L-lactic acid)
PMDETA	*N*,*N*,*N*',*N*',*N*''-pentamethyl diethylenetriamine

PMI	*N*-(2,6-diisopropylphenyl)-perylene-3,4-dicarbonacidimide
PMMA	poly(methyl methacrylate)
PMMA-*co*-PVBC	poly(methyl methacrylate)-*co*-poly(vinylbenzyl chloride)
PPC	poly(propylene carbonate)
PPO	poly(2,6-dimethyl-1,4-phenylene oxide)
PS	poly(styrene)
PS-*b*-P4VP	poly(styrene)-*block*-poly(4-vinylpyridine)
PS-*b*-PBD	poly(styrene)-*block*-poly(butadiene)
PS-*b*-PDMAEMA	poly(styrene)-*block*-poly(2-dimethylaminoethyl methacrylate)
PS-*b*-PFEMS	poly(styrene)-*block*-poly(ferrocenylethylmethylsilane)
PS-*b*-PMMA	poly(styrene)-*block*-poly(methyl methacrylate)
PS-*co*-PVBC	poly(styrene)-*co*-poly(vinylbenzyl chloride)
PSS	Polymer Standard Service
PVA	poly(vinylalcohol)
PVAc	poly(vinylacetate)
PVBC	poly(vinylbenzyl chloride)
PVCi	poly(vinylcinnamate)
PVF	poly(vinylformal)
PVFc	poly(vinylferrocene)
$PVFc^+$	poly(vinylferrocenium)
PVFc-*b*-P2VP	poly(vinylferrocene)-*block*-poly(2-vinylpyridine)
PVFc-*b*-PMMA	poly(vinylferrocene)-*block*-poly(methyl methacrylate)
RAFT	reversible addition-fragmentation chain transfer
SANS	small-angle neutron scattering
SDS	sodium dodecylsulfate
SEC	size exclusion chromatography
SEC-MALLS	size exclusion chromatography with multi angle light scattering detection
SEED	solvent evaporation from emulsion droplets
SEM	scanning electron microscope
SEM-EDX	scanning electron microscope energy-dispersive X-ray spectroscopy
SFM	scanning force microscope
TBAF	tetra-(*n*-butyl)-ammonium fluoride
TBAHFP	tetra-(*n*-butyl)-ammonium hexafluorophosphate
TDI	toluene diisocyanate
TEM	transmission electron microscope
TEOS	tetraethoxysilane
TFA	trifluoroacetic acid
THF	tetrahydrofuran
VBC	vinylbenzyl chloride
VPA	9-vinylphenanthrene
XPS	X-ray photoelectron spectroscopy

B. List of Symbols

A	aggregation ratio
$A_{i,j,k}$	interfacial area between the components i, j or k
b	blue
br	blue and red
c	concentration
C_n	concentration of a fluorophore in channel n
D	hydrodynamic diameter
$\delta F(t)$	temporal fluctuation of the fluorescence intensity
D_z	coefficient of diffusion
E	energy
η	dynamic viscosity
f_i	fraction of species i in the observation volume V
G	Gibbs enthalpy
γ_{ij}	surface tension between components i and j
$g_1(t)$	auto-correlation function
$G_n(\tau)$	auto-correlation function in channel n
h	Planck's constant, $h = 6.626\,069\,57 \times 10^{-34}$ Js
i	component in a multi-component system
I	intensity
I_{group}	integral of the signal in the NMR spectrum of a certain group
j	component in a multi-component system
k	component in a multi-component system
k_B	Boltzmann constant
M	molecular weight
m	mass
m_d	number of types of freely diffusing species in a given volume
M_n	number-averaged molecular weight
M_w	weight-averaged molecular weight
N	absolute number of a species in an experiment in the given volume
n	general variable
n/m	molar ratio in copolymers
N_A	Avogadro constant, $N_A = 6.022\,141\,29 \times 10^{23}\,\mathrm{mol}^{-1}$
ν	frequency
$p_{Laplace}$	Laplace pressure
Φ_{FRET}	FRET quantum yield
π	ratio of a circle's circumference to its diameter, $\pi \approx 3.1415926$
$\Pi_{osmotic}$	osmotic pressure
Ψ	normalized surface density
q	wave vector
r	red
R_{FRET}	Förster radius
R_{gas}	universal gas constant
r_0	lateral dimension of the observation volume
r_{FRET}	distance of donor and acceptor in FRET pairs

r_h	hydrodynamic radius
$r_{monomer}$	copolymerization parameter of the monomer
ρ	density
S	ratio of axial to lateral dimension of volume V
$S_{a,b}$	electronic singlet state with an energy a and a vibrational state b
$s_{i,j,k}$	spreading coefficient of component i, j or k
T	temperature
t	time
$T_{a,b}$	electronic triplet state with an energy a and a vibrational state b
τ	diffusion time
τ_D	lateral diffusion time
V	volume or observation volume
V_n	observation volume of a laser in channel n
x	general variable

C. Acknowledgments

D. Curriculum Vitae

E. Scientific Contributions

Publications

- R. H. Staff, K. Landfester, D. Crespy: Marrying Janus Particles to Click-Chemistry, *in preparation*
- R. H. Staff, M. Gallei, C. Schmidt, K. Landfester, D. Crespy: Hydrophobic nanocapsules encoded for stimuli-selective release in water, *in preparation*
- R. H. Staff, K. Landfester, D. Crespy: Recent Advances in the Emulsion Solvent Evaporation Technique for the Preparation of Polymer Nanoparticles, *Adv. Polym. Sci.*, **2013**, DOI: 10.1007/12_2013_233
- R. H. Staff, D. Schaeffel, A. Turshatov, D. Donadio, H.-J. Butt, K. Landfester, K. Koynov, D. Crespy: Particle Formation in the Emulsion Solvent Evaporation Process, *Small*, **2013**, *9*, 3514-3522
- D. Schaeffel, R. H. Staff, H.-J. Butt, K. Landfester, D. Crespy, K. Koynov: Fluorescence Correlation Spectroscopy Directly Monitors Coalescence during Nanoparticle Preparation, *Nano Lett.*, **2012**, *12*, 6012-6017
- R. H. Staff, M. Gallei, M. Mazurowski, M. Rehahn, R. Berger, K. Landfester, D. Crespy: Patchy Nanocapsules of Poly(vinylferrocene)-Based Block Copolymers for Redox-Responsive Release, *ACS Nano*, **2012**, *6*, 9042-9049
- D. Crespy, R. H. Staff, T. Becker, K. Landfester: Chemical Routes toward Multicompartment Colloids, *Macromol. Chem. Phys.*, **2012**, *213*, 1183-1189
- R. H. Staff, I. Lieberwirth, K. Landfester, D. Crespy: Preparation and Characterization of Anisotropic Submicron Particles from Semicrystalline Polymers, *Macromol. Chem. Phys.*, **2012**, *213*, 351-358
- R. H. Staff, P. Rupper, I. Lieberwirth, K. Landfester, D. Crespy: Phase Behavior of Binary Mixtures of Block Copolymers and a Non-Solvent in Miniemulsion Droplets as Single and Double Nanoconfinement, *Soft Matter*, **2011**, *7*, 10219-10226

Conferences

- Oral presentation "Synthesis of Functional Polymer Nanocapsules Prepared by Solvent Evaporation from Emulsion Droplets", DWI - RWTH Aachen Summer School, Aachen, 24.-25.06.2013, awarded the "Lanxess Talent Award 2013"
- Invited oral presentation "Synthesis of Functional Polymer Nanoparticles Prepared by Solvent Evaporation from Emulsion Droplets", BASF, Ludwigshafen, 25.04.2013
- Oral presentation "Mechanism and applications of the solvent evaporation process from emulsion droplets", 9th Zsigmondy-Colloquium, Essen, 06.-08.03.2013
- Poster "Redox-Responsive Patchy Nanocapsules" (R. H. Staff, R. Berger, K. Landfester, D. Crespy), Max Planck Poster Day, Max Planck Institute for Polymer Research, Mainz, 10.10.2012

- Poster "Redox-Responsive Patchy Nanocapsules" (R. H. Staff, M. Gallei, M. Mazurowski, M. Rehahn, K. Landfester, D. Crespy), Smart Polymers, Mainz, 07.-09.10.2012
- Poster "New functional Colloidal Morphologies from Block Copolymer Assemblies in nanoparticulate Systems" (R. H. Staff, D. Crespy, K. Landfester), 124th International BASF Summer Courses, Ludwigshafen, 14.-24.08.2012
- Poster "Mechanism and Applications of the Solvent Evaporation Process from Emulsion Droplets" (R. H. Staff, D. Schäffel, K. Koynov, K. Landfester, D. Crespy), Warwick Polymer Conference, Warwick, 09.-12.07.2012
- Oral presentation "Block Copolymer Assembly in Single- and Double Nanoconfinement", JCF-Frühjahrssymposium Rostock, 18.-21.03.2012
- Poster "Particle Formation by the Emulsion-Solvent Evaporation Technique: A comprehensive Study" (D. Schäffel, R. H. Staff, H.-J. Butt, K. Koynov, K. Landfester, D. Crespy), 8th Zsigmondy-Colloquium, Darmstadt, 05.-07.03.2012
- Poster "New Functional Colloidal Morphologies from Block Copolymer Assembly in Droplets" (R. H. Staff, M. Gallei, M. Mazurowski, M. Rehahn, K. Landfester, D. Crespy), Makromolekulares Kolloquium Freiburg, 23.-25.02.2012, awarded first place in poster competition
- Poster "On the Morphology of Block Copolymer Nanoparticles in Mono- and Double Spherical Confinement" (R. H. Staff, K. Landfester, D. Crespy), Jülich Soft Matter Days, 16.-18.11.2011
- Poster "Unraveling the Kinetics of Nanoparticle Formation by Fluorescence Correlation Spectroscopy" (R. H. Staff, D. Schäffel, K. Koynov, K. Landfester, D. Crespy), Max Planck Poster Day, Max Planck Institute for Polymer Research, Mainz, 28.09.2011